U-Th-Pb fractionation in selected carbonate and silicate systems

Thesis

U-Th-Pb Fractionation in Selected Carbonate and Silicate Systems

A thesis submitted for the degree

of Doctor of Philosophy

Yi-Ming Huang

B. Eng., M. Eng.

The Department of Earth Science

The Open University

Milton Keynes, U.K.

February,1995

The Open University

Abstract

U-Th-Pb fractionation trends, and the associated variations in Pb-isotopes, provide important constraints on the nature, and age, of a wide range of geological processes. This thesis presents three detailed case studies from a carbonatite intrusive complex, lower crustal granulite xenoliths, and young volcanic rocks which represent a range of processes that fractionate U, Th and Pb.

New major, trace element and Sr, Nd and Pb isotope results are presented for carbonatites and pyroxenites from the 130 Ma old Jacupiranga complex in southern Brazil. The data preclude simple models in which the Sr-Nd and Sr-Pb isotope arrays are the result of crustal contamination processes, or liquid immiscibility between the carbonatites and magmas similar to those from which the pyroxenites crystallised. The initial Sr, Nd and Pb isotope ratios in the Jacupiranga complex are similar to those in the Parana high-Ti basalts and to the oceanic basalts of the Walvis Ridge and Tristan da Cunha, and were apparently inherited from the mantle source regions associated with incipient magmatism of the Tristan da Cunha hotspot and the opening of the South Atlantic. Most carbonatites have high U/Pb and low Rb/Sr ratios and infiltration and/or metasomatism by such melts is one process that may be responsible for the negative correlation of U/Pb and Rb/Sr inferred for the source of certain oceanic basalts such as Tristan da Cunha.

Correlations between trace and major elements in mostly mafic granulite xenoliths from southern Africa probably result from magmatic processes such as fractional crystallisation and crystal accumulation. From Pb and Nd isotope systematics it can be inferred that the northern Lesotho xenoliths are Proterozoic in age, whereas Cape province xenoliths appear to have been formed in the Archaean and to have had their Nd isotopes reset in the Proterozoic. Most Pb isotope ratios from the granulites xenoliths are unradiogenic relative to the Geochron, which indicates relatively low U/Pb ratios in the later parts of their histories. The correlation between Pb isotope ratios and K_2O/Al_2O_3 in the granulites from Markt is considered to reflect magmatic control of the U/Pb fractionation. The Archaean, and some of the younger mantle derived rocks on the Kaapvaal craton, plot on similar Pb isotope trends. It is argued that segments of the crust and uppermost mantle beneath southern Africa stabilised together in the Archaean, and that both were remobilised in subsequent magmatic and orogenic events.

Volcanic rocks in the Northland-Auckland peninsula, New Zealand, range from silica-undersaturated basanites to tholeiites and andesites. Although all the volcanic fields are in intraplate settings, two types of mantle source enrichment can be recognised. One is subduction-related and characterised by high Sr and low Nd isotope ratios and negative Nb anomalies. The other type has geochemical features characteristic of intraplate enriched mantle sources with Sr and Nd isotope ratios and Nb/Ba, Ba/La, similar to HIMU OIB, which has been attributed to the deep recycling of oceanic crust. The differences in Pb isotopes between the two mantle sources, i.e. higher Δ 8/4 and 7/4, but lower $^{206}Pb/^{204}Pb$ in the subduction-related material than in the inferred HIMU source, indicate that U/Pb in shallow recycled crustal material tend to be lower than in the deeper recycled material.

These case studies confirm that (i) metasomatism by small degree melts can have significant effects on mantle trace element characteristics, (ii) the lower crust is a relatively low μ environment and crystal accumulation may be an important mechanism in the fractionation of Th and U from Pb, and (iii) incorporation of recycled crustal material at different levels can result in different U-Th-Pb fractionation and so, with time, different Pb isotope ratios.

Acknowledgements

First of all, my special thanks go to my supervisors, Dr. Peter van Calsteren and Professor Chris Hawkesworth for their continuous help, encouragement and supervision throughout the period of my studies at the Open University. Without their enthusiastic help and interest, this project would not have been possible.

I also would like to thank Drs. Frank McDermott, Nick Rogers, Pamela Kempton and Graeme Pearson for many discussions and detailed comments on my thesis drafts. Dr. Ian Smith is thanked for the New Zealand samples, data and comments on the relevant chapters. I wish to thank Frank McDermott and Andy Sutton for their help with correcting my English. Drs. Keith Bell, Catherine Chauvel and Mike Roden are thanked for their detailed reviews of Chapter two, when it was submitted for publication in Chemical Geology. Mabs Johnston and David Wright are thanked for their enthusiastic help in Radiogenic Isotope Laboratory, where I spent most of my time collecting the data. Andy Tindle was very helpful with electron-probe work, and when Macs went wrong. John Watson, Peter Webb and Nick Rogers helped with XRF and INAA analyses, and Kay Chambers and Brian Elis helped in making thin sections. Dentinho helped in electron-probe analyses and metamorphic P-T condition calculations. Janet Dryden helped me with her professional skill on WORD and prepared the final manuscripts for publication.

John Holbrook, Rita, Mike and Lynn are thanked for their kindly help, especially during the early days when I came here. Andy, Kate, Fran, Marcus, Jessica, Penny, Josanne, Jason and Arlëne shared offices with me, and all members of the department were very helpful and provided a nice environment for my study. I would like to thank my lab colleagues for the numerous lab parties and knowledge of wines, but learning drinking large volumes of wine, as they do, seems even more difficult for me than writing-up a thesis .

The China State Education Commission and Changchun University of Earth Sciences (CUES) are acknowledged for one year funding, which enabled me to come and start this project here. I wish to thank Professor Lin Er-Wei and many others of the Isotope Geology Laboratory, CUES, who introduced me into the Isotope Geology and helped me during the time of my studies at UK.

Finally, I would like to thank my wife and parents, for their love, understanding and persistent support, which gave me the strength to overcome all difficulties I encountered in the course of my studies. I dedicate this thesis to them.

Contents

List of Tables

Chapter II

Chapter III

Chapter IV

Chapter V

List of Figures

Chapter II

Chapter III

Chapter IV

Chapter V

Chapter One

Introduction

Fundamental objectives of terrestrial geochemistry include the determination of the fluxes of elements between different reservoirs of the Earth through geological time, and the fractionation patterns of trace elements that can be used to understand the processes involved. Discussions of chemical changes with time and rates of element transport processes require information from trace elements and isotopes generated by radioactive decay. The U-Th-Pb system has several unique properties which are helpful for a better understanding of element transport and fractionations during various geological processes.

1-1. U-Th-Pb system

U and Th are radioactive trace elements which can be used in geochemical studies and they have several features in common. U and Th have similar electron configurations and so have similar chemical properties. They occur in nature in the tetravalent oxidation state and have similar ionic radii (U^{+4} =1.05 Å, Th^{+4} = 1.10Å), although under oxidizing conditions, U has a valence of +6 and then forms the water soluble uranyl ion $(UO_2)^{-}$. U and Th can substitute extensively for each other in most silicate minerals, and therefore the Th/U ratio in most terrestrial rocks is relatively constant (2-6). Pb is found as a trace element in most rock-forming minerals but it also forms galena (PbS), and it has both siderophile and chalcophile characteristics. U/Pb is also relatively constant in most silicate rocks ($^{238}U/^{204}Pb$ = 7-12) except in some carbonate and hydrothermal

environments.

Th has one long-life isotope, ^{232}Th, and U has two, ^{235}U and ^{238}U. ^{232}Th and both ^{235}U and ^{238}U decay, via a number of short-lived intermediaries, through their individual series, to three Pb isotopes, ^{208}Pb, ^{207}Pb and ^{206}Pb with half-lives of 14, 4.5 and 0.7 Ga, respectively. This indicates that about half the ^{238}U and most of ^{235}U has decayed to Pb during Earth history. This system has a number of properties that other isotope systems, such as Rb-Sr and Sm-Nd, do not possess. First, ^{235}U and ^{238}U are radioactive isotopes of the same element, and so will not be fractionated during geological processes; second, they decay with different decay rates to two isotopes of Pb, and so the Pb isotope ratio, $^{207}Pb/^{206}Pb$, can be used for dating. ^{232}Th also decays to one isotope of Pb, ^{208}Pb, and thus $^{208}Pb/^{206}Pb$ can be used to evaluated the time integrated Th/U ratios in reservoirs in which the Pb resides. U/Pb and Th/Pb ratios are changed by various geological processes, such as partial melting, hydrothermal and metamorphic processes, and with time such changes result in variable Pb isotope ratios. Thus, a better understanding of U-Th-Pb fractionation in various geological processes will help the interpretation of the range in Pb isotope compositions observed in different geological environments, and this, in turn, will improve the general understanding of geological histories. In addition, the U-Th-Pb system often does not correlate with other systems, such as Rb-Sr and Sm-Nd, and so their fractionation cannot be predicted by other systems. This means that the U-Th-Pb system is able to provide extra information, and so it is both the most interesting, but also the most complicated geochemical tracer (Allègre et al. 1986).

The available data provided by many studies exhibit a general picture of U, Th and Pb distributions in different reservoirs in the Earth. The Th, U and Pb abundances have been measured in a wide range of rock types, and estimates of the average of Th, U and Pb contents in the upper crust have

been compiled (Rogers and Adams 1975). All three elements are highly incompatible with very small partition coefficients in most rock forming minerals. In magmatic processes Th, U and Pb therefore tend to be enriched in the melt, and so their abundances are higher in acid than in basic rocks, and in the crust relative to the mantle. Because U is more incompatible than Pb during partial melting (Sun and McDonough 1989), the upper crust has high U relative to Pb and so high U/Pb ratios, which results in radiogenic Pb isotope ratios. The MOR mantle is depleted by magma extraction and so is expected to have low U/Pb. However, Pb isotope ratios from MORB are radiogenic relative to the Geochron. This is so-called Pb-paradox. The lower crust is thought to be characterised by unradiogenic Pb isotope compositions and so to complement the radiogenic Pb in the mantle and the upper continental crust (Davis 1984; Newsom et al. 1986). Another hypothesis suggests that U is more incompatible during the generation of oceanic crust but less incompatible than Pb in the generation of continental crust (Sun and McDonough 1989). Recent Models (Kramers and Tolstikhin 1994) propose that the Earth took ~0.18 Ga for accretion rather than being generated instantly ~4.55 Ga years ago, and suggest that the Geochron should therefore be at higher $^{206}Pb/^{204}Pb$, which resolves the Pb paradox.

Whatever the reasons for the Pb-paradox, the U-Th-Pb fractionation in different reservoirs provides genetic information which needs to be fully understood. The lower crust is much more difficult to sample than the upper crust, and high grade metamorphic terrains and granulite xenoliths are considered to be at least partially representative of the lower crust. A number of studies (Moorbath et al., 1969; Grey and Oversby, 1972; Weaver and Tarney, 1981) on Precambrian high grade metamorphic terrains documented a relative depletion of LILE and U. However, in a wide survey of granulite terrains Taylor and Mclennan (1985) concluded that they were not always depleted in LILE, U and Th. Many granulite xenoliths have been

shown to have relatively radiogenic Pb isotope ratios (Esperanca et al. 1988; Rudnick and Goldstein 1991; and Kempton et al. 1993). Thus, both U, Th depleted and un-depleted pictures for the lower crust have emerged from different studies. The nature of U-Th-Pb in the lower crust is important for any modeling of the bulk Earth and for understanding lower crustal processes.

The chemical heterogeneity of the upper mantle has been well documented in a large number of studies (e.g. Faure and Hurley 1963; Gast et al 1964; Dupré and Allègre 1983; Hart 1984; McDonough et al. 1985; Song and Frey 1989; Staudigel et al. 1991). The continental lithosphere mantle is considered to be cold and isolated from other parts of the mantle and so with time it has developed geochemical features different from the convecting upper mantle. Oceanic mantle regions have also been shown to have variable compositions and studies of oceanic basalts have proposed four principle end-member isotopic components (Zindler and Hart 1985). DM is depleted by magma extraction and characterised by relatively low $^{206}Pb/^{204}Pb$, $^{207}Pb/^{206}Pb$ and $^{208}Pb/^{206}Pb$. The high U/Pb (HIMU) end-member has very high $^{206}Pb/^{204}Pb$ with relatively low $^{208}Pb/^{206}Pb$, which indicates time integrated high U/Pb but low Th/U ratios. In contrast, EMI, EMII have relatively low $^{206}Pb/^{204}Pb$ associated with high $^{208}Pb/^{206}Pb$ which suggests that it has been derived from sources with relatively low U/Pb and high Th/U ratios. Several processes have been proposed to have been responsible for causing such heterogeneities in the mantle. For example, EMI, EMII and HIMU end-member components inferred from Oceanic Island Basalts (OIB) in intraplate settings have all been attributed to recycling of different crustal material by subduction. However, at destructive plate margins, subduction related magmatism provides different fractionation patterns from those in OIB. Mantle metasomatism is another mechanism operating in the mantle (Harte 1983; Dawson 1984; Hawkesworth et al 1984) which can modify mantle compositions and it has

been identified in a number of studies of mantle xenoliths (Kempton 1987; Lloyd 1987, Harte et al. 1987; Erlank et al. 1987; Chen et al. 1989; Ben Othman et al. 1990; Hawkesworth et al. 1990). Melts generated by small degrees of partial melting are considered to be very efficient agents for transporting elements and hence modifying compositions in the mantle (Spera 1987; Eggler 1987; Green and Wallence 1988; Menzies 1990). The data from metasomatised mantle xenoliths from the continental lithosphere also indicate significant fractionation of Th and U. Because Th and U are not supposed to be fractionated during fractional crystallization and relatively large degrees of partial melting, fractionation of Th/U may be specifically related to the metasomatism and small degrees of partial melting.

1-2. Objectives

As discussed above, the geological fractionation of U-Th-Pb in various geological processes are particularly interesting. This project was planned to look into several different kinds of rocks with different petrogenesis, to obtain further insights into U-Th-Pb fractionation in different geological environments. Therefore, the aims of this project are as follows:-

(i) To examine the geochemical characteristics of a suite of carbonatites, and to use trace element and radiogenic isotope data to re-evaluate the petrogenetic models for carbonatites. In addition, carbonatite melts have been suggested as an important agent for mantle metasomatism, and so their geochemical features are important in any discussion of trace element fractionation by mantle metasomatism.

(ii) To investigate the origins of two suites of granulite xenoliths from kimberlites, which represent direct samples from the lower crust. New major, trace element and isotope data provide evidence for the ages of granulites, whether they were generated by underplating in the lower crust,

or as residues after partial melting, and new insights into the causes of U/Pb and Th/U fractionation in the lower crust.

(iii) To study young intraplate volcanic rocks, mainly basalts, from Northland-Auckland Peninsula, New Zealand, to determine the conditions of melt generation, and the nature of their source components.

(iv) To review briefly the results of each study in the context of U-Th-Pb fractionation and its application to Earth evolution models.

1-3. Thesis layout

This thesis consists of detailed studies of different kinds of rocks ranging from carbonatites to silicates, and including both metamorphic and volcanic rocks. Each chapter presents a different case study and they are relatively independent from one another, except for the volcanic rocks from New Zealand, which comprise Chapters IV and V. At the time of submission, Chapter II has been published in Chemical Geology (119) and Chapter III has been provisionally accepted by Geochim. Cosmochim. Acta for publication.

Chapter II deals with the Jacupiranga carbonatites from Brazil. It provides new analytical results on major, trace element and Sr, Nd and Pb isotope compositions. It discusses their geochemical characteristics, examines the possible processes which might have been responsible for the observed compositional variations, and considers the relationship between the carbonatites and some associated silicate rocks. On the basis of the major, trace element and isotope evidence, generation models for the carbonatites are discussed, as are the effects of carbonatite metasomatism on mantle U/Pb ratios.

Chapter III presents a study of granulite xenoliths from kimberlites in southern Africa. The study includes two suites of granulite xenoliths, one

from locations around Britstown in South Africa and another from northern Lesotho. The generation ages of the granulites are complicated because some isotope systems have been reset during metamorphism in their long histories. This chapter provides evidence that the two suites of granulites have different generation ages, Archaean and Proterozoic. Using the available data, the Pb isotope composition in the lower crust beneath the southern Africa is evaluated. In addition, the processes responsible for fractionation of U/Pb and Th/U and relationship between generation of the Archaean crust and continental lithosphere mantle are discussed.

Chapter IV is concerned with the petrogenesis of the Auckland basanites and alkali basalts. It is argued that although they occur in a continental intraplate tectonic setting, they have trace element patterns and isotope compositions similar to OIB, which leads to implications for their tectonic model, time constraints on mantle enrichment by deep recycled crustal material.

Chapter V deals with tholeiites and andesites from Northland and Mercury Island. It provides data which show that the samples can be divided into different groups, and discusses possible roles of various processes and mantle sources in their compositions. Mantle enrichment models involving components related to deep recycling and shallow subduction are proposed to explain the observed geochemical characteristics.

Chapter VI summarises the discussions in the previous chapters and provides general discussion and speculation of fractionation of the U-Th-Pb system in different reservoirs.

Chapter Two
Geochemical characteristics and origin of the Jacupiranga carbonatites, Brazil

2-1. Introduction

Carbonatites have very low SiO_2, but high incompatible trace element abundances and so they are markedly different from most other igneous rocks. Previous studies have demonstrated that carbonatites are more likely to have been generated by partial melting of the mantle than by limestone syntexis (Bell et al., 1982; Bell and Blenkinsop, 1987). Many carbonatites occur in continental areas and so they are useful probes of the sub-continental upper mantle. However, on the basis of similar radiogenic isotope compositions, it has been argued that carbonatites were derived from an ocean island basalt (OIB)-type source (Basu and Tatsumoto, 1980; Bell et al., 1982; Bell and Blenkinsop, 1987; Nelson et al., 1988).

The generation of carbonatites is still debated, but they are important to any discussion of magma generation and element fractionation processes in the upper mantle. Many carbonatites are associated with alkaline rocks and the relationship between them is relevant to understanding carbonatite petrogenesis. Experimental studies on carbonate and silicate systems show that carbonate melt may be segregated by liquid immiscibility from a carbonate-enriched silicate melt at certain P–T conditions (Kjarsgaad and Hamilton, 1989). Alternatively, carbonatites may be generated by small degrees of partial melting in the upper mantle (Nelson et al., 1988; Gittins,

1989). However, the primary carbonatites are expected to have high Mg# and relatively low Ca#(Ca/(Ca+Mg)) (Eggler, 1989; Dalton and Wood, 1993), and these characteristics are rare in carbonatites worldwide. Dalton and Wood (1993) suggested that calcio-carbonatites may be formed by interaction of primary magnesian carbonatite melts with the upper mantle lithosphere.

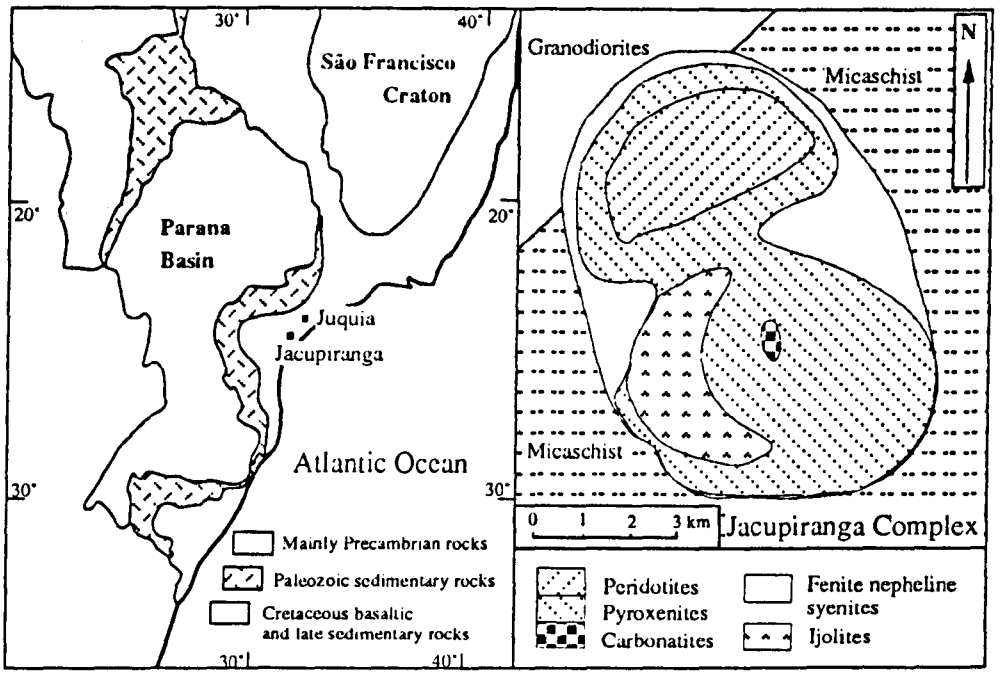

Fig. 2-1 Simplified geological sketch maps of southern Brazil and the Jacupiranga complex, modified after Ulbrich and Gomes (1981) and Melcher (1966).

The Jacupiranga carbonatite complex was intruded into a late Precambrian mica schist and syntectonic granodiorite belt ~130 Ma ago (Fig. 2-1) (Amaral, 1978; Roden et al., 1985) and, together with several nearby alkaline complexes, it comprises the Jacupiranga alkaline province (Ulbrich and Gomes, 1981). It occurs in an oval shaped alkalic complex (Fig. 2-1, about 65 km^2), which includes pyroxenites, peridotites, ijolites and fenite nepheline syenites. Two separate intrusive stages of silicate rocks, and up to five distinct carbonatite intrusions, have been identified (Melcher, 1966;

Gaspar and Wyllie, 1983). To the west is the present outcrop of the Parana–Etendeka continental flood basalts (CFB) which erupted contemporaneously 138–128 Ma ago (Hawkesworth et al., 1992; Renne et al., 1992, Turner et al., 1994). Herz (1977) proposed that a triple junction had developed in this area with two arms related to the initial opening of the South Atlantic Ocean, and the third marked by tholeiitic and alkalic volcanism on the South American continent. Thus, both tholeiitic and alkalic magmatism appears to have been related to the initial opening of the south Atlantic. Roden et al. (1985) reported Sr and Nd isotope ratios for the Jacupiranga carbonatites and suggested that they were derived from source regions similar to those sampled by the Walvis Ridge basalts. This study was undertaken to investigate the relationship between the Jacupiranga complex, the Parana CFB, and subsequent hot spot related magmatism in the South Atlantic, and to evaluate the element fractionation effects of carbonatite generation in the upper mantle.

2-2. Analytical techniques

The Jacupiranga carbonatites and associated silicate rocks were collected from recently blasted outcrops to avoid weathering effects. The whole rock samples were crushed in acid cleaned agate satellite ball mills to minimize contamination, and their petrography and mineralogy are described in Appendix B.

Major elements were measured using a ARL Fisons–8420 dual goniometer WD XRF spectrometer on fused glass discs at Open University. Carbonatite samples for major elements were prepared at 50% SiO_2 dilution, using the normal silicate calibration. SiO_2 was adjusted relative to BCS368 and BCS393 carbonate standards and the data corrected for the dilution. The trace elements Rb, Sr, Y, Zr, Nb, Ba, Sc, V, Cr, Co, Ni, Cu, Zn and Ga were determined by XRF on pressed powder pellets. Abundances of

the REE and remaining trace elements in Table 2-1 were obtained by INAA, following the procedures described by Potts et al. (1985).

The nine whole rock samples and selected mineral separates were analysed for Sr, Nd and Pb isotopes. In order to reduce the contamination in other minerals from calcite, which has very high Sr contents, mineral separates other than calcite were washed in acid. Apatite and phlogopite were washed with cold 0.25 N HCl in an ultra-sonic bath for ~15 minutes, and pyroxenes were washed with 2.5 N HCl for ~15–30 minutes. Routine blanks for Sr and Nd were 0.5 ng and 1 ng respectively, and that for Pb was ~1 ng. Isotope measurements were carried out on a Finnigan-MAT 261. Repeat analyses of standards with samples gave averages and errors (1 standard deviation) as follows: NBS 987, $^{87}Sr/^{86}Sr$ = 0.710245±14, $^{86}Sr/^{86}Sr$ normalised to 0.1194; Johnson Mattey Nd, $^{143}Nd/^{144}Nd$ = 0.511853±11, $^{146}Nd/^{144}Nd$ normalised to 0.7219. Average ratios of NBS 981 are $^{206}Pb/^{204}Pb$ = 16.909±12, $^{207}Pb/^{204}Pb$ = 15.454±16, $^{208}Pb/^{204}Pb$ = 36.577±49. The Pb isotope ratios in Table 2-3 have been corrected for fractionation relative to repeated analyses of NBS 981. Isotope dilution analyses for the trace element concentrations in Table 2-2 and 3 were carried out on a VG 54E.

2-3. Results

2-3.1 Major and trace elements

The major, trace element and REE analyses are tabulated in Table 2-1. Three groups can be recognised on the basis of major elements: the pyroxenites (HB001 and HB008–1) are characterised by high SiO_2 and Al_2O_3; the carbonatites (HB005, HB009–2, HB010 and HB011) have low SiO_2 (<10%), MgO, K_2O and Al_2O_3, but high CaO (35–50%); and the third group of samples (HB004, HB008–2 and HB009–1) has SiO_2 ~25%, high MgO and K_2O (15–35% and 2–4.5% respectively). These extreme variations in major

TABLE 2-1

Major and trace element abundances in the whole rock samples from the Jacupiranga carbonatite complex

Sample	HB001	HB004	HB005	HB008-1	HB008-2	HB009-1	HB009-2	HB010	HB011
SiO_2	43.29	22.58	2.3	40	23.24	21.04	2.38	4.3	6.08
TiO_2	3.704	2.27	0.66	3.924	0.24	1.23	0.05	1.32	0.14
Al_2O_3	6.07	3.3	1.16	6.65	4.1	2.76	0	0.86	0.12
Fe_2O_3	15.58	10.98	33.64	16.83	10.9	8.82	4.48	33.04	3.08
MnO	0.128	0.2	0.25	0.139	0.2	0.22	0.014	0.31	0.14
MgO	11.24	18.04	4.34	11.32	14.84	24.02	4.18	7.3	6.98
CaO	19.33	18.88	30.78	19.96	20.06	19.62	47.34	28.56	45.28
Na_2O	0.38	0.41	0.18	0.42	1.16	0.28	0.01	0.2	0.08
K_2O	0.02	3.98	0.26	0.03	4.3	2.1	0.04	0.36	0.06
P_2O_5	0.009	1.12	9.04	0.017	0.86	1.97	0.87	9.78	3.07
LOI	0.59	17	15.96	1.09	17.82	17.32	36.36	13.4	34.36
S	0.06	0.54	0.26	0	0.04	0.02	2.00		0.4
Total	100.34	99.3	98.83	100.38	99.92	99.4	97.85	99.43	99.79
Rb	n.d.	100	9	1	75	69	4	10	6
Sr	282	2172	2749	332	2123	2404	5848	2772	5130
Y	10	18	34	10	24	18	38	33	35
Zr	182	62	1678	208	109	20	n.d.	1710	287
Hf	6.67	2.98	22.6	6.91	4.9	1.62	0.23	29.2	6.28
Nb	6	294	78	5	100	159	5	97	68
Ta	0.73	7.15	24.6	0.79	1.45	16.4	0.25	26.5	16.8
Ba	45	466	734	38	822	1412	629	491	525
Pb	16	9	38	9	8	5	19	34	14
Th	0.57	13.3	4	0.32	17.7	5.25	3	6.08	34.4
U	n.d.	0.74	0.253	n.d.	2.58	1	n.d.	1.86	4.61
Sc	52	20.9	56.2	53.6	79.7	29.6	17	76.1	24.2
V	287	131	287	314	141	83	4	331	31
Cr	65	50	11	118	72	167	5	12	6
Co	59	45	41	63	37	63	61	49	6
Ni	150	160	n.d.	141	92	21	67	2	11
Cu	454	279	34	33	35	14	205	40	85
Zn	58	91	202	74	104	98	16	186	22
Ga	17	12	7	18	13	7	n.d.	9	n.d.
La	13.2	45	98.3	13.8	69.8	47.4	91.3	113	105
Ce	33.6	93.4	213	37.6	141	102	184	248	224
Nd	23.7	46.8	118	27.8	72.1	54.6	89.7	134	118
Sm	4.57	8.53	19.6	4.84	11.9	9.32	15.2	21.5	19.8
Eu	1.45	2.73	5.88	1.56	3.76	2.93	5.01	6.45	6.14
Tb	0.44	0.92	1.75	0.53	1.21	1	1.74	1.94	1.97
Yb	0.65	1	1.29	0.56	1.43	0.9	2.18	1.25	2.5
Lu	0.08	0.16	0.18	0.12	0.2	0.17	0.32	0.19	0.28

n.d. - not detected

element compositions are reflected in the mineralogy described in the Appendix B. The third group of samples consisting of olivine, calcite and microcrystalline phlogopite, is here termed ol–phl–carbonatites. Disequilibrium textures between the mineral phases were observed in thin sections of the ol–phl–carbonatites, in which olivines are corroded and surrounded by phlogopite and calcite. Thus, the ol–phl–carbonatites are considered to be peridotites or dunites altered by fluid infiltration with growth of new phlogopite and carbonate.

The trace element data are presented in Fig. 2-2, and they display distinctive patterns for the three groups. The carbonatites have high Ba, Sr and REE contents, similar to other carbonatites worldwide (Nelson et al., 1988; Woolley et al., 1991), variable concentrations of the high field strength elements (HFSE), and relatively low Cr, Ni, Ti, Rb and K contents. The pyroxenites have flatter mantle-normalised patterns with negative anomalies at K, Rb and P. The ol–phl–carbonatites exhibit features intermediate between those of the carbonatites and pyroxenites, but without the negative K and Rb anomalies that are present in both the carbonatites and pyroxenites. Mineral analyses indicate that apatite has the highest REE abundances (Nd >400 ppm, Table 2-2). However, the observed variation in phosphorus in the carbonatites, without much change in REE (Fig. 2-2), suggests that apatite does not control the whole-rock REE abundances.

Several trace elements, such as K, Rb and the HFSE vary much more widely in the carbonatites, than in the pyroxenites and the ol–phl–carbonatites (Fig. 2-2). The mineral assemblage in the carbonatites is predominantly carbonate, with variable amounts of silicate minerals (olivine and phlogopite) and apatite. The ratio $(SiO_2 + Al_2O_3*2)/CaO$ (silica is substituted by aluminium in some mineral phases, such as phlogopite) can be used as a measure of the proportions of silicate and carbonate

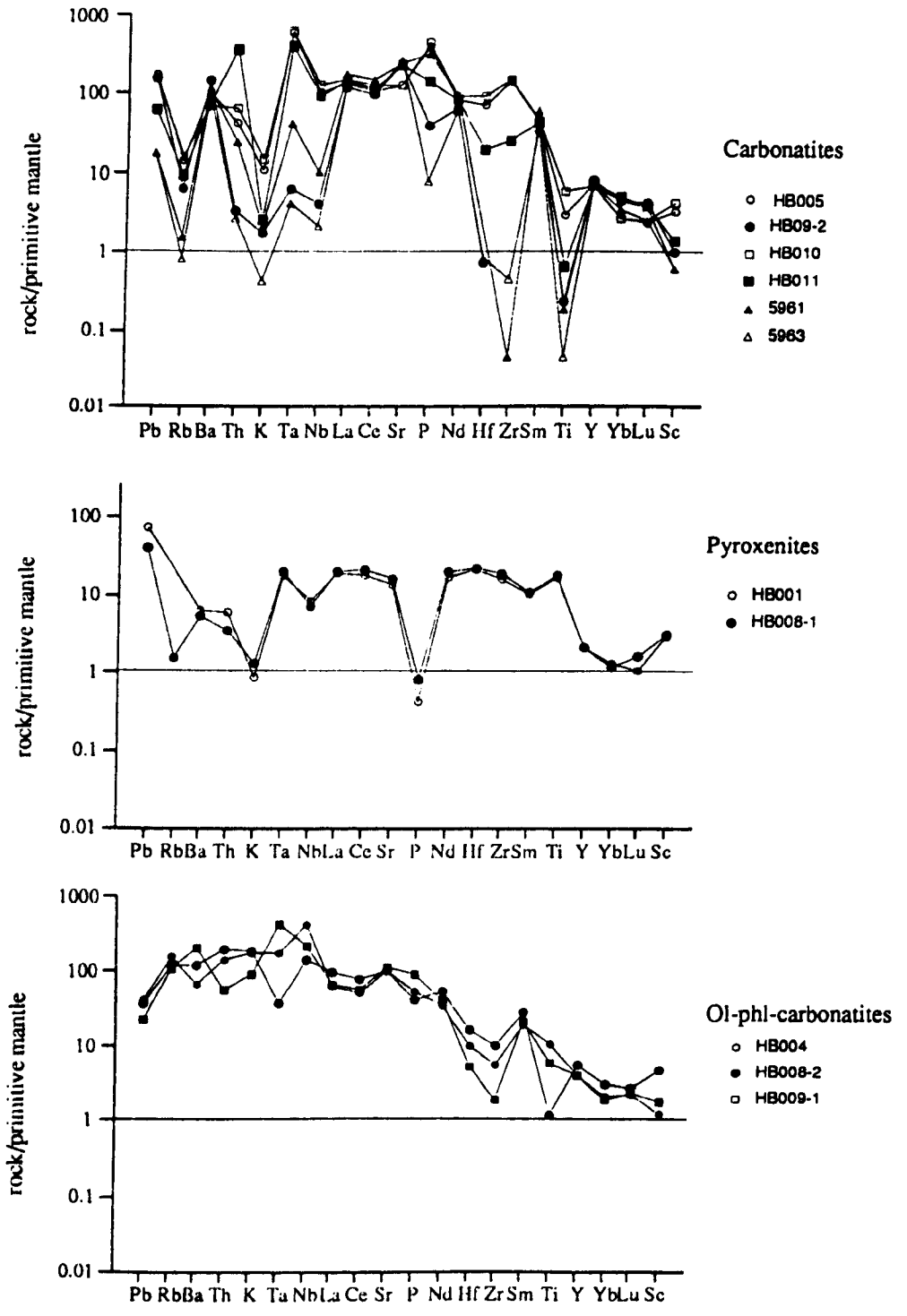

Fig. 2-2 Minor and trace element data for samples from the Jacupiranga samples illustrated on primitive-mantle normalised diagrams. Two samples are from Nelson et al. (1988), and the others are from this study. Three groups are distinguished on the basis of their major element compositions; (i) carbonatites, which have negative Rb, K and Ti anomalies; (ii) pyroxenites, which have generally flat patterns with slight negative K and P anomalies; and (iii) ol–phl–carbonatites, which have intermediate characteristics without the negative K, Rb and P anomalies.

components in the carbonatites. Thus, the relationship between (SiO_2 + Al_2O_3*2)/CaO and minor and trace elements should reflect the distribution of these elements between the silicates and the carbonates. Fig. 2-3 shows that (SiO_2 + Al_2O_3*2)/CaO ratios correlate with selected trace elements in the carbonatites; for example, there are positive correlations with K, Sc, Zr, Ta and Ti, and negative correlations with Sr (and Ba, not shown).

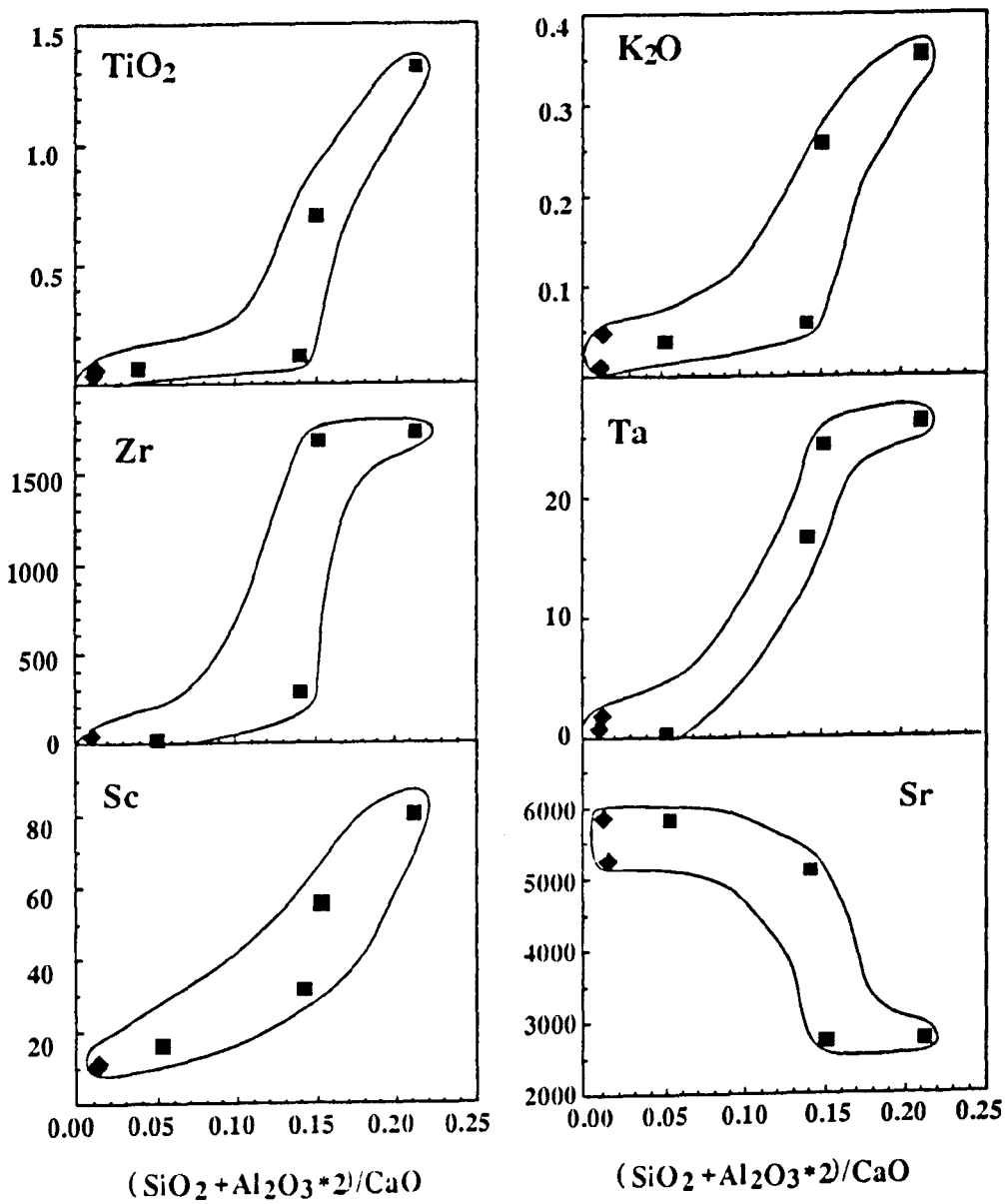

Fig. 2-3 Diagrams illustrating the correlations between (SiO_2 + Al_2O_3*2)/CaO and selected minor and trace elements in the carbonatites. The squares are data from this study and diamonds are samples from Nelson et al. (1988). See text for discussion.

2-3.2 Sr and Nd isotopes

Sr and Nd isotope data are presented in Table 2-2 and illustrated in Fig. 2-4. Present-day Sr isotope ratios range from 0.70467–0.70551, similar to those published previously by Nelson et al. (1988) and Roden et al. (1985). There is a broad correlation between Sr isotopes and Rb/Sr within different sample groups in that, for example, the ol–phl–carbonatites have slightly higher $^{87}Sr/^{86}Sr$ (0.70538–0.70551), consistent with their higher Rb/Sr ratios ($^{87}Rb/^{86}Sr$ = 0.13–0.08). However, in general, the measured Sr isotope and Rb/Sr ratios scatter on a $^{87}Sr/^{86}Sr$ vs $^{87}Rb/^{86}Sr$ diagram (not shown) and no age information can be reasonably inferred.

Initial $^{87}Sr/^{86}Sr$ ratios have been calculated at 130 Ma, and they vary from 0.70466–0.70540. Several explanations are possible for the range in initial Sr isotope ratios, including post emplacement alteration of Rb/Sr and/or $^{87}Sr/^{86}Sr$. The replacement of phlogopites by chlorites in HB005 might be due to post emplacement fluid infiltration. Calcites have high Sr and little Rb, and there is no evidence that they have been altered by hydrothermal fluid. Thus, the Sr isotope ratios of the calcites may provide the best estimate of initial $^{87}Sr/^{86}Sr$, and in general they are indistinguishable from the initial $^{87}Sr/^{86}Sr$ ratios of their whole rocks.

The range of initial $^{87}Sr/^{86}Sr$ in the carbonatites and ol–phl–carbonatites is from 0.70489 to 0.70540, whereas the Sr isotope ratios in the pyroxenites are significantly lower (0.70466 and 0.70467, Fig. 2-4 and Table 2-2). Because the pyroxenites have low Rb/Sr and present day $^{87}Sr/^{86}Sr$, this difference cannot be attributed to inadequate age corrections. Moreover, HB008–1 and HB008–2, which are splits from one banded hand specimen, have different mineral compositions and initial Sr isotope compositions (0.70466 and 0.70527, respectively). Thus, a more likely explanation is that the Jacupiranga complex is isotopically heterogeneous. On the basis of field observations Gaspar and Wyllie (1983) pointed out that the Jacupiranga

complex underwent multiple intrusion, and it is certainly possible that different intrusions had different initial Sr isotope ratios. Relative to other carbonatites worldwide, those from Jacupiranga have higher initial $^{87}Sr/^{86}Sr$ ratios than those from most central intrusive carbonatites (~0.703), but similar $^{87}Sr/^{86}Sr$ to the Walloway vein carbonatite from Australia (Nelson et al., 1988). Thus, the Jacupiranga rocks plot in the high $^{87}Sr/^{86}Sr$ portion of the ε_{Nd}-ε_{Sr} field for carbonatites from different continental settings (Fig. 2-4).

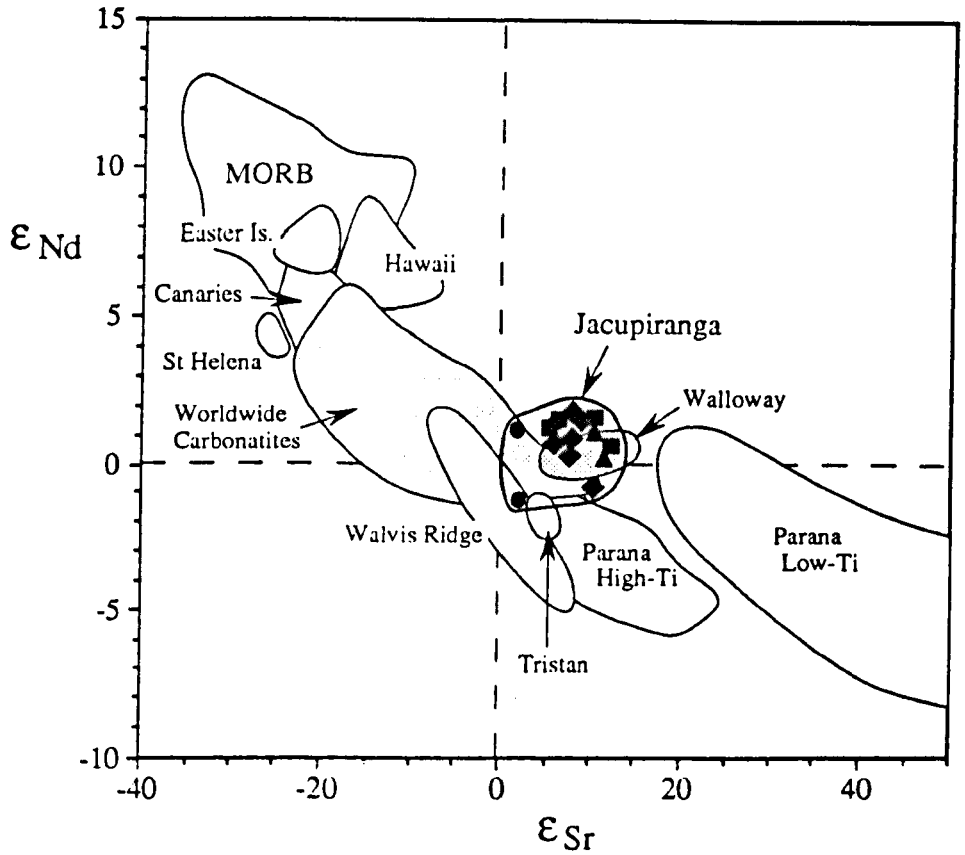

Fig. 2-4 ε_{Nd} vs ε_{Sr} diagram. The Jacupiranga complex rocks plot in the high ε_{Sr} portion of the carbonatite field (Nelson et al., 1988; Bell and Blenkinsop, 1989), and they have initial Sr and Nd isotope ratios similar to those of the Walvis Ridge and Tristan da Cunha basalts. The filled circles are pyroxenites, squares are carbonatites, and triangles are ol-phl-carbonatites from this study. The diamonds are the Jacupiranga carbonatite data from Roden et al. (1985) and Nelson et al. (1988). The data for oceanic basalts are from Ito et al. (1987), Richardson et al. (1982), Zindler and Hart (1986) and references therein; and the data from the Parana basalts are from Hawkesworth et al. (1986) and Peate et al. (1992 and references therein).

TABLE 2-2

Sr and Nd isotope ratios in mineral and whole rock samples

Sample	Rb	Sr	$^{87}Sr/^{86}Sr$	Sm	Nd	$^{143}Nd/^{144}Nd$	$^{87}Sr/^{86}Sr_i$	ε_{Sr_t}	$^{143}Nd/^{144}Nd_i$	ε_{Nd_t}
HB001	0.082	282	0.70467	3.992	19.72	0.512638	0.70466	1.7	0.51253	1.2
HB001 py				4.998	22.89	0.512585			0.51247	0.0
HB004	100	2172	0.70538	8.648	45.11		0.70513	8.3		
HB004 cc			0.70513							
HB005	9	2749	0.70498	20.84	116.2	0.512636	0.70497	6	0.51254	1.4
HB005 cc			0.70494	12.86	75.41					
HB005 apt	0.037	3447	0.70493	72.24	403.3					
HB008-1	1	332	0.70469	5.13	26.49	0.512509	0.70467	1.9	0.51241	-1.2
HB008 py	152	394		5.32	24.62	0.512492			0.51238	-4.2
HB008-2	75	2123	0.70546	12.28	67.2	0.512620	0.70527	10.3	0.51253	1.1
HB009-1	69	2404	0.70551		50.69	0.512584	0.70535	11.5	0.51248	0.2
HB09-2	4	5448	0.70540	15.53	82.75	0.512602	0.7054	12.1	0.51251	0.7
HB009 cc			0.70534	15.33						
HB010	10	2772	0.70494	23.03	129.6	0.512626	0.70492	5.4	0.51253	1.2
HB010 cc			0.70489	13.98	87.72		0.70489	4.9		
HB010 apt	0.016	3473		75.41	427.3					
HB010 phl				0.66	3.61					
HB011	6	5130	0.70521	20.15	108.8	0.512642	0.70520	9.4	0.51255	1.5
HB011 cc			0.70521				0.70521	9.5		
HB011 apt	0.041	3832		78.96	431.4					
HB011 phl				1.52	7.06					

Sm and Nd analyses confirm that the $^{147}Sm/^{144}Nd$ ratios are systematically different in the three sample groups (pyroxenites 0.122–0.117, ol–phl–carbonatites 0.116–0.111 and carbonatites 0.112–0.107), consistent with the REE data in Fig. 2-2. Present-day Nd isotope compositions in all three groups are very similar ($^{143}Nd/^{144}Nd$ = 0.51264–0.51251). Unlike Sr, the initial Nd isotope ratios show no systematic differences between pyroxenites, carbonatites and ol–phl–carbonatites. The ε_{Nd_t} values range from -1.2 to +1.5, which are very close to the bulk Earth composition, and the two Nd analyses on silicate rocks bracket those from the carbonatites (Fig. 2-4).

2-3.3 Pb, U and Th data

The measured Pb, U and Th contents for the whole rock and mineral samples are also listed in Table 2-3. Whole rock Pb contents range from 2.3–9.0 ppm, except for the pyroxenite HB008–1 which has 0.29 ppm Pb. However, another pyroxenite HB001 has 6.4 ppm Pb, which is higher than most carbonatites. There are no systematic differences between the three groups. However, in general, the whole rocks have higher Pb contents than the separated major rock forming minerals, such as calcite, apatite, phlogopite and magnetite. This suggests that there is another phase containing significant quantities of Pb. Sulphide is a candidate, and it was observed in HB009–2 which has highest Pb content (9 ppm).

U abundances in the pyroxenites are much lower than those in the carbonatites (except for HB009–2) and the ol–phl–carbonatites. However, like Pb, the U concentrations in calcite and apatite are lower than those in their whole rocks. The implication is that much of the U is also carried by accessory minerals. Pyrochlore and baddeleyite have been reported from the Jacupiranga carbonatite complex (Melcher, 1966; Hussak, 1892) and they may control the U distribution.

TABLE 2-3

Pb isotope ratios in bulk rock samples and mineral separates

Sample	Pb	U	Th	μ	Th/U	$^{206}Pb/^{204}Pb$	$^{207}Pb/^{204}Pb$	$^{208}Pb/^{204}Pb$	$(^{206}Pb/^{204}Pb)_i$	$(^{207}Pb/^{204}Pb)_i$	$(^{208}Pb/^{204}Pb)_i$
HB001	6.407	0.055	0.446	0.53	8.17	17.685	15.447	38.068	17.674	15.446	38.040
HB001 py						17.705	15.442	38.020			
HB004	4.506	0.703	12.24	9.77	17.4	17.421	15.404	38.899	17.222	15.394	37.802
HB004 cc						17.230	15.421	37.752			
HB005	3.520	2.178	3.489	38.86	1.60	18.256	15.446	38.170	17.464	15.407	37.769
HB005 cc	1.244	0.102	0.338	5.07	3.31	17.358	15.405	37.849	17.255	15.400	37.741
HB005 apt	2.247	0.473	17.16	13.62	36.27	17.644	15.443	41.003	17.367	15.429	37.816
HB008-1	0.293	0.018	0.226	3.77	12.79	17.702	15.447	38.241	17.626	15.443	37.931
HB008-2	3.492	2.217	17.59	40.61	7.93	17.963	15.421	39.854	17.135	15.381	37.775
HB009-1	3.613	0.385	5.438	6.59	14.12	17.194	15.379	38.187	17.060	15.372	37.586
HB09-2	9.021	0.007	0.088	0.05	12.46	17.049	15.380	37.610	17.048	15.380	37.606
HB009 cc	4.702	0.0002		0.003		17.049	15.388	37.636	17 049	15.387	
HB010	2.327	1.138	5.924	30.83	5.21	17.954	15.430	38.791	17.326	15.399	37.755
HB010 cc	1.881	0.021		0.68		17.294	15.431	37.859	17.280	15.430	
HB010 apt	2.128	0.439		12.74							
HB010 phl	0.506	0.110		13.37		17.402	15.427	38.543	17.129	15.414	
HB011	6.315	3.46	34.4	35.39	9.94	18.191	15.448	40.320	17.470	15.413	38.049
HB011 cc	5.104	0.003		0.041		17.231	15.415	37.766	17 230	15.419	
HB011 apt	3.036	0.368		7.77		17.435	15.431	40.558	17.277	15.423	
HB011 phl	6.112	5.120		55.08		18.417	15.432	41.456	17.295	15.377	

Th concentrations are low (<1 ppm) in the pyroxenites, but they are rather higher in the carbonatites (3–26.8 ppm), except for HB009–2, which has <0.1 ppm Th. Apatite data from HB005 show that it has much higher Th contents and $^{208}Pb/^{206}Pb$ than its whole rock. The samples which have low P_2O_5 also have low Th, such as HB001, HB008–1 and HB009–1, suggesting that apatite is an important Th carrier. However, the samples which have high Th do not always have high P_2O_5. The lack of a positive correlation between P_2O_5 and Th shows that some other mineral phase(s) also contains significant amounts of Th.

Measured μ ($^{238}U/^{204}Pb$) values in six of the whole rock samples range from 10 to 41 (Table 2-2), although the pyroxenites (HB001 and HB008–1) and one carbonatite (HB009–2) have low μ (0.5–3). Among the analysed mineral separates, calcite has the lowest μ (0.68–5.7), and those for apatite (7.8–14) are lower than μ in the whole rocks. This may also reflect the presence of other mineral phases with high μ in carbonatites. Most Th/U ratios are >5, except for HB005 which has relatively low Th and a Th/U ratio of 1.

The Pb isotope results for the Jacupiranga carbonatites are presented in Table 2-3 and Fig. 2-5. Present-day $^{206}Pb/^{204}Pb$ ratios in the whole rocks range from 17.05 to 18.26, $^{207}Pb/^{204}Pb$ = 15.38–15.45, and $^{208}Pb/^{204}Pb$ = 37.61–40.32. The measured Pb isotopes from the pyroxenites have similar $^{206}Pb/^{204}Pb$ to those in the carbonatites, but slightly elevated $^{207}Pb/^{204}Pb$. Initial Pb isotope ratios were calculated at 130 Ma, and, with the exception of HB009, the initial Pb ratios of the calcites are lower than those of their whole rocks (Table 2-3). This may be due to relatively recent mobilisation of U. However, the phlogopites from HB010 and HB011 also appear to have different initial Pb isotope ratios with lower $^{206}Pb/^{204}Pb$ and/or $^{207}Pb/^{204}Pb$ than the calcites (Table 2-3). More measurements are needed to confirm the scale of such heterogeneities, but because most of the calcites analysed have

low U/Pb ratios, their initial ratios may be more reliable than those from the whole rocks. Nonetheless, the initial Pb isotope ratios are consistent with three groups of samples, in that the pyroxenites have the highest ratios with $^{206}Pb/^{204}Pb$ = 17.67–17.63, the ol–phl–carbonatites tend to have the lowest initial ratios and the carbonatites have intermediate values, except for HB009–2 which is similar to HB009–1.

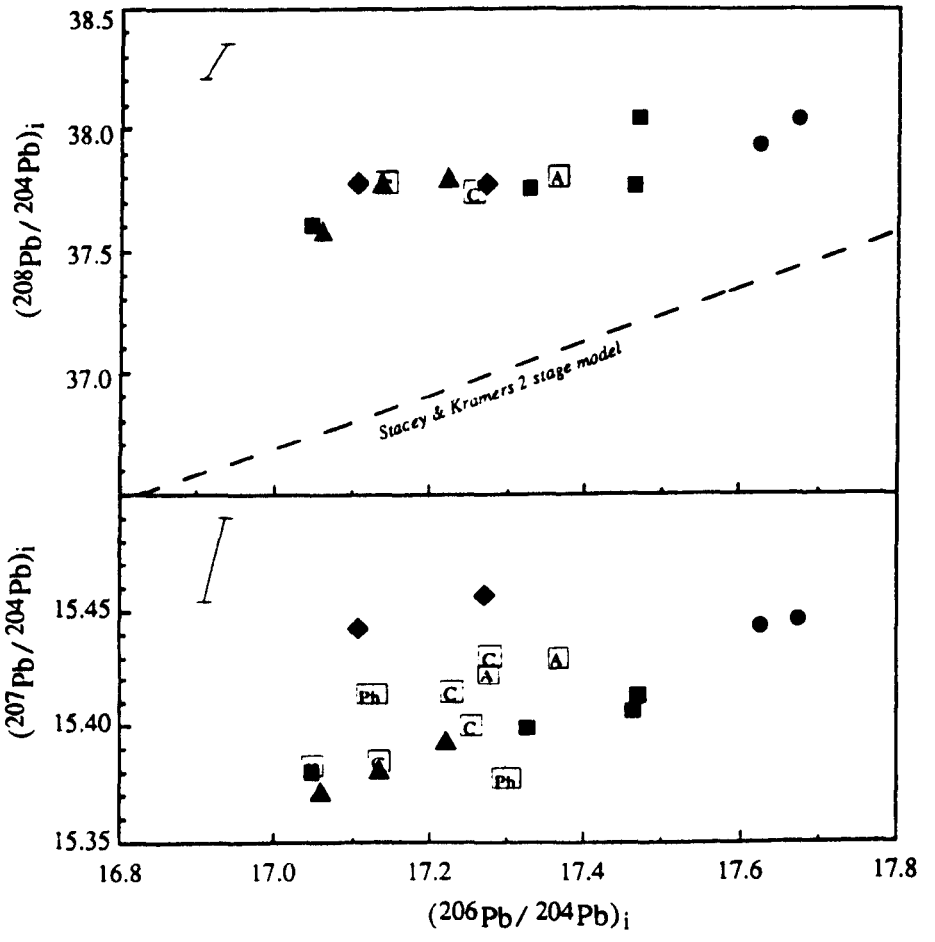

Fig. 2-5a Initial Pb isotope ratios for the whole rocks and mineral separates from the Jacupiranga carbonatite complex. The symbols are as in Fig. 2-4, and A – apatite, C – calcite, Ph – phlogopite. The bars illustrate the degree of fractionation on repeated measurements of NBS 981. The $^{207}Pb/^{204}Pb$ ratios reported by Nelson et al. (1988) are slightly higher than our data at similar $^{208}Pb/^{204}Pb$ and $^{206}Pb/^{204}Pb$, but these cannot be simply explained by the small differences in the measured values of NBS 981.

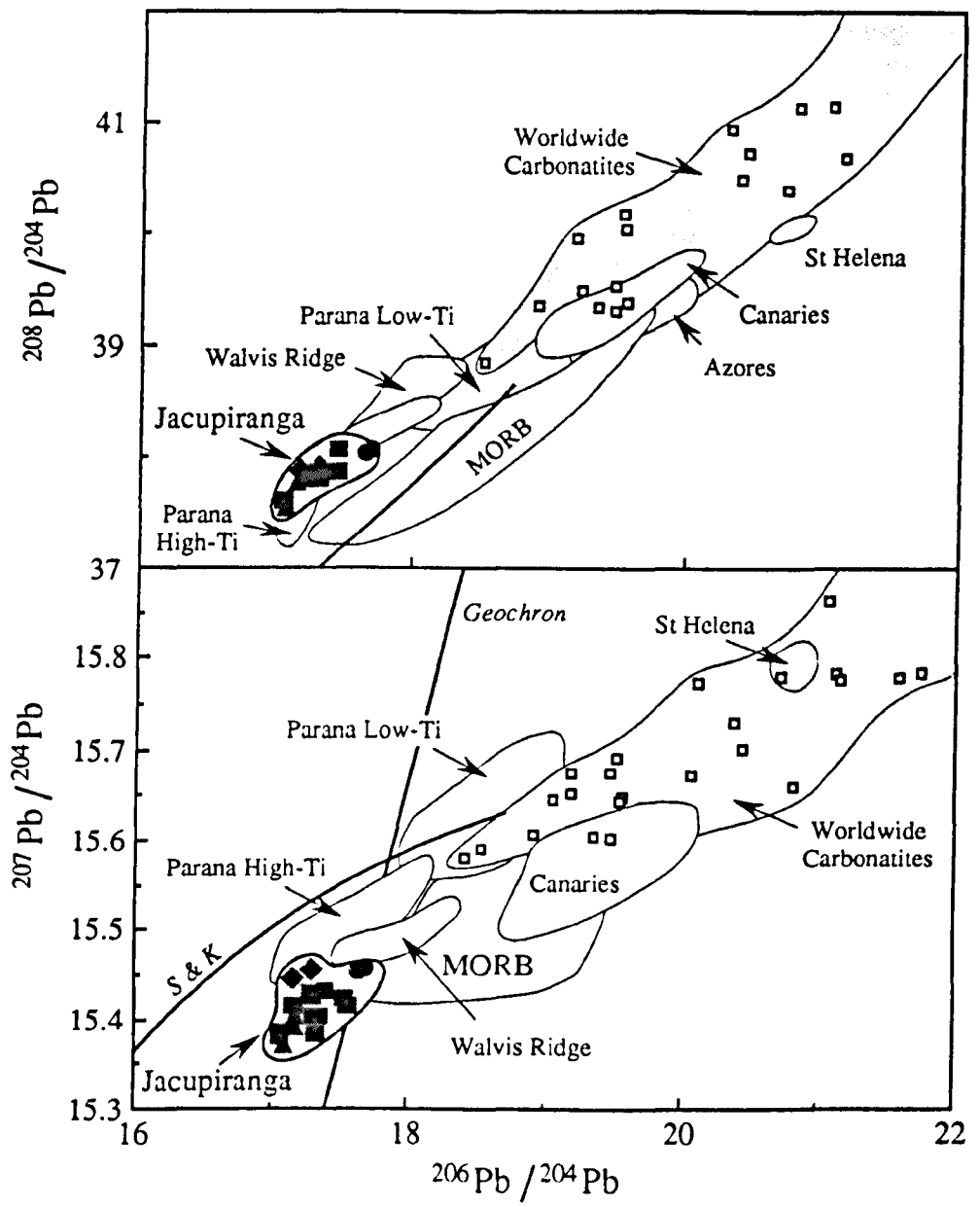

Fig. 2-5b The initial Pb isotope ratios of the Jacupiranga rocks compared with those from selected oceanic basalts, the Stacey and Kramers (1975) 2 stage evolution curve (S and K), and the Geochron. Small open squares are present day ratios for worldwide carbonatites from Nelson et al. (1988) and Andersen and Taylor (1988), although some of the more radiogenic Pb isotope ratios fall outside the range of this diagram. By contrast, the present day Pb isotope ratios for Jacupiranga (not shown) are relatively restricted (e.g. $^{206}Pb/^{204}Pb$ = 17.05–18.26, Table 2-3). Other symbols and data sources as for Figure 4.

These initial ratios define a trend on a $^{207}Pb/^{204}Pb$–$^{206}Pb/^{204}Pb$ diagram (Fig. 2-5a) with the pyroxenites at the upper end. All the initial $^{208}Pb/^{204}Pb$ and $^{206}Pb/^{204}Pb$ ratios plot above the 2 Stage evolution line of Stacey and Kramers (1975) (Fig. 2-5a) which, in a single stage model, requires time-integrated Th/U ratio >4. Relative to other carbonatites (Nelson et al., 1988) the Jacupiranga carbonatite has unradiogenic Pb, but it has similar $^{206}Pb/^{204}Pb$ and $^{208}Pb/^{204}Pb$ to the Parana high-Ti and the Walvis Ridge basalts (Fig. 2-5b).

2-4. Petrogenesis

Most carbonatites are spatially and temporally associated with mafic or alkaline complexes, and thus the relationship between the silicate and carbonatite rocks is important in any explanation of the petrogenesis of carbonatites. The initial isotope ratios in the Jacupiranga carbonatite complex are similar to those of basalts from the Walvis Ridge, Tristan da Cunha and the Parana. Helium data on a pyroxene from the pyroxenite exhibit a mantle signature (Basu et al., 1993), and it is inferred that the Jacupiranga complex has a mantle origin as invoked for other carbonatites worldwide (Basu and Tatsumoto, 1980; Bell et al., 1982; Nelson et al., 1988). However, in detail the new isotope data presented here demonstrate significant isotope variations within the Jacupiranga complex. Although the initial $^{143}Nd/^{144}Nd$ ratios in the pyroxenites and carbonatites are broadly similar, their initial Sr and Pb isotope ratios are systematically different (Fig. 2-6). The pyroxenites have lower initial Sr (0.7047) and higher initial Pb isotope ratios ($^{206}Pb/^{204}Pb$ ~17.6), whereas in the carbonatites, initial Sr and Pb isotope ratios vary from 0.7049–0.7054 and 17.05–17.46. Overall, there is negative correlation between initial $^{206}Pb/^{204}Pb$ and $^{87}Sr/^{86}Sr$ both in the pyroxenites and carbonatites, and within the carbonatite group (Fig. 2-6). Initial Pb isotope ratios also exhibit a linear trend between the carbonatites and pyroxenites (Fig. 2-5a). These

isotope heterogeneities in the Jacupiranga carbonatite complex may provide useful constraints for models of carbonatite generation. However, the first step is to evaluate the effects of crustal contamination.

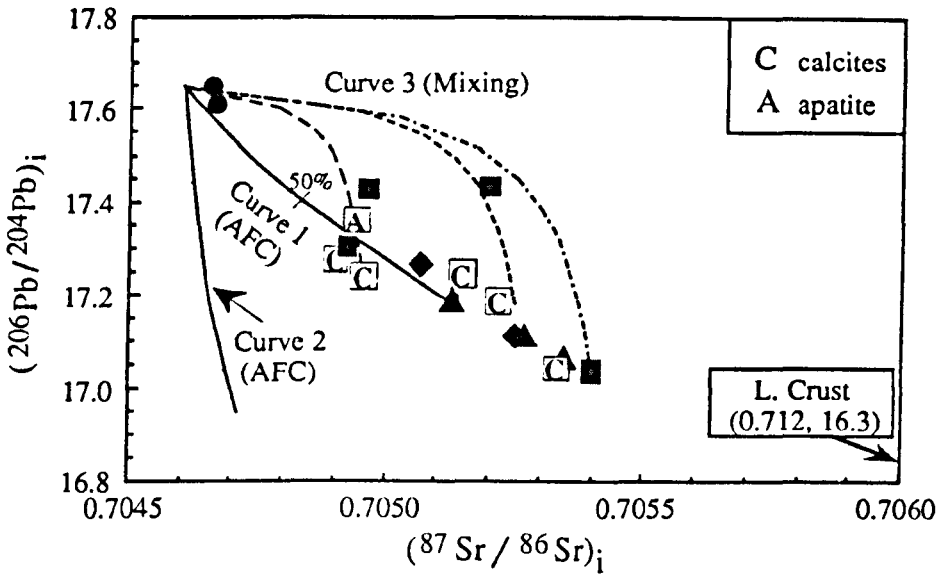

Fig. 2-6a $(^{206}Pb/^{204}Pb)_i$ vs $(^{87}Sr/^{86}Sr)_i$. Curve 1 illustrates an AFC model (r = 20%) for a primary silicate magma with isotope ratios similar to the pyroxenites, contaminated with lower crustal material. The Sr and Pb contents are 900 and 5 ppm in the primary silicate magma and 200 and 6 ppm in the lower crustal component respectively. The bulk partition coefficients used were 0.6 for Sr and 0.9 for Pb. Curve 2 is an AFC model for a primary carbonatite melt with Sr and Pb isotope ratios similar to those of the pyroxenite, but with 3000 ppm Sr, contaminated with the lower crustal component. Curve 3 lines illustrate mixing between the pyroxenite and carbonatites. The symbols are as for Fig. 2-4.

2-4.1 Crustal Contamination Processes

Crustal contamination is responsible for the isotope variations in many continental magmatic rocks (DePaolo, 1981), and it was considered by Roden et al. (1985) to explain the Sr heterogeneity in the Jacupiranga carbonatites. With more data this hypothesis can now be re-evaluated and a number of problems identified. First, because the pyroxenites have much lower Sr contents than the carbonatites, they should be more easily contaminated. Although there are no Sr and Pb isotope data for the wall-rocks, such micaschists and granodiorites which are likely to have had high

$^{87}Sr/^{86}Sr$. Yet the pyroxenites have the lowest initial $^{87}Sr/^{86}Sr$ in the complex, and they therefore appear to have been least affected by any crustal contamination processes.

Second, if the carbonatites were formed from a contaminated silicate magma by liquid immiscibility, the observed within-suite variations indicate that they cannot have been formed by segregation from a single batch of contaminated magma. Moreover, crustal rocks which have high Rb/Sr also tend to have elevated U/Pb, as seen in most estimates of the bulk or upper continental crust (e.g. Taylor and McLennan, 1985). Thus, with time, they have both high $^{87}Sr/^{86}Sr$ and $^{206}Pb/^{204}Pb$, and so such material cannot have been responsible for the observed negative Pb-Sr correlation in the pyroxenites and carbonatites.

Alternatively, crustal contamination might have involved a component from the lower continental crust, since that is regarded as a major reservoir of unradiogenic Pb. Such unradiogenic Pb may be due to U depletion, together with other LIL elements, during granulite facies metamorphism (Moorbath et al., 1969; Gray and Oversby, 1972; Weaver and Tarney, 1981; Cohen et al., 1991; Rudnick and Presper, 1990), or to primary low U/Pb ratios in areas of significant underplating with gabbroic cumulates (van Calsteren et al 1986, 1993; Huang et al., 1994). The result of both processes is lower crustal rocks with low U/Pb and low Rb/Sr and, with time, unradiogenic Pb and relatively unradiogenic Sr isotope ratios, as seen for example in the Lewisian granulites (Cohen et al., 1991). Thus, whereas the lower crust is a source of unradiogenic Pb, it is unlikely to be the source of a suitable contaminant with elevated $^{87}Sr/^{86}Sr$ and low $^{206}Pb/^{204}Pb$. Moreover, even if it is simply assumed that the Proterozoic basement had suitable isotope ratios of $^{87}Sr/^{86}Sr = 0.712$ and $^{206}Pb/^{204}Pb = 16.3$, simple calculations (Curve 1, Fig. 2-6a) indicate that an assimilation-fractional crystallisation (AFC) model (DePaolo, 1981) does not generate the

full isotope range observed in the pyroxenites and carbonatites with a realistic contamination rate (r = 20%, Fig. 2-6a). Moreover, even then the $^{143}Nd/^{144}Nd$ ratios of such old crust (0.5116 in average 2 Ga old crust) would be too low to explain the observed Nd–Pb data (Fig. 2-6b)

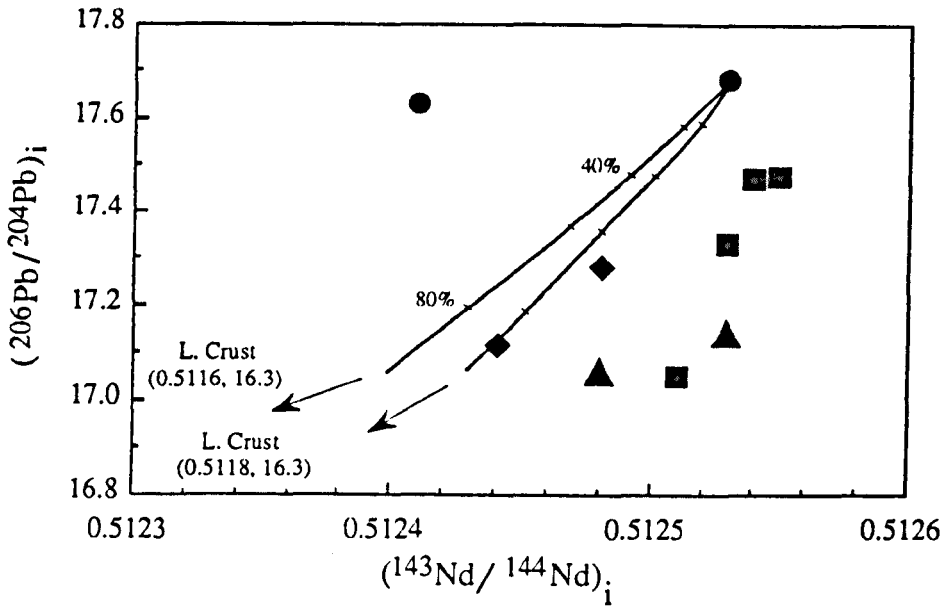

Fig. 2-6b $(^{206}Pb/^{204}Pb)$ vs $(^{143}Nd/^{144}Nd)_i$ illustrating the AFC model (r = 20%). Nd = 20 ppm in the lower crustal material, and 60 ppm in the initial silicate magma, and the Pb isotopes and abundances are as for Curve 1 in (a) above.

Third, if crustal contamination occurred after segregation of the carbonatites, for example by AFC, the high Sr/Pb ratios of the carbonatites compared with those of the pyroxenites would result in significant changes in Pb isotopes with relatively little change $^{87}Sr/^{86}Sr$. This is illustrated by Curve 2 on Figure 6a and it is discordant to the observed data array. Curve 3 further demonstrates that the variation in Sr and Pb isotopes within the carbonatites cannot be due to simple mixing between pyroxenites and a carbonatitic end-member, because the mixing line is strongly convex-upward. Two whole rock data plot on such mixing lines. This may indicate that they were formed with some mixture of a pyroxenite-like component, or it may be due to inadequate age corrections of the initial Pb isotope ratios as discussed above.

Finally, the available O and C isotope compositions of the Jacupiranga carbonatite show that they have mantle stable isotope ratios which have not been significantly affected by assimilation of crustal material (Nelson et al., 1988). The initial Sr, Nd and Pb isotope ratios of the Jacupiranga samples are also similar to those observed in the oceanic basalts of the Walvis Ridge and Tristan da Cunha, and in the Parana high-Ti basalts (Figs. 2-4 and 2-5). Thus, despite little direct information on the composition of the lower crust in this area, the more likely explanation of the isotope variation is that the carbonatites and pyroxenites have different primary Sr and Pb isotope compositions which reflect differences in their mantle source regions, rather than contamination and/or magma mixing processes within the continental crust.

2-4.2 *Liquid Immiscibility*

Experimental studies indicate that there is an immiscibility gap between carbonatite and alkali-rich (phonolite) or alkali-poor silicate melts at pressures up to 25 kb (Baker and Wyllie, 1990). However, in practice, carbonatites may only be generated by liquid immiscibility at relatively low pressures (~15 kb) (Kjarsgaad and Hamilton, 1989, and references therein), because at pressures of 25 kb the liquids are very different in composition from natural mantle melts (Baker and Wyllie, 1990). Some studies (e.g. Beccaluva et al., 1992) have demonstrated that silicate rocks in carbonatite complexes have major element compositions close to the experimental solvus. Moreover, that is consistent with the observation that carbonatites are normally associated with alkaline rocks, and that the volumes of carbonatites are small compared with those of the associated silicates. In principle, the liquid immiscibility model can be evaluated further using minor and trace elements, although the available partition coefficients are rather variable (Wendlandt and Harrison, 1979; Hamilton et al., 1989). The experiments of Wendlandt and Harrison (1979) indicate that the

carbonatites should have relatively high HREE abundances, but this is inconsistent with the commonly observed high LREE/HREE ratios (Nelson et al., 1988). Subsequently published partition coefficients for the REE are strikingly pressure dependent in that at ~1 kb the REE partition into the silicate, whereas at 5–6 kb they are preferentially partitioned into the carbonate melt (Hamilton et al., 1989).

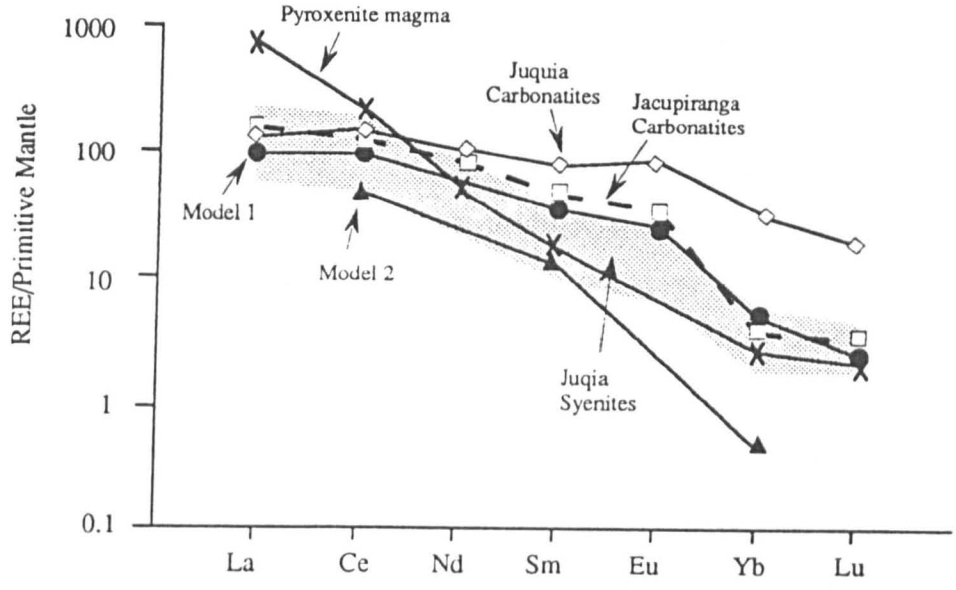

Fig. 2-7 REE mantle-normalised diagram, illustrating potential silicate parent magmas for the Jacupiranga carbonatite magmas, calculated on the basis of available experiment data for REE distribution between carbonatite and silicate melts. The pyroxenite magma (crosses) is that calculated to have been in equilibrium with the pyroxenites. Open squares represent the average of the Jacupiranga carbonatites, and open diamonds are the average of Juquia carbonatites; the shaded field is for the Juquia syenites. The REE profiles for silicate magma in equilibrium with the Jacupiranga carbonatites were calculated using the partition coefficient data from Wendlandt and Harrison (1979) (Model 2, filled triangles) and for 6 kb from Hamilton et al. (1989) (Model 1, filled circles). See text for discussion.

Using an average for the REE in the Jacupiranga carbonatite and available partition coefficient data, the REE profile in an inferred parental magma can be calculated (Fig. 2-7). Model 1 is the REE profile calculated using data from Hamilton et al. (1989), and Model 2 is that obtained using the data of Wendlandt and Harrison (1979). The LREE contents in both the

calculated parent magmas and the carbonatite melts are similar, but similar HREE abundances are only obtained using the partition coefficients of Hamilton et al. (1989), (Model 1, Fig. 2-7). Fig. 2-7 also includes data from syenite and carbonatite rocks from the Juquia complex situated ~50 km north of Jacupiranga (Fig. 2-1). This complex is approximately coeval (130–135 Ma) with that at Jacupiranga and it has similar Sr isotope ratios ($^{87}Sr/^{86}Sr$ = 0.7052 to 0.7056) (Beccaluva et al., 1992). It was argued by Beccaluva et al. (ibid.) that the Juquia carbonatites were derived by liquid immiscibility from the syenites, but this can only be reconciled with the REE data if the partition coefficients of Wendlandt and Harrison (1979) are used, rather than those of Hamilton et al. (1989). It would appear that more experimental data are required on REE partition coefficients.

The Jacupiranga pyroxenites consist largely of clinopyroxene, as seen in the similar Nd and Sm contents in separated clinopyroxenes and the bulk rock pyroxenites (Table 2-2). The REE profile of a magma in equilibrium with the pyroxenites can therefore be calculated using REE partition coefficients for clinopyroxene (Hart and Dunn, 1993) and that in equilibrium with the Jacupiranga pyroxenites has relatively high LREE and high LREE/HREE ratios (Fig. 2-7). Thus, it is different from both the calculated magmas in equilibrium with the carbonatites, and from the Jacupiranga carbonatites themselves (Fig. 2-7). Since the LREE are incompatible ($D << 1$), these differences cannot easily be attributed to fractional crystallisation processes. If the carbonatites were derived from the same magma from which the pyroxenites crystallised, but at a later stage than the pyroxenites, they should have steeper REE profiles and higher LREE contents than those observed. Although early experimental work indicated that LREE might be preferentially removed in CO_2 vapour (e.g. Wendlandt and Harrison, 1979), Paterson (1993) argued that REE variations in carbonatites from New Zealand conflict with these experimental data. One explanation might be that carbonatite crystallised earlier than the

pyroxenites but that is not consistent with the field observations (Gaspar and Wyllie, 1983). Since the Jacupiranga pyroxenites and carbonatites also have different initial Sr and Pb isotope ratios, it is more likely that they crystallised from different parental magmas.

2-4.3 Partial melting

Sr and Nd isotope differences between carbonatites and alkaline silicate rocks in some complexes have been cited as evidence that their associated silicate rocks may not be directly genetically related to the carbonatites (Nelson et al., 1988; Bell and Peterson, 1991). Nelson et al. (1988) invoked very small degrees of melting (<1%) from eclogitic sources to generate primary carbonatite melt with extreme LREE abundances. Experimental studies in mantle peridotite-CO_2–H_2O systems have revealed a P–T window (Meen et al., 1989; Falloon and Green, 1989) in which partial melting of depleted lherzolites can generate primary carbonatite melts with low alkali contents (Dalton and Wood, 1993). Our calculations show (Fig. 2-8) that the minor and trace element patterns of the Jacupiranga carbonatites can be reproduced by small degrees (0.5%) of partial melting of mantle peridotite in the presence of phlogopite (1%) and garnet (0.5%) using the partition coefficients listed in Table 2-4. The reason that so little garnet is required is that the recent experimental data (e.g. Sweeney et al., 1992) show that HREE partition coefficients for garnet/carbonate melt are 3–9 times higher than those for garnet/silicate melt (Fujimaki et al., 1984). Clearly, further studies are required to confirm this difference in HREE partition coefficients for garnet in silicate and carbonate systems, and hence to evaluate better the source mineralogy in the generation of carbonatites.

One problem with this model is that primary carbonatite melts are predicted to have high Mg# and Ca/(Ca+Mg) between 0.72–0.74 (Eggler, 1989; Dalton and Wood, 1993). Calcio-carbonatites worldwide rarely meet these criteria, but Dalton and Wood (1993) pointed out that calcio-

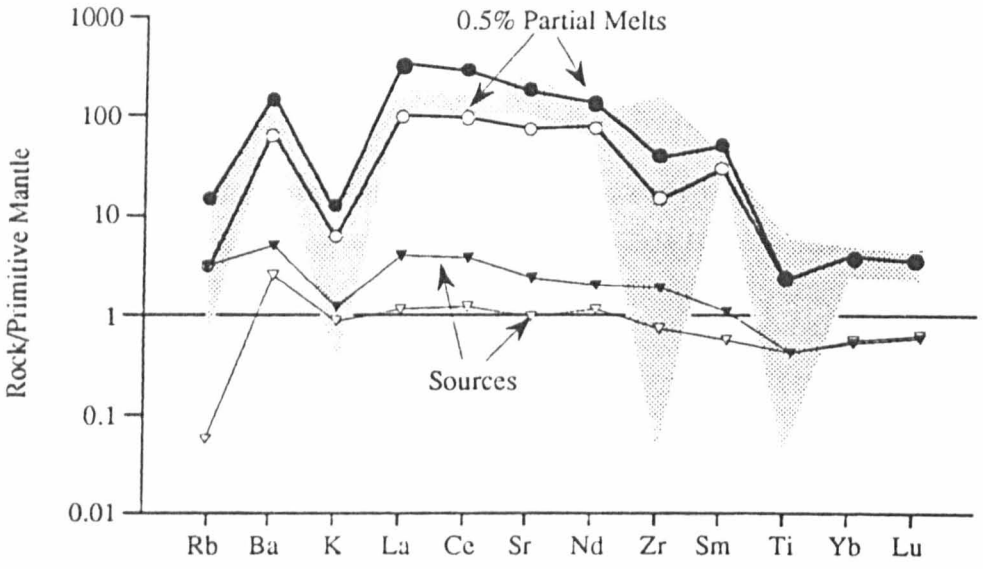

Fig. 2-8 Mantle-normalised trace element diagram, illustrating the batch melting model for the generation of the carbonatite magmas. The residual mantle is assumed to be peridotite with 1% phlogopite and 0.5% garnet, and with trace element abundances similar to the spinel peridotite xenoliths studied by McDonough (1990). Partial melting calculations were undertaken using both the average (filled symbols) and the mean (open symbols) values for the spinel peridotites. The shaded field is the data for the Jacupiranga carbonatites (Nelson et al., 1988 and this study).

TABLE 2-4

The mineral compositions and partition coefficients used in the partial melting calculations

	%	La	Ce	Nd	Sm	Yb	Lu	Zr	Ba	Ti	K	Rb
ol	0.63	0.0005	0.0005	0.0003	0.0006	0.009	0.0109	0.0005	0.0001	0.06	0.0001	0.0001
opx	0.24	0.01	0.01	0.01	0.01	0.12	0.163	0.0067	0.007	0.3	0.0001	0.0001
cpx	0.095	0.02	0.03	0.06	0.1	0.43	0.435	0.3055	0.067	0.5	0.001	0.0005
phl	0.01	0.04	0.05	0.03	0.03	0.05	0.0471	0.2806	2	0.3	20	20
gar	0.005	0.0001	0.005	0.03	0.09	12	14	1.7	0.0006	1.7	0.0001	0.0001
spinel	0.02	0.03	0.03	0.035	0.04	0.1	0.09	0.2	0.0001	0.15	0.0001	0.0001

carbonatites can be generated by reaction between primary magnesian carbonatite melts and harzburgite in the upper mantle, and several such reactions have been proposed (Brey et al., 1983; Green and Wallace, 1988). The effects of these processes on trace element patterns are not clear, but they might modify both the trace element and isotope compositions of the resultant calcio-carbonatites. However, there are no systematic differences between the minor and trace element patterns of calcio-carbonatites and dolomite-carbonatites, even though the latter may be closer to primary compositions than the former.

2-4.4 Fractional crystallisation

Some elements, including K, Ta, Nb, P, Hf, Zr and Ti, exhibit considerable variation in the Jacupiranga carbonatites, as seen in other carbonatites worldwide. The partial melting calculations outlined above indicate that these variations cannot be due to different degrees of partial melting, because the highly incompatible elements, such as Ba and La, vary less than Nb, Ti and Zr, which vary by over two orders of magnitude (Fig. 2-2). The variations in elements, such as P, Nb (Ta) and Zr (Hf), which are not concentrated in minerals like olivine, phlogopite or magnetite, may reflect the presence of accessory mineral phases (Nelson et al., 1988). Apatite, pyrochlore and baddeleyite have been observed in the Jacupiranga carbonatites (Melcher, 1966 and Hussak, 1892), and other phases which may cause significant variations in such elements include perovskite, monazite and sphene (Nelson et al., 1988). The samples with high (SiO_2 + Al_2O_3*2)/CaO have higher Ti and Zr, and lower Sr and Ba (Fig. 2-3). Since the major observed mineral phases are phlogopite, olivine, magnetite and carbonate, the ratio of (SiO_2 + Al_2O_3*2)/CaO represents the proportion of silicate and carbonate mineral phases. If it is inferred that the silicates crystallised before most of carbonates, the observed correlations between Ti, Zr, K, and Nb and (SiO_2 + Al_2O_3*2)/CaO might be explained by

accumulation of the silicates, with these elements preferentially distributed into either silicate or associated accessory mineral phases. The negative correlation between Sr (as well as Ba, not shown) and $(SiO_2 + Al_2O_3*2)/CaO$ indicates that Sr was compatible into the carbonate phases, consistent with its known geochemical characteristics.

2-5. Mantle Sources of the Jacupiranga Complex

The Jacupiranga carbonatites have ε_{Sr_t} = 0–12 and ε_{Nd_t} = -1.2–1.5 (Fig. 2-4), and their Pb isotope ratios straddle the Geochron (Fig. 2-6a, b). Relative to other carbonatites worldwide (Fig. 2-4), the Jacupiranga carbonatite complex has higher Sr and lower Nd initial isotope ratios. Thus, their source regions were less depleted than those for many carbonatites and for Sr, Nd and Pb isotopes they were similar to estimates of the bulk Earth.

The low Pb, low ε_{Nd}, and high ε_{Sr} isotope ratios of the Jacupiranga carbonatite are broadly similar to those of the Parana high-Ti basalts, and the Walvis Ridge and Tristan da Cunha oceanic basalts. Such compositions are different from MORB, and other OIB, such as Hawaii, St. Helena and the Canaries (Figs. 2-4, 2-5). Rather, they have been termed the Dupal anomaly (Hart, 1984) and while it is still debated whether the Dupal anomaly is a deep seated or a shallow phenomenon, it appears to be present in basalts from both oceanic (Walvis Ridge and Tristan da Cunha) and continental areas (Parana high-Ti) (Hawkesworth et al., 1986). The Jacupiranga complex exhibits similar isotope ratios, consistent with the presence of a regional mantle isotope signature. Moreover, the negative correlation between Sr and Pb isotope compositions in the carbonatite complex is also similar to those observed in the basalts of the Parana (high-Ti), the Walvis Ridge and Tristan da Cunha.

2-6. U/Pb and Rb/Sr Fractionation by Carbonatite Melts

The negative $^{206}Pb/^{204}Pb$–$^{87}Sr/^{86}Sr$ correlation in the Jacupiranga carbonatite complex is likely to have been inherited from their mantle source. Kwon et al. (1989) also documented a negative correlation between initial Pb and Sr ratios in a variety of carbonatites of different ages, except for a group at 2.7 Ga, and they emphasised that such trends are observed in certain oceanic basalts, such as those from the Walvis Ridge. If U is more incompatible than Pb during partial melting in the upper mantle (Sun and McDonough, 1989; McKenzie and O'Nions, 1991), both Rb/Sr and U/Pb should be low in depleted mantle, high in enriched mantle and with time there should be positive correlations between Pb and Sr isotopes. The implication is that other processes or components were involved, and a number of authors have invoked the subduction of altered ocean crust to explain such isotopic variations in mantle derived rocks (Chase, 1981; Hofmann and White, 1982; Chauvel et al., 1992). However, Kwon et al. (1989) emphasized the importance of mineralogy in the control of different fractionation patterns during mantle partial melting. Since experiments reveal that U is more incompatible than Pb in clinopyroxene (Watson et al., 1986), Kwon et al. (1989) postulated that Pb may be more incompatible than U in garnet. If so, different Rb/Sr–U/Pb arrays might be generated by partial melting mantle with variable garnet/clinopyroxene ratios.

Alternatively, mantle metasomatism may play an important role in fractionation of trace elements in the upper mantle (Harte, 1983; Menzies, 1983; Dawson, 1984; Hawkesworth et al., 1990) and it has been argued that some small degree melts have very fractionated U/Pb ratios (Hawkesworth et al., 1990; Rogers et al., 1992). Although experiments indicate that CO_2–H_2O-rich fluids are ineffective agents for transporting trace elements in the mantle (Eggler, 1987), carbonatite melts are much more effective transport agents (Green and Wallace, 1988; Jones, 1989; Meen et al., 1989; Haggerty,

1989). Several geochemical features, such as high Ca/Al and La/Yb and low Ti/Eu have also been recognised in some mantle xenoliths and attributed to carbonatite mantle metasomatism (Yaxley et al., 1991; Rudnick et al., 1993; Hauri et al., 1993).

Although the compositions of primary carbonatite melts remain controversial, a striking feature of carbonatites is that they tend to have low Rb/Sr, and variable, but often high U/Pb. Experimental studies (Dalton and Wood, 1993) have shown that primary melts generated by partial melting of depleted lherzolite can have low alkaline contents. Most of the carbonatites studied here and by Nelson et al. (1988) have Sr contents in the range of 2000–6000 ppm and Rb/Sr <0.003. Thus, the emplacement of a few per cent of carbonatite melt would change the Sr budget and significantly reduce Rb/Sr ratio in the host mantle. Mantle xenoliths which are considered to have undergone carbonatite metasomatism have low Rb/Sr, and positive correlations between Sr contents (or Rb/Sr) and (La/Yb)n or Ca/Al, which have been attributed to the introduction of carbonatitic melts (Yaxley et al., 1991; Rudnick et al., 1993).

Although a few carbonatites have low U/Pb ratios, more than half of the carbonatites analysed by Nelson et al. (1988) appear to have high U/Pb (Fig. 2-9) and, consequently, radiogenic present day Pb isotope compositions (Fig. 2-5). Some extreme present-day Pb isotope ratios, such as those from the Fen carbonatite in Norway ($^{206}Pb/^{204}Pb_p$ = 30–53, Andersen and Taylor, 1988), also indicate that U/Pb can be high in carbonatitic melts. Thus, mantle enriched or metasomatised by carbonatitic melt will have low Rb/Sr with high and variable U/Pb, and with time it will develop relatively low $^{87}Sr/^{86}Sr$ and high and variable $^{206}Pb/^{204}Pb$.

Carbonatite metasomatism may not only change the mantle compositions directly, but also affect the stability of certain mineral phases in the upper mantle and, in turn, the compositions of extracted melts. For

example, Rogers et al. (1992) argued that a CO_2-rich environment has an important role in keeping phlogopite stable during small degrees of melting in the generation of melilitites. Such small degree silicate melts have high U contents and U/Pb, but with low Rb/Sr because of the presence of residual phlogopite (Fig. 2-9). Thus, mantle metasomatism by either carbonatitic melt or a melilitite-like silicate melt will fractionate U/Pb and Rb/Sr, and with time will result in low Sr and high Pb isotope ratios, in addition to low Sm/Nd and hence low ε_{Nd}. At present, the effects of carbonatite emplacement cannot be distinguished from those of melilitite on the basis of radiogenic isotopes alone, primarily because low Rb/Sr ratios can be due to the high Sr contents of carbonatites and/or to low Rb retained in residual potassic phases.

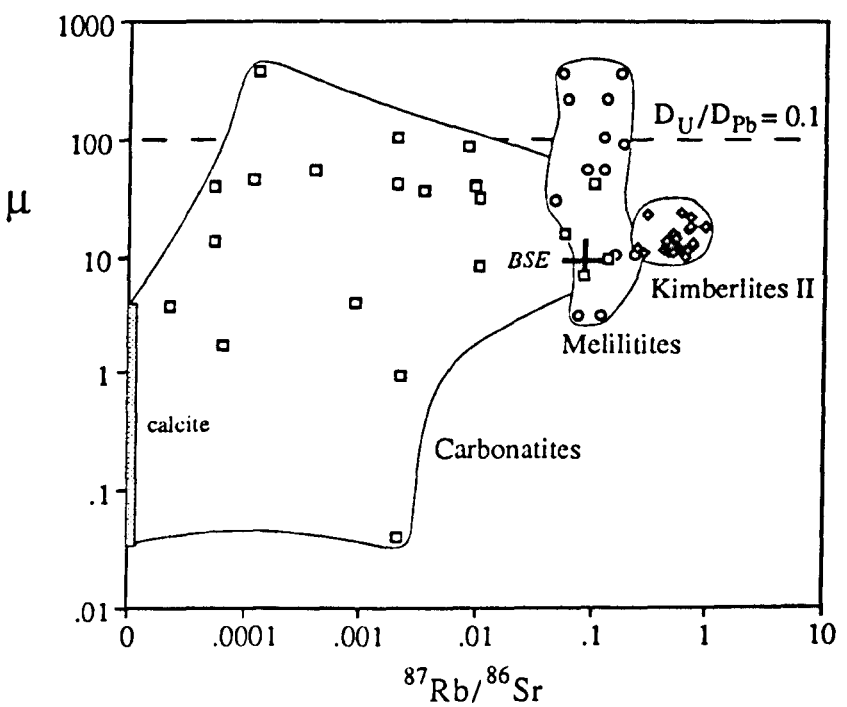

Fig. 2-9 μ ($^{238}U/^{204}Pb$) vs $^{87}Rb/^{86}Sr$ illustrating the measured ratios from carbonatites, melilitites and Group II kimberlites (Fraser and Hawkesworth, 1992; Rogers et al., 1992). Most of the carbonatites have high μ and low $^{87}Rb/^{86}Sr$. Some carbonatites with very high μ may reflect large amounts of fractional crystallisation. The D_U/D_{Pb} = 0.1 line represents the maximum μ generated by batch partial melting of primitive mantle material using the partition coefficients summarised in McKenzie and O'Nions (1991). BSE – bulk silicate Earth.

2-7. Conclusions

(1) The initial Sr, Nd and Pb isotope ratios in the Jacupiranga carbonatite complex are similar to those of basalts from the Parana (high-Ti), the Walvis Ridge and Tristan da Cunha. They appear to have been derived from similar mantle source regions, and not to have been affected significantly by crustal contamination processes. They also exhibit a broad negative correlation between Pb and Sr isotopes similar to that in certain oceanic basalts.

(2) The initial Sr and Pb isotope ratios in the Jacupiranga carbonatites are different from those in the associated pyroxenites. These differences are considered to be primary features related to their mantle source regions.

(3) Model calculations indicate that liquids in equilibrium with the carbonatites and the pyroxenites had different REE profiles, and that these differences cannot readily be attributed to fractional crystallisation or segregation of immiscible liquids. Thus, both the isotope and trace element data indicate that the Jacupiranga carbonatites were not derived from the same magma as the pyroxenites. Instead, it is argued that the Jacupiranga complex was generated in multiple episodes of small degree melting.

(4) Both experimental and mantle xenolith studies have demonstrated that carbonatite melts are important agents of mantle metasomatism, and some distinctive geochemical features have been recognised (Yaxley et al., 1991; Meen et al., 1989; Rudnick et al., 1993; Haggerty, 1989). Carbonatites are characterised by very high Sr contents, high and variable U/Pb, but low Rb/Sr. Thus, infiltration and/or metasomatism by carbonatite melts may significantly reduce Rb/Sr and increase U/Pb in the upper mantle. This is consistent with the low Rb/Sr and elevated Sr contents observed in the mantle xenoliths modified by carbonatite melts. With time this will result

in negative correlations between Sr and Pb isotopes, and thus carbonatite metasomatism is one process which may have been responsible for the negative fractionation of U/Pb and Rb/Sr inferred for the source of certain oceanic basalts.

Chapter Three

The evolution of the lithosphere in southern Africa: A perspective on the basic granulite xenoliths from kimberlites in South Africa

3-1. Introduction

It is widely believed that the lower continental crust is composed of granulite facies metamorphic rocks, and there have been a number of studies of both high grade surface metamorphic terrains and lower crustal xenoliths entrained in volcanic rocks. Although xenoliths do not record their original spatial relationships, they are valuable both as a window on the lower crust in areas where high grade rocks are not exposed on the surface (Rogers, 1979; Leeman et al., 1985), and because they suggest that the lower crust may actually have a bulk composition different from that inferred from surface terrains (Rogers, 1979; Taylor and McLennan, 1985; Rudnick and Goldstein, 1990; Rudnick, 1992a). The lower crust may be regarded in a number of ways: first, as a reservoir of material residual after partial melting and fractional crystallisation associated with the formation of the upper crust (Taylor and McLennan, 1985); second, as a site of magmatic underplating that is a significant process in the generation of new crust (Rogers and Hawkesworth, 1982; Rudnick et al., 1986; Downes et al., 1990 Kempton et al., 1990; Loock et al., 1990); and third, as a reservoir of unradiogenic Pb isotope compositions to complement the more radiogenic Pb isotope ratios of the upper continental crust (Moorbath et al., 1969; Gray and Oversby 1972; Weaver and Tarney, 1981). Thus, knowledge of the composition, genesis and age of the lower crust is important to models for

the generation and evolution of the bulk continental crust, and the relationship between the crust and mantle.

In southern Africa crustal xenoliths have had an important role in both mapping out the margins of the Archaean craton, and in the development of models for crust generation processes in the Archaean and the Proterozoic. Previous studies established that mafic granulites are extremely rare in kimberlite pipes on the Kaapvaal craton, but that they are a feature of the surrounding Proterozoic mobile belts, even though mafic rocks are only occasionally exposed at the surface. The granulite xenoliths from Northern Lesotho preserve temperatures and pressures of 550–1000° C and 4.5–20 kb (Griffin et al., 1979, van Calsteren et al., 1986, and references therein), and a whole rock Sm-Nd errorchron corresponding to an age of 1.4 ±0.1 Ga (Rogers and Hawkesworth, 1982). This chapter presents new major, trace element, and isotope data on 21 granulite xenoliths, mainly from Markt, in the central Cape province, South Africa, and new Pb isotope data for the granulite xenoliths from northern Lesotho. The project was designed to evaluate the characteristics and genesis of the lower crust in southern Africa near the boundary between the Archaean craton and Proterozoic Namaqua-Natal mobile Belt, and the links between crust generation and the stabilisation of lithospheric mantle.

3-2. Background Geology and Samples Analysed

The Kaapvaal and Zimbabwe cratons in southern Africa consist of Archaean granite-greenstone terrains with ages between 3.6 Ga and 2.6 Ga (De Wit et al., 1992 and references therein). These cratons are surrounded by middle Proterozoic mobile belts, such as the Namaqua-Natal Belt, which contain a considerable amount of new crustal material (Barton and Burger, 1981; Rogers and Hawkesworth, 1982). In contrast, the adjacent Pan African terrains in Namibia have been shown to have formed primarily by

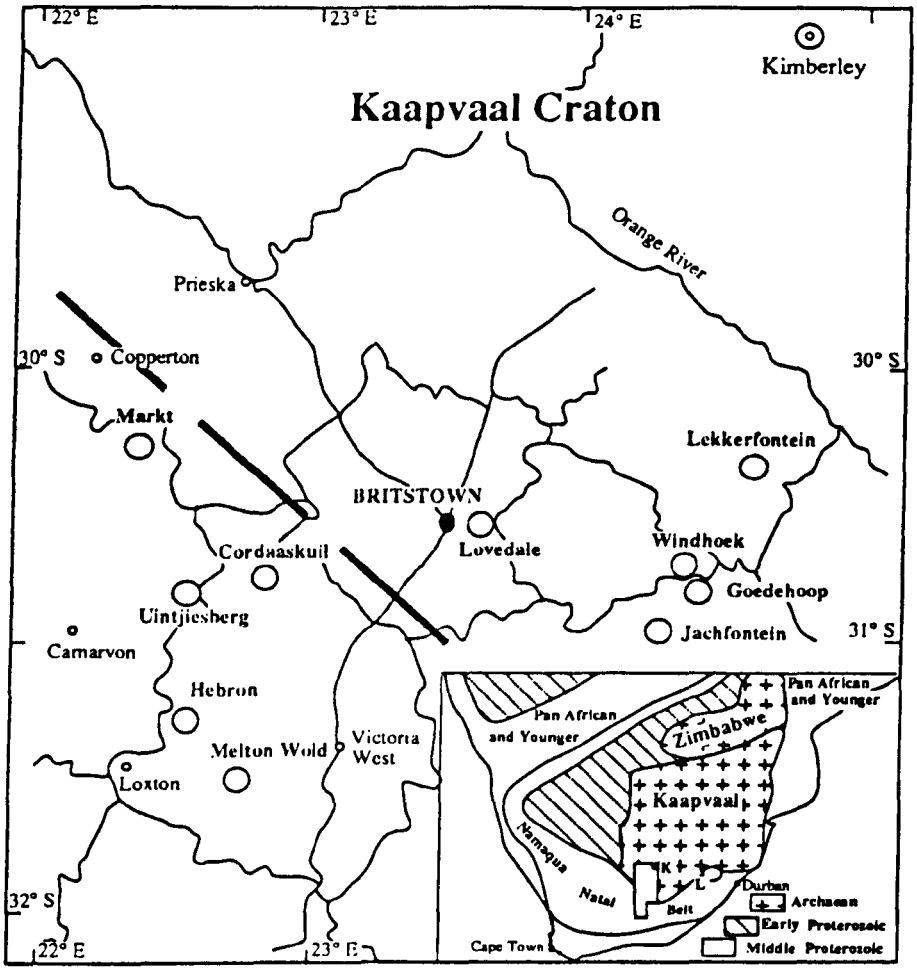

Fig. 3-1 Sample localities and schematic Geological map of southern Africa, modified from Robey (1981), Cornell et al. (1986) and De Wit et al. (1992). The dashed line is the boundary between the Kheis Province (Archaean) and the Namaqua-Natal Belt (Proterozoic) after Cornell et al. (1986).

reworking of pre-existing crust (Hawkesworth and Marlow, 1983; Barton and Burger, 1983). The early Jurassic Karoo continental flood basalts (e.g. Erlank, 1984) and the Cretaceous kimberlites which contain comprehensive xenolith suites from the upper mantle and the crust, occur both on the Kaapvaal Craton and in the surrounding mobile belts. The 21 basic granulites analysed here are from a number of sites in the central Cape Province, South Africa (Fig. 3-1): 10 are from the kimberlite pipes in Markt and the rest are from kimberlite pipes in other localities around Britstown, including Uintjesberg, Lovedale, Lekkerfontein, Cordaatskuit, Hebron and

Windhoek. To facilitate the discussion, they are collectively referred to as the Britstown Group.

Cornell et al. (1986) studied the surface rocks in the Prieska-Copperton region and confirmed the Proterozoic origin of the Copperton formation, ~50 km north-west of Markt (Fig 3-1), and the Archaean age of the Marydale Group in the Kheis Province. Thus, in the context of the surface boundaries of the Archaean craton, Markt is within the Proterozoic mobile belt and the samples in Britstown Group are from both on the Archaean craton and in the Proterozoic mobile belt (Fig. 3-1). The Markt granulite xenoliths are from Group 2 kimberlite pipes, but the northern Lesotho granulites and the Britstown Group xenoliths are mainly from the Group 1 kimberlite pipes (Skinner et al., 1992; Smith et al., 1993). Pb isotope ratios were also measured on the basic granulite xenoliths from northern Lesotho, which have been studied previously (Rogers and Hawkesworth, 1982; Griffin et al., 1979; Rogers, 1977 and references therein).

Most granulite xenolith specimens from Markt are 10–20 cm in diameter; they are not banded and they have medium grained, equigranular granoblastic textures. The minerals are typically homogeneous, and the assemblages include plagioclase+garnet (HSA22), plag+cpx+gt+ky±phl (HSA19), cpx+gt±plag (HSA13 and HSA24) and plag+cpx+gt±opx±bi (most other samples). The accessory mineral phases are predominantly apatite and zircon. P-T conditions have been determined on two samples (HSA19 and 32) and they are 900° C, 17.3 kb (Huang, unpublished data) and 780° C and 15 kb (van Calsteren et al., 1986) respectively, which indicate metamorphic conditions between granulite and eclogite facies and similar to those for the granulite xenoliths from northern Lesotho (Rogers, 1977; Griffin et al., 1979; van Calsteren et al., 1986).

3-3. Geochemical Results

Major and trace elements were analysed by XRF and INAA at the Open University (Potts et al., 1985), except for Pb and U which were measured by isotope dilution, and the isotope compositions of Sr, Nd and Pb were analysed on a Finnigan-MAT 261 mass spectrometer. Isotope standards were measured frequently and the following average values were obtained: NBS987 $^{87}Sr/^{86}Sr$ = 0.710253 ±16, Johnson and Matthey Nd $^{143}Nd/^{144}Nd$ = 0.511791 ±14, and NBS 981: $^{206}Pb/^{204}Pb$ = 16.904 ±14, $^{207}Pb/^{204}Pb$ = 15.450 ±13, $^{208}Pb/^{204}Pb$ = 36.568 ±40 (1σ).

Minerals were separated from washed and sieved splits of crushed rocks that were analysed for Sr, Nd and Pb. Garnet, clinopyroxene and plagioclase were separated using an electro-magnetic separator and then hand-picked under a binocular microscope. Garnet and clinopyroxene were washed for 15 min. in 2.5 HCl, and plagioclase in H_2O in an ultrasound bath. The total blanks were less than 1 ng for Nd, Sr and Pb.

3-3.1 Major and Trace Elements

The major element results on the granulite xenoliths from Markt and the Britstown Group are summarised in Table 3-1 and illustrated in Fig. 3-2. The samples from Markt have SiO_2 contents ranging from 46.4 to 51.8%, Al_2O_3 from 12 to 24% (Fig. 3-2), and Mg# from 53 to 76. There is a broad negative correlation between SiO_2 and Mg# in the Markt granulites, except for HSA24, which has low SiO_2 and low Mg#. The xenoliths from both northern Lesotho and Britstown Group have similar major element compositions to those from Markt (Fig. 3-2).

Trace element abundances in the Markt and Britstown Group granulites are given in Table 3-2, together with data from the northern Lesotho granulites (Rogers and Hawkesworth, 1982). Mg# in the Markt granulites correlates positively with highly compatible trace element abundances, such as Cr, but negatively with Rb (Fig. 3-3a), which is

consistent with magmatic differentiation. However, there is no correlation between Ba, another highly incompatible element, with Mg# in the Markt granulites, which is very different from that in the northern Lesotho granulites (Fig. 3-3a). The variation of Ba in the northern Lesotho granulites is more than an order of magnitude with very limited variation of Mg# and SiO_2. This wide variation is unlikely to be solely due to magmatic processes, and so the Ba contents in the granulites xenoliths may have been modified significantly by later events.

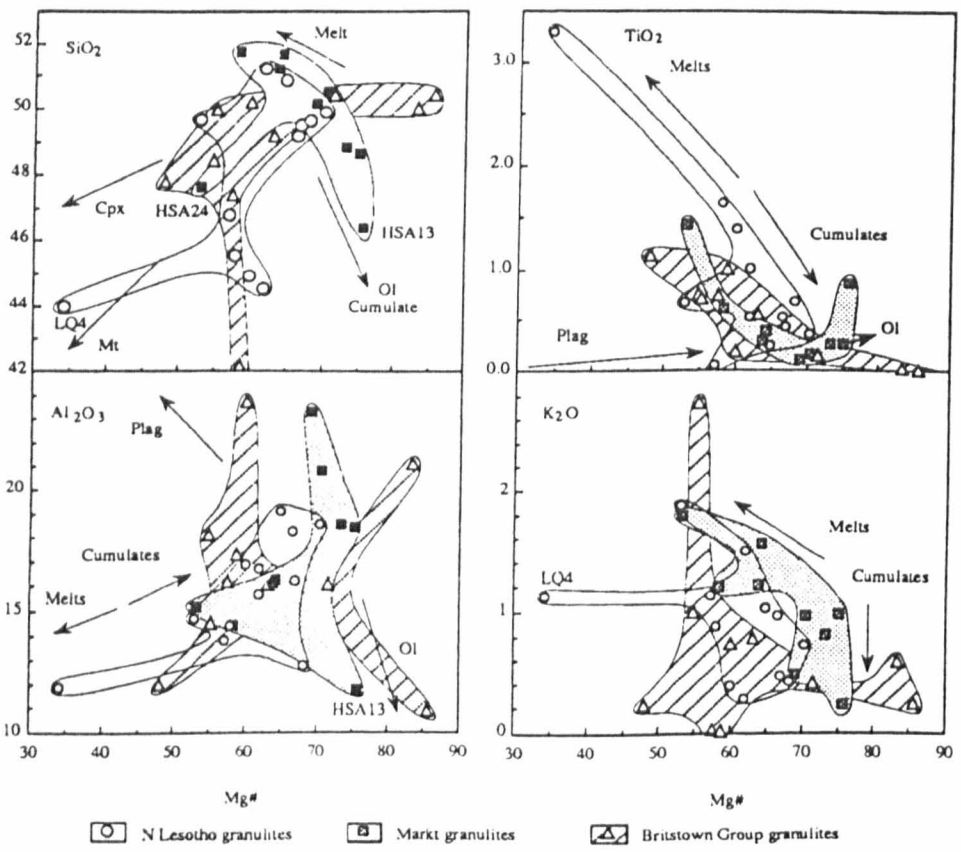

Fig. 3-2 Variation diagrams showing the relationship between selected major elements in the Markt and Britstown Group granulite xenoliths, and in northern Lesotho granulite xenoliths (Rogers, 1977, 1979)

TABLE 3-1

Major element abundances in the whole rock samples from the southern African granulite xenolites

Names	Locality	SiO_2	TiO_2	AL_2O_3	Fe_2O_3	MnO	MgO	CaO	Na_2O	K_2O	P_2O_5	H_2O^+	H_2O^-	LOI	Tol	Mg#
HSA12	Markt	51.22	0.302	16.15	9.36	0.142	8.34	9.6	3.03	1.22	0.04			0.70	100.10	63.8
HSA13	Markt	46.42	0.88	11.74	9.57	0.16	15.05	14.62	0.57	0.23	0.02			1.33	100.58	75.7
HSA19	Markt	48.67	0.27	18.45	7.12	0.11	10.80	9.45	2.70	0.98	0.02			1.63	100.19	75.0
HSA22	Markt	50.16	0.11	23.32	3.83	0.06	4.29	10.84	4.27	0.48	0.03			2.26	99.64	68.9
HSA24	Markt	47.65	1.44	15.16	12.88	0.18	7.37	9.33	2.50	1.80	0.01			2.31	100.63	53.1
HSA28	Markt	50.52	0.16	20.86	5.71	0.08	6.87	9.19	3.51	0.96	0.02			2.36	100.24	70.4
HSA32	Markt	48.83	0.26	18.58	7.67	0.19	10.61	9.48	2.98	0.81	0.01			0.90	100.32	73.3
HSA35	Markt	51.78	0.62	14.41	9.81	0.13	6.94	9.35	4.29	1.21	0.06			1.30	99.90	58.4
12133	Markt	51.66	0.39	16.27	9.07	0.12	8.19	8.61	3.47	1.55	0.07	0.88	0.13		100.41	64.1
12133a	Markt	49.73	0.25	18.79	8.19	0.11	12.17	9.13	1.72	0.33	0.00	0.50	0.01		100.93	74.6
31--1	Goedehoop	50.44	0.16	16.06	6.92	0.11	8.80	11.36	3.80	0.41	0.02	1.85	0.01		99.94	71.6
2223	Lovedale	50.42	0.02	10.92	3.94	0.09	11.79	11.71	2.33	0.24	0.47	0.75	0.23		92.91	85.6
2243	Lovedale	50.02	0.03	21.12	3.28	0.07	8.21	12.54	2.92	0.59	0.01	1.07	0.12		99.98	83.2
6043	Cordaatskuit	48.43	0.76	18.13	9.11	0.17	5.58	9.68	5.06	1.00	0.20	1.59	0.08		99.79	54.8
7403	Hetron	47.85	1.14	12.00	11.09	0.16	5.17	9.54	3.04	0.23	0.34	0.91	0.07		91.54	48.0
9123	Uintjesberg	42.17	1.01	17.27	16.09	0.30	11.54	10.22	0.99	0.01	0.22	0.01	0.06		99.89	58.7
9153	Uintjesberg	47.44	0.75	16.19	12.24	0.22	8.37	9.65	4.52	0.03	0.46	0.92	0.12		100.91	57.5
25023	Windhoek	49.22	0.56	16.07	8.40	0.14	7.26	10.62	4.74	0.78	0.15	2.20	0.03		100.17	63.1
33013	Lekkerfontein	50.01	0.72	14.51	12.22	0.21	7.60	7.59	2.36	2.75	0.03	0.73	0.01		98.74	55.2
33023	Lekkerfontein	50.21	0.19	23.75	4.98	0.05	3.77	12.14	3.64	0.74	0.00	0.82	0.06		100.35	60.0

$$Mg\# = \frac{Mg}{(Mg+TFe)}$$

TABLE 3-2

Trace element abundance in the whole rock samples of the southern African granulite xenoliths

Names	Ba	Rb	Nb	Sr	Zr	Y	V	Sc	Ni	Co	Zn	Cr	Cu	Pb	U	La	Ce	Nd	Sm	Eu	Tb	Yb	Lu	Eu/Eu*
HSA12	1135	15	3	376	14	8	140	31	160	50	69	227	43	2.21	0.074	6.3	12.4	9.1	1.57	0.54	0.23	0.77	0.14	1.05
HSA13	239	5	3	86	30	12	415	61	343	55	61	888	9			2.7	6.9	7.5	2.35	0.61	0.36	0.97	0.16	0.78
HSA19	1032	10	2	399	5	4	110	21	208	36	47	698	58	1.71	0.268	3.4	5.9	1.8	0.42	0.28	0.15	0.32	0.06	1.52
HSA22	477	5	3	653	1	3	36	13	123	15	31	157	25	1.96	0.101	3.3	5.6	3.5	0.49	0.42	0.05	0.24		2.81
HSA24	420	17	2	532	5	8	346	40	126	57	84	112	22	2.79	0.651	0.7	1.2	1.6	0.62	0.42	0.16	0.94	0.15	1.75
HSA28	438	9	2	481	6	4	45	13	173	25	48	411	38	2.54		7	11.4	4.9	0.85	0.5	0.13	0.56	0.07	1.77
HSA32	703	9	2	430	5	4	96	19	219	40	46	651	56	2.64	0.168	2.7	5.1	3.5	0.4	0.27	0.07	0.37	0.06	1.97
HSA35	1358	15	4	1070	5	11	197	35	173	49	75	205	99	3.47	0.339	4.7	8.7	7.2	1.82	0.75	0.32	1.1	0.18	1.20
12133	702	20	<2	570	26	13	133	26	222	52	72		46											
12133a	1079	4.3	<2	242	5.8	2.9	104		209	55	5		5											
31--1	2353	4.8	7	674	5	5.4	80	25	239	44	45		25											
2223	581	1.6	<2	311	12	4	7	20	145	46	22		27											
2243	3026	7.6	<2	261	8.3	2.1	52	18	165	32	14		14											
6043	4.2	8.3	3.5	514	104	24	134	24	57	33	108		42											
7403	1194	70	4.9	1123	244	24	206	30	31	33	115		19											
9123	267	2.7	2.3	198	15	37	294	63	149	72	139		255											
9153	692	3.2	3.1	545	39	25	230	33	84	45	129		9											
25023	1721	10	30	1994	38	17	168	21	<2	41	78		48											
33013	1953	39	<2	1298	40	24	297	36	245	53	100		59											
33023	614	4.9	<2	989	14		63	15	63	23	61		<2											

$Eu^* = (2*Sm_N + Tb_N)/3$

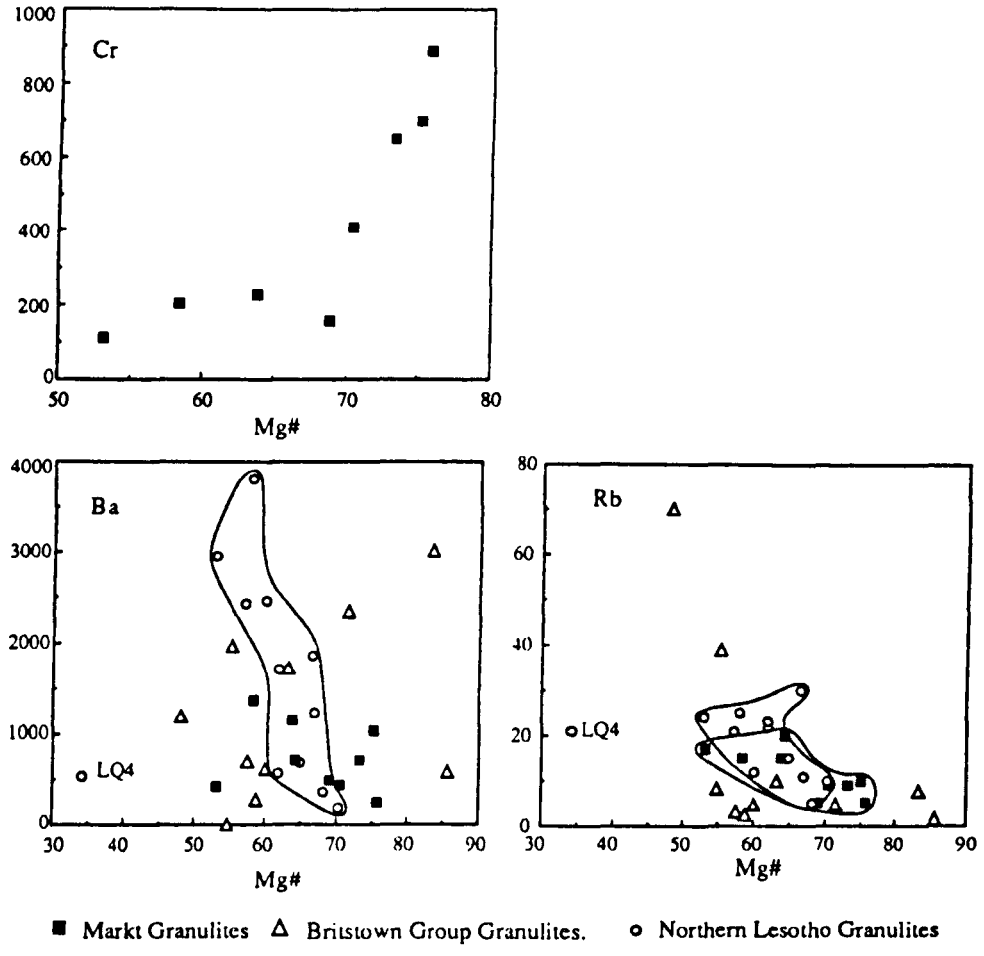

Fig. 3-3a Trace elements vs. Mg#, illustrating the variation between Mg# and selected compatible and highly incompatible elements

Many other trace elements which are more compatible in ferromagnesian phases than in plagioclase, such as Sc, V, Y, Yb and Co, correlate negatively with Al_2O_3 (Fig. 3-3b). Sr is more compatible in plagioclase and correlates positively with Al_2O_3, except for the relatively high Sr in HSA35. The Rb/Sr ratios in the Markt granulites are largely controlled by their Sr contents and so there is a negative correlation between Rb/Sr and Al_2O_3 (Fig. 3-3b). In general, the range of trace element abundances in the Markt granulites is less than those in the granulite xenoliths from northern Lesotho. Granulites from the Britstown Group tend to have similar major, but more variable trace element contents than those from Markt (Fig. 3-2 and 3a, b). However, because they are from

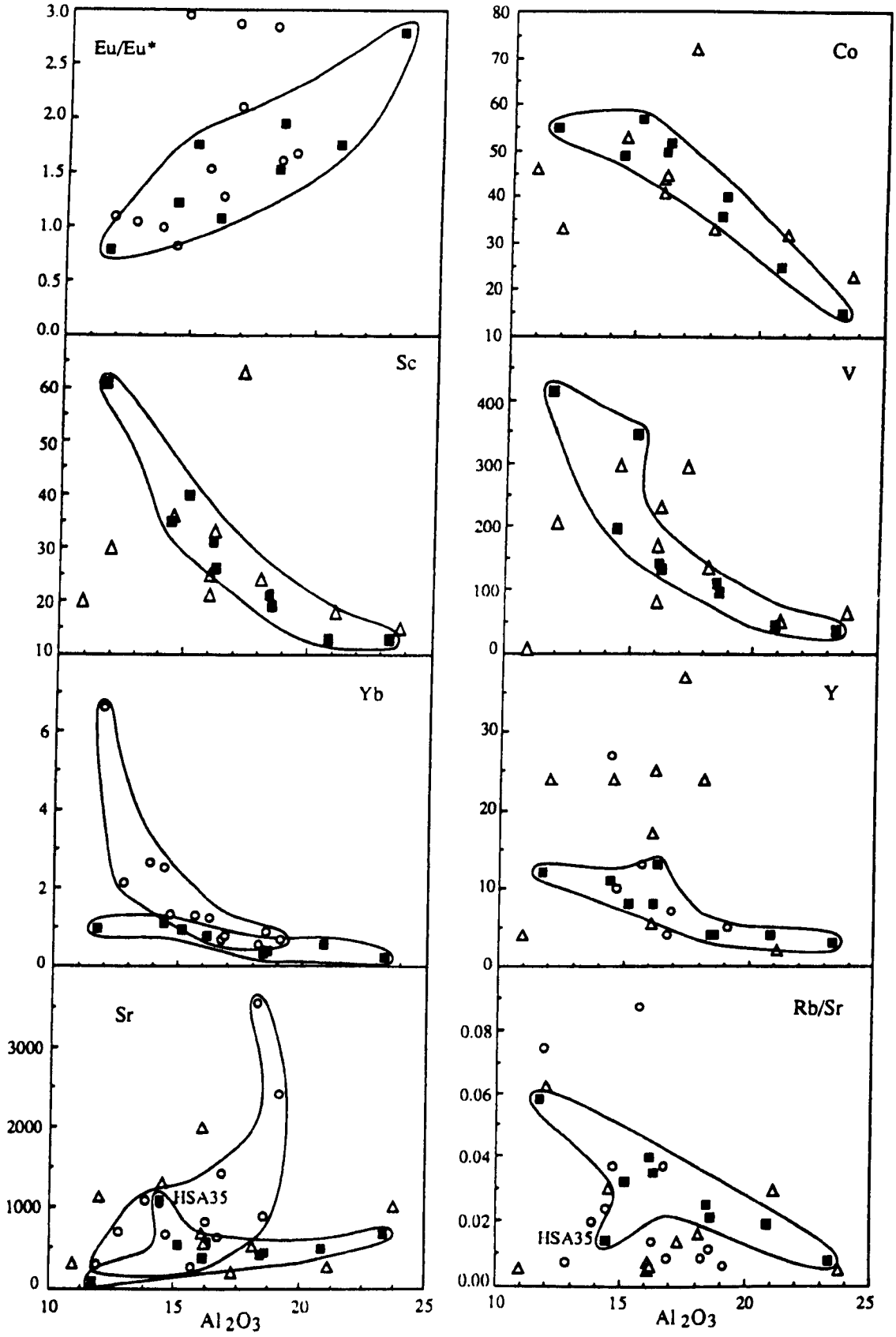

Fig. 3-3b Trace elemnts vs. Al_2O_3, illustrating the relation between moderately incompatible trace elements and Al_2O_3. Data from: this study; Rogers and Hawkesworth (1982); Griffin et al. (1979).

different kimberlite pipes scattered over a wide area, it is not surprising that no clear correlations are observed.

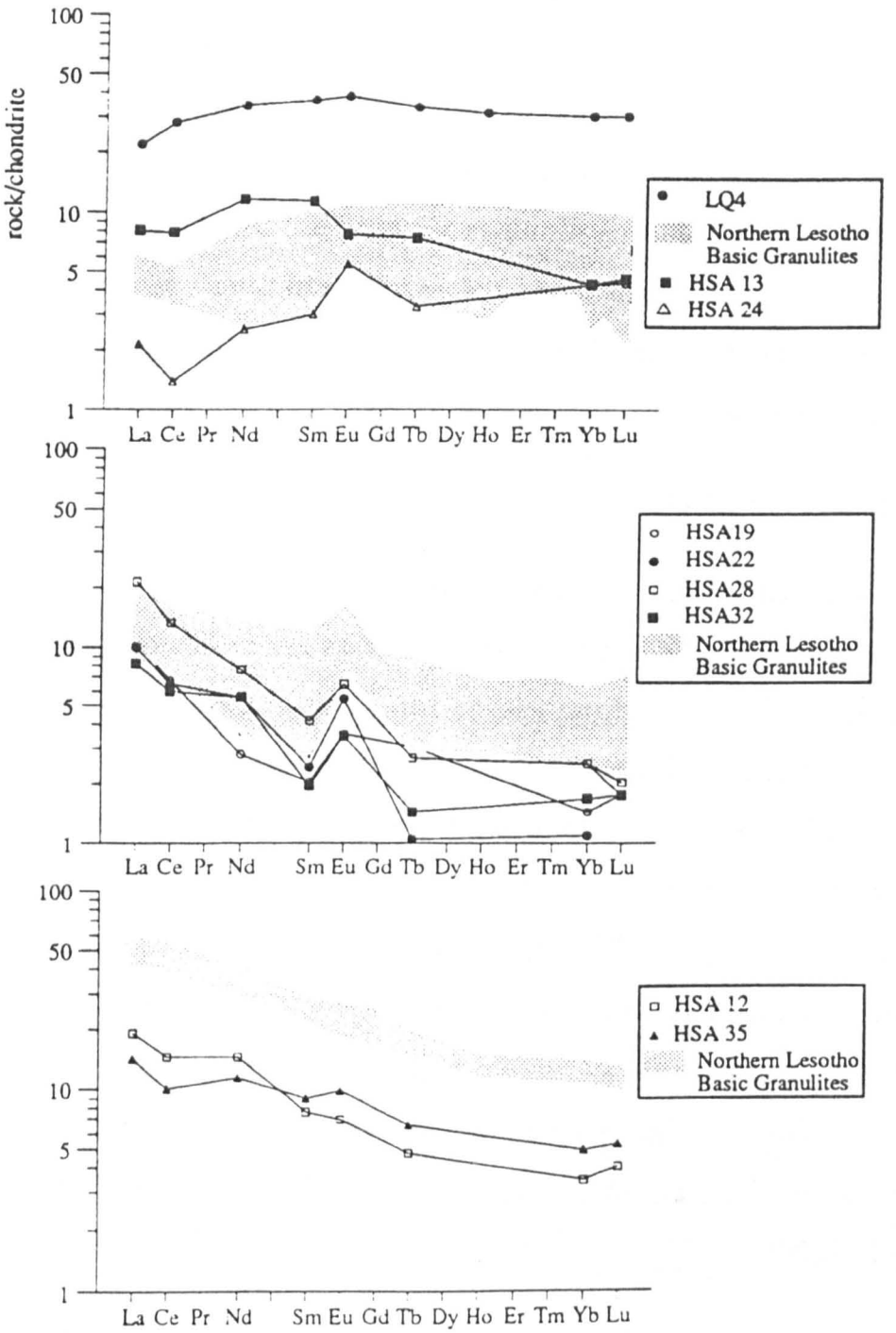

Fig. 3-4 Chondrite normalised REE diagrams. With the exception of HSA13 and HSA 24 two types of REE pattern are recognised in the Markt granulites. The northern Lesotho granulite (Rogers and Hawkesworth, 1982) are shown for comparison.

The REE data from the Markt granulites are presented in Table 3-2 and Fig. 3-4. Two groups are recognised: one with LREE-enriched patterns and large positive Eu anomalies (HSA19, HSA22, HSA28 and HSA32), and the other with similar LREE enriched profiles, but without significant Eu anomalies (HSA12 and HSA35). The first group has relatively high Mg# (68–75) and the second group has low Mg# (53–65). The two exceptions are HSA13, which has high LREE with low SiO_2 and high Mg#, and HSA24 which is LREE depleted with low SiO_2 and low Mg#. Eu/Eu^* correlates with Al_2O_3 in the Markt granulites (Fig. 3-3b), reflecting the plagioclase control. Overall, REE patterns in the Markt granulites are similar to those in the granulites from northern Lesotho (Rogers and Hawkesworth, 1982), but at lower REE abundances (Fig. 3-4).

3-3.2 Sr and Nd Isotopes

Sr and Nd isotope data are listed in Table 3-3 and shown in Fig. 3-5. The measured $^{87}Sr/^{86}Sr$ ratios from the Markt granulites range from 0.7048 to 0.7118, and $^{87}Rb/^{86}Sr$ from 0.02 to 0.18. Two of the high $^{87}Sr/^{86}Sr$ ratios are from HSA13 and HSA35 and they have SiO_2 of 46.4 and 51.8 wt%, respectively. There is no Rb-Sr isochron relationship observed in the data from the Markt granulites, although HSA13 has the highest $^{87}Rb/^{86}Sr$ ratio (0.174) and the highest $^{87}Sr/^{86}Sr$ ratio (0.7118). Another high $^{87}Sr/^{86}Sr$ sample, HSA35, has low $^{87}Rb/^{86}Sr$ (0.035). The average present-day $^{87}Sr/^{86}Sr$, even excluding the two high ratios from HSA13 and HSA35, is 0.706±1. This is higher than the average from the northern Lesotho granulites (~0.704, Fig. 3-5), even though both suites have similar Rb/Sr ratios (~0.028).

The Britstown Group granulites have similar $^{87}Sr/^{86}Sr$ ratios (0.704~0.708) and $^{87}Rb/^{86}Sr$ ratios (0.014~0.18), but again no isochron relations are preserved. The present-day $^{143}Nd/^{144}Nd$ ratios in the Markt xenoliths range from 0.51172 to 0.51352 with $^{147}Sm/^{144}Nd$ = 0.064–0.327.

The Britstown Group granulites have $^{143}Nd/^{144}Nd$ = 0.51159–0.51294, similar to those from Markt. Overall, these granulite xenoliths have higher present day $^{87}Sr/^{86}Sr$ and lower $^{143}Nd/^{144}Nd$, (except for the samples HSA24 and 33013 from Markt and Lekkerfontein, respectively) than the granulites from the northern Lesotho in the Natal belt (Fig. 3-5). There are no correlations between Mg# and either Sr and Nd isotope ratios in the xenoliths from Markt, unlike those observed in the granulite xenoliths from Chudleigh (Rudnick et al., 1986).

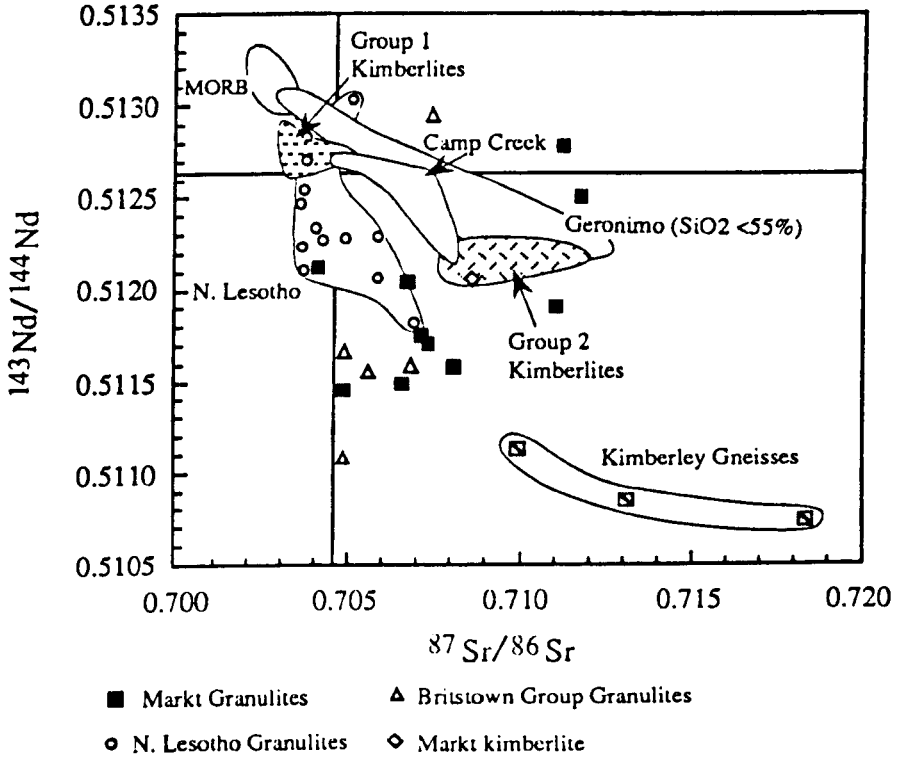

Fig.3-5 Nd-Sr isotope diagram illustrating the range of present day isotope ratios. $^{87}Sr/^{86}Sr$ in the granulites from Markt and the Britstown Group scatter but tend to higher than those from northern Lesotho, whereas the $^{143}Nd/^{144}Nd$ ratios are lower. Data from: Rogers and Hawkesworth (1982); Kempton et al. (1990); Esperanca et al. (1988); Smith (1983) and Skinner et al. (1992).

TABLE 3-3

Sr, Nd and Pb isotope ratios in the whole rock samples

Name	$\frac{^{87}Rb}{^{86}Sr}$	$\frac{^{87}Sr}{^{86}Sr}$	$\frac{^{147}Sm}{^{144}Nd}$	$\frac{^{143}Nd}{^{144}Nd}$	$\frac{^{206}Pb}{^{204}Pb}$	$\frac{^{207}Pb}{^{204}Pb}$	$\frac{^{208}Pb}{^{204}Pb}$	T_{DM}
PHN1646	0.069	0.70396	0.143	0.51210	17.344	15.602	37.115	2.05
PHN1670	0.024	0.70372	0.118	0.51211	17.344	15.592	37.175	1.50
PHN1919	0.208	0.70483	0.151	0.51228	17.564	15.592	37.517	1.87
PHN2533	0.128	0.70373	0.129	0.51247				1.04
PHN2588	0.107	0.70507	0.242	0.51302	16.502	15.511	36.372	
PHN2852	0.040	0.70412	0.139	0.51232	17.134	15.561	36.904	1.48
M1	0.035	0.70373	0.139	0.51223	17.614	15.622	37.577	1.66
MAT12	0.054	0.70408	0.138	0.51209				1.93
L12A	0.039	0.70359	0.223	0.51295	17.033	15.554	36.966	
L12B	0.021	0.70376	0.206	0.51282	17.442	15.496	37.370	
L13	0.033	0.70374	0.196	0.51270	17.166	15.444	36.938	3.56
LT2	0.030	0.70700	0.101	0.51176	17.254	15.581	37.175	1.73
LQ4	0.215	0.70423	0.177	0.51246	16.282	15.540	36.733	2.48
HSA12	0.121	0.70712	0.127	0.51175	16.442	15.235	36..850	2.31
HSA13	0.174	0.71179	0.182	0.51251				2.66
HSA19	0.071	0.70731	0.099	0.51172	17.666	15.543	37.585	1.76
HSA22	0.019	0.70657	0.105	0.51149	15.200	14.916	35.379	2.19
HSA24	0.087	0.70831	0.327	0.51352	17.985	15.548	37.930	
HSA24 duplicate				0.51351	17.995	15.562	37.974	
HSA28	0.054	0.70479	0.064	0.51164	15.893	15.045	36.138	1.43
HSA32	0.058	0.70666	0.113	0.51204	17.577	15.551	37.476	1.53
HSA35	0.036	0.71112	0.165	0.51189	16.681	15.289	36.815	3.90
12133	0.102	0.70807	0.134	0.51159	17.706	15.546	37.601	2.84
HSA60	0.106	0.70487		0.51108	14.266	14.667	34.712	
7403	0.180	0.70701	0.128	0.51160	17.077	15.428	36.707	2.62
9153	0.018	0.70506	0.123	0.51166	17.298	15.464	37.026	2.35
25023	0.015	0.70411	0.1	0.51212				1.25
33013	0.087	0.70723	0.203	0.51294	17.349	15.450	37.155	1.42
33023	0.014	0.70550	0.135	0.51159	14.666	14.647	33.751	2.89

Pb isotope ratios have been corrected for fractionation relative to NBS981.
T_{DM} are calculated after Ben Othman et al (1984)

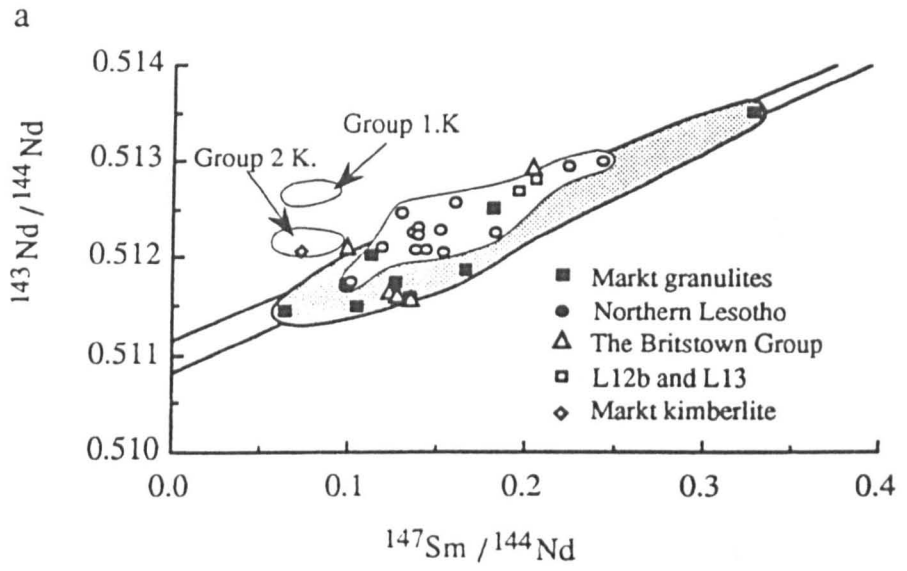

Fig. 3-6a Sm-Nd whole rock errochron diagram. The whole rock data from Markt scatter about an errorchron corresponding to an age of 1.24 ±0.17 Ga, whereas those from northern Lesotho yield an age of 1.18 ±0.20 Ga, recalculated after Rogers and Hawkesworth (1982). The two granulite suites therefore yield similar ages, but the Markt granulites have lower initial $^{143}Nd/^{144}Nd$ ratios.

Rogers and Hawkesworth (1982) reported a Sm-Nd errorchron on 15 granulite xenoliths from northern Lesotho, corresponding to an age of 1.4 ±0.1 Ga. New data on two basic granulite xenoliths from the same area plot on that whole-rock errorchron (Fig. 3-6a), and the recalculated age is 1.24 ±0.17 Ga (MSWD=25). The results from the Markt granulites are also plotted in Fig. 3-6a and they scatter about a similar errorchron, corresponding to an age of 1.18 ±0.20 Ga (MSWD = 64), which is indistinguishable from the age for the northern Lesotho granulites. The T_{DM} model ages of the northern Lesotho mafic granulites range from 1.0 to 2.0 Ga, except for L13 and LQ4 (3.6 and 2.5 Ga, respectively), with an average of 1.7 Ga. For the Markt and Britstown Group granulites T_{DM} = 1.3 to 3.9 Ga.

Sm, Nd and $^{143}Nd/^{144}Nd$ have also been measured for selected mineral separates, including garnet, clinopyroxene and plagioclase, from a northern Lesotho granulite xenolith PHN2852 and two Markt granulite

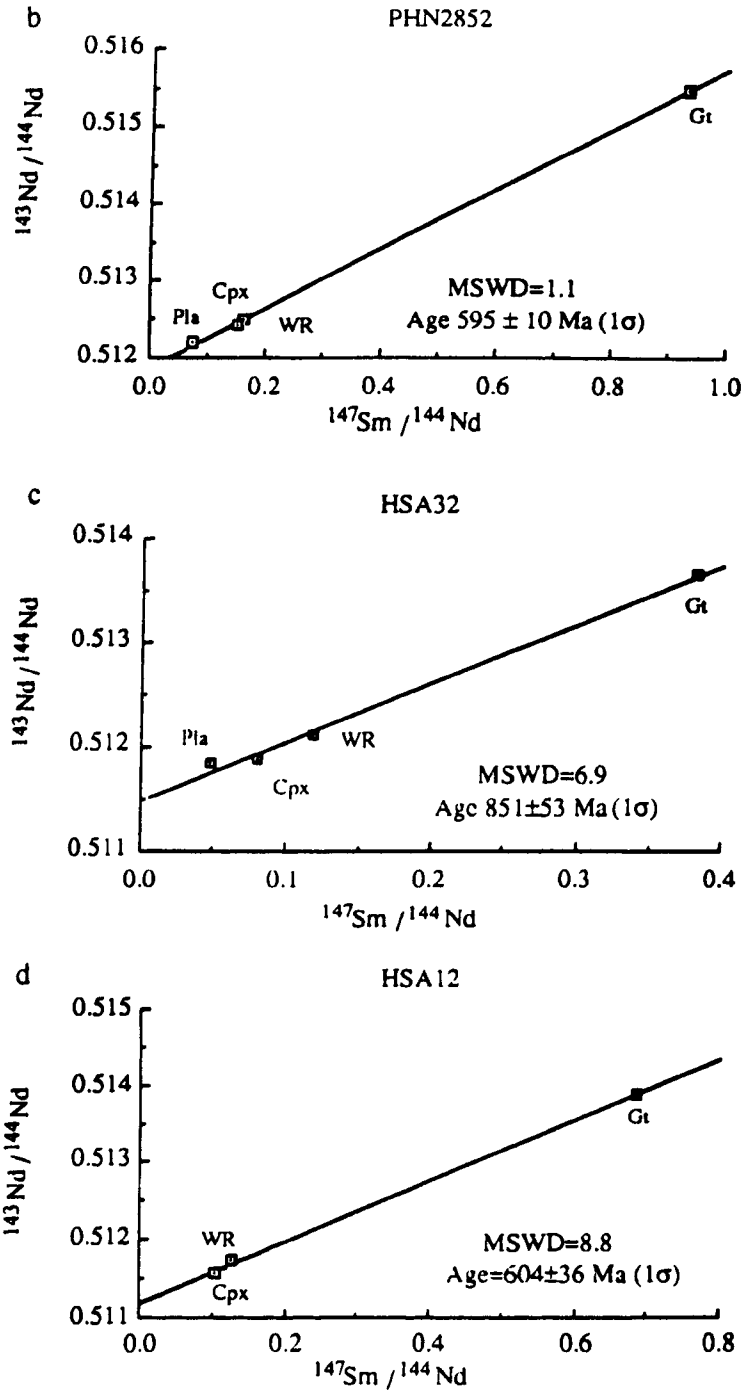

Fig. 3-6 (b) PHN2852 mineral-whole rock isochron 595 ±10 Ma. (c) HSA32 mineral-whole rock isochron, 851 ±53 Ma. (d) HSA12 mineral-whole rock isochron, 604 ±36 Ma.

xenoliths, HSA12 and HSA32, and data are listed in Table 3-4. Garnet has the higher Sm/Nd ratio, although normally clinopyroxene has the highest Sm and Nd contents. Plagioclase has both the lowest Sm and Nd contents

and Sm/Nd ratio. These are consistent with published Sm and Nd partition coefficients for these mineral phases (e.g., Fujimaki et al., 1984; Irving, 1978). The three mineral-whole rock isochrons yield ages of 595 ±10, 604 ±36 and 851 ±56 Ma, respectively (Fig. 3-6b, c and d). All the mineral-whole rock ages are significantly younger than the whole rock isochron ages of ~1.2 Ga, and although HSA12 and PHN2852 are from Markt and northern Lesotho respectively, they have indistinguishable Sm-Nd mineral-whole rock ages.

TABLE 3-4

Nd and Pb isotope ratios in the mineral separates of granulite xenoliths

Name		Sm	Nd	$\frac{^{147}Sm}{^{144}Nd}$	$\frac{^{143}Nd}{^{144}Nd}$	$\frac{^{206}Pb}{^{204}Pb}$	$\frac{^{207}Pb}{^{204}Pb}$	$\frac{^{208}Pb}{^{204}Pb}$
PHN2852	WR	1.30	5.65	0.139	0.51232	17.134	15.561	36.904
	Garnet	1.02	0.67	0.916	0.51539			
	Py	3.15	13.00	0.146	0.51239			
	Plag	0.11	1.60	0.057	0.51207			
HSA12	WR	1.20	5.70	0.127	0.51175	16.442	15.235	36.850
	Garnet	1.23	1.07	0.685	0.51389	17.632	15.498	37.606
	Py	2.51	14.17	0.107	0.51141	16.117	15.150	36.627
	Plag					15.321	15.010	35.878
HSA28	WR	0.44	4.17	0.064	0.51164	15.893	15.045	36.138
	Garnet					17.150	15.323	37.108
	Py					17.282	15.278	37.373
	Plag					14.516	14.724	34.964
HSA32	WR	0.36	1.93	0.113	0.51204	17.577	15.551	37.476
	Garnet	0.29	0.47	0.375	0.51357			
	Py	0.56	4.49	0.075	0.51181			
	Plag	0.03	0.48	0.042	0.51177			

3-3.3 *Pb data*

The Pb isotope data from all the granulite xenoliths are listed in Table 3-3 and shown in Fig. 3-7. Those from northern Lesotho have present day $^{206}Pb/^{204}Pb$ ratios in range of 16.28 to 17.61 and $^{207}Pb/^{204}Pb$ = 15.24–15.62. Most granulites from northern Lesotho, except L12b and L13, fall on a

relatively shallow array on a $^{207}Pb/^{204}Pb$ vs $^{206}Pb/^{204}Pb$ diagram (Fig. 3-7a), which yields an age of 0.82 ±0.3 Ga. However, the slope is dominated by the two unradiogenic samples, LQ4 and PHN2588. LQ4 is a felsic granulite and it falls off the trends of the mafic samples on trace element-Mg# diagrams (Fig. 3-3b), and it plots above the trend of the other samples on a $^{207}Pb/^{204}Pb$ vs $^{206}Pb/^{204}Pb$ diagram (Fig. 3-7a). If it is excluded, the Pb-Pb errorchron yields an age of 1.49 ±0.36 Ga, and if both LQ4 and PH2588 are excluded, the age is 1.59 ±0.4 Ga.

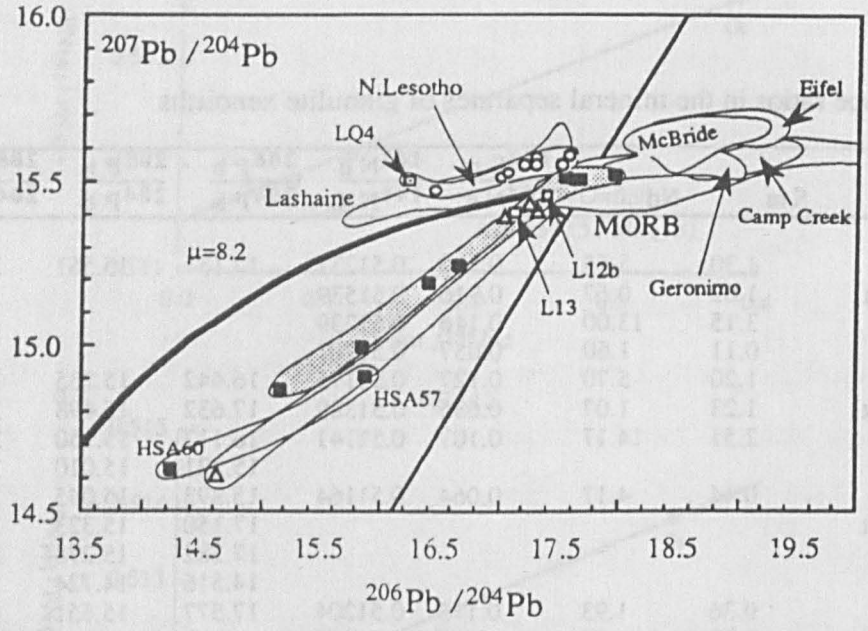

Fig. 3-7a $^{207}Pb/^{204}Pb$ vs $^{206}Pb/^{204}Pb$. The data from the Markt granulites define an errorchron with a slope corresponding to an age of 3.19 ±0.07 Ga, and those from the Britstown Group exhibit a similar trend yielding an age of ~3.4 Ga. The granulites from northern Lesotho scatter about a shallow sloping errorchron, see text for the age discussion.

Measured Pb isotope ratios for the Markt granulite xenoliths show a wide variation in $^{206}Pb/^{204}Pb$ (15.20 to 17.67) and $^{207}Pb/^{204}Pb$ (14.92 to 15.55), and they appear to plot in two groups which yield ages of 3.29 ±0.08 Ga and 2.96 ±0.17 Ga. If all the data are considered together the age is 3.19 ±0.07 Ga (Fig. 3-7a), significantly older than that for the northern Lesotho granulites. The Britstown Group xenoliths and two samples from northern Lesotho

(L12b and L13) plot close to this Archaean array. Two samples (33013 and 33023) in the Britstown Group from Lekkerfontein, which is on the Archaean craton, have very different Pb isotope ratios which yield a two point age of 3.4 Ga. Most of the whole rock Pb isotope data plot to the left of the Geochron (Fig. 3-7a), indicating relatively low time-integrated U/Pb ratios.

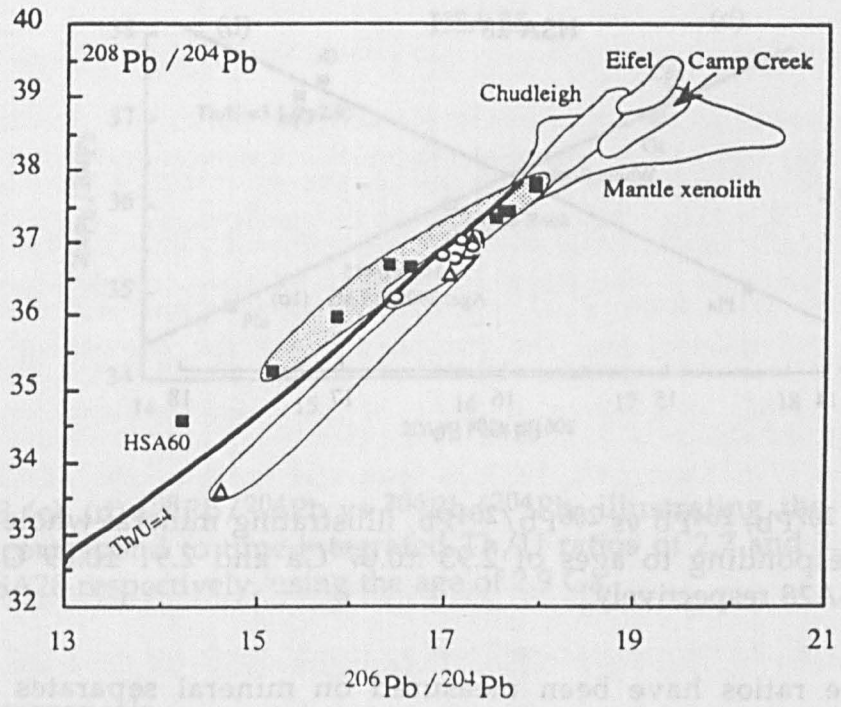

Fig. 3-7b $^{208}Pb/^{204}Pb$ vs $^{206}Pb/^{204}Pb$. Similar arrays are observed for both suites of granulites, and they plot closely to an integrated Th/U = 4 line. The results from the Archaean granulites from Markt and the Proterozoic granulites from northern Lesotho yield time-integrated Th/U ratios of 3.2 and 3.6 respectively. Symbols as for Fig. 3-6.

The Pb isotope data from all the granulite xenolith samples from southern Africa define similar arrays on a $^{208}Pb/^{204}Pb$ vs $^{206}Pb/^{204}Pb$ diagram (Fig. 3-7b). Those from northern Lesotho plot nearest to the time integrated Th/U = 4 line, whereas the Markt granulites have a slightly shallower trend and so they may have had lower time integrated Th/U.

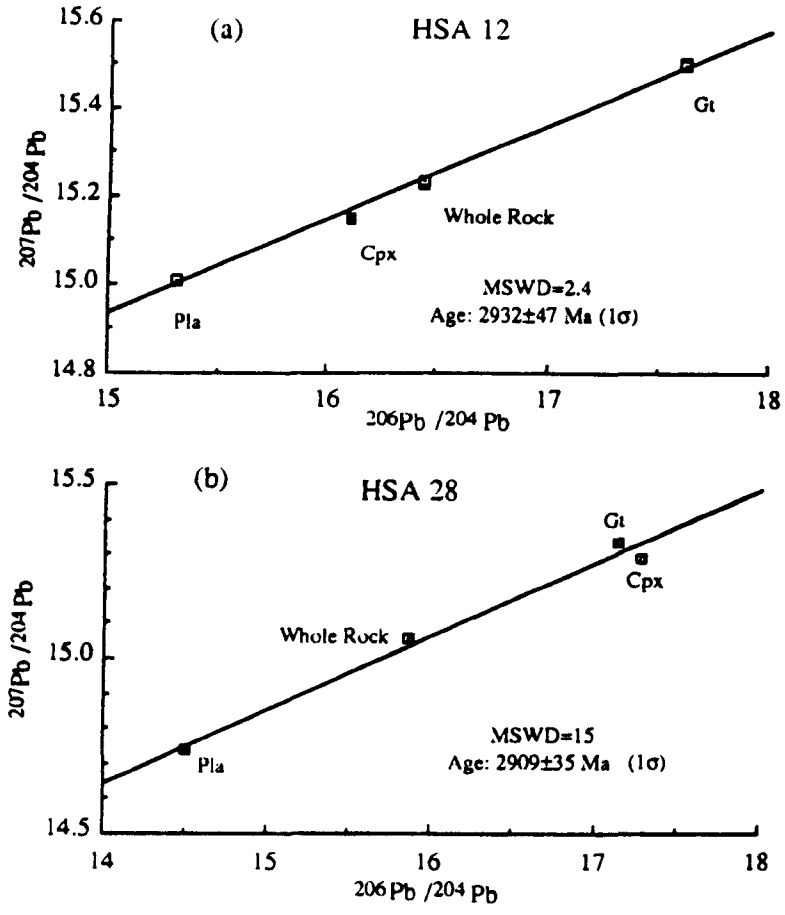

Fig. 3-8 (a), (b) $^{207}Pb/^{204}Pb$ vs $^{206}Pb/^{204}Pb$, illustrating mineral-whole rock isochrons corresponding to ages of 2.93 ±0.07 Ga and 2.91 ±0.09 Ga for HSA12 and HSA28 respectively.

Pb isotope ratios have been measured on mineral separates from HSA12 and HSA28 (Table 3-4). Garnet has the highest Pb isotope ratios, plagioclase has the lowest, and clinopyroxene has intermediate ratios. The mineral-whole rock isochrons for HSA12 and HSA28 yield ages of 2.93±0.07 and 2.91±0.08 Ga respectively (Figs. 8a, b). These are much older than both the Sm-Nd mineral-whole rock isochron ages, and the Sm-Nd whole rock age of ~1.2 Ga. However, they are younger than the whole rock Pb-Pb errorchron age of 3.19 ±0.07 Ga. On $^{208}Pb/^{204}Pb$ vs $^{206}Pb/^{204}Pb$ diagrams (Fig. 3-8c, d), HSA12 and HSA28 also display linear arrays with slopes corresponding to Th/U ratios of 2.7 and 3.1 assuming ages of 2.9 Ga.

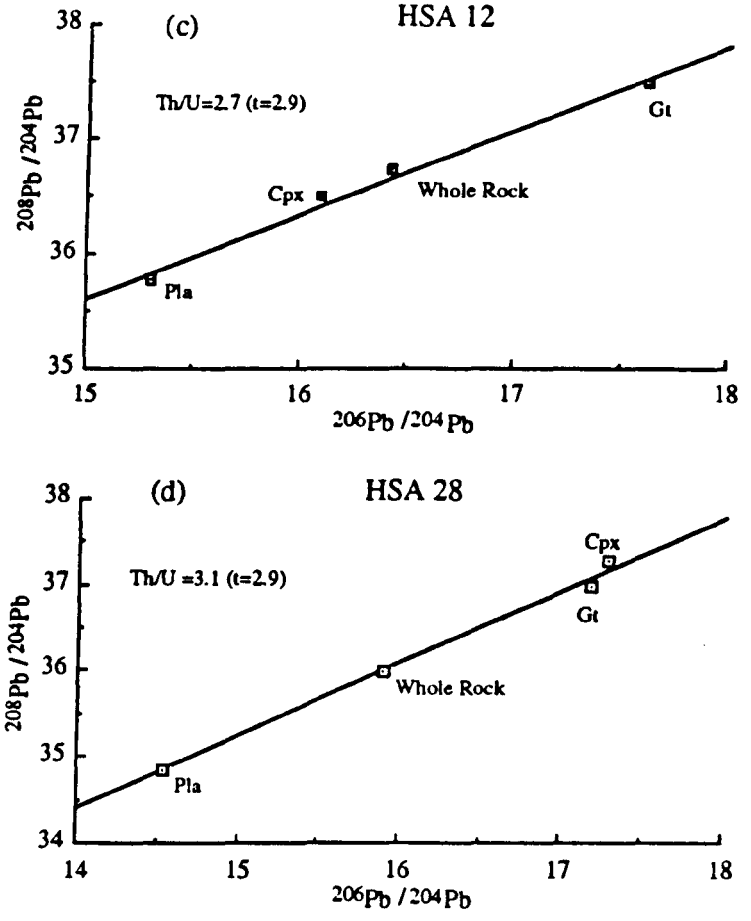

Fig. 3-8 (c), (d) $^{208}Pb/^{204}Pb$ vs $^{206}Pb/^{204}Pb$, illustrating the linear arrays which correspond to time-integrated Th/U ratios of 2.7 and 3.1, for HSA12 and HSA28 respectively, using the age of 2.9 Ga.

3-4. Petrogenesis

The new major and trace element data from the Markt and the Britstown Group granulites are similar to those from northern Lesotho, with a relatively restricted range of major elements (SiO_2 mainly 46–51%) and a wide range of trace element abundances. Their basic compositions (SiO_2 <52%) are consistent with the data on most lower crustal xenolith suites worldwide (Rogers, 1977; Taylor and McLennan, 1985; Kempton et al., 1990; Rudnick, 1992a, b). The samples from the Britstown Group were taken from different locations and so they are unlikely to be simply related to one another, however, correlations between major and trace elements in

the Markt granulite xenoliths suggest that they may be genetically related to one another.

As basic lower crustal rocks, they may have been formed by differentiation of underplated basic magma, or as restites from intracrustal partial melting. The granulites from northern Lesotho have been interpreted as underplated basalts and associated cumulates. Similarly, most of the basic granulites analysed here are LREE enriched, and have within-suite variations consistent with fractional crystallisation processes.

3-4.1 Fractional Crystallisation

Mg# is widely used as an index of magmatic evolution and it broadly correlates with SiO_2 (Fig. 3-2). A number of parameters affect Mg#, including the original variation of modal olivine, othopyroxene, clinopyroxene and oxides, and the composition of the coexisting melt (Rudnick et al., 1986). However, in view of the evidence from layered intrusions (New, 1976; Campbell, 1977; Wilson and Larsen, 1985), Rudnick et al. (1986) argued that variations of ferromagnesian phases were not responsible for the large range of Mg# (17 units) in granulites from Queensland, Australia, and Mg# in the Markt rocks varies by 23 units. On the basis of the Mg#, and Al_2O_3 data, the samples may be subdivided into two groups: HSA13, 19, 22, 28 and 32 have higher Mg# (>68), and preserve a correlation between Mg# and Al_2O_3, whereas those in the second group (12133, HSA 12, 24, and 35) have lower Mg# (<68). These groups are the same as those recognised from the REE profiles.

The first group of samples have higher compatible, but lower incompatible element contents. The variation of Mg# with Al_2O_3 can be interpreted as varying proportions of ferromagnesian phases and plagioclase, suggesting that this group is of cumulates. However, the low Mg# in HSA 12, HSA35 and 12133, together with their high incompatible

(high Rb and La) and low compatible (Cr and Ni) element contents, is consistent with crystallisation from more evolved melts. HSA24 has low SiO_2 and Mg# but with high TiO_2 (1.44%) and relatively high V and Sc, indicating magnetite accumulation. That some moderately incompatible elements, such as Sc, V, Y and Co, correlate with Al_2O_3, as do Eu/Eu* and Rb/Sr, suggests significant plagioclase control on the original major and trace element fractionation in the Markt granulites.

3-4.2 Contamination Processes

Xenoliths may have been contaminated in the kimberlite en route to the surface, and so the significance of such contamination must be assessed before further inferences are drawn from the new data. Even though the ascent rate of kimberlites is very rapid (McGetchin and Ullrich, 1973) and at relatively low temperatures, which may be a reason why Archaean biotite ages are preserved in upper crustal xenoliths (van Calsteren et al., 1986), some samples clearly have experienced mineral alteration (Griffin et al., 1979).

Rogers and Hawkesworth (1982) argued that most of the granulite xenoliths from northern Lesotho had not been significantly contaminated by the host Group 1 kimberlites. The Group 2 kimberlites (Smith, 1983; Fraser and Hawkesworth, 1986, 1992; Skinner et al., 1992) have low Al_2O_3 (< 5%), and relatively low Sc (17–23 ppm), V and Y (22 ppm), and so they are unlikely to have been responsible for the overall trends within the Markt granulite xenoliths (Fig. 3-3a). Although kimberlites have much higher Sr (>700 ppm) and Nd (>50 ppm) contents than the granulite xenoliths (mostly Sr <650 and Nd <10), there is no relationship between the Sr and Nd isotope ratios of the granulites and those of the Group 2 kimberlites at the time of emplacement, at 116 Ma (see also Fraser and Hawkesworth, 1992; Skinner et al., 1992; Smith et al., 1993). In addition, the Group 2 kimberlites plot above the errorchrons for the granulites from northern Lesotho and

Markt in Figure 3-6a, and so contamination with host kimberlite does not appear to have been responsible for the errorchron. van Calsteren et al. (1986) demonstrated that the Sm/Nd and $^{143}Nd/^{144}Nd$ ratios across a gneiss xenolith are remarkably uniform, even in the zone which was visibly affected by the host kimberlite. Griffin et al. (1979) undertook an electron microprobe study on northern Lesotho granulites and concluded that the abundances of even the highly mobile elements such as K, Rb, Sr and Ba were established before or during the granulite-facies metamorphism. It is difficult, therefore, to envisage that interaction with the host kimberlites was responsible for the overall major and trace element, and isotope characteristics in the granulites.

It has been consistently argued that crustal contamination is an important process which affects the compositions of magmas within continental crust (Taylor, 1980; Marsh, 1989; DePaolo, 1981), and such processes may have influenced the magmatic evolution of the granulite precursors (Rudnick et al., 1986, 1990; Downes et al., 1990; Kempton et al., 1990). Rudnick et al. (1986) proposed that a negative correlation of LIL elements, and measured Sr and Nd isotope ratios, with Mg# implied that xenoliths from Queensland, Australia, crystallised from a continuously evolving melt as the result of assimilation and fractional crystallization (AFC). Although such correlations are not observed in the Markt granulites, it may be that more complex processes resulted in no simple correlations in the analysed xenoliths (Kempton et al. 1990; Kempton and Harmon 1992).

The possibility that the protoliths of the Markt granulite xenoliths were significantly contaminated during differentiation is difficult to assess with little information on the likely crustal contaminants. Nonetheless, these are likely to have had high SiO_2, low Mg# with high Sr, but low Nd isotope ratios. Major element data from the Markt granulites exhibit

limited variation of SiO_2 (46–51.8%). Mg# in the first group of samples (cumulates) is between 68–76. The second group of samples (HSA12, 35 and 12133) has Mg contents in range of 7–8%, although the Mg# is slightly lower (58–64). Accepting the Pb-Pb isochron age of 3.2 Ga for the Markt granulites (see below), the initial $^{87}Sr/^{86}Sr$ ratios, calculated on the basis of measured Rb/Sr, range from 0.702 to 0.706, except for 0.71 in HSA35 which has anomalously high Sr (Fig. 3-3b). However, since no good Rb-Sr isochron relations are preserved, the Rb/Sr ratios may have been altered and such initial ratio calculations may not be reliable. Assuming that $^{87}Sr/^{86}Sr$ = 0.702 in mantle derived rocks at 3.2 Ga (Faure, 1987), the time integrated Rb/Sr ratios for each sample can be calculated and most of them are <0.05. This is slightly higher than 0.033, suggested as the average Rb/Sr ratio for Archaean basalts (Hart et al., 1970), but within the expected range for rocks of mantle origin. The higher $^{87}Sr/^{86}Sr$ ratios in HSA13 and HSA35 (>0.711) require Rb/Sr ratios = ~0.07, and they are also similar to some peridotite xenoliths from southern Africa (0.704 to 0.714, Erlank et al., 1987). Moreover, the initial Nd isotope ratios at 3.2 Ga correlate negatively with Sm/Nd, which is inconsistent with contamination by a crustal component with lower Nd isotope and Sm/Nd ratios than the mantle derived components. Thus, in general, it appears that crustal contamination of the protoliths of the Markt granulite xenoliths was not significant in the development of the observed present-day compositions.

3-5. Age Information

Age information on lower crustal components is important for models for the generation and evolution of the continental crust. However, because xenoliths may have been derived from material which was in the lower crust for long periods of time, their chronological systems may have been disturbed, and their true ages may be difficult to establish. The new data presented here indicate that the Pb-Pb ages may be much

older than those recorded by Sm-Nd.

3-5.1 Granulite Xenoliths from the central Cape province

The Sr isotope data for the Markt and Britstown Group xenoliths scatter on a $^{87}Sr/^{86}Sr$~$^{87}Rb/^{86}Sr$ diagram (not shown), and no age information can be inferred. The trend displayed by the granulites from Markt on a $^{143}Nd/^{144}Nd$~$^{147}Sm/^{144}Nd$ diagram (Fig. 3-6a) corresponds to an age of 1.18 ±0.20 Ga. This Sm-Nd isochron age is consistent with their geological setting in a Proterozoic belt (Hartnady et al., 1985) and the isotope data from surface rocks, which yield Proterozoic model Nd ages (Clifford et al., 1981; Cornell et al., 1986). Thus, it might be that the precursors to the Markt granulite xenoliths were generated in the Proterozoic, in which case the 3.2–3.4 Ga whole rock Pb isotope arrays (Fig. 3-6), would presumably represent source ages consistent, for example, with derivation from Archaean lithospheric mantle.

The mineral-whole rock Pb-Pb isochrons of HSA12 and HSA28, however, yield two analytically indistinguishable ages of 2.93 ±0.05 and 2.91 ±0.04 Ga respectively (Fig. 3-8a, b). It is possible that such ages are the result of mixing Pb from an Archaean reservoir with either laboratory blank or with the kimberlite that brought the xenoliths to the surface. The laboratory blank would be most significant for the garnets, since they have Pb contents in the range of 0.1 to 0.3 ppm. Typically 150 mg was dissolved, and so the laboratory blank could potentially contribute up to 7% to the Pb analysed. However, the plagioclase and whole rock samples have Pb contents of ~4 and ~2 ppm respectively, and so their isotope ratios would not be significantly affected by the laboratory blank. The ages obtained from the plagioclase-whole rock pairs of HSA12 and HSA28 are 2.8 and 3.1 Ga respectively, similar to the ages of 2.9 Ga from their Pb-Pb mineral-whole rock isochrons. Thus, we infer that the Pb-Pb mineral-whole rock isochrons were not affected significantly by laboratory blanks.

An alternative interpretation is that these trends represent mixing between unradiogenic Pb from an Archaean lower crust or from the Archaean mantle lithosphere and radiogenic Pb from kimberlites, which carried xenoliths to the surface. However, there is no petrographic evidence that the selected xenoliths have been significantly altered by fluid from the kimberlites, and it is not clear how kimberlite infiltration could have been responsible for the mineral isochrons. In addition, the Group 2 kimberlites have much higher Pb concentration (14 ppm on average) than the granulite xenoliths (1.7–3.5 ppm, Table 3-2). Thus, if the Pb isotope ratios in the granulite xenoliths had been significantly contaminated by kimberlite, there should be a correlation between Pb contents and Pb isotope ratios which is not observed. Consequently, we accept the mineral - whole rock ages as calculated.

The minerals analysed (gt, cpx, plag) are metamorphic, and so the mineral-whole rock Pb-Pb ages of 2.9 Ga are presumably metamorphic ages. The crust generation ages for HSA12 and HSA28 must therefore be older than 2.9 Ga, and the whole rock Pb-Pb age of 3.2 Ga may well represent the time of generation of their protoliths from the upper mantle. The previous discussion of the major and trace element data suggested that the Markt granulite xenoliths were genetically related, and that they were relatively unaffected by crustal contamination. In addition, the other xenolith samples from Markt have Sr and Nd isotope compositions similar to those of HSA12 and HSA28. Thus, it would appear that the protoliths of the Markt granulites were extracted from the mantle ~3.2 Ga ago.

In contrast to the Pb-Pb mineral-whole rock ages, the mineral-whole rock Sm-Nd isochrons from the same mineral assemblage in HSA12 yields a much younger age of 0.6 Ga. Thus, it seems clear that Nd isotope system of this sample has been reset on the scale of the individual mineral phases. Moreover, the Nd whole rock errorchron age of 1.2 Ga for the Markt

granulites is also much younger than the Pb-Pb ages. The Nd model ages of the Markt granulites vary from 0.3 to 3.9 Ga, and both HSA12 and HSA28 have Nd model ages (T_{DM} = 2.5 and 1.6 Ga, respectively), which are lower than the metamorphic age of 2.9 Ga inferred from the Pb-Pb mineral-whole rock isochron.

Mezger et al. (1992) undertook a geochronological study on several suites of granulite facies rocks, and showed that Sm-Nd garnet-whole rock ages were younger than the latest regional metamorphism, and significantly younger than U-Pb ages on the same minerals and zircons. On the bases of age differences and T-t path of these samples, they suggested that the Sm-Nd closure temperature in garnet is ~600 ±30 °C. Burton et al. (1993) also presented some high precision data on garnet-clinopyroxene-plagioclase assemblages from a corona structure in garnet-bearing granulites, which showed that Sm-Nd exchange in the corona continued for ~250 Ma after the closure of the U-Pb system. They concluded that the diffusion rates for Sm-Nd are significantly higher than those for U-Pb. Previous studies on granulite xenoliths from northern Lesotho yielded a range of metamorphic temperatures, from 500–1000° C, but most are higher than 600° C (Griffin et al., 1979; van Calsteren et al., 1986). The metamorphic temperature estimated from a Markt granulite (HSA32) is 780 ±40° C (van Calsteren et al., 1986). At this stage we infer that Nd isotopes were disturbed by a later event than that recorded by Pb isotopes, but closing temperature rates for U-Th-Pb systems are poorly constrained, and new experimental data should be a high priority.

3-5.2 *Granulite xenoliths from northern Lesotho*

The recalculated Sm-Nd errorchron for the whole rock granulite xenoliths from northern Lesotho gives an age of 1.24 ±0.17 Ga (Fig. 3-6), indistinguishable from that for the Markt granulites. In constrast to the granulites from Markt, however, the Pb isotope ratios from all but two of the northern Lesotho granulites (L12b and L13) lie on a relatively shallow $^{207}Pb/^{204}Pb$–$^{206}Pb/^{204}Pb$ array. If LQ4 is excluded, for the reasons outlined above, the calculated age is 1.49 ±0.36 Ga, similar to the Sm-Nd whole rock errorchron age. Thus, there is no evidence from either Pb or Nd isotopes for a significant contribution from Archaean material in the generation of these granulite precursors. The exceptions are L12b and L13, which have lower $^{207}Pb/^{204}Pb$ (Fig. 3-7a), and indicate that some Archaean material was present in northern Lesotho. The Sm-Nd mineral-whole rock data yield an age of 0.85 ±0.06 Ga for PHN2852, consistent with the age of 0.7 Ga for a garnet-whole rock pair from PHN1646 (van Calsteren et al., 1986).

In summary, the Pb-Pb trends for the granulite xenoliths from Markt and the Britstown Group yield Archaean ages, which appear to represent the time of separation from the upper mantle and an early granulite facies metamorphic event. Those from northern Lesotho, however, with the exception of two xenoliths with possible Archaean characteristics, yield Proterozoic ages. The Sm-Nd whole-rock age of the Markt granulite xenoliths, which is indistinguishable from that of the northern Lesotho granulites, appears to reflect the resetting of the Sm-Nd system in Archaean lower crust during the Proterozoic. The mineral-whole Nd data on both the northern Lesotho and Markt granulite xenoliths yield ages of 0.6–0.85 Ga, indicating that they had similar thermal histories after the formation of the Namaqua-Natal mobile belts. In the preferred explanation, the U-Pb system appears to be more likely to reflect a primary event than the Sm-Nd system, consistent with the results of other studies (Mezger et al., 1992;

Burton et al., 1993). Age information on samples from the lower crust should clearly be interpreted with extreme caution.

3-6. Composition of the Lower Crust in southern Africa

The above discussion suggests that the granulite xenoliths from localities around the margin of the Kaapvaal Craton came from both Archaean (the Markt and Britstown Group granulites) and Proterozoic lower crust (the northern Lesotho granulites). Both sets of granulite xenoliths have mafic major element compositions and similar trace element patterns. However, on $^{143}Nd/^{144}Nd$–$^{87}Sr/^{86}Sr$ (Fig. 3-5) and $^{207}Pb/^{204}Pb$–$^{206}Pb/^{204}Pb$ (Fig. 3-7a) diagrams, there are clear differences in the present day isotope ratios of the Markt/Britstown and northern Lesotho suites. The former exhibit greater scatter and, on average, lower present day Nd and higher Sr isotope compositions than the northern Lesotho granulites, and they have markedly different Pb-Pb arrays. As discussed above, these reflect whether xenoliths came from Archaean or Proterozoic lower crust, and hence the margin of the Archaean craton in the lower crust. On the surface, the margin of the Kaapvaal Craton is obscured by the sediments and lavas of the Karoo Supergroup. On the basis of seismic and gravity studies, the inferred margin passes through the north of the Markt/Britstown study area (Nixon, 1987). Cornell et al. (1986) analysed surface samples from Prieska and the Copperton area, and obtained crust generation ages of ~3 Ga for the Kheis Province around Prieska and 1.5~1.3 Ga for the samples from the Copperton formation in the Namaqua -Natal Belt. On the basis of those data, the surface boundary of the Archaean craton would pass through the centre of the Markt/Britstown Group xenolith localities (Fig. 3-1). However, the granulite samples analysed have yielded Archaean Pb-Pb ages, suggesting that in the lower crust the margin of the craton is displaced to the southwest.

3-7. Pb Isotope Evolution in the lithosphere

3-7.1 U Depletion

The Pb isotope composition of the lower crust is critical to whole Earth evolution models for U, Th and Pb. The upper crust has high U/Pb and so, with time, radiogenic Pb. Most of the Pb isotope data from upper mantle-derived rocks also tend to plot to the right of the Geochron and indicate that Pb, at least in the upper mantle, is also relatively radiogenic. From an investigation of siderophile and chalcophile element abundances in oceanic basalts, Newsom et al. (1986) argued that there is no evidence that mantle Pb isotopic compositions result from the continued extraction of Pb into the Earth's core over geologic time. The lower crust may have relatively low U contents and so be a reservoir for unradiogenic Pb to balance the radiogenic Pb of the upper crust and mantle (Newsom et al., 1986). Many Precambrian granulite terrains show depletion of U, K and Rb attributed to high grade metamorphism (Moorbath et al., 1969; Gray and Oversby, 1972; Weaver and Tarney, 1981), but this is not always the case (Ben Othman et al., 1984). In addition, many lower crustal xenoliths from alkali basalts, such as those from Camp Creek (Esperanca et al., 1988), Geronimo (Kempton et al., 1990) and the Kola Penisula (Kempton et al., 1993), have relatively radiogenic Pb isotope ratios.

A number of processes may fractionate U/Pb. U is more incompatible than Pb in silicate systems, particularly when plagioclase is present, and so gabbroic cumulates are likely to have low U/Pb as a primary feature (Rogers and Hawkesworth, 1982; Rudnick et al. 1990, Stosch et al., 1986). van Calsteren et al. (1986, 1988) suggested that (U/Pb in cumulates)/(U/Pb in magma) is ~0.5 on the basis of the cumulate model used by Rogers and Hawkesworth (1982) for appropriate U and Pb partition coefficients. Similarly, high grade metamorphism can cause U depletion because U is

preferentially removed in small degree melts or fluids, particularly in response to the breakdown of micas.

The present-day Pb isotope ratios of most granulites from southern Africa plot to the left of the Geochron, and so they have relatively unradiogenic Pb (Fig. 3-7). These low $^{206}Pb/^{204}Pb$ values reflect low time-integrated U/Pb, and Fig. 3-9a shows that they are generally accompanied by low K_2O/Al_2O_3. In addition, on a plot of Mg# vs K_2O/Al_2O_3 (Fig. 3-9b), two groups can be recognised which correspond to the two groups identified earlier, i.e. Mg# >68 and Mg# <68. The samples with low K_2O/Al_2O_3 have high Mg# as well as positive Eu anomalies (Fig. 3-9c), suggesting that they originated as cumulates. The petrogenesis of the second group is more difficult to assess, but may represent solidified melts. Pb isotope ratios correlate positively with K_2O/Al_2O_3 in each group. This relation can be explained if the liquid (or K-rich phases) control U, and plagioclase contains most of the Pb. Furthermore, the cumulate group tend to have lower Pb isotope ratios than the melt group (Fig. 3-9a). Thus, the low time integrated U/Pb ratios of the Markt granulites appear to reflect magmatic processes, which adds further support to the suggestion that the Pb-Pb errorchron age represents that of their protoliths.

The Archaean isochron displayed by the Markt granulite xenoliths yields an age of c. 3.2 Ga and a first stage μ ($^{238}U/^{204}Pb$) = 8.3. If their protoliths were derived from mantle with μ = 8.3, they had second stage μ between 3 and 8.3, with an average μ = 6. If the Pb isotope composition of PHN2588 has not changed much since 1.2 Ga, because of its low μ (0.01), the northern Lesotho granulite xenoliths have had an average μ of 3.5 since their generation. The granulite xenoliths from Markt and northern Lesotho display two trends on the $^{206}Pb/^{204}Pb$–$^{208}Pb/^{204}Pb$ diagram, indicating they have time integrated Th/U of ~3.3 and 3.9 respectively.

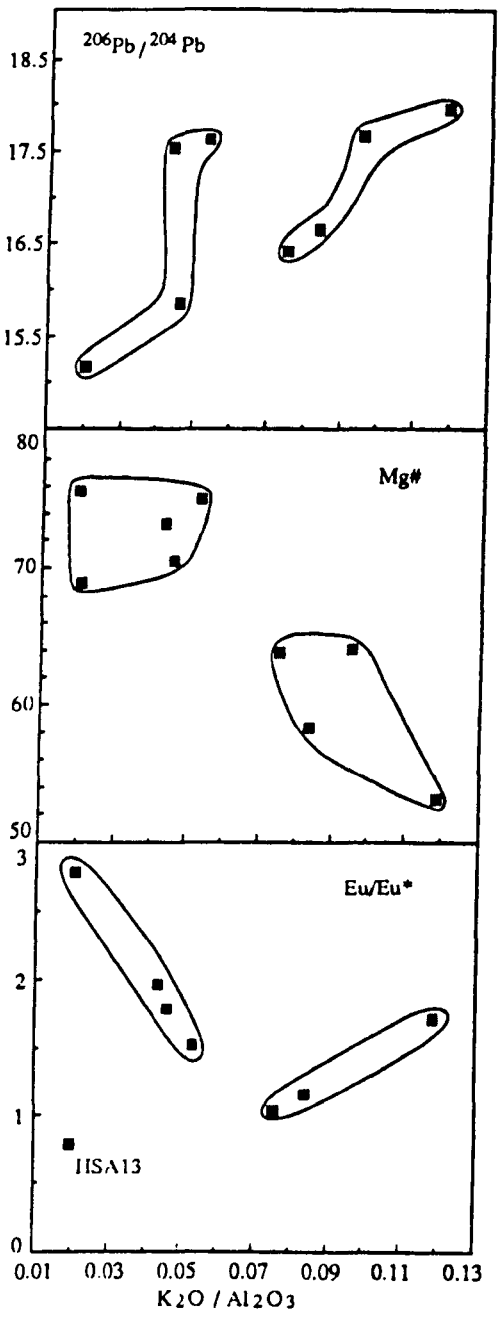

Figure 9 Diagrams illustrating the broad correlations between Pb isotopes Mg*, Eu/Eu* and K_2O/Al_2O_3 in the Markt granulites. The two trends observed on $^{206}Pb/^{204}Pb$ vs K_2O/Al_2O_3 correspond to the two Mg# groups. K_2O/Al_2O_3 represents relative proportion of K-phases to plagioclase feldspar and $^{206}Pb/^{204}Pb$ ratio reflects time integrated μ ($^{238}U/^{204}Pb$). The broad correlation between Pb isotopes and K_2O/Al_2O_3 ratios suggests that μ increases generally with K_2O/Al_2O_3 and so a K-phase and plagioclase control the U/Pb ratio in the granulites, and then, this control is attributed to the original magmatic processes.

3-7.2 Pb isotope evolution in the lower crust

The new Pb isotope data from the Proterozoic and Archaean granulite xenoliths provide a basis for more extended modelling of the Pb isotope compositions in the lower crust beneath southern Africa. Such crust can be considered to consist of segments generated during different orogenic events, each of which include juvenile material derived from the mantle, and remobilized crust. Since it was generated, each segment of the lower crust evolved with its own U/Pb ratio and consequently has its own characteristic Pb isotope ratios. In general, the Pb isotope ratios in a new segment are more radiogenic than those in older segments of the lower crust.

Using Nd isotope and $^{147}Sm/^{144}Nd$ ratios, and the inversion technique developed by Allègre and Rousseau (1984), continental crustal growth curves (CCGC) for southern Africa were computed by Harris et al. (1987) and Dia et al. (1990). Dia et al. (1990) concluded that more than 50% of the crust was generated in the Proterozoic, whereas Harris et al. (1987) suggested that half the southern Africa crust is Archaean and more than 90% was generated in the Precambrian. With these CCGC, and estimated Pb isotope ratios for different age segments, the evolution of Pb isotopes in the lower crust beneath southern Africa can be modelled. It is assumed that the Pb concentrations in each segment are similar, and that the geological history may be subdivided into four intervals: 0–0.5 Ga, 0.5–1 Ga, 1–2.5 Ga and >2.5 Ga.

Table 3-5 lists the time intervals, the percentage of crust formed during each episode, and the estimated Pb isotope ratios in each lower crustal segment. There are no data on 0–0.5 Ma and 0.5–1 Ga lower crust in southern Africa, and so their Pb isotope ratios were taken from Rudnick and Goldstein (1990). The data on the Proterozoic basic granulite xenoliths

in Table 3-3 were used for 1–2.5 Ga lower crust, and the Archaean granulite xenoliths were used for the >2.5 Ga segment. Model 1 and Model 2 are based on the CCGC Dia et al. (1990) and Harris et al. (1987), respectively, and the proportions of segments of the lower crust used in Model 3 are modified from Rudnick and Goldstein (1990).

TABLE 3-5 Models of present-day Pb isotope composition in the southern Africanlower crust

	0–500 Ma	500–1000 Ma	1000–2500 Ma	>2500 Ma
$^{206}Pb/^{204}Pb$	18.0	17.5	17.3	16.25
$^{207}Pb/^{204}Pb$	15.6	15.55	15.55	15.25
Model 1	9%	14%	60%	17%
Average of total the lower crust:		$^{206}Pb/^{204}Pb$: 17.2;		$^{207}Pb/^{204}Pb$: 15.5
Model 2	4%	6%	35%	55%
Average of total the lower crust:		$^{206}Pb/^{204}Pb$: 16.8;		$^{207}Pb/^{204}Pb$: 15.4
Model 3	32%	28%	22%	18%
Average of total the lower crust:		$^{206}Pb/^{204}Pb$: 17.4;		$^{207}Pb/^{204}Pb$: 15.5

The models are summarised in Table 3-5 and the results are displayed in Fig. 3-10. The present day Pb ratios for the lower crust in Model 1 are similar to those in Rudnick and Goldstein (1990) model 2, and Model 3 gives similar results to Model 1. Model 2 results in lower Pb isotopic ratios because it contains a greater contribution from Archaean crust. Such calculations demonstrate that the Pb isotope evolution of the lower continental crust can be modelled qualitatively. However, given the marked compositional differences between granulite terrains and xenolith suites the major uncertainty is which is more representative of the bulk lower crust (Rogers, 1977; Rudnick, 1990). Taylor and McLennan (1985)

pointed out that granulite terrains with very complex tectonic histories 'may be incomplete, atypical or non-random exposures of a highly heterogeneous lower crust', and that 'xenoliths may be less biased samples of the lower crust'. Griffin et al. (1979) suggested that the Lesotho lower crust contained 30–50% intermediate granulites, on the basis of its geophysical properties, but that is contrary to the low proportion of intermediate granulites in the kimberlite xenoliths. It is increasingly accepted that the relatively low U/Pb ratios in mafic granulites are primarily due to magmatic processes, and that intermediate surface granulites tend to be more depleted in U because of the breakdown of hydrous minerals (e.g. van Calsteren et al., 1986) and the preferential partitioning of U into fluids during granulite metamorphism. Thus, a major uncertainty in modelling the Pb isotope evolution of the lower crust is closely linked to the current uncertainty over its average major element composition.

3-7.3 Pb Isotope Evolution Model for the Continental Lithosphere

As argued above, the Pb isotope and U/Pb ratios of the basic granulite xenoliths from northern Lesotho and Markt primarily reflect the magmatic processes involved in the generation of their protoliths from the mantle. Thus, the data on these xenoliths can be compared with those from other mantle derived rocks to evaluate the Pb isotope evolution in the continental lithosphere beneath southern Africa.

The present day Pb isotope ratios of komatiites from the Kaapvaal Craton (Wilson and Carlson, 1989) lie on a similar array to the Markt granulites, and yield an age of 3.2 Ga (Fig. 3-10). Since both suites were derived from the upper mantle it is inferred that they reflect the U/Pb fractionation associated with melt generation in the mantle, and that other suites subsequently derived from similar source regions should plot within similar Pb-Pb arrays. Karoo picrites from Nuanetsi, and Group 2

kimberlites are characterised by unradiogenic Pb isotope ratios, compared with those from most oceanic basalts, and they are widely believed to have been largely derived from old, trace element enriched source regions within the mantle lithosphere (Ellam and Cox, 1989; Fraser and Hawkesworth, 1992, and reference therein). Both suites yield mid-Proterozoic model Nd ages, and they plot close to the intersection of the Proterozoic and Archaean arrays in Fig. 3-10.

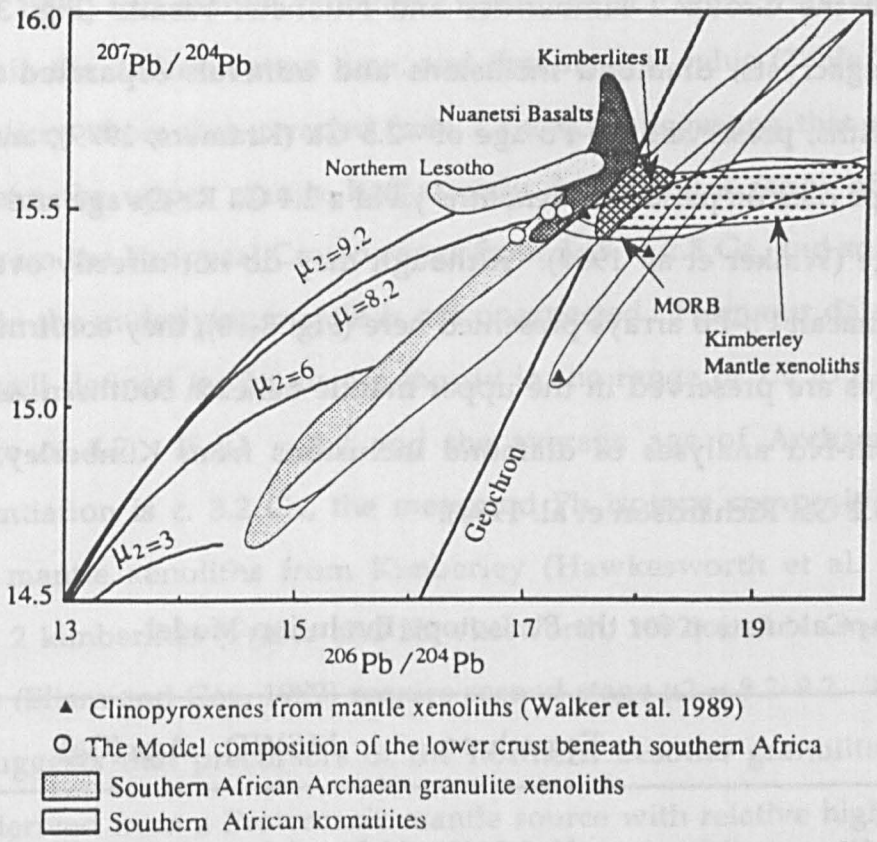

Fig. 3-10 Pb isotope evolution diagram. A two stage model illustrates the Pb isotope evolution in the continental mantle beneath southern Africa: stage one started at 4.55 Ga with μ_1 = 8.2, and differentiated at c. 3.2 Ga to 8.4 and 9.2 to account for the Pb compositions in the mantle, and in the granulite xenoliths from northern Lesotho. The trends formed by the Archaean granulite xenoliths and komatiites pass through the inferred Pb isotope composition of the continental mantle beneath southern Africa. See text for discussion. Data from: Esperanca et al. (1988); Dupre and Arndt (1990); Hawkesworth et al. (1990); Ellam and Cox (1989); Fraser and Hawkesworth (1992); Smith (1983), and this study. See Zindler and Hart (1986) for reference of MORB and OIB data.

Pb isotope data have also been published for several suites of mantle materials from southern Africa (Fig. 3-10). Amphibole- and phlogopite-bearing mantle xenoliths define a linear Pb-Pb array, with a shallow slope corresponding an age of 207 ±150 Ma, that is indistinguishable from the age of 150 ±20 Ma inferred from the Rb-Sr results (Hawkesworth et al., 1990). The present day Pb isotope ratios reflect a significant range in recent μ, but those of samples with low μ (<0.5) should be similar to the upper mantle at the time of metasomatism at ~150 Ma. Their unradiogenic Pb compositions overlap with the Group 2 kimberlites and Nuanetsi basalts (Fig. 3-10). Diopside megacrysts, diamond inclusions and minerals separated from mantle xenoliths, preserve a Pb-Pb age of ~2.5 Ga (Kramers, 1979), and Os and Pb isotope data on peridotite xenoliths yield a 2.4 Ga Re-Os age and a 3.4 Ga Pb-Pb age (Walker et al. 1989). Although they do not directly overlap with the Archaean Pb-Pb arrays presented here (Fig. 3-10), they confirm that Archaean ages are preserved in the upper mantle beneath southern Africa, as do the Sm-Nd analyses of diamond inclusions from Kimberley and Finsch (3.4–3.2 Ga, Richardson et al. 1984).

TABLE 3-6, μ_1 Calculation for the Pb Isotope Evolution Model

Data set	Errorchron	MSWD	Age (Ga)	μ_1
Markt granulite xenolith	Y=0.244*x+11.21	4.8	3.19±0.04	8.3
All the Archaean Granu.xeno.	Y=0.283*x+10.51	7.4	3.30±0.02	8.3
Kaapv. komatiite	Y=0.249*x+11.03	9.4	3.17	8.0
Barberton	Y=0.258*x+10.81	28	3.23	7.9
Belingwe	Y=0.184*x+12.30	0.05	2.69	8.4
Jagersfontein Cpx	Y=0.291*x+10.08		3.4	7.4
Kaapv. greenstone belt	Y=0.287*+10.64		3.4	8.4

Data from Wilson and Carlson (1989), Dupre and Arndt (1990), Walker et al. (1992) and this study. The errorchrons are recalculated by using Isochron Programme (Wright and van Calsteren, 1988). 0.1% errors for $^{206}Pb/^{204}Pb$ and $^{207}Pb/^{204}Pb$ ratios, T= 4.55 Ga, $\lambda_{235}=9.8485*10^{-10}$ and $\lambda_{238}=1.55125*10^{-10}$ are taken in our calculation.

The above discussion suggests that the Pb isotope ratios of Archaean crustal and mantle material reflect coupled mantle-crust evolution, and we have therefore used a simple two stage evolution to model the Pb isotope evolution in the upper mantle beneath southern Africa (Fig. 3-10). The Pb-Pb isochron of the granulite xenoliths from Markt defines an age of 3.2 Ga, and a first stage $\mu = 8.3$. If all the granulite xenoliths are included, the Pb-Pb array yields an age of 3.4 and first stage $\mu = 8.3$. Pb data published for the greenstone belts in southern Africa (Wilson and Carlson, 1989; Dupre and Arndt, 1990) and mantle xenoliths (Walker et al., 1989) were also used to constrain the differentiation time, and first stage μ value (Table 3-6). Such calculations show that μ varied from 7.3 to 8.9, suggesting that even in the Archaean the upper mantle had already developed a range of μ values. Ages from the Kaapvaal Craton range from 3.65 to 2.8 Ga, and so a range in U/Pb in the underlying mantle is not unexpected. From our data, μ values from well defined isochrons are mostly in the range of 7.9 to 8.4, with an average of 8.2. If $\mu 1 = 8.2$ and the average age of Archaean mantle differentiation is c. 3.2 Ga, the measured Pb isotope compositions of the low-μ mantle xenoliths from Kimberley (Hawkesworth et al. 1990), the Group 2 kimberlites (Fraser and Hawkesworth, 1992) and Nuanesti picritic basalts (Ellam and Cox, 1989) require second stage $\mu 2 = 8.2$–9.2. This model also suggests that precursors of the northern Lesotho granulite xenoliths were derived from a Proterozoic mantle source with relative high $\mu 2$, i.e. c. 9.2 to account for their relatively low $^{206}Pb/^{204}Pb$ and high $^{207}Pb/^{204}Pb$.

3-8. Conclusions

The Markt granulite xenoliths appear to be genetically related, and they have been subdivided into two groups; high Mg# samples with high Al_2O_3 represent cumulates and those with low Mg# and Al_2O_3 reflect more evolved compositions. The correlations between incompatible trace element abundances, Rb/Sr and Eu/Eu* and Al_2O_3 indicate that plagioclase

accumulation played a significant role in primary differentiation of the granulite precursors.

New Pb isotope data for granulite xenoliths from northern Lesotho yield an age similar to that from previous Sm-Nd studies (Rogers and Hawkesworth 1982), indicating extraction from the mantle at 1.2–1.4 Ga. In contrast, a Pb-Pb isochron from the granulites from Markt gives an age of 3.19 ±0.07 Ga, and the Britstown Group granulites have a similar Archaean age. These ages are supported by Pb-Pb mineral-whole rock ages of 2.9 Ga which are inferrred to be metamorphic ages. Thus, the generation of both the protoliths of the Markt and the Britstown Group granulites, was older than 2.9 Ga, consistent with their Pb-Pb whole rock ages of 3.2–3.4 Ga. However, these data contrast with the mineral and whole rock Sm-Nd results from the Markt and Britstown Group granulite xenoliths which yield ages of 0.6–0.85 Ga and ~1.4 Ga respectively. It appears the Sm-Nd, but not the Pb-Pb, system was reset during the formation of at least the lower crust in the Namaqua-Natal Belt.

The Archaean granulites tend to have higher $^{87}Sr/^{86}Sr$ and lower $^{143}Nd/^{144}Nd$ than the Proterozoic granulites, and markedly different Pb isotope arrays. A model for the evolution of Pb isotopes in the lower crust beneath the southern Africa is similar to that obtained by Rudnick and Goldstein (1990) for average lower crust. Most of the Pb isotope results from the southern African granulite xenoliths plot to the left of the Geochron and so reflect relatively low U/Pb ratios. It appears that the U-Pb system was surprisingly little affected by secondary processes, and that the time integrated U/Pb ratios primarily reflect magmatic processes associated with the generation of new crust.

Nuanetsi picrites and Group 2 kimberlites are thought to have been derived from old, trace element enriched source regions in the subcontinental mantle (Ellam and Cox, 1989; Fraser and Hawkesworth,

1992). Their Pb isotope ratios plot close to the Archaean fractionation trend expressed by the Markt granulite xenoliths which represent underplating of mantle derived magma in the Archaean. It is argued that much of the subcontinental mantle beneath southern Africa stablised in the Archaean, as also suggested by mantle xenolith studies (Richardson et al., 1984; Kinny et al., 1986; Boyd, 1989; Walker et al., 1989).

Chapter Four

Geochemistry and Petrogenesis of Basic Volcanism in Auckland, New Zealand

4-1. Introduction

The investigation of basaltic volcanism on continental terrains can provide information for melt generation processes and source compositions. However, the possibility of reactions between mantle-derived magmas and the continental crust contributes to the complexity of the investigations. Since the crust, in general, is silica rich, alkali basalts which are silica-undersaturated may be more likely to represent primitive, uncontaminated melts from mantle source regions.

In many areas, mafic continental volcanism has been attributed to source regions within the mantle lithosphere (Norry and Fitton, 1983; Hawkesworth et al., 1983; McDonough et al., 1985; Wörner et al., 1986; Gallagher, K. G. and Hawkesworth, 1992), which are generally considered to have high LILE abundances and enriched isotope compositions relative to oceanic basalts. Radiogenic isotope compositions in oceanic basalts are widely modelled in terms of contributions from different mantle components, i.e. DM, EMI, EMII and HIMU, and each component appears to be associated with distinct trace element patterns (Weaver 1991a, b), and the source regions of some oceanic island basalts are thought to be associated with deep seated mantle plumes. However, recent studies on continental alkali basalts show the similarities of trace element and isotope compositions between some continental and oceanic island basalts which indicate that they were derived from similar mantle source regions, and

therefore inferred to be within the sub-lithospheric mantle (Wörner et al. 1986; Adam, 1990; Francis and Ludden, 1990).

Continental intraplate volcanism is often attributed to lithosphere extension or mantle plumes, which may in turn be related to each other, and their relationship may vary from one area to another (Peate et al. 1990, Fitton et al. 1991, Smith 1993). However, where intraplate volcanism occurs soon after the cessation of subduction, such as those occur in Northland-Auckland Peninsula and Antarctic Peninsula, there is another possible magma generation mechanism in operation, such as in slab window models (Hole et al., 1991).

This study reports major, trace element and radiogenic isotope data on young volcanic rocks from the Auckland volcanic field in the Northland-Auckland Peninsula, New Zealand. It discusses their petrogenesis, and considers how these data shed new light on the geochemical features of their mantle sources and related mantle processes. It is argued that these rocks were derived from mantle source regions with geochemical features similar to HIMU, but at relatively shallow levels in the upper mantle.

4-2. General geology and previous research

New Zealand consists of two main islands, North and South Island, and it straddles an active boundary between the Pacific and Indo-Australian plates (Fig. 4-1). New Zealand is recognised as having been part of Gondwana, although relative to the continental crust of Australia and Antarctica, that in New Zealand is much younger. Recent geochronological studies of detrital zircons (Ireland, 1992) indicate that the basement paragneisses of the Western Province have maximum deposition ages of Ordovician to Devonian, followed by metamorphism in the Cretaceous, and the Torlesse greywake in North Island, New Zealand has a Permian - Triassic sedimentary age. However, some Archaean and Proterozoic

zircons have been identified and the age patterns are similar to those in some basement rocks from eastern Australia (Ireland, 1992).

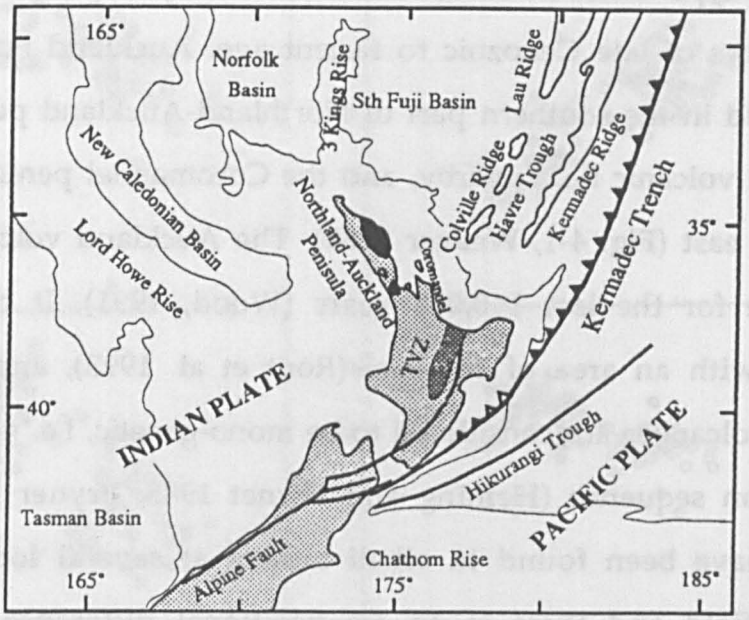

Fig. 4-1 A sketch map of the New Zealand plate tectonic setting. North Island sits on the Indian Plate which overrides Pacific Plate along Kemadec Trench. Present-day subduction related volcanism occurs at the Taupo Volcanic Zone (TVZ). The Auckland volcanic field is at the south end of the Northland-Auckland Peninsula, which is in the Indian Plate, 500 km away from the subduction zone.

The Pacific Plate is being subducted along a Wadati-Benioff zone westward under North Island which sits on the Indo-Australian plate. However, the Wadati-Benioff zone cuts through the north of South Island and dips eastward, indicating subduction of the Indo-Australian plate under the main part of South Island on the Pacific plate. The interaction of the two plates has directly or indirectly resulted in widespread volcanism. Cole (1986) proposed three volcanic regions, i.e. oceanic volcanism to the north of New Zealand, volcanism in North Island and in South Island.

Volcanism has been widespread in the north-west and central part of the North Island, with the latter including the currently active, subduction-

related Taupo Volcanic Zone (TVZ). In the Northland-Auckland Peninsula, three volcano/tectonic associations have been recognised (Smith et al., 1993): (i) an obducted ophiolite (Malpas et al. 1992), (ii) a lower Miocene arc-type andesitic suite, and (iii) a variety of predominantly basic volcanic rocks of late Cenozoic to Recent age. Auckland is the youngest volcanic field in the southern part of Northland-Auckland peninsula, with the Kerikeri volcanic field nearby, and the Coromandel peninsula volcanic field to the east (Fig. 4-1, Weaver 1989). The Auckland volcanic field has been active for the last 140,000 years (Wood, 1991). It consists of 49 volcanoes with an area of 360 km^2 (Rout et al. 1993), and most of the Auckland volcanoes are considered to be mono-genetic, i.e. generated from one eruption sequence (Heming and Barnet 1985; Bryner 1991). Mantle xenoliths have been found in alkali basalts at several locations of the Auckland field and there is no compositional difference between the volcanic rocks containing mantle xenoliths and those without the xenoliths (Rodgers et al. 1975). The Auckland volcanic field is about 500 km west of the present day subduction-related TVZ. Thus, volcanic activity is not directly related to present-day subduction (Fig. 4-1), but whether it should be attributed to back-arc basin volcanism behind a subduction zone, or to a mantle plume, is unclear (Weaver 1989). Previously published data show that the Auckland volcanic rocks are mainly silica under-saturated, unlike the present-day subduction related volcanic rock of the TVZ, or even those of the Northland volcanic field.

4-3. Geochemical Results

Major and trace elements on 9 samples and isotope ratios on 13 samples have been analysed at the Open University. To show the full range of compositions characteristic of the Auckland volcanic rocks, published (Heming and Barnet, 1985) and unpublished data (from Smith and Bryner) are also used in the discussion. Although the samples were collected from

different locations in the Auckland volcanic field, they seem to have a number of common geochemical characteristics.

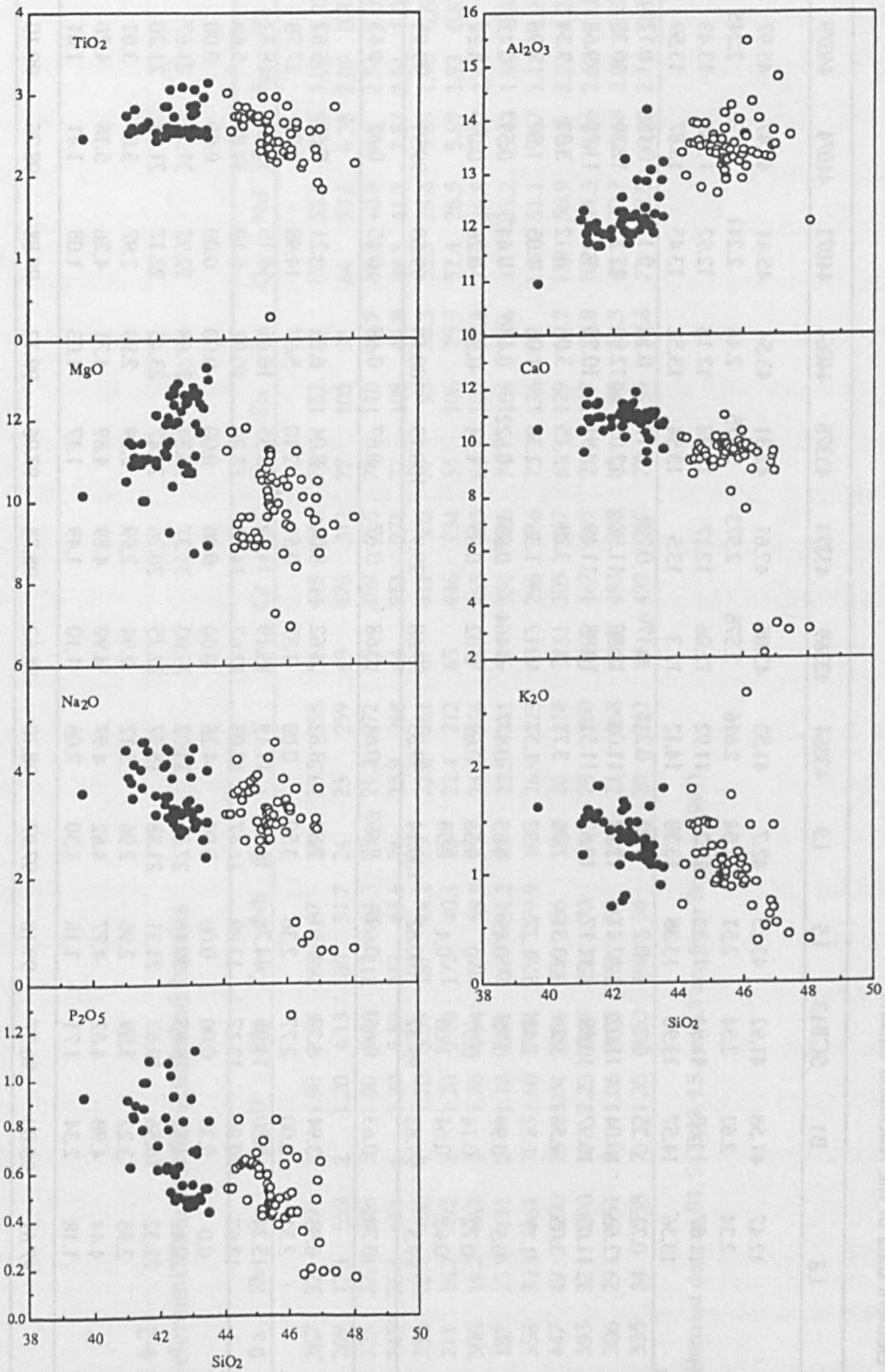

Fig. 4-2 Major element diagrams, illustrating the variations in major element compositions. The rocks can be divided into two groups; basanites (filled circles) with SiO_2 < 44% and alkali basalts (open circles) with SiO_2 mainly > 44%. The basanites tend to have lower Al_2O_3, but higher MgO, CaO and P_2O_5 than the alkali basalts.

TABLE 4-1
Major element data of the Auckland basalts

No.	L8	B1	SCB13	L5	L9	43364	43369	43374	43378	44064	44071	44074	44079	44093
SiO_2	42.47	41.58	41.92	43.25	42.7	41.53	43.05	42.61	42.31	43.54	45.44	42.47	45.97	41.27
TiO_2	2.34	2.62	2.54	2.51	2.54	2.616	2.578	2.573	2.575	2.48	2.241	2.726	2.245	2.823
Al_2O_3	11.87	11.63	11.94	12.23	12.24	11.92	12.06	12.17	12.28	12.18	12.92	11.68	13.43	12.00
Fe_2O_3	13.36	14.57	13.98	13.38	13.38	14.12	13.3	13.5	13.54	13.52	13.45	13.87	13.59	15.05
MnO	0.21	0.25	0.2	0.2	0.22	0.213	0.179	0.201	0.196	0.18	0.179	0.186	0.179	0.202
MgO	12.66	10.04	11.02	12.41	12.22	11.06	12.82	11.98	12.05	12.99	11.21	12.39	10.35	11.09
CaO	11.02	10.97	10.89	11.17	10.87	11.51	10.88	11.49	10.91	10.75	9.89	11.28	9.68	10.82
Na_2O	3.05	4.58	3.2	3.31	2.96	3.72	3.21	3.29	3.15	3.05	3.12	3.32	3.34	4.16
K_2O	1.17	1.82	1.41	1.27	1.32	1.57	1.12	1.36	1.36	1.06	1.05	1.3	0.96	1.56
P_2O_5	0.5	0.99	0.72	0.49	0.55	0.877	0.464	0.631	0.622	0.436	0.442	0.597	0.425	0.893
LOI	0.22	0.14	0.97	0	0.56	0.69	0.02	0.09	1.14	-0.06	-0.26	0.09	-0.24	-0.21
H_2O-	0.63	0.64	1.03	0.4	0.58									
Total	99.5	99.83	99.82	100.62	100.14	99.83	99.68	99.9	100.13	100.13	99.68	99.91	99.93	99.66
Mg#	0.701	0.63	0.661	0.697	0.693	0.64	0.68	0.67	0.67	0.68	0.65	0.67	0.63	0.62
or	6.91	3.94	8.33	7.51	7.80	3.82	6.62	8.04	8.04	6.26	6.21	7.68	5.67	3.95
ab	2.51	0.00	2.77	2.36	3.50	0.00	3.87	0.51	2.10	5.67	14.98	0.72	17.78	0.00
an	15.24	5.80	14.05	14.76	16.21	11.19	15.19	14.42	15.35	16.41	18.15	13.13	18.82	9.46
ne	12.62	20.99	13.17	13.89	11.67	17.05	12.62	14.80	13.30	10.91	6.19	14.83	5.68	19.07
lc	0.0	5.35	0.00	0.00	0.00	4.28	0.00	0.00	0.00	0.00	0.00	0.00	0.00	4.13
di	29.42	34.82	28.95	30.46	27.81	33.02	29.03	31.37	28.34	27.68	22.92	31.72	21.67	31.61
ol	22.32	16.56	19.87	21.31	21.88	18.57	22.35	20.26	21.47	23.45	22.17	21.01	21.20	19.72
mt	2.95	3.22	3.09	2.96	2.96	3.12	2.94	2.99	2.99	2.99	2.97	3.07	3.01	3.33
il	4.44	4.98	4.82	4.77	4.82	4.97	4.90	4.89	4.89	4.71	4.26	5.18	4.26	5.36
ap	1.18	2.34	1.71	1.16	1.30	2.08	1.10	1.49	1.47	1.03	1.05	1.41	1.01	2.12
SUM	97.61	98.00	96.77	99.18	97.97	98.10	98.62	98.78	97.96	99.12	98.88	98.75	99.10	98.76

Fe_2O_3=TFeO*0.2; major element data of L8, B1, SCB 13, L5 and L9 are from Bryner (1991)

TABLE 4-2
Trace element data for the Auckalnd basalts

	Ba	Rb	Sr	Pb	U	Th	Zr	Nb	Sc	Y	V	Co	Cr	Ni	Cu	Zn	La	Ce	Nd	Sm	Eu	Tb	Yb	Lu
43364	367	32	891	4	1.90	7.93	288	87	28	30.5	255	56	445	230	74	132	61	121	53.4	9.98	3.08	1.22	1.8	0.26
43369	269	17.1	559	2	1.20	4.13	180	51.7	24	23	259	69	476	312	77	105	31	64	30.6	6.38	2.09	0.9	1.55	0.23
43374	325	27.1	676	5	1.80	5.56	212	64.3	25	26.2	272	65	499	265	76	110	44.9	88.2	40.8	7.9	2.54	1.05	1.73	0.25
43378	345	26.6	624	6	2.30	5.59	213	64.6	24	25.9	268	64	513	271	71	108	44.9	89.8	41.2	7.87	2.54	1.09	1.78	0.25
44064	230	22.1	496	4	1.20	3.39	167	44.1	25	22.8	261	67	411	302	77	95	28.3	55.5	28.4	5.89	1.96	0.85	1.71	0.23
44071	211	16.7	492	1	1.20	3.20	172	40.1	23	22.4	212	65	446	234	55	106	25.3	52.4	26.5	5.69	1.93	0.87	1.61	0.22
44074	306	19.2	663	3	1.70	4.94	207	59.9	25	24.4	266	66	465	295	84	109	37.8	77.2	36.8	7.37	2.44	1	1.43	0.21
44079	187	15.9	491	2	1.10	2.91	166	34.2	22	23.5	211	59	354	226	74	106	23.4	47.9	25.2	5.42	1.88	0.84	1.56	0.23
44093	358	30.4	861	7	2.60	7.24	278	79.9	16	26.9	223	63	296	236	73	136	57	114	51.1	9.67	3.12	1.21	1.72	0.23
B1	447	49	900	24	3.04	8.56	308	86	18.8	26	218	74	305	187	61	129	69.2	130	56.9	10.8	3.22	1.2	1.65	0.25
SCB13	393	32	790	10	2.23	6.48	250	70	24	26	260	74.1	467	247	75	117	53.8	102	44.3	8.86	2.67	1.05	2.02	0.27
L5	306	29	551	9	1.06	4.03	181	50	25.2	21	268	66.4	493	298	85	98	33.5	65.1	30.7	6.48	2.06	0.85	1.65	0.22
L9	335	34	558	7	1.35	4.53	190	56	25.5	20	262	64	499	287	77	99	37.6	73	32.5	6.99	2.14	0.85	1.71	0.25

Trace element data of B1, SCB 13, L5 and L9 are from Bryner (1991)

4-3.1 Major and trace elements

The new results obtained at the Open University on 9 samples (Table 4-1, 2) are generally consistent with the previous data, and together they show that the Auckland samples are silica undersaturated (SiO_2 40 - 48%, Fig. 4-2) with total alkali contents in the range 4 - 6.2%. This is very different from the Northland volcanic rocks which tend to have SiO_2 > 48% and are discussed in the next chapter. In addition, although the Auckland basalts are from different volcanoes, they display broad correlations in major elements and similar geochemical characteristics, and they appear to fall into two groups on the TAS classification (Le Maitre 1989). The higher silica samples have SiO_2 > ~44% (including new samples 44071 and 44079) and are here termed alkali basalts, and the lower silica samples with SiO_2 < ~44% are termed basanites (including the rest of the new data).

On major element diagrams (Fig. 4-2), it can be seen that the Auckland alkali basalts and basanites have different compositions with a compositional gap at SiO_2 ~44%. On the TiO_2-SiO_2 diagram some of the alkali basalts tend to have lower TiO_2 and so define a broad negative correlation between TiO_2 and SiO_2, whereas the basanites have higher TiO_2 and no clear correlation between TiO_2 and SiO_2 (Fig. 4-2a). The alkali basalts have higher Al_2O_3, in addition to higher SiO_2, than the basanites and they plot together on a positive trend between Al_2O_3 and SiO_2 (Fig. 4-2b). In contrast, CaO and MgO are lower in the alkali basalts than in the basanites, although, the Na_2O contents are similar (Fig. 4-2c, d, e). The alkali basalts and basanites both have broad negative correlations between K_2O and P_2O_5 with SiO_2, and the alkali basalts have lower K_2O as well as higher SiO_2 than the basanites. However, the former have higher SiO_2 relative to K_2O and P_2O_5, and so the alkali basalts and basanites plot on different trends on these diagrams (Fig. 4-2f, g). A few alkali basalts, which are from Heming and Barnet (1985), have significantly lower CaO, K_2O, Na_2O and P_2O_5 than

the other samples in this group (Fig. 4-2d-g) and the reason for this is unknown.

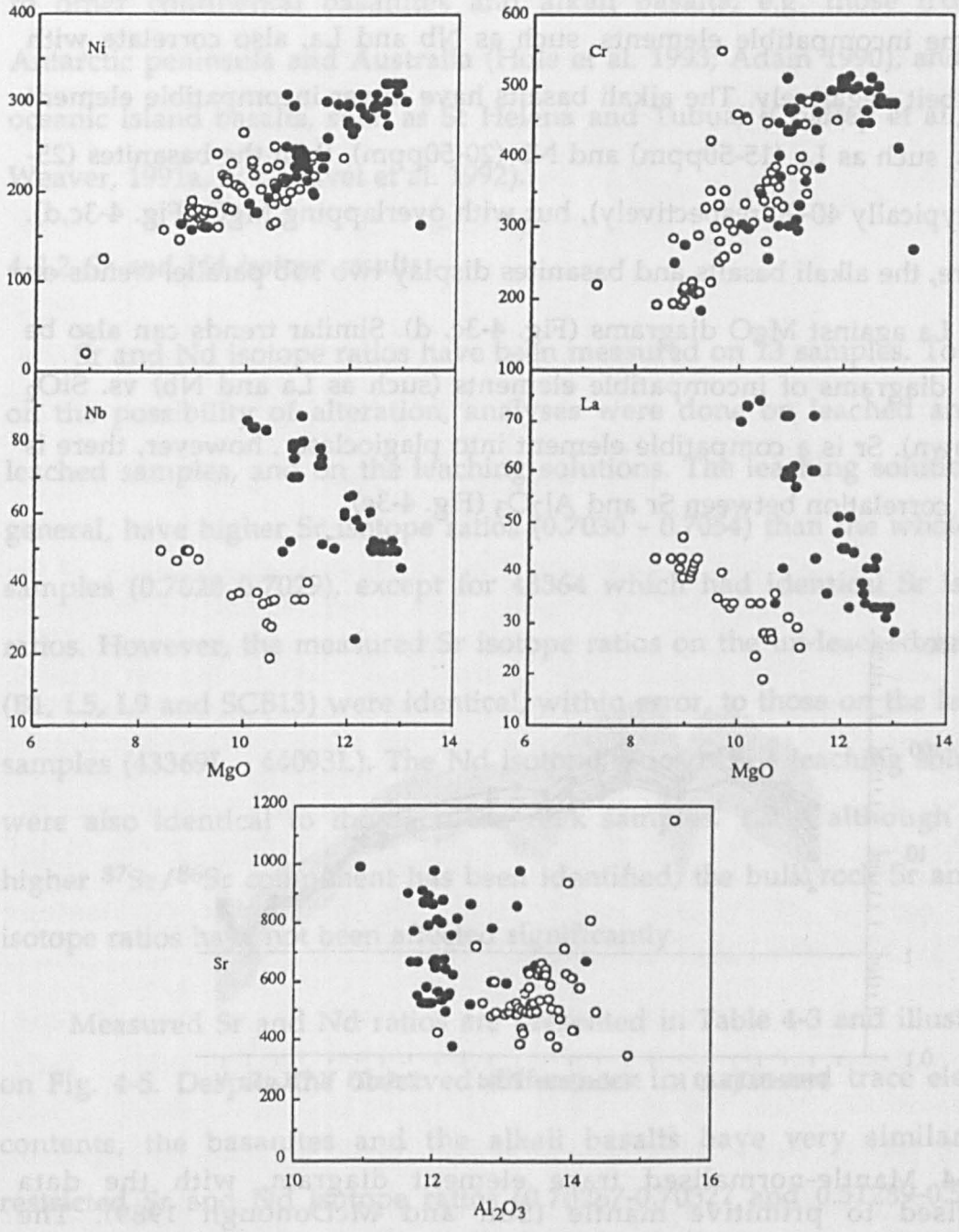

Fig. 4-3 Major and trace element variation diagrams; showing compatible elements correlate positively with MgO in both the basanites and alkali basalts (a, b), and incompatible element correlation negatively between Nb and La, with MgO (c, d). The basanites and alkali basalts exhibit parallel trends in these diagrams. (e) Sr vs. Al_2O_3 diagram, even though Sr is compatible in plagioclase, there is no clear correlation between Sr and Al_2O_3.

Compatible elements, such as Ni and Cr, correlate with MgO in both the alkali basalts and basanites and plot on similar trends on Fig. 4-3a, b.

However, the basanites tend to have higher MgO and higher Ni and Cr contents than the alkali basalts.

Some incompatible elements, such as Nb and La, also correlate with MgO, albeit negatively. The alkali basalts have lower incompatible element contents, such as La (15-50ppm) and Nb (20-50ppm), than the basanites (25-70 and typically 40-90 respectively), but with overlapping MgO (Fig. 4-3c,d). Therefore, the alkali basalts and basanites display two sub parallel trends on Nb and La against MgO diagrams (Fig. 4-3c, d). Similar trends can also be seen on diagrams of incompatible elements (such as La and Nb) vs. SiO_2 (not shown). Sr is a compatible element into plagioclase , however, there is no clear correlation between Sr and Al_2O_3 (Fig. 4-3e).

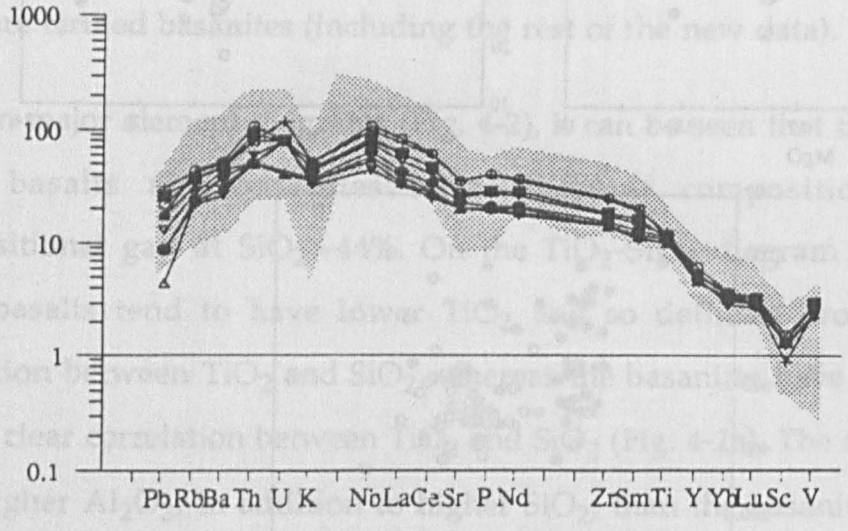

Fig. 4-4 Mantle-normalised trace element diagram, with the data normalised to primitive mantle (Sun and McDonough 1989). The Auckland basalts show incompatible element enriched patterns with maxima at Nb, Th and U. The low LIL elements relative to Nb are similar to HIMU OIB (Chaffey et al., 1989; Chauvel et al. 1992), which is shown by shaded field.

Although there are several differences in the geochemical features of the alkali basalts and basanites, they all exhibit broadly similar mantle-normalised incompatible element profiles (Fig. 4-4). These are characterised by high incompatible element contents, maxima in the region of Nb and

Ta, and relatively low LILE and LREE. Consequently, they have high Nb/Ba, Nb/Rb and Nb/La ratios (Table 4-5). These characteristics are similar to other continental basanites and alkali basalts, e.g. those from the Antarctic peninsula and Australia (Hole et al. 1993; Adam 1990), and some oceanic island basalts, such as St Helena and Tubuai (Chaffey et al., 1989; Weaver, 1991a, b; Chauvel et al. 1992).

4-3.2 Sr and Nd isotope results

Sr and Nd isotope ratios have been measured on 13 samples. To check on the possibility of alteration, analyses were done on leached and un-leached samples, and on the leaching solutions. The leaching solutions, in general, have higher Sr isotope ratios (0.7030 - 0.7054) than the whole-rock samples (0.7028 0.7029), except for 43364 which had identical Sr isotope ratios. However, the measured Sr isotope ratios on the un-leached samples (B1, L5, L9 and SCB13) were identical, within error, to those on the leached samples (43369L - 44093L). The Nd isotope ratios of the leaching solutions were also identical to those on the rock samples. Thus, although some higher $^{87}Sr/^{86}Sr$ component has been identified, the bulk rock Sr and Nd isotope ratios have not been affected significantly.

Measured Sr and Nd ratios are presented in Table 4-3 and illustrated on Fig. 4-5. Despite the observed differences in major and trace element contents, the basanites and the alkali basalts have very similar and restricted Sr and Nd isotope ratios (0.70287-0.70327 and 0.51289-0.51315, respectively). Thus, they are all depleted relative to the bulk Earth, but relative to MORB, they have lower $^{143}Nd/^{144}Nd$ at a given $^{87}Sr/^{86}Sr$, and they are therefore displaced from the MORB field, towards HIMU OIB, such as St Helena (Fig. 4-5).

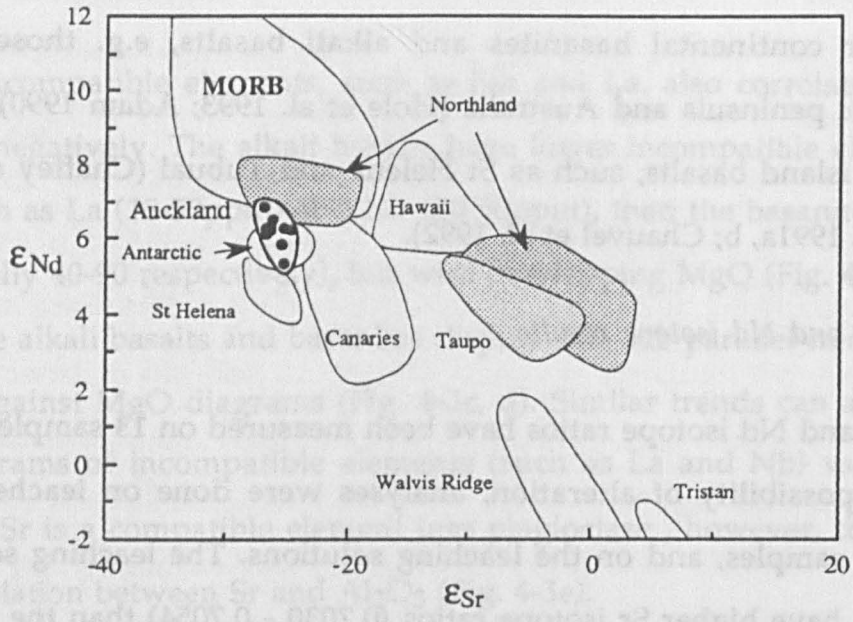

Fig. 4-5 εNd vs. εSr, illustrating the Nd and Sr isotope compositions of the Auckland basalts, together with other data from Northland, Antarctic Peninsula, MORB and OIB for comparison (White and Hofmann 1982; Richardson et al. 1982; Ito et al. 1987; Chaffey et al., 1989; Le Roex et al. 1990; Hoernle et al. 1991; Graham et al. 1992; Chauvel et al. 1992; Hole et al. 1993; and Chapter V in this study). The basanites and alkali basalts have similar Nd and Sr isotope ratios, and these are also similar to the basalts from Antarctic Peninsula. Relative to MORB they have similar Sr but lower Nd isotopes. The samples from the Northland volcanic field, north of the Auckland field in Northland-Auckland Peninsula plot in two separate fields, one of which has much higher Sr and lower Nd isotope compositions. These will be discussed in ChapteV.

4-3.3 Pb isotope ratios

Pb isotope ratios have been analysed for 13 samples and data on leached and un-leached samples (Table 4-4) appear to vary more than Sr and Nd isotopes. $^{206}Pb/^{204}Pb$ in the un-leached samples varies from 17.04 to 19.27 and those in the leached samples = 18.2 - 19.27. Measured $^{206}Pb/^{204}Pb$ in the leaching solutions (16.77 -19.25) are in general lower than those from both the un-leached and leached rock samples. The differences between the leached and un-leached samples can be expressed as $D^{206}Pb = (^{206}Pb/^{204}Pb)_{leached} - (^{206}Pb/^{204}Pb)_{un\text{-}leached}$. In Fig. 4-6, it can be seen that there is a negative correlation between $D^{206}Pb$ and $^{206}Pb/^{204}Pb$. Thus, the

TABLE 4-3
Sr and Nd isotope data of the Auckland basalts

	$^{87}Sr/^{86}Sr_l$	εSr	$^{143}Nd/^{144}Nd_l$	εNd	$^{87}Sr/^{86}Sr_{ls}$	$^{143}Nd/^{144}Nd_{ls}$
43364	0.70280	-26.98	0.51296	6.28		0.512910
43369	0.70290	-25.54	0.51296	6.83	0.705403	0.512920
43374	0.70283	-26.55	0.51297	6.34	0.703954	0.512978
43378	0.70279	-27.09	0.51299	6.89	0.703354	0.512984
44064	0.70283	-26.48	0.51296	6.26	0.702989	0.512988
44071	0.70281	-26.76			0.703499	
44074	0.70286	-26.07				
44079	0.70275	-27.66				
44093	0.70280	-27.00	0.51295	6.13		
B1	0.70290	-25.59	0.51294	5.87		
SCB13	0.70294	-25.03	0.51296	6.28		
L5	0.70284	-26.35	0.51298	6.53		
L9	0.70291	-25.43	0.51292	5.36		

l - measurements from leached samples; ls - measurements of leaching solution;

TABLE 4-4
Pb isotope data of the Auckland basalts

	$\frac{^{206}Pb}{^{204}Pb^u}$	$\frac{^{207}Pb}{^{204}Pb^u}$	$\frac{^{208}Pb}{^{204}Pb^u}$	$\frac{^{206}Pb}{^{204}Pb^l}$	$\frac{^{207}Pb}{^{204}Pb^l}$	$\frac{^{208}Pb}{^{204}Pb^l}$	$\frac{^{206}Pb}{^{204}Pb^{ls}}$	$\frac{^{207}Pb}{^{204}Pb^{ls}}$	$\frac{^{208}Pb}{^{204}Pb^{ls}}$
43364	19.307	15.585	38.895	19.329	15.584	38.914	19.303	15.561	38.827
43369	19.195	15.568	38.770	19.184	15.563	38.764	19.109	15.575	38.713
43374	19.126	15.587	38.759	19.193	15.578	38.786	17.695	15.539	37.484
43378	19.315	15.595	38.923	19.327	15.574	38.882	18.972	15.565	38.559
44064	19.243	15.594	38.867	19.107	15.525	38.624	19.097	15.575	38.7
44071	19.178	15.589	38.811	19.183	15.569	38.764			
44074	19.295	15.574	38.855	19.176	15.58	38.778	19.136	15.578	38.731
44079	19.170	15.593	38.807	19.294	15.572	38.851	19.08	15.579	38.693
44093	19.106	15.569	38.703	19.314	15.569	38.863	18.869	15.554	38.475
B1	18.625	15.575	38.379	18.885	15.594	38.627			
SCB13	17.55	15.451	37.094	18.319	15.529	37.949	17.281	15.473	36.949
L5	17.059	15.422	36.611	18.227	15.523	37.859	16.813	15.44	36.484
L9	19.1834	15.531	38.627	19.251	15.59	38.862	18.984	15.558	38.548

u - unleached sample; l - leached sample; ls - leaching solution;

samples with low un-leached Pb isotope ratios have larger differences (high $D^{206}Pb$) between the un-leached and leached measurements, whereas those with high Pb isotope ratios show little difference between the un-leached and leached measurements ($D^{206}Pb \sim 0$). In addition, there is a negative correlation between Pb isotope ratios and Pb contents, such that those samples with lower Pb isotope ratios have higher Pb contents. Whatever the cause it would appear that the three samples (L5, SCB13 and B1), with lower Pb isotope ratios and higher Pb contents than the rest of the samples, may have had their Pb isotope ratios modified significantly.

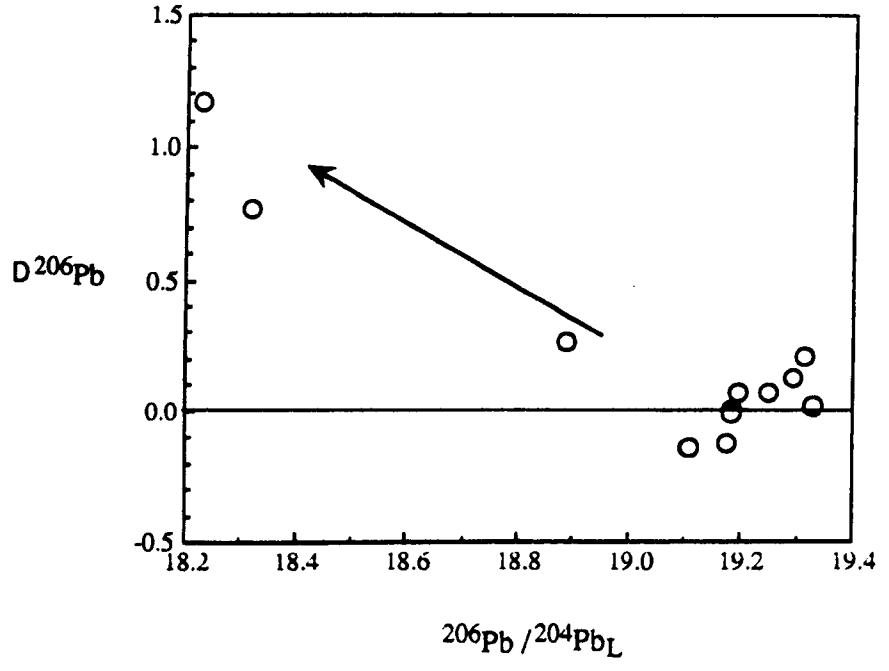

Fig. 4-6 $D^{206}Pb$ vs. $^{206}Pb/^{204}Pb$, showing the relationship between $^{206}Pb/^{204}Pb$ and the difference in $^{206}Pb/^{204}Pb$ between the unleached and leached samples. There is a negative correlation which is considered to be evidence that the samples with low $^{206}Pb/^{204}Pb$ experienced more alteration.

It is difficult to estimate what the alteration component may have been but it would appear to have had lower Pb isotope ratios than the lowest one measured in either the un-leached samples or the leaching solutions. The lowest $^{206}Pb/^{204}Pb$ (16.77) was obtained from the leaching

solution on sample L5, which also has the lowest un-leached Pb isotope ratios (17.06). Because there are no significant differences in the major and trace element patterns, and the Sr and Nd isotope compositions between the altered and unaltered samples, the alteration component either had very low concentrations of these elements or similar Nd and Sr isotope ratios to the bulk rocks. This may exclude any crustal component. Lead addition from petrol is a possible component. Most additives have more radiogenic Pb isotope ratios ($^{206}Pb/^{204}Pb \sim 18$) than that inferred from these samples, however, some have unradiogenic Pb isotope signature (Chow, 1970), with $^{206}Pb/^{204}Pb \sim 16.0$, and that might have been responsible for the lower Pb isotope ratios in some of the samples.

The variation of Pb isotope ratios in the unaltered samples is very limited ($^{206}Pb/^{204}Pb$ 19.06~19.2; Fig.4-8a,b), and they plot at relatively high ratios within the MORB field on the North Hemisphere Reference Line (NHRL, Hart 1984). Thus, they are similar to some young continental basalts, such as those from the Antarctic peninsula (Hole et al. 1993), but significantly less radiogenic than those from HIMU OIB (e.g. St Helena, Fig. 4-7).

The geochemical features of the Auckland basalts are summarised in Table 4-5 and it can be seen that they are similar to some OIB. Their Sr and Nd isotope and trace element ratios, Nb/Ba, Nb/Rb, and Nb/La, are more similar to the HIMU OIB than the others, however, with lower Pb isotope ratios than HIMU OIB, i.e. St Helena and Tubuai.

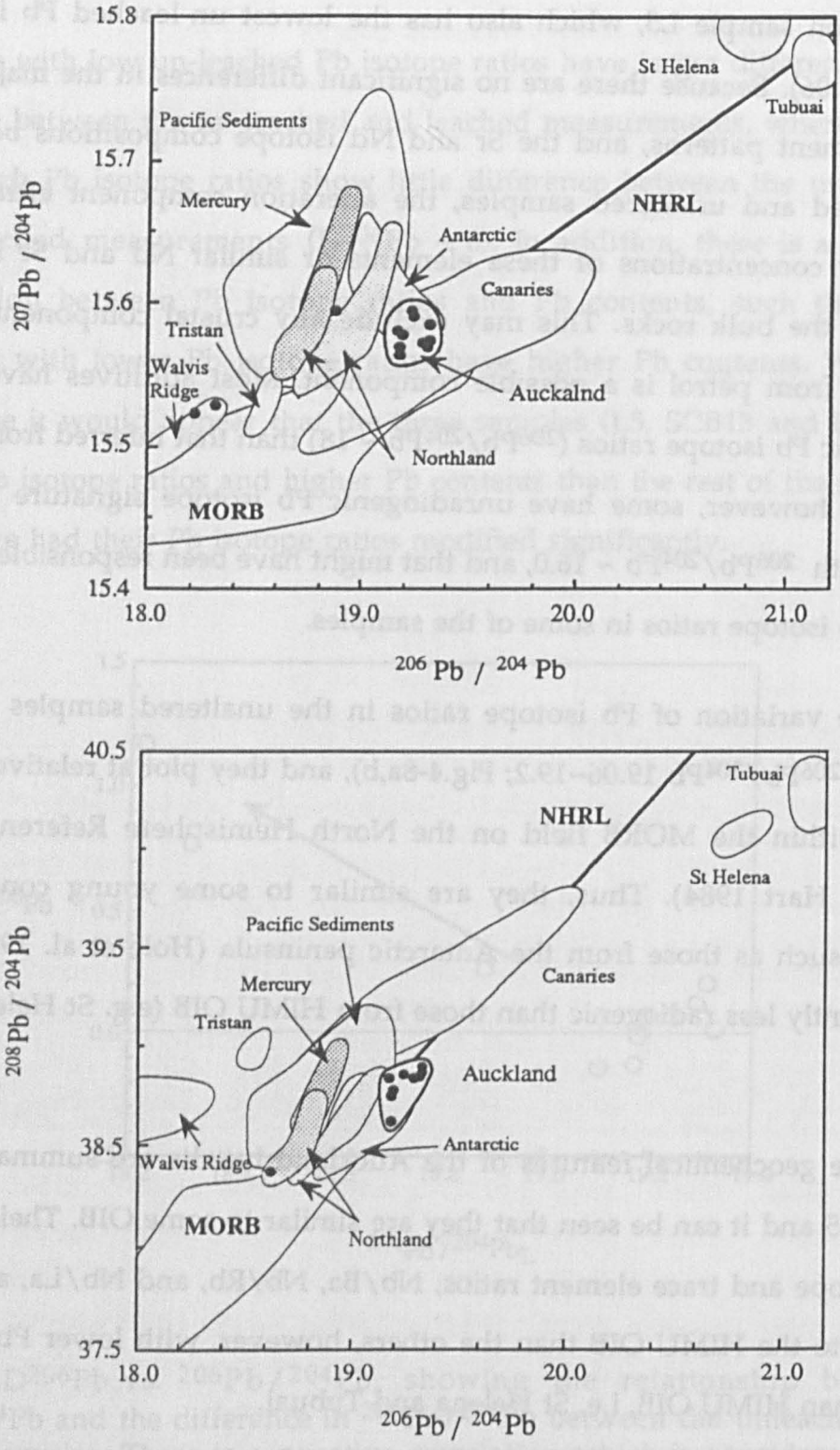

Fig. 4-7 (a) $^{207}Pb/^{204}Pb$ and (b) $^{208}Pb/^{204}Pb$ against $^{206}Pb/^{204}Pb$ diagrams, illustrating the Pb isotope compositions in the Auckland samples. Other data from the Northland volcanic field, Mercury Island in the Coromandel Volcanic Zone, Antarctic Peninsula, some OB and Pacific sediments are also plotted for comparison (Ben Othman et al. 1989; McDermott and Hawkesworth 1991 and others see Fig. 4-5 for data sources). The Auckland basalts have very restricted on Pb isotope ratios, and they are plot on NHRL (Hart 1984) between MORB and HIMU OIB, e.g. St Helena and Tubuai. Their relatively low $^{207}Pb/^{204}Pb$ and $^{208}Pb/^{204}Pb$ are very different from those for the Pacific sediments, consistent with their intraplate tectonic setting. The samples from Northland, north of Auckland on the Northland-Auckland Peninsula, show two groups of Pb isotopes and their implications will be discussed in Chapter V.

TABLE 4-5
Comparison of incompatible trace element and isotope ratios

	Nb/Ba	Nb/Rb	Nb/La	Ba/La	Ba/Th	$^{87}Sr/^{86}Sr$	$^{144}Nd/^{143}Nd$	$^{206}Pb/^{204}Pb$
N-MORB	0.23	2.78	0.93	4.0	60	0.7029	0.5132	18.5
Continental crust	0.02	0.21	0.45	25.0	124			
EMI								
Walvis Ridge (227)	0.08		1.09	15.1		0.70412	0.51256	18.24
Tristan	0.09	1.14	1.16	13.2	103	0.70505	0.51254	18.55
EMII								
Tutuila	0.14	1.69	1.12	8.3	67	>0.706		
HIMU								
St Helena	0.17	2.63	1.45	8.7	77	0.70293	0.51289	20.71
Tubuai	0.20	2.86	1.39	6.9	49	0.70285	0.51289	21.09
Young basalts								
Auckland	0.18	2.55	1.32	7.4	62	0.70284	0.51296	19.25
Antarctic Peninsula	0.24	2.38	1.32	6.1	45	0.70297	0.51293	19.07

Data from Weaver (1991), Hole et al (1993), Richarson et al. (1982) and this study

4-4. Crustal Assimilation Processes

The Auckland basalts have low silica contents (40-48%), but high MgO contents (most > 9%). Except for a few samples with apparently altered Pb isotope ratios, they generally have narrow ranges of isotope compositions, with low $^{87}Sr/^{86}Sr$ and high $^{143}Nd/^{144}Nd$. Although the Auckland alkali basalts have higher silica contents than the basanites, they have indistinguishable Sr, Nd and Pb isotope ratios. Crustal components may vary widely in their major, trace element and isotope ratios, but, in general, they tend to have high SiO_2, low MgO contents, and high Sr but low Nd isotope ratios. Thus, it appears that the Auckland basalts have not been contaminated significantly by crustal material en route to the surface.

4-5. Fractional Crystallisation

The samples analysed show systematic variations in major and trace element contents, but they have very similar Sr, Nd and Pb isotope ratios.

Fractional crystallisation processes may therefore have been, at least partly, responsible for the compositional variations in the basanites and alkali basalts.

MgO and the compatible trace elements are sensitive to low pressure fractionation, and there is a positive correlation between MgO and Ni in the Auckland rocks (Fig. 4-3a) and negative correlations between MgO and incompatible trace elements. Such correlations seem consistent with olivine fractional crystallisation, which may in turn imply that some of these rocks may be related to one other by fractional crystallisation processes. Because the alkali basalts and basanites plot on different trends they seem unlikely to be related each other by fractionation.

Phenocrysts in the Auckland basalts include olivine, clinopyroxene and plagioclase, although the latter two are not common (Smith per. comm.), and there are some microprobe analyses data (Bryner 1991). One way to test for fractional crystallisation is to use major element least-squares models (Mason 1987). The essential idea is that mineral phases which crystallise from a magma will segregate from it and so change the composition of the melt. Thus, the composition of a less evolved melt can be expressed as certain proportions of the crystallised mineral phases and the composition of a more evolved melt.

Using the average values of microprobe data from phenocrysts in the Auckland basalts (Bryner 1991), major element least-square calculations have been undertaken and the results (shown in Appendix C-3-1) indicate that the alkali basalts cannot be generated by fractional crystallisation from basanites, because the calculated least-square residual is very large (~ 1, see Appendix C-3-1). This is consistent with separate trends for incompatible trace elements plotted against MgO (Fig. 4-3). Such calculations indicate that the basanites could be related to one another by fractional crystallisation, and that the most evolved rocks, such as B1, B3 and B7 which tend to have

relatively low MgO and high incompatible element contents, may have undergone up to more than 30% fractional crystallisation.

However, there are some problems with this model. The calculated fractionation assemblages contain, in average, only 32% olivine, and 34% plagioclase. In contrast, most of the phenocrysts observed in the Auckland basalts are olivine, plagioclase is mainly in the groundmass, rather than as phenocrysts which might be separated from the melts and clinopyroxene is not common (Smith per. comm.; Bryner 1991), consistent with their high MgO contents (most > 9%). In addition, that Sr variation does not correlate with Al_2O_3 in the alkali basalts and basanites (Fig. 4-3) indicates the Sr contents are not controlled by fractionation of plagioclase. Thus, olivine may be considered as the major mineral phase which segregated from the Auckland basalts (see also McKenzie and O'Nions 1993).

The effects of olivine fractionation are relatively easily calculated. Olivine is a major component in the mantle with Mg#~90 or [Fe/Mg] ~0.111. Melts generated in equilibrium with mantle olivine should have Mg# ~73 or [Fe/Mg] ~0.37, provided $[Fe/Mg]_{olivine}/[Fe/Mg]_{melt} = 0.3$ (Roedder and Emslie, 1970). To correct for olivine fractionation, $[Fe/Mg]_{melt}$ was calculated from the bulk rock composition of the samples, and the olivine composition in equilibrium with each sample was calculated using $[Fe/Mg]_{olivine}/[Fe/Mg]_{melt} = 0.3$ and (Fe+Mg)/Si=2. Then 1% olivine was added and the composition of the whole rock was recalculated; this was repeated until Mg# (assuming that Fe_2O_3 = 20% total FeO) in the calculated whole rock reached the primary value. Because the calculated Ni values, using the model of Hart and Davis (1978), in some samples are unrealistically high (> 700 ppm) if Mg# ~73 is used for primary melts for the Auckland basalts, all the Auckland samples have been corrected to Mg#~71, with which equilibrated olivine would have had Mg# ~ 89.

Such calculations show that olivine fractionation in the alkali basalts was in the range 1% to 17% with an average of ~ 7%, and 1- 12% in the basanites. The corrected data have different MgO and TFeO, slightly different SiO_2, relative to uncorrected data, whereas the other major and incompatible trace element abundances are simply diluted by the olivine fractionation correction. Ni contents in those samples with relatively low Mg# but high incompatible element abundance are increased significantly, so that the negative correlation in the uncorrected data between Ni and Nb becomes a positive correlation with the corrected data. Because of uncertainties in partition coefficient for Cr, its corrected values were not calculated.

Some of the corrected data are illustrated on Fig. 4-8. The corrected data show that the alkali basalt primary magmas have 44 - 48% SiO_2 and MgO = 10 to 14%, whereas the basanites have SiO_2 and MgO between 41 - 44% and 11 - 15%, respectively. The other major element relationship between the corrected alkali basalts and basanites are similar to those of the uncorrected data on Fig. 4-2, and the corrected alkali basalts still have higher SiO_2 and Al_2O_3, and lower CaO, K_2O and P_2O_5 than the corrected basanites, but similar MgO and, in general, there is a significant range in SiO_2 and total Fe (TFeO) for a relatively restricted range in MgO.

Most trends between the corrected major and incompatible trace elements and between different incompatible trace elements, are similar to those in the uncorrected data. The corrected alkali basalts still tend to have lower incompatible element contents than the basanites. For example, average values of corrected Nb and La are 34±7 (1σ) and 30 ± 6 (1σ) ppm in the former and 60±11 (1σ) and 47 ± 12 (1σ) ppm in the basanites. These incompatible trace elements correlate negatively with SiO_2 and Al_2O_3, although, the alkali basalts and basanites define two broadly parallel clouds in the MgO-c and CaO-c vs. Nb-c diagrams (Fig. 4-8).

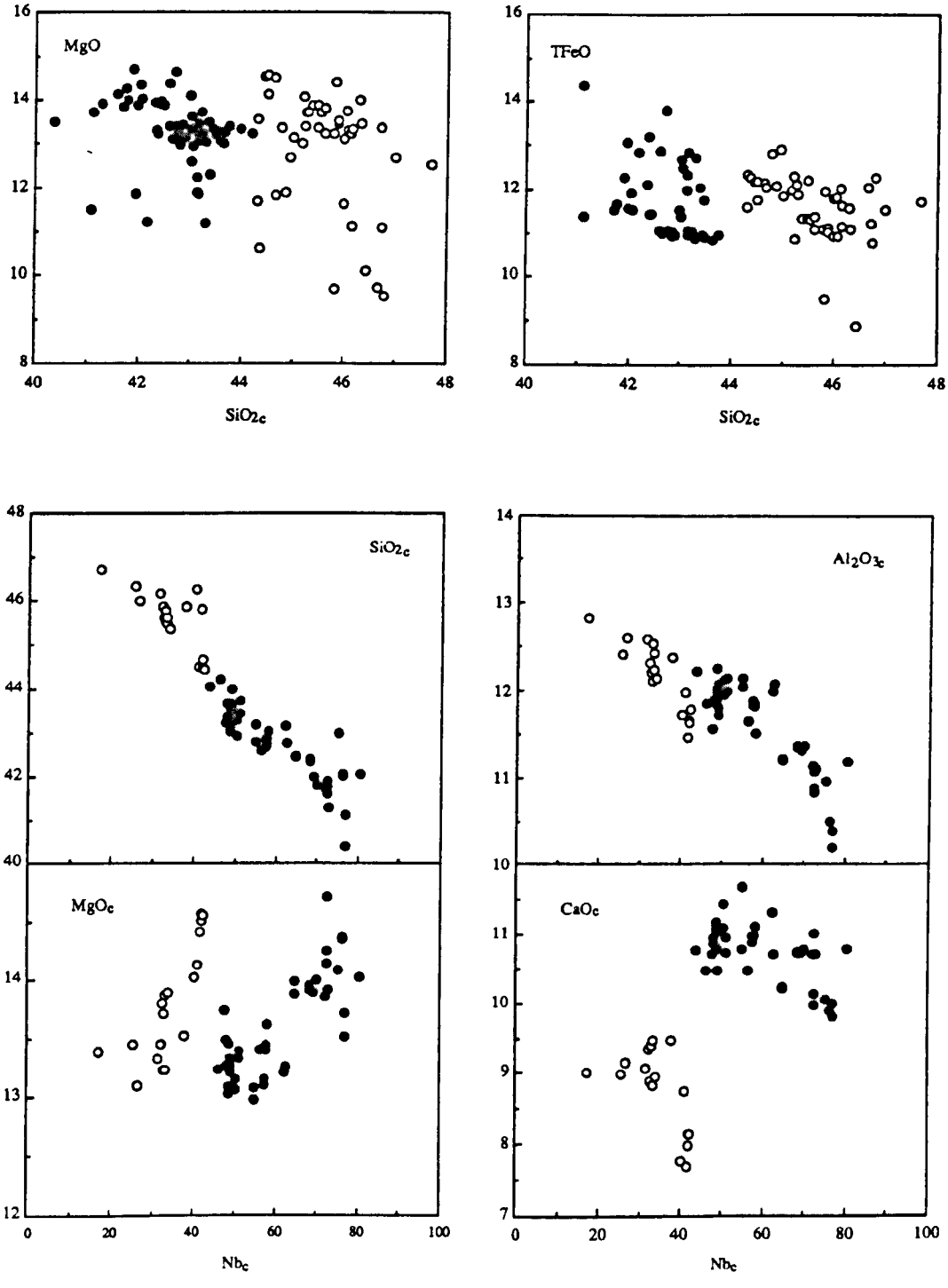

Fig. 4-8 Major and trace element diagrams, showing the variations in the Auckland samples after correction for olivine fractionation. The corrected data show that the alkali basalts have higher $SiO_{2\text{-}c}$, $Al_2O_{3\text{-}c}$, similar $MgO_{\text{-}c}$ and $TFeO_{\text{-}c}$, but lower $CaO_{\text{-}c}$ and incompatible elements, such as $Nb_{\text{-}c}$, than the basanites. See text for discussion.

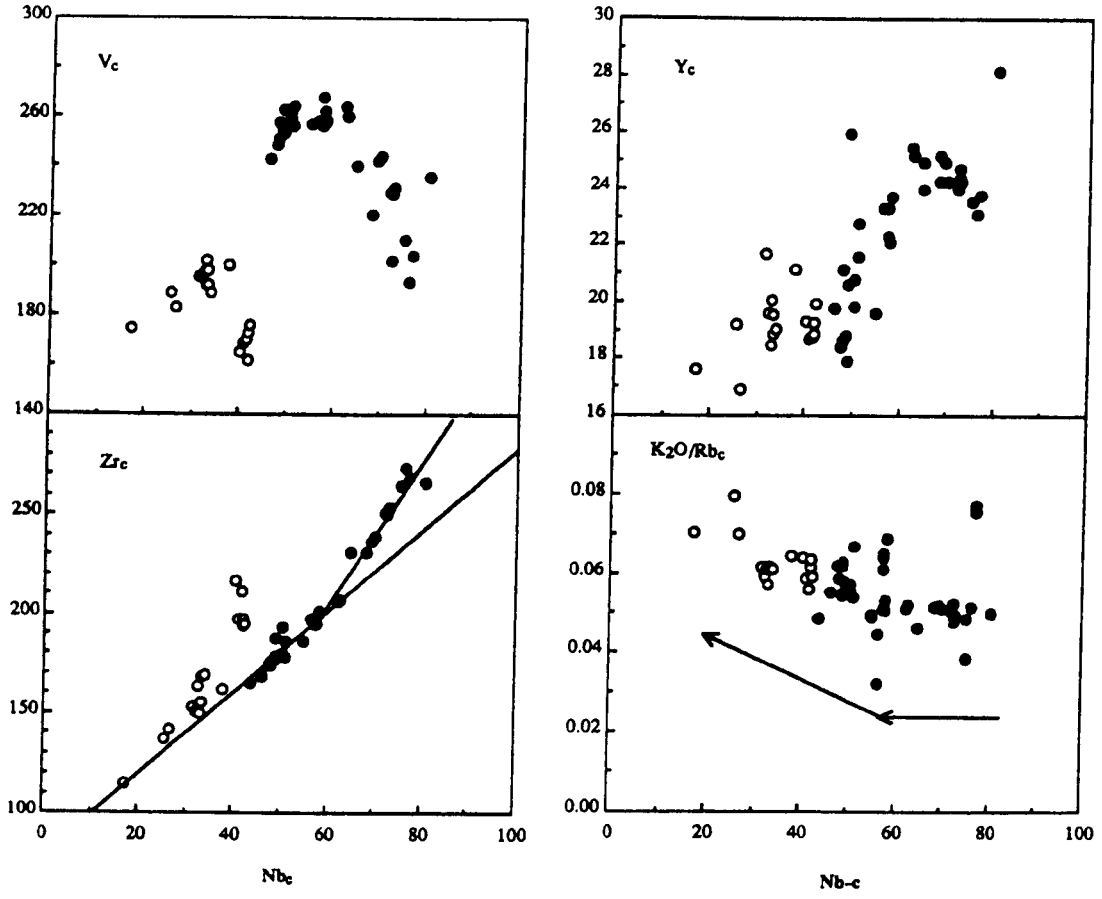

Fig. 4-9 (a) V_{-C}, (b) Y_{-C}, (c) Zr_{-C} and (d) K_2O/Rb against Nb_{-C} using the data corrected for olivine fractionation. The alkali basalts have lower incompatible elements but higher K_2O/Rb ratios than the basanites. However, there are also systematic variations within the basanites. The samples with high Nb exhibit negative correlations between Nb with Y and V and they have lower K_2O/Rb whereas with lower Nb exhibit positive correlations and higher K_2O/Rb. These features are more likely to be attributed to partial melting and difference in their mantle source regions rather than fractionation crystallisation.

Within the basanites, there are also some systematic trends with, for example, the corrected data showing a broad positive correlation between Nb and Ni (not shown), instead of a negative array shown by the uncorrected data. The basanites have quite broad positive correlations between incompatible trace elements. However, some trace elements, such as the moderately incompatible elements V, Zr and Y are characterised by different trends (Fig. 4-9). The samples with high incompatible elements, for example Nb > 60ppm and La > 50ppm, have relatively low V contents

and high Zr. which are associated with relatively low K_2O/Rb ratio (Fig. 4-9).

The systematic variation of Y_{-c} and V_{-c} with Nb_{-c} (Fig. 4-9) cannot be attributed to olivine fractionation, but might be due to fractionation of other mineral phases. Magnetite has a high partition coefficient for V, but not for Y, and so it is unlikely to have been responsible for the variation in both Y and V in the basanites. Fractional crystallisation of clinopyroxene could have been important because V and Y are relatively compatible in the clinopyroxene, and Nb highly incompatible. Recent experimental studies (Hart and Dunn, 1993) on partition coefficients for clinopyroxene suggest that V is compatible with a partition coefficient of about 3.1, although Woodhead et al. (1993) suggested a value of 1 for V in clinopyroxene. Experimental data for partition coefficients for Y in clinopyroxene also scatter from 0.47 to 1.1 (Hart and Dunn, 1993; Green et al., 1989; and Adam et al., 1993). Calculations show that about 15% fraction of clinopyroxene would reduce the V content of liquid from 260 to 150, if Kd_V=3.1, and that might also explain the buffer of Y in high Nb basanites if the partition coefficient for Y in the clinopyroxene was > 1.1. However, fractionation of clinopyroxene cannot explain the associated variation of K_2O/Rb. Thus, the variations of major and incompatible trace elements in the data corrected for olivine fractionation cannot be readily attributed to fractional crystallisation of other phases. Rather, those compositional differences may be largely due to partial melting processes or to source compositions, these are discussed further below.

4-6. Partial Melting

As discussed above, fractional crystallisation cannot account for most of the major and trace element variations in the Auckland basalts. The data corrected for olivine fractionation to Mg#=71 show that highly incompatible elements, such as Nb and La, vary about by 40% within the

basanites (80 - 45 and 70 - 30ppm, respectively), and by even more if the alkali basalts are included. For the major elements, the corrected data show that the alkali basalts have higher SiO_2 (44 - 48%) but lower CaO (on average of 9.25%) than the basanites (in range of 41-44% and an average of 10.5% respectively). These are unlikely to be due to fractional crystallisation and so we now consider partial melting processes and source compositions.

Basalts with silica undersaturated compositions, similar to the Auckland rocks, are likely to be generated by low degrees of partial melting (McKenzie and O'Nions 1991). With increasing of degrees of partial melting, e.g. from basanites to alkali basalts, SiO_2 and Al_2O_3 increase, K_2O, Na_2O and P_2O_5 decrease, and K_2O/Na_2O remains < 1 in both the alkali basalts and basanites. CO_2-H_2O enriched mantle sources have been invoked, together with small degrees of partial melting, to generate silica undersaturated melts, such as melilitites from South Africa (Rogers et al. 1992). Experimental studies (Brey and Green 1975; 1977) have documented the effects of CO_2 on the composition of upper mantle melts. At pressures above 25 kb and at sub-solidus temperatures, CO_2 reacts with clinopyroxene to form dolomite. Partial melting generates initial melts with high MgO, CaO, but low SiO_2 contents. The basanites have SiO_2 contents of 39-45%, generally higher than melilitites (32-43%), but lower than, for example MOR tholeiites which are thought to represent 10-20% degrees of partial melting (McKenzie and Bickle 1988; McKenzie and O'Nions 1991). Thus, the basanites may reflect higher degrees of partial melting than melilitites and their silicate undersaturated features are attributed both to the presence of CO_2 in their source regions, and to the small degrees of partial melting.

Previous studies have noted that basanites have compositions similar to mantle amphibole. Oxbough (1964) proposed that residue amphibole would buffer K_2O/Na_2O in the melts. Other experimental and petrological evidence also indicates that amphibole-bearing mantle sources may be

required to generate silica undersaturated melts. Francis and Ludden (1990) showed that glasses in amphibole lherzolite tend to have lower silica and higher alkali contents than the glasses from anhydrous lherzolites. Adam (1990) reported experimental work which indicates that primary basanites can be generated from amphibole-bearing garnet lherzolite source in the presence of H_2O+CO_2. Thus, partial melting of amphibole-bearing mantle is likely to generate melts with compositions similar to the basanites and alkali basalts, i.e. silicate undersaturated with K_2O/Na_2O <1. A mantle source metasomatised by amphibole-garnet clinopyroxenite veins, which may have similar compositions to some mantle xenoliths from Nunivak Island (Roden et al. 1984), has been invoked for the basanites at Fort Selkirk, Canada (Francis and Ludden 1990).

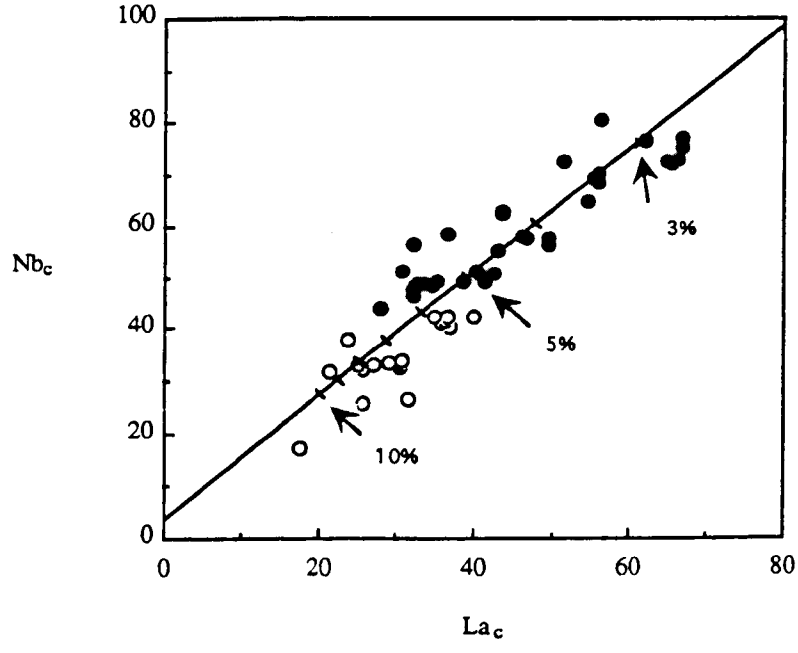

Fig. 4-10 Nb_{-c} vs. La_{-c} diagram illustrating partial melting model calculations. Because they are highly incompatible elements, the results are not sensitive to the choice of mineralogy and they indicate that the basanites and alkali basalts can have been generated by 3-7% and 5-10% degrees of partial melting, respectively.

Although the Auckland alkali basalts have low incompatible element contents and major element compositions different from the basanites, they may still have been derived from similar sources regions. Both suites have similar isotope compositions and the higher SiO_2 and lower incompatible element abundances of the alkali basalts may simply reflect larger degrees of partial melting than the basanites. Moreover, on a diagram of Nb-c vs La-c (Fig. 4-10), the alkali basalts plot on the extension of the trend of the basanites, further suggesting that they were derived from source regions with similar trace element contents. However, this seems unable to explain fully some of the differences in major elements between the alkali basalts and basanites. For example, highly incompatible elements can be used as indicators of degrees of partial melting, and when plotted against major elements, rocks generated by different degrees of partial melting should lie on a trend. Fig. 4-11 shows La corrected for olivine fractionation against $SiO_{2\text{-}c}$, the alkali basalts tend to have higher $SiO_{2\text{-}c}$ (and lower $CaO_{\text{-}c}$) than the basanites. This cannot be explained simply by changing the degrees of partial melting and it implies that other factors, such as melting conditions, may also have effects in compositions of the melts .

Experimental studies on partial melting have shown that SiO_2 and MgO contents are related to physical conditions during partial melting. Hirose and Kushiro (1993) proposed that SiO_2 contents vary with pressure negatively and MgO contents correlate with temperature positively on the basis of experimental data. Thus, the two parallel trends for the alkali basalts and basanites on a diagram of SiO_2 against MgO (Fig. 4-8a) may reflect different conditions of partial melting, with the higher SiO_2 in the alkali basalts being due to melting at shallower depths.

However, since Hirose and Kushiro (1993) proposed that CaO should be controlled by degrees of partial melting and compositions in the sources, the different trends of the alkali basalts and basanites on the CaO-c vs Nb-c

diagram (Fig. 4-8) are less likely to be due to differences in the depths of melting. Moreover, because highly incompatible element abundances are an index of the degree of partial melting, the alkali basalts and basanites should plot on the same trend if that was also primarily responsible for the CaO contents in the Auckland basalts. Thus, the different relationship between CaO and incompatible elements, such as Nb, may reflect differences in the major element compositions of the sources.

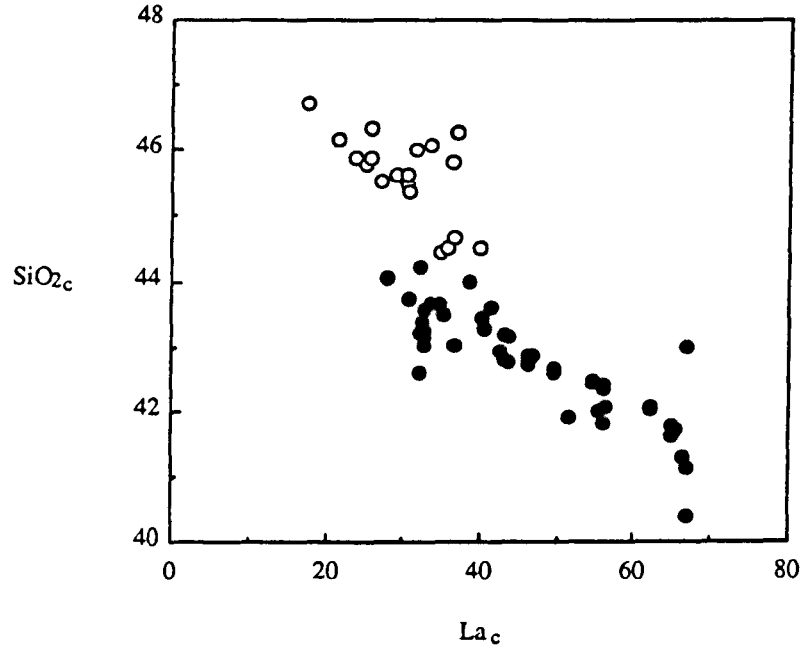

Fig. 4-11 $SiO_{2\text{-}c}$ vs. $La_{\text{-}c}$, illustrating the different silica contents between the alkali basalts and basanites. Although both the alkali basalts and basanites exhibit negative correlations between $SiO_{2\text{-}c}$ and $La_{\text{-}c}$, the alkali basalts tend to have higher $SiO_{2\text{-}c}$ and $La_{\text{-}c}$ than the basanites, and they do not plot on the same trend. The higher $SiO_{2\text{-}c}$ relative to their $La_{\text{-}c}$ of the alkali basalts may be attributed to different depths of partial melting.

With a knowledge of the partition coefficients for incompatible elements, and their abundances in the source regions, the degrees of partial melting can be estimated. The partition coefficients of elements such as Nb and La have been extensively studied and they are relatively well constrained for common rock-forming mineral phases (e.g. Kelemen et al. 1993; Green et al. 1989). Although recent experimental data are not available

for olivine, the partition coefficients for Nb are likely to be lower than those for orthopyroxene. Thus, taking account of the inferred abundance of each mineral phase in the mantle, reasonable estimates can be made for the bulk La and Nb partition coefficients. Because both of them are highly incompatible, their bulk partition coefficients are not much affected by varying the proportion of minerals in their source regions. Simple batch melting model calculations suggest that the Auckland basanites were generated by 3-7% and alkali basalts by 5-10% partial melting (Fig. 4-10) from a enriched mantle source with incompatible element abundances of 3-4 times primitive mantle.

Trace element features also constrain the residual mineralogy during partial melting. In the alkali basalts and the lower Nb basanites, Y correlates positively with highly incompatible elements (Fig. 4-9b). This indicates that Y was essentially incompatible during the generation of many of the alkali basalts and basanites, and that garnet was therefore not residual in their mantle sources. Because garnet has a partition coefficient for Y of 10, even if there was only 5% garnet in the mantle source, Y in the melt would remain constant while the more incompatible elements vary significantly. Y is buffered in the high Nb basanites (Fig. 4-9b), suggesting that garnet may have been residual during the generation of these rocks over the first few percents of partial melting.

Rogers et al. (1992) argued that phlogopite is more likely to be residual during small degrees of partial melting in CO_2-rich mantle. Residual phlogopite in mantle source regions with relatively high CO_2 has also been suggested to be responsible for low K_2O contents and high Nb/K ratios in some basalts (Clague and Frey, 1982; Hawkesworth et al. 1990). Because both K_2O and Rb are compatible in phlogopite they should be buffered by residual phlogopite with relatively little fractionation of K_2O/Rb. However, K_2O/Rb increases with decreasing Nb from the basanites to the alkali basalts

(Fig. 4-9d). Amphibole has high K_2O/Rb, and high K partition coefficient relative to Rb (Adam et al. 1993), and so residual amphibole is likely to result in relatively low K_2O/Rb in the melts (Hawkesworth et al. 1990). Recent experimental work (Adam et al. 1993) reported that amphibole also has a relatively high V partition coefficient of 1.25 (see also Woodhead et al. 1993). Thus, the main features of the Auckland basalts may be consistent with the presence of residual amphibole during the generation of the high Nb basanites, which was then exhausted when the low Nb basanites and alkali basalts were generated at relatively higher degrees of partial melting. Because the degrees of partial melting to generate the basanites must be small, if the different trace element patterns between the high and low Nb basanites are due to amphibole, or any other residual phase, it can only have been present in very small amounts.

Inferred mineral assemblages may also be used to constrain the depths of their mantle source regions. Since Y is not buffered in the low Nb basanites, that suggests a source region without residual garnet. If the model discussed above, in which amphibole was involved in the generation of the high Nb basanites, is correct, it implies that the source regions for the basanites were not very deep (Wass, 1980, Menzies and Murthy, 1980). However, using the correlation between SiO_2 and pressure derived from experimental work (Hirose and Kushiro 1993), the average SiO_2 of 45% for the alkali basalts suggests a pressure of 30 kb (or 75 km), and the average of SiO_2 =43% for the basanites suggests mantle source regions at depths greater than 100 km. It is clear that it remains difficult to estimate the real depth of the source regions and more experimental work is needed.

4-7. A potential HIMU source

The distinctive features of the Auckland basalts include their high Nb and LREE relative to LILE (Fig. 4-12 and Table 4-5), together with Sr and Nd isotope compositions similar to HIMU basalts. Because the continental

crust is characterised by a negative Nb anomaly, these trace element features cannot be related to recycled bulk continental crust. Instead, these signatures are also observed in HIMU OIB (Table 4-5, Weaver 1991b) and it has been argued that the HIMU component is derived from subducted oceanic crust from which LIL elements have been preferentially removed during dehydration of the slab. The signature associated with high Nb/Rb, Nb/Ba and Nb/La is inferred to be high U/Pb because Pb has been removed preferentially relative to U by dehydration of the slabs (Weaver 1991a, b; Chauvel et al. 1992). Therefore, source regions containing a component of recycled oceanic crust are thought to be characterised by depleted Sr, Nd, but high Pb isotope ratios, together with high Nb/Ba and Nb/La, as inferred for HIMU mantle sources.

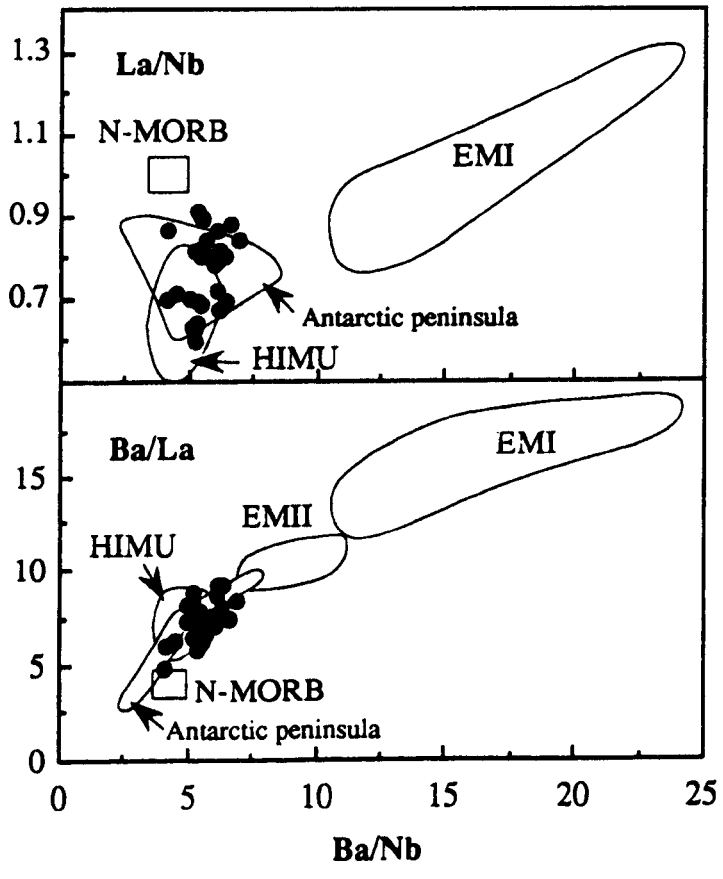

Fig. 4-12 La/Nb and Ba/La against Ba/Nb after Weaver (1991). This diagram shows that the Auckland basalts have low La/Nb, Ba/La and Ba/Nb ratios, which are similar to HIMU OIB rather than to other OIB end-members.

However, in principle, the relative enrichment of Nb relative to at least some of the LIL elements is likely to be due to partial melting processes, if for example Nb and the LREE are more incompatible than Rb, Ba and K in the presence of residual amphibole. Relative partitioning during partial melting can be investigated using trace element diagrams (Hofmann and Feigenson 1983). Nb_{-C} is plotted against Nb/Ba and Nb/K_2O ratios for the Auckland basanites and alkali basalts in Fig. 4-13. Some tholeiites from the Northland volcanic field, which are discussed in the next chapter, are also plotted in the diagrams, together with data from St Helena and Walvis Ridge. These two diagrams show that the Auckland rocks exhibit broad arrays which tend to have positive slopes. This suggests that Nb was more incompatible than Ba and K during partial melting, and the high Nb/Ba and Nb/K_2O in the Auckland basalts is therefore at least in part due to partial melting with the presence of amphibole in their sources since amphibole has higher partition coefficients for K, Ba and Rb relative to Nb (Adam et al. 1993).

The Pb isotope ratios ($^{206}Pb/^{204}Pb$ ~19.2) in the Auckland samples are much lower than those from HIMU OIB ($^{206}Pb/^{204}Pb$ >20.5, Fig. 4-7). Possible reasons for their lower Pb isotope ratios could be either that they had lower U/Pb ratios in their source regions and/or insufficient time has passed since high U/Pb ratios developed. The precise U/Pb ratios in the mantle sources are difficult to assess. However, the Auckland basalts have lower Nb/U ratios (~35) and higher Ce/Pb (~33) than the average values in MORB and OIB, which are 47 and 25, respectively (Fig. 4-14a, b). Since these ratios are not fractionated during partial melting (Hofmann et al. 1986; Newsom et al. 1986), it appears that U is relatively enriched and Pb is relatively depleted in the mantle sources of the Auckland basalts. Thus, although there is no clear correlation between Nb/U and Pb isotope ratios in the OIB end members HIMU and EMI, the measured high U/Pb ratios in

the Auckland basalts give an average of ~0.72, which is equivalent to μ ~45, and these are likely to reflect high μ in their mantle sources.

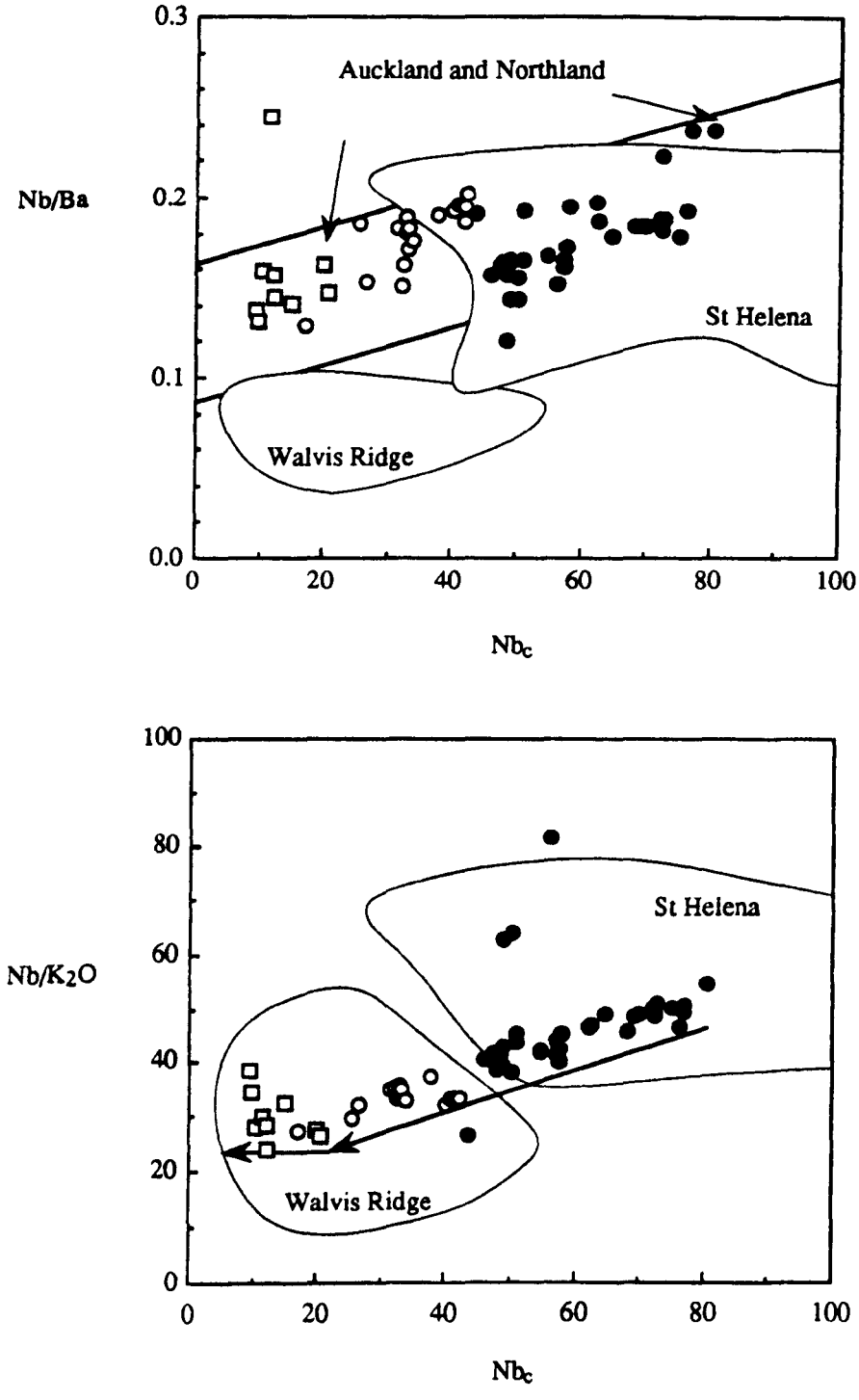

Fig. 4-13 Nb/Ba vs. Nb_C and Nb/K_2O vs. Nb_C. The positive data arrays suggest that Nb was more incompatible than Ba and K during the generation of the Auckland basalts. Therefore, these Nb/Ba and Nb/K_2O features are likely to be due to, at least partially, partial melting processes.

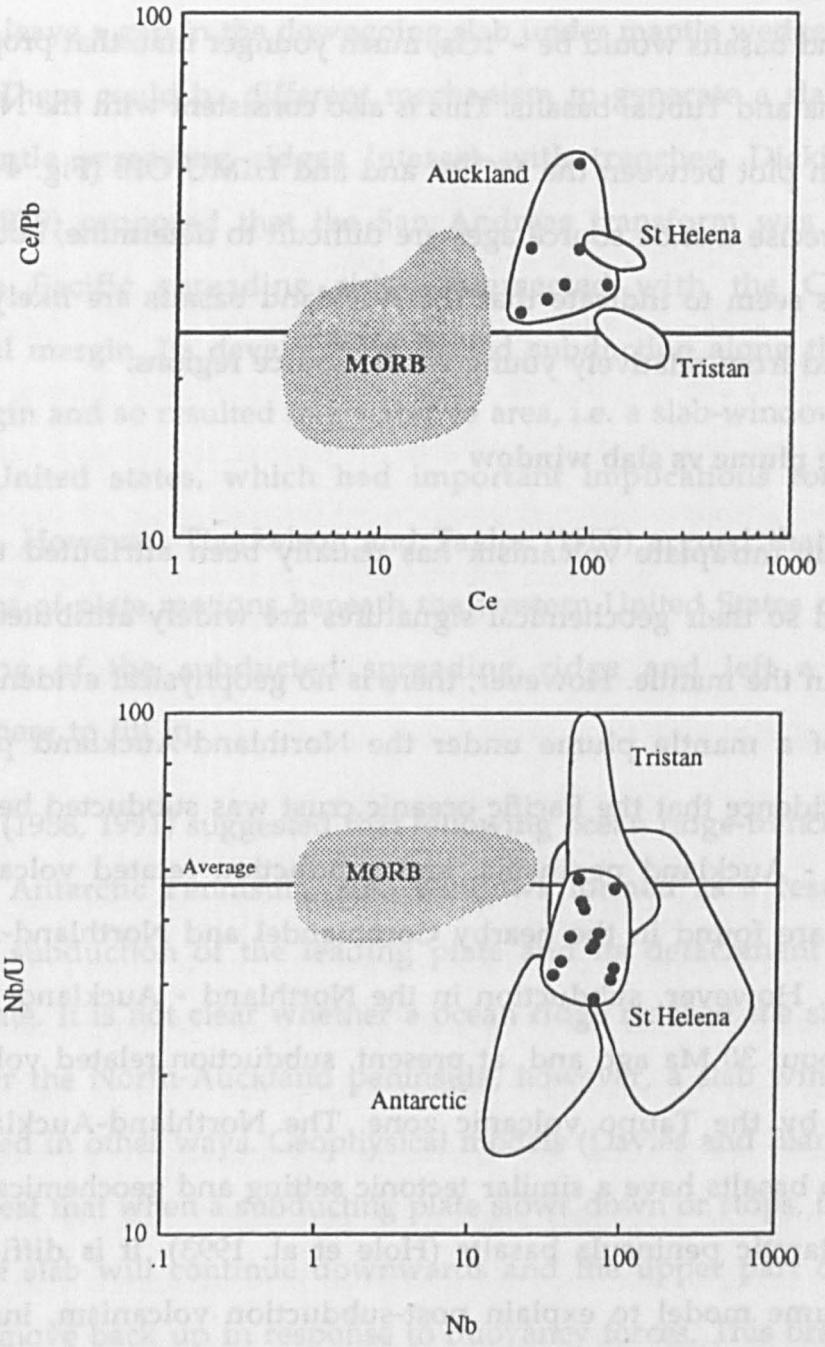

Fig. 4-14 (a) Ce/Pb vs. Ce, (b) Nb/U vs. Nb diagram. The Auckland basalts have high Ce/Pb and low Nb/U relative to the average of MORB (Hofmann et al. 1986; Newsom et al. 1986). Since these ratios are not fractionated by partial melting and fractional crystallisation, they indicate that Pb is relatively depleted and U is relatively enriched in the mantle source regions of the Auckland basalts. These features are again similar to HIMU OIB.

Chauvel et al. (1992) proposed a model for the mantle of the HIMU OIB, i.e. St Helena and Tubuai basalts, in which the mantle source age is ~2 Ga. Following their model, calculations indicate that the mantle source for the Auckland basalts would be ~ 1Ga, much younger than that proposed for for St Helena and Tubuai basalts. This is also consistent with the Nd isotope ratios which plot between the MORB and and HIMU OIB (Fig. 4-5). Thus, although precise mantle source ages are difficult to determine, both Pb and Nd systems seem to indicate that the Auckland basalts are likely to have been derived from relatively young HIMU source regions.

4-8. Mantle plume vs slab window

Oceanic intraplate volcanism has usually been attributed to mantle plumes and so their geochemical signatures are widely attributed to deep reservoirs in the mantle. However, there is no geophysical evidence for the presence of a mantle plume under the Northland-Auckland peninsula. There is evidence that the Pacific oceanic crust was subducted beneath the Northland - Auckland peninsula, and subduction related volcanic rocks (Miocene) are found in the nearby Coromandel and Northland-Auckland peninsulas. However, subduction in the Northland - Auckland peninsula stopped about 30 Ma ago and, at present, subduction related volcanism is expressed by the Taupo volcanic zone. The Northland-Auckland post-subduction basalts have a similar tectonic setting and geochemical features to the Antarctic peninsula basalts (Hole et al. 1993). It is difficult for a mantle plume model to explain post-subduction volcanism, instead, the geological setting of the Auckland volcanism is more easily explained in terms of a slab window model. (e.g. Hole et al. 1991).

Slab window models were proposed from studies of the interaction between mantle spreading ridges and continental lithosphere (Dickinson and Snyder 1979, Thorkelson and Taylor 1989, Hole et al 1991). When oceanic crust is being subducted beneath a continental plate and its

subduction rate is higher than the generation rate at its midocean ridge, the ridge will move closer and closer to the subduction zone, until it reaches the trench then so-called ocean ridge subduction starts and subducted ocean ridge will leave a gap in the downgoing slab under mantle wedge, i.e. a slab window. There could be different mechanism to generate a slab window when mantle spreading ridges interact with trenches. Dickinson and Snyder (1979) proposed that the San Andreas transform was generated when the Pacific spreading ridge intersected with the Californian continental margin. Its development ceased subduction along this part of plate margin and so resulted in a slab-free area, i.e. a slab-window, beneath western United states, which had important implications for regional volcanism. However, Thorkelson and Taylor (1989) argued that changing orientations of plate motions beneath the western United States resulted in a widening of the subducted spreading ridge and left a void for asthenosphere to fill in.

Hole (1988, 1991) suggested that following ocean ridge-trench collision along the Antarctic Peninsula, slab windows formed as a result of the continued subduction of the leading plate and its detachment from the trailing plate. It is not clear whether a ocean ridge reached the subduction zone under the North-Auckland peninsula, however, a slab window may be generated in other ways. Geophysical models (Davies and Blanckenburg 1995) suggest that when a subducting plate slows down or stops, the deeper part of the slab will continue downwards and the upper part of oceanic crust will move back up in response to buoyancy forces. This break in the slab leaves a gap which allows asthenosphere to upwell and partially melt by decompression within the mantle wedge. Furthermore, it is speculated that this initial upwelling of asthenosphere may be a trigger of extension of lithosphere, which could result in relatively large scale magmatism (Dickinson and Snyder 1979, Thokelson and Taylor 1989).

Hole et al. (1991) examined volcanic rocks from three proposed slab-window areas around the margin of Pacific Ocean. They appear to share some common trace element features, such as enrichment of incompatible element and more enriched Nb (Ta) relative to LIL elements (Hole et al. 1991). This is similar to those from the Auckland volcanic field. Although the rocks from different locations have variable isotope ratios (Hole et al. 1991), the rocks from the Northland and Auckland fields have isotope ratios similar to either MORB or OIB, which implies involvement of asthenosphere in their generation.

4-9. Summary

New data presented in this study indicate that the Auckland basalts are silica undersaturated with high MgO contents, consistent with Heming and Barnet (1986). They have low Sr, high Nd isotope ratios and it appears that they have not been significantly contaminated, except for three samples with very low Pb isotope ratios.

On the basis of major and trace element compositions, the Auckland basalts can be subdivided into the alkali basalts and basanites. They cannot be simply related to each other by fractional crystallisation processes, and it appears that they underwent ~ 10% fractionation. Most of the major and trace element variations are therefore attributed to partial melting processes, and the relatively high silica contents of the Auckland alkali basalts may indicate that they were derived from shallower mantle source regions than the basanites. It is argued that the geochemical features in the Auckland basalts are consistent with CO_2 and amphibole bearing mantle source regions.

Since Y correlates positively with Nb in most of the Auckland samples, i.e. the alkali basalts and some basanites, there was little or no residual garnet in their mantle sources during their generation. Together

with the evidence for amphibole in their mantle source regions, the depths where the Auckland basalts derived were relatively shallow, perhaps within in the continental lithosphere.

The Auckland basalts have Sr isotopes similar to MORB, but lower $^{143}Nd/^{144}Nd$ isotope ratios, thus, they plot towards the HIMU OIB. They also have similar trace element patterns to the HIMU OIB, such as high Nb/Rb, Nb/Ba and Nb/La, but they also have much lower Pb isotope ratios than the HIMU OIB, albeit with very high measured μ ($^{238}U/^{204}Pb$). Since the HIMU mantle sources are attributed to recycling of old oceanic crust, it is likely that the mantle source regions for the Auckland basalts may be metasomatised by melts derived from young recycled oceanic crust. If this is correct, they may provide time constraint for recycling.

Intraplate continental magmatism is often attributed either to mantle plumes or extension in many areas. Since there is no evidence for a mantle plume under the Northland-Auckland Peninsula, or for significant lithosphere extension, a slab window hypothesis is proposed for the post - subduction volcanism on the Northland-Auckland Peninsula.

Chapter Five

Geochemistry of Basic Volcanism in Northland, New Zealand and implications for mantle enrichment processes

5-1. Introduction

Mantle derived magmatism provides samples which can be used to investigate mantle compositions, and a number of studies have documented various scales of compositional heterogeneities (Faure and Hurley 1963; Gast et al 1964; Dupré and Allègre 1983; Hart 1984; McDonough et al. 1985; Song and Frey 1989; Staudigel et al. 1991). For example, in general, continental mantle is different from oceanic mantle because the former is cold and isolated from convection in the asthenosphere; and magmas at destructive plate margins have different isotope and trace element features from those generated in intraplate settings.

Subduction related volcanic rocks typically have high large ion lithophile (LIL) elements, but low high field strength (HFS) element contents, often with slightly higher Sr and lower Nd isotope ratios than MORB. These are different from the key geochemical features of intraplate magmas, and they have been attributed to recycling of continental material back into the mantle, although the reason for the depletion of HSF elements is still debated. Studies on oceanic basalts recognised several end member compositions, e.g. DM, HIMU, EMI and EMII (Zindler and Hart, 1986). They were defined largely on the basis of isotope compositions, however, some trace element features appear to be associated with the isotope signatures of these end-members, and certain aspects of mantle

heterogeneity have been related to relatively deep recycling of crustal components back into the mantle (Hawkesworth et al. 1979, Zindler et al. 1982, Cohen and O'Nions 1982, White 1985, Palacz and Sanders 1986, Weaver et al. 1986, 1991a, b). Moreover, since many ocean island basalts (OIB) are associated with mantle plumes, it is inferred that the components inferred from OIB exist deep in the mantle.

In the Northland Volcanic Field (NVF) a wide variety of young volcanic rocks occur in a relatively small area. The isotope and trace element characteristics of these rocks range from those similar to subduction related volcanic rocks to some also seen in OIB, even though there is no independent evidence for a mantle plume. In this chapter further geochemical evidence is reconciled with data from the literature and various processes of magma genesis are reviewed and a geochemical model is proposed to interpret mantle enrichment.

5-2. General geology and previous research

The Northland volcanic field is situated on the eastern side of the Northland Peninsula, about 100 km north of the Auckland volcanic field (Fig. 5-1). The Northland volcanic field consists of several volcanic areas, including those at Kaikohe-Bay, Waipu-Ti Point, Waiheke Island and Puhipuhi Wangarei. Some samples from Mercury Island, in the Coromandel volcanic zone (Fig. 5-1), are also included for comparison.

The basement rocks of the Northland Peninsula exposed along the eastern margin are westward dipping Permian-Jurassic metagraywackes. The base of the metagraywackes is not exposed, but geophysical data suggest a maximum depth in the order of ~4-5 km (Woodward, 1970; Stern et al., 1987). Some Cretaceous to Oligocene clastic sedimentary rocks unconformably or tectonicaly overlie the basement rocks; they have been folded, fractured and sheared and are estimated to be ~ 7000 m thick

(Ballance and Sporli, 1979; Malpas et al., 1992). Extensive (2600 km^2) predominantly basaltic and associated intrusive rocks rest on and within the Cretaceous-Oligocene sequence. They are chemically similar to MORB and are inferred to represent, at least in part, oceanic crust obducted on to the Northland Peninsula (Brothers and Delaloye, 1982; Malpas et al., 1992). In the Miocene, arc-type magmas erupted at several locations along the length of Northland, and they, together with the obducted oceanic crust, reflect an old episode of subduction. The arc-type volcanism is considered to have migrated southeastward during the late Miocene and Pliocene, and it was then replaced by intraplate basaltic volcanism from the late Pliocene to the Quaternary (Brothers 1986). Thus, the geotectonic setting of Northland changed from that of a convergent margin to an intraplate setting. A recent K-Ar study (Smith et al. 1993) on the youngest volcanic rocks in Northland provide time constraints on the volcanism and development of associated mantle source regions.

The Mercury Islands are situated outside the Coromandel Volcanic Zone (CVZ) in the Hauraki Volcanic Region (HVR), which is the largest and longest lived region of andesite - dacite volcanism (Skinner 1986). The basement of the CVZ is composed of late Jurassic marine sedimentary rocks, which are overlain by restricted Oligocene - Miocene sediments. Volcanism in the CVZ started as early as ~20 Ma ago, and the youngest eruption age is less than 1 Ma (Skinner 1986). Most eruptions were of andesites and rhyolites, however, at a few locations, including the Mercury Islands, basalts were erupted. The isotopic compositions of the volcanic rocks in the CVZ is similar to those from the present subduction related the Taupo Volcanic Zone (TVZ). However, the CVZ are considered to be the result of NE extension, even though the chemical features may have been inherited from the previous history of subduction before 22 Ma ago (Skinner 1986).

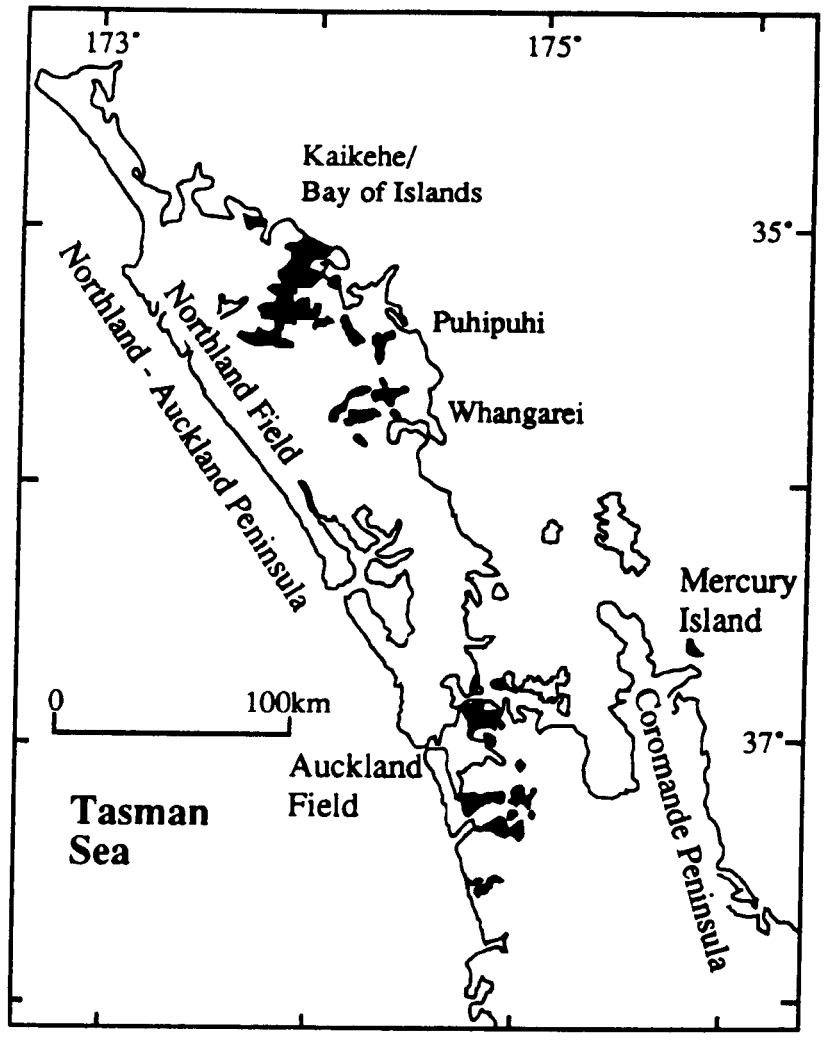

Fig. 5-1 Sketch map of the Northland-Auckland and Coromandel Peninsula, North Island New Zealand, and nearby areas, after Weaver and Smith (1989).

5-3. Geochemical Results

The samples studied in this chapter show some systematic differences especially in trace element and isotope compositions, and these differences are summarised briefly in Fig. 5-2. In general, the Northland samples can be divided into three groups; Group 1 (filled squares) is characterised by high Nb/La and Nb/Sr, low Ba/La and $^{87}Sr/^{86}Sr$ ratios, and plot outside field for N-MORB and E-MORB (e.g. Gill, 1981). Group 2 (open squares) of the

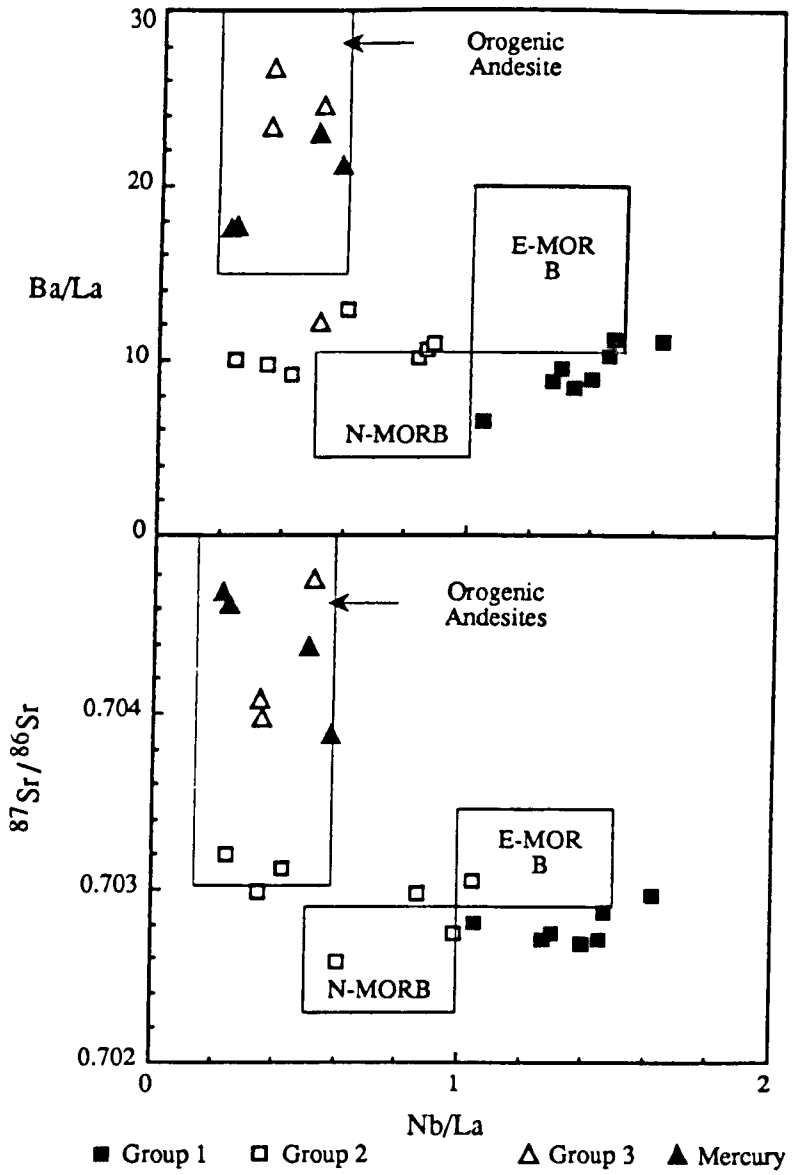

Fig. 5-2 (a) Ba/La vs Nb/La and (b) $^{87}Sr/^{86}Sr$ vs Nb/La, illustrating the key geochemical characteristics of the three groups of Northland volcanic rocks. Group 1 has low Ba/La and $^{87}Sr/^{86}Sr$ but high Nb/La (> 1); in contrast, Group 3 and the Mercury basalts have high Ba/La and $^{87}Sr/^{86}Sr$, but low Nb/La ratios; whereas Group 2 has compositions intermediate between Groups 1 and 3, with Ba/La and $^{87}Sr/^{86}Sr$ similar to Group 1, but low Nb/La similar to Group 3. N-MORB, E-MORB and orogenic andesite fields from Gill (1981) are plotted for comparison.

Northland samples has low Ba/La and $^{87}Sr/^{86}Sr$ ratios, similar to Group 1, but also low Nb/La and Nb/Sr ratios, similar to Group 3 and the Mercury Island basalts. Group 3 of the Northland samples is different from Groups 1 and 2 in that it is characterised by high Ba/La, $^{87}Sr/^{86}Sr$, low Nb/La ratios, and plot mainly in the field for orogenic andesite defined by Gill (1981). The

basalts from Mercury Islands are similar to Group 3 of the Northland samples. The geochemical characteristics of the three groups of Northland samples, together with the Mercury Island basalts are described below.

5-3.1 Major elements

Major element data are listed in Table 5-1 and selected elements are illustrated in Fig. 5-3. The samples discussed in this chapter are silica saturated, in contrast to the undersaturated nature of rocks from the Auckland volcanic field. Group 1 of the Northland basalts have silica contents from 48 to 51%, higher than the Auckland basalts discussed in Chapter IV, but lower than the other groups of Northland samples. Alkali contents (Na_2O+K_2O) in Group 1 basalts range from 3.5 to 5.5%, lower on average than the Auckland basanites, and MgO contents are between 6.4 to 9.4%. The samples in Group 2 tend to have higher SiO_2 contents, higher Al_2O_3 and Na_2O, but similar MgO, CaO and K_2O to those in Group 1 (Fig. 5-3). Group 3 samples have much a wider variation of major elements than the previous groups, for example SiO_2 = 49 - 58%, and the Mercury basalts are chemically similar to the basalts in Group 3.

5-3.2 Trace elements

Abundances of compatible elements, Ni and Cr, in the different groups overlap each other and correlate broadly with MgO (Fig. 5-4a, b), which may be attributed to similar degrees of low pressure olivine fractional crystallisation.

However, incompatible elements show different patterns in the different groups. Group 1 and 2 basalts have similar LIL element contents, such as Ba, while Group 3 and Mercury samples tend to have high and variable LIL elements (Fig. 5-5). For example, Ba in the Mercury samples varies from 160 to 600ppm and the Mercury and Group 3 have consistently higher Ba/Y than Group 1 and 2 (Fig. 5-5). The LREE contents and

TABLE 5-1
Major element data of the Northland and Mercury Island sample

	Locality	SiO_2	TiO_2	Al_2O_3	Fe_2O_3	MnO	MgO	CaO	Na_2O	K_2O	P_2O_5	LOI	H_2O	Totle
37653	W-Ti	49.88	1.18	17.3	8.89	0.14	8.31	10.27	3.52	0.4	0.19	0	0.4	100.48
37669	W-Ti	50.92	1.61	16.32	10.65	0.16	6.87	8.36	3.55	0.93	0.31	0.08	0.41	100.17
37682	P-W	50.69	1.26	17.94	7.95	0.14	7.41	9.92	4.05	0.46	0.28	0	0.26	100.36
37697	W-Ti	50.65	0.94	18.72	7.98	0.13	5.98	10.49	3.29	0.32	0.24	0.58	0.69	100.01
37702	W-Ti	50.03	0.94	17.62	8.83	0.14	8.22	9.37	3.5	0.24	0.25	0.43	0.55	100.12
37702ou	W-Ti	49.88	0.982	17.59	8.67	0.138	8.58	9.31	3.61	0.24	0.219	0.65		99.87
42547	W-Ti	52.17	0.83	15.47	8.44	0.13	9.85	9.35	2.71	0.89	0.17	0.43	0.3	100.74
42548	W-Ti	49.59	1.785	14.92	9.01	0.151	8.01	9.25	3.65	1.68	1.085	0.99		100.12
42550	W-Ti	49.79	0.99	16	8.41	0.17	8.24	9.67	3	0.7	0.17	1.58	1.52	100.24
42556	W-Ti	57.18	0.709	16.99	7.91	0.147	5.21	7.87	2.97	1	0.12	0.32		100.43
42565	W-Ti	53.18	1.2	16.87	8.37	0.12	5.46	9.07	3.22	0.83	0.2	0.57	1.19	100.28
44020ou	P-W	50.38	1.334	17.64	9	0.153	7.26	10.37	4.36	0.2	0.174	-0.11		100.76
44034	K-B	57.33	0.977	18.42	6.15	0.097	3.44	7.8	3.92	0.72	0.196	0.93		99.98
44040	K-B	48.88	1.42	16.34	9.33	0.14	9.35	10.46	3.34	0.46	0.24	0.07	0.22	100.25
44042	K-B	48.15	1.29	16.63	11.77	0.17	7.24	8.92	3.3	0.32	0.2	0.93	1.09	100.01
44048	K-B	50.81	1.35	17.38	8.89	0.14	7.21	9.42	3.38	0.26	0.18	0.29	0.57	99.88
44055	P-W	47.78	1.308	17.23	10.03	0.151	8.16	11.08	3.09	0.4	0.192	0.54		99.96
44380	Mercury	49.54	0.97	18.57	10.14	0.17	6.11	10.97	2.32	0.4	0.14	0.47		99.8
44386	Mercury	51.58	1.16	15.8	9.73	0.15	8.62	9.7	2.71	0.53	0.2	0.04		100.22
44398	Mercury	49.83	1.22	17.63	9.2	0.16	6.8	10.97	2.75	0.49	0.2	0.67		99.92
44400	Mercury	51.45	1.22	18.17	9.96	0.16	5.23	9.89	2.69	0.51	0.17	0.38		99.83
44410ou	Mercury	50.97	1.05	17.1	8.69	0.15	8.13	9.28	3.09	0.88	0.3	0.46		100.1
44411	Mercury	50.94	1.11	17.24	8.74	0.12	7.28	9.21	3.27	0.88	0.31	0.86		99.96

W-Ti,Waipu Ti Point area; P-W, Puhipuhi-Whangarei area; K-B, Kaikohe-Bay of Island area;

TABLE 5-2
Trace element data of the Northland and Mercury Island samples

	Ba	Rb	Sr	Th	U	Zr	Nb	Y	La	Ce	Nd	Sm	Eu	Yb	lu	V	Cr	Ni	Cu	Zn
37653		10	367	0		94	8	21	7.7	16.8	10.7	3	0.99	1.7	0.3	131	286	110	59	66
37669	168	24	371	0		144	18	23	15.5	31.9	16.9	4.1	1.32	1.7	0.3	167	269	112	44	102
37682	0	12	329	0		130	9	23	9.1	20.8	13.1	3.1	1.09	1.7	0.3	135	178	94	53	62
37697	123	6	395	0		111	3	25	12.3	21.6	14	3	1.14	2	0.3	157	149	49	38	50
37702	83		312	0		113	3	20	8.5	19.3	11.5	2.6	0.98	1.7	0.3	152	276	120	46	67
37702ou	95	1.7	318	1.26	0.4	113	7.9	22.7	9.4	21.1	12.2	3.01	1.1	2.15	0.33	175	328	141	56	68
42547	337	20	455	6		97	5	18	14.4	30.1	15.2	3.3	0.99	1.8	0.3	213	492	168	55	67
42548	653	19.9	1386			320	19.6	35.8								224	298	35	171	56
42550	299	8	384	0		105	4	22	11.2	24.2	13.4	3.1	1.06	1.8	0.3	235	254	96	55	63
42556	305	10	236			96	5.3	22.7								198	117	49	57	71
42565	285	19	362	5		122	6	26	11.6	26.3	15.3	3.6	1.15	2.3	0.3	210	54	16	57	70
44020	85	0	290	0		146	4	30	6.6	18.6	13	3.6	1.31	2.4	0.3	173	211	59	76	61
44020ou	70	5.7	296	0.66	0.3	136	5.7	28.1	6.4	17.5	12.2	3.39	1.33	2.48	0.38	185	240	68	69	65
44034	151	14.3	312			161	9.1	26.7								145	46	22	36	68
44040	106	4	381	0		104	15	23	10.3	23.6	12.5	3.5	1.29	1.7	0.3	157	292	177	58	75
44042	84	0	202	0		99	11	30	7.5	17.4	11.01	2.9	1.07	2.6	0.4	161	262	174	73	95
44048	73	0	300	0		98	10	27	7.7	14	10	2.9	1.18	1.7	0.3	144	258	151	53	68
44055	49	6	358	0.81	0.3	102	12	22.1	8.9	19.4	12.1	3.1	1.2	1.98	0.31	171	276	147	78	72
44380	168	7.2	327	1.15	0.4	60	3.7	21.5	7.3	14.8	10	2.59	0.97	1.77	0.28	282	87	36	74	78
44386	189	12.9	267	1.64	0.6	114	7.5	476	108	90.3	121	29.4	9.96	32.9	5.46	253	438	184	54	99
44398	145	6.7	295	0.98	0.4	95	9.5	152	45.1	21.6	64.8	15.5	5.51	9.97	1.58	255	173	40	37	80
44400	153	10.8	292	1.42	0.6	89	4.2	23.4	7.2	16.1	11.7	3	1.2	2.1	0.34	298	95	28	32	86
44410ou	595	18.7	676	4.83	0.8	136	7.7	26.1	33.9	70	32.3	5.76	1.73	2.4	0.37	220	325	160	45	81
44411	576	18.7	667	4.58	1.1	136	8	28.9	32.6	65.4	31.7	5.77	1.79	2.6	0.41	223	339	174	28	77

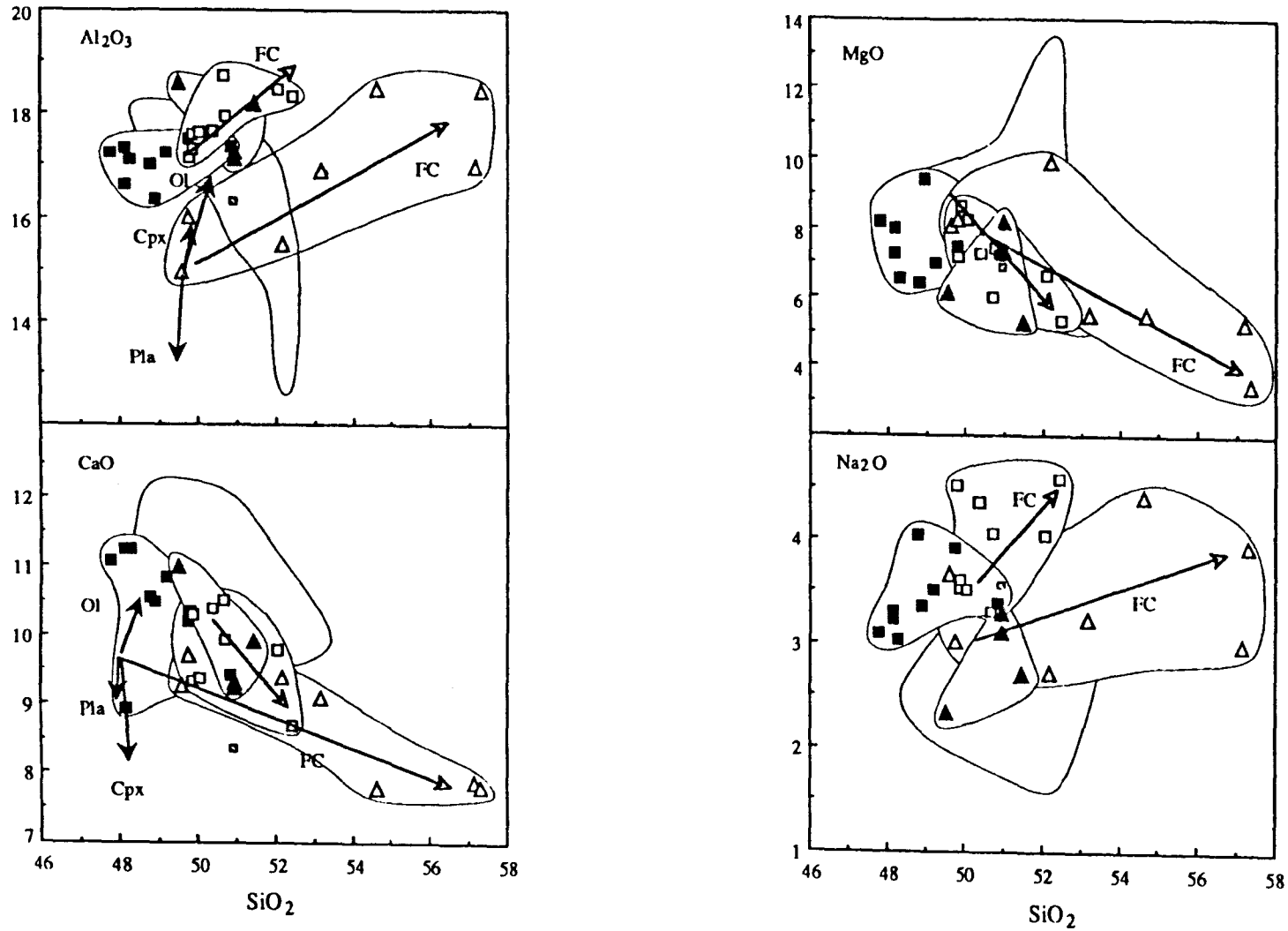

Fig. 5-3 Major element variation diagrams showing selected major element compositions. The effects of olivine, clinopyroxene and plagioclase fractionation (small arrows) in major elment composition and fractional crystallisation trends (long arrows) indicated by least-square mixing models are also shown.

LREE/HREE ratios are similar in the different groups as shown by La and La/Yb against SiO_2 (Fig. 5-5c, f). In addition, Group 1 rocks have significantly higher Nb contents, from 9 to 24 ppm, whereas, most of those in the other groups have Nb contents between 2 - 9 ppm (Fig. 5-5b).

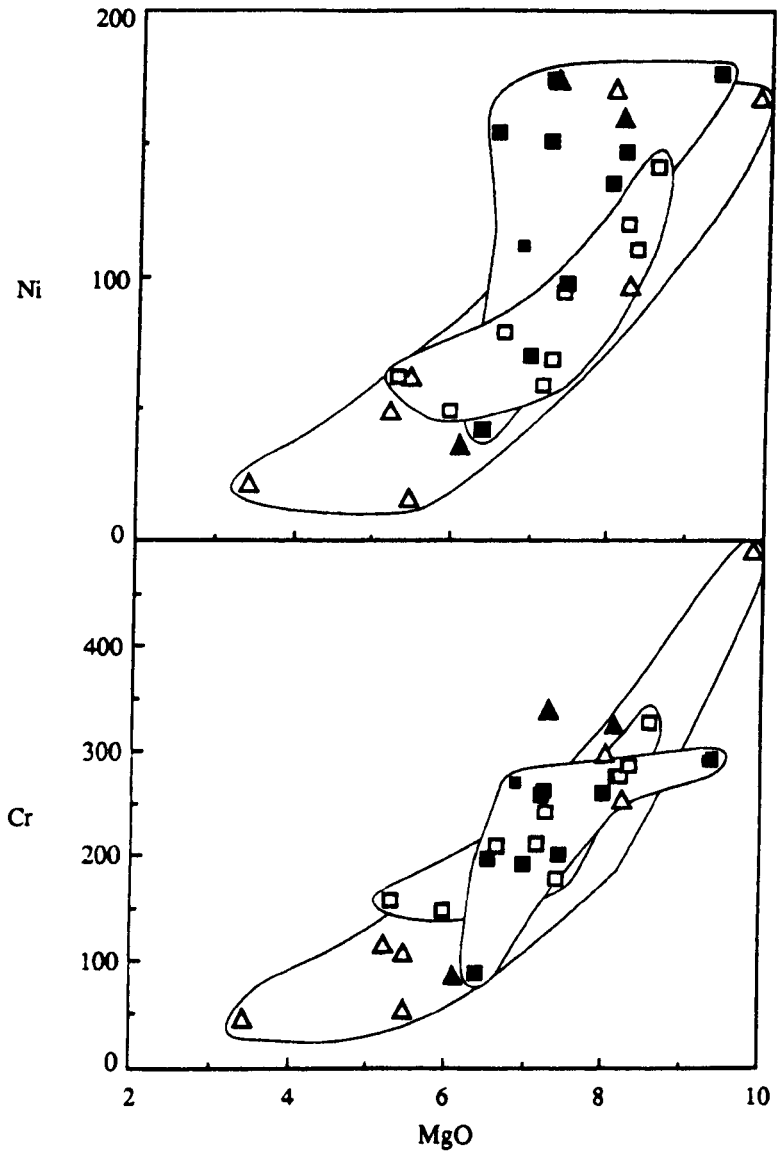

Fig. 5-4 Compatible elements, Ni and Cr, vs MgO in the Northland and Mercury Island rocks.

These features are also observed in mantle-normalised trace element diagrams (Fig. 5-6). Group 1 shows high incompatible element abundances, with Nb more enriched than the LIL elements such as Ba, Rb and K_2O.

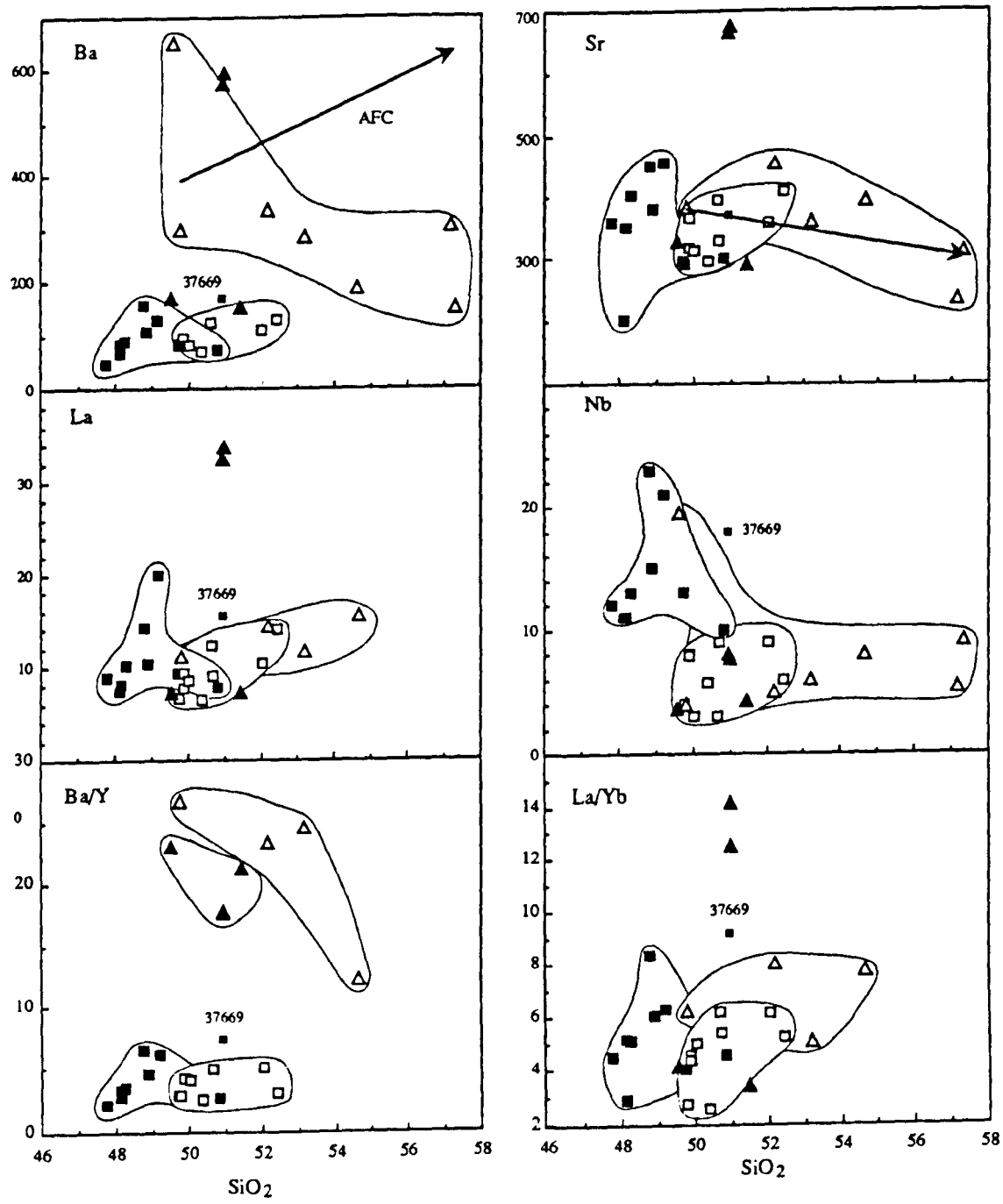

Fig. 5-5 Incompatible element abundances and ratios vs SiO_2. Group 1 has low Ba and Ba/Y, but high Nb, in contrast to high Ba and Ba/Y, but low Nb in the Group 3 and Mercury samples. Group 2 has low Ba content similar to Group 1, but low Nb similar to Group 3 and Mercury samples. Group 2 seems to exhibit a positive correlations between Ba, La and Sr with SiO_2, whereas Group 3 samples appear to have broadly negative correlation between Sr and SiO_2. For discussion, see text.

These patterns are similar to those for the Auckland basalts. Fig. 5-6 shows that Group 2 samples have similar incompatible element abundances to Group 1, but with a clear negative Nb anomaly. The result is a low Nb/La

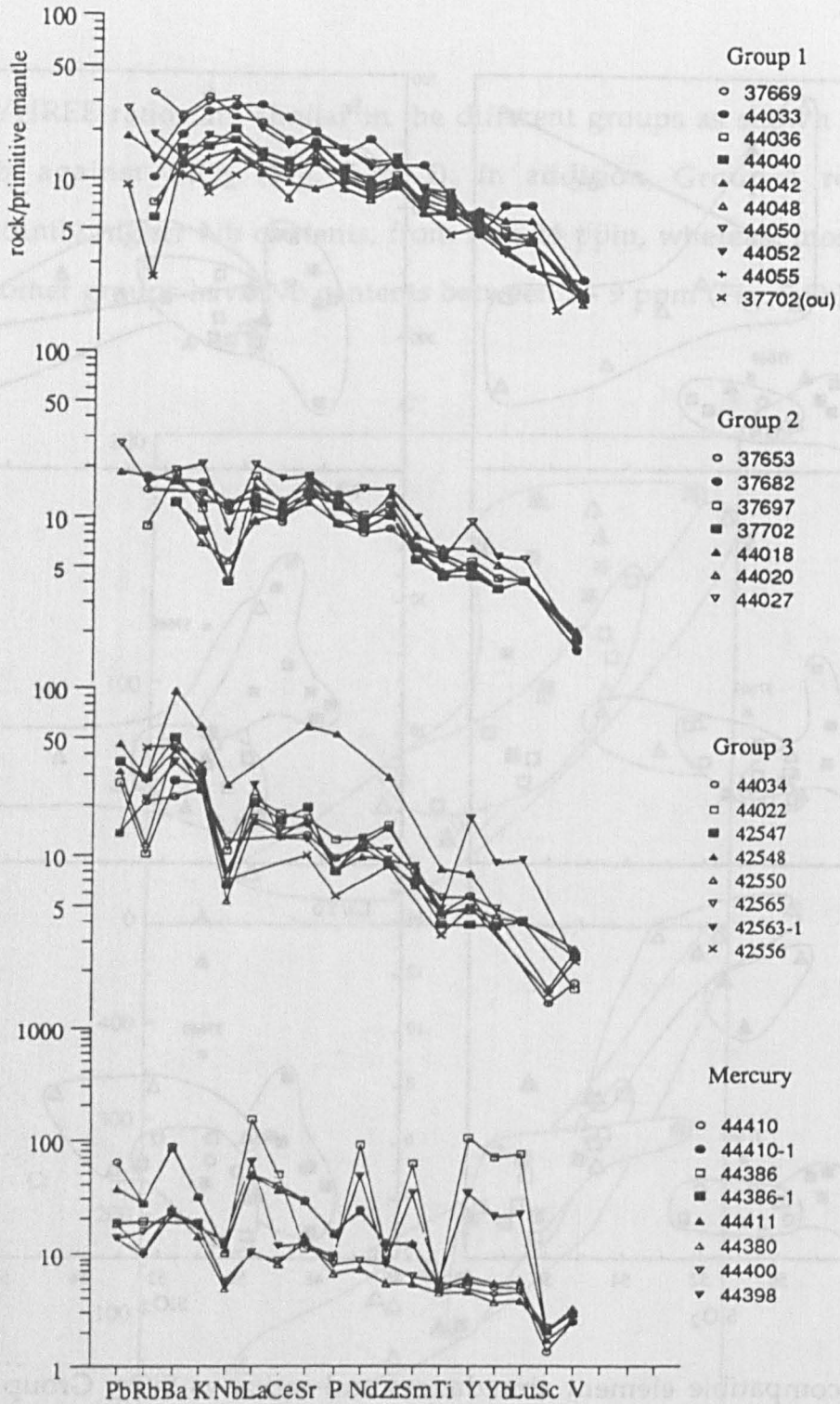

Fig. 5-6 Trace element normalised diagrams for Group 1(a), Group 2 (b) and Group 3 (c) and Mercury Island samples (d). They are normalised to primitive mantle (Sun and McDonough 1989). Group 1 has a smooth pattern with high incompatible element contents and a positive Nb anomaly, whereas Group 2 has incompatible element abundances similar to Group 1, but with a negative Nb anomaly. Group 3 and Mercury have similar trace element patterns with high LILE and significant negative Nb anomalies. Three samples, one from Group 3 and two from Mercury, are very different from the others with very high Y and LREE contents, flat REE patterns and negative Ce anomalies.

ratio in Fig. 5-2, which is very different from Group 1. Group 3 and Mercury samples have similar mantle normalised incompatible element patterns, i.e. variable and generally high LIL and LRE elements, with large negative Nb anomalies. These patterns are similar to those from TVZ basalts.

Three samples, one from Group 3 (42563) and two from the Mercury rocks (44386, 44398), have anomalously high Y contents (78 - 476ppm). They also have high REE contents, especially HREE, and therefore, rather flat REE patterns with a Ce negative anomaly (not shown). This REE profile is very different to those of the other samples. Whether these samples have been contaminated by REE and Y enriched components, or they are related to hydrothermal fluid veins, is not clear. P_2O_5 and LOI in the samples do not appear to be correlated with HREE and Y.

5-3.3 Sr and Nd isotope results

Sr and Nd isotope compositions are illustrated in Fig. 5-7, together with data from Auckland basalts and selected OIB and MORB. Group 1 and 2 basalts have similar Sr and Nd isotope ratios, and they plot in the same field in Fig. 5-7. Relative to the Auckland basalts they have similar Sr but higher Nd isotope ratios, and so plot within the MORB field. One sample (37669) from Group 1 has significantly higher $^{87}Sr/^{86}Sr$ (0.70340) and lower $^{143}Nd/^{144}Nd$ (0.51288) than the rest of the samples (Fig. 5-7).

The Group 3 and Mercury samples have similar Sr and Nd isotope ratios, which are similar to those from the Taupo basalts but significantly different from Groups 1 and 2 (Fig. 5-7). Since they have higher Sr and lower Nd isotope ratios, they are displaced towards the basement rocks on a Nd-Sr isotope diagram.

TABLE 5-3
Isotope data of the Northland and Mercury Island samples

	Age	$^{87}Sr/^{86}Sr$	$^{143}Nd/^{144}Nd$	$^{206}Pb/^{204}Pb$	$^{207}Pb/^{204}Pb$	$^{208}Pb/^{204}Pb$
37653		0.703052	0.513011	18.781	15.586	38.541
37653-1				18.765	15.602	38.565
37669		0.703399	0.512897	18.845	15.606	38.654
37682				18.767	15.576	38.484
37697		0.703209	0.513028	18.82	15.599	38.656
37702		0.702989	0.512985	18.793	15.585	38.575
42547	8.62	0.704082	0.512882	18.761	15.58	38.622
42548				18.945	15.674	38.997
42550	8.37	0.703977	0.512933	18.793	15.610	38.608
42556		0.704768	0.512828	18.776	15.595	38.608
42563-1				18.823	15.616	38.709
42563-2				18.82	15.612	38.694
42565	8.34			18.801	15.601	38.654
44018	0.32	0.70298	0.512992	18.805	15.611	38.665
44020	2.38			18.655	15.569	38.396
44020		0.702583	0.513051	18.655	15.569	38.396
44020ou				18.631	15.552	38.351
44027	1.06	0.703125	0.512976	18.779	15.602	38.633
44033	0.36	0.702805	0.513016	18.865	15.557	38.507
44034	9.35	0.704329	0.512933	18.825	15.612	38.659
44034-1				18.848	15.621	38.699
44036	1.33	0.70269	0.51304	18.796	15.581	38.528
44040	2.7	0.702712	0.513051	18.734	15.579	38.441
44040-1				18.731	15.541	38.336
44042	8.1	0.702868	0.513002	18.774	15.572	38.531
44048	4.61	0.702742	0.513002	18.960	15.58	38.652
44050	0.19	0.702958	0.512991	18.933	15.584	38.595
44052	5.7	0.702715	0.512998	19.006	15.569	38.594
44055	9.7	0.702697	0.512986	19.141	15.651	38.879
44380		0.704386	0.51282	18.824	15.608	38.673
44386		0.70412	0.512813	18.825	15.621	38.710
44386-1				18.809	15.604	38.650
44398		0.703629	0.512861	18.862	15.608	38.684
44400		0.703883	0.512916	18.801	15.606	38.657
44410ou		0.704694	0.512781	18.837	15.615	38.713
44410				18.836	15.614	38.709
44411		0.704622	0.512804	18.84	15.615	38.720

Age, Sr and Nd isotope data from I Smith (1992 and unpubl.)

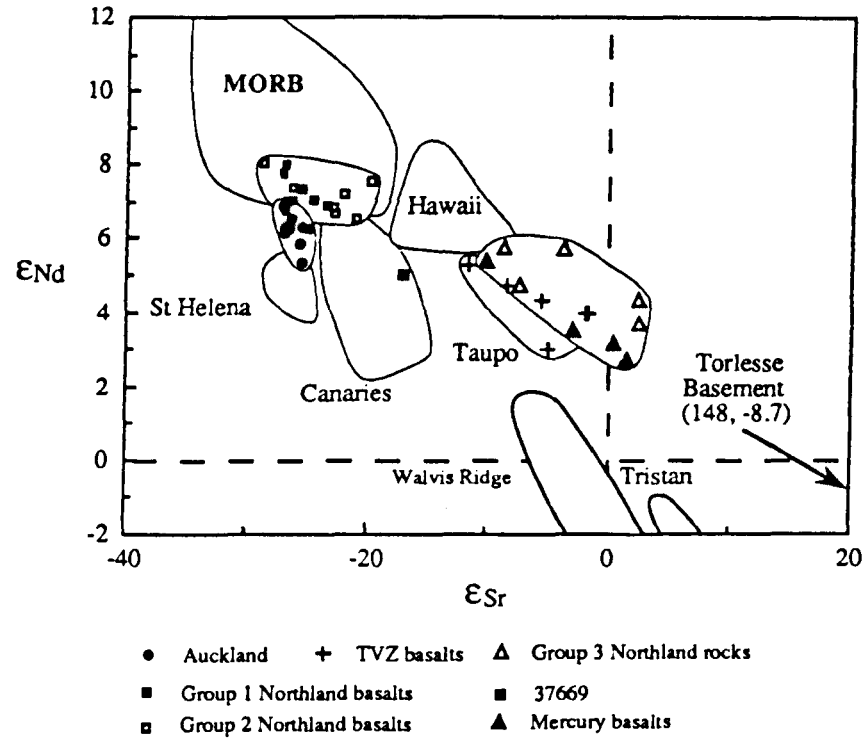

Fig. 5-7 εNd vs. εSr diagram, illustrating the Nd and Sr isotope compositions of the Northland and Mercury samples, together with those from Auckland basanites, Taupo MORB, and some OIB (White and Hofmann 1982; Richardson et al. 1982; Ito et al. 1987; Chaffey et al., 1989; Le Roex et al. 1990; Hoernle et al. 1991; Graham et al. 1992; Chauvel et al. 1992; Hole et al. 1993). Nd and Sr isotope ratios in Groups 1 and 2 are similar, and they plot within the MORB field. Group 1 has similar Sr but higher Nd isotope ratios than the Auckland basanites. Group 3 and Mercury have much lower Nd and higher Sr isotope ratios than Groups 1 and 2, similar to the Taupo basalts.

5-3.4 Pb isotope compositions

The Pb isotope ratios are illustrated in Fig. 5-8 and define two trends. One trend is formed by the Group 1 basalts with a relatively shallow slope, because they have relatively high $^{206}Pb/^{204}Pb$ but low $^{207}Pb/^{204}Pb$ and $^{208}Pb/^{204}Pb$ ratios. These Pb isotope ratios are lower, but close to those for

the Auckland basalts in the Northland basalts. Sample 37669 is again an exception, with a Pb isotope composition similar to the Group 2 samples.

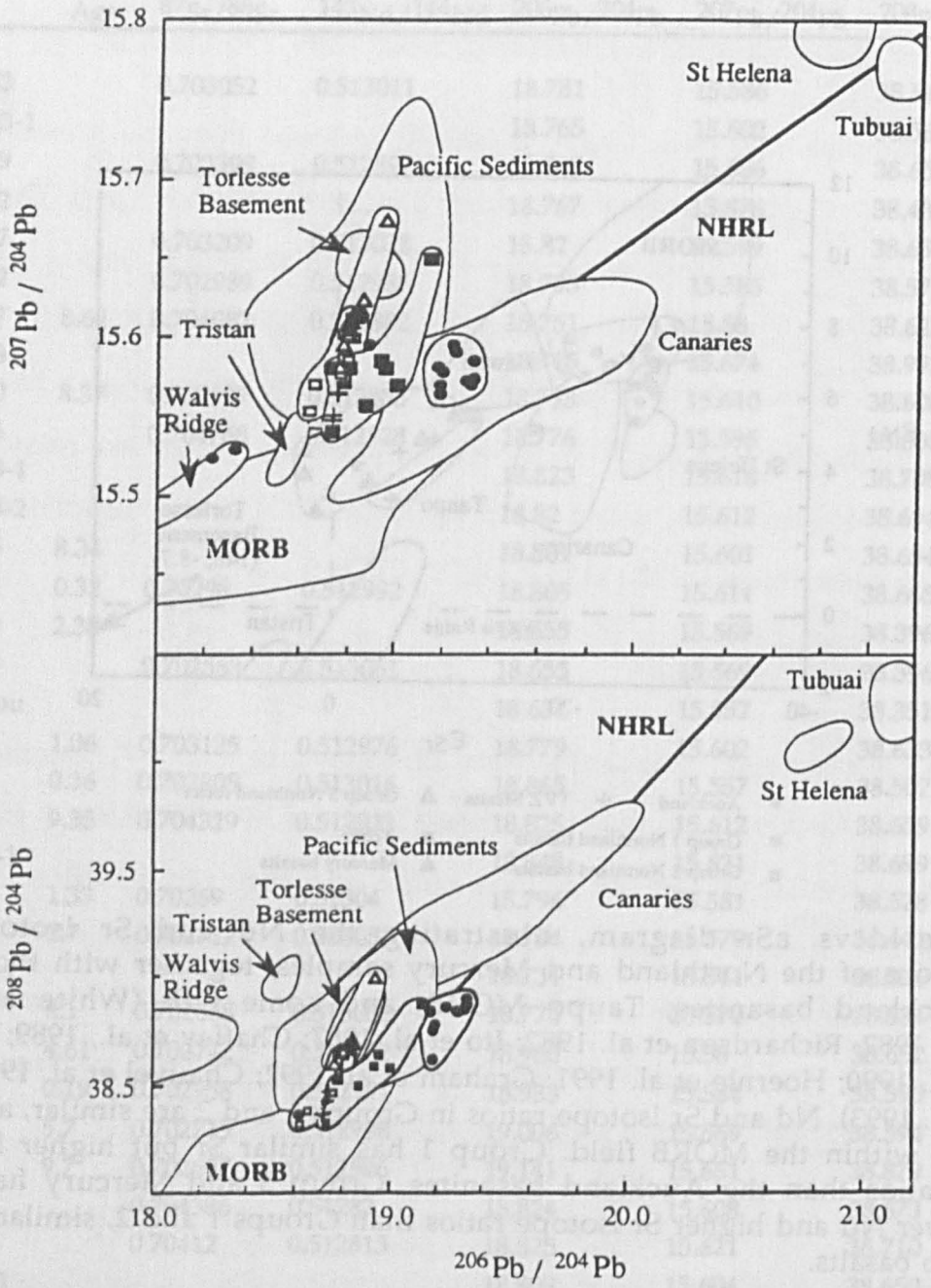

Fig. 5-8 (a) $^{207}Pb/^{204}Pb$ vs. $^{206}Pb/^{204}Pb$ and (b) $^{208}Pb/^{204}Pb$ vs. $^{206}Pb/^{204}Pb$, illustrating Pb isotope compositions in the Northland and Mercury samples. Data from the Auckland basanites, Torlesse basement and Pacific sediments, MORB and OIB are shown for comparison (Ben Othman et al. 1989; McDermott and Hawkesworth 1991 and others see Fig. 5-7 for data sources). Northern Hemisphere Reference Line is from Hart (1984). The Groups 2, and 3, and Mercury samples are similar to the Taupo basalts and they plot in a broad trend on both diagrams. The Group 1 basalts have higher $^{206}Pb/^{204}Pb$ but lower $^{207}Pb/^{204}Pb$ and $^{208}Pb/^{204}Pb$ than Groups 2 and 3. These differences are expressed by lower $\Delta^{207}Pb/^{204}Pb$ and $\Delta^{208}Pb/^{204}Pb$ in Table 5-4.

Although the group 2 rocks have similar Sr and Nd isotope ratios to group 1, they share some Pb isotope features with the Group 3 and Mercury samples, i.e high $^{207}Pb/^{204}Pb$ and $^{208}Pb/^{204}Pb$ relative to $^{206}Pb/^{204}Pb$, and so high $\Delta^{207}Pb/^{204}Pb$ and $\Delta^{208}Pb/^{204}Pb$ (following definition of Hart, 1984). Thus, the Group 2, 3 and the Mercury samples form a second trend in Fig. 5-8 with a steeper slope than the Group 1 and Auckland rocks. These Pb isotope ratios are similar to those for the Taupo basalts (Graham et al. 1992).

TABLE 5-4
The major compositional differences in the different sample groups

	Group 1	Group 2	Group 3	Mercury
SiO_2	48.2-50.8%	49.8-52.4%	49.6-57.3%	49.5-51.6%
Nb/Nb*	1.2-1.7	0.24-0.84	0.20-0.46	0.17-0.38
$^{87}Sr/^{86}Sr$	0.7027-0.7030	0.7026-0.7031	0.7040-0.7048	0.7039-0.7047
$^{143}Nd/^{144}Nd$	0.51299-0.51304	0.51298-0.51305	0.51283-0.51293	0.51278-0.51292
$\Delta^{207}Pb/^{204}Pb$	4.1±2.2 (1σ)	6.1±1.3 (1σ)	8.2±2.2 (1σ)	7.9±0.3 (1σ)
$\Delta^{208}Pb/^{204}Pb$	10.7±6.7 (1σ)	13.7±5.0 (1σ)	31.1±6.5 (1σ)	30.1±1.3 (1σ)

$Nb/Nb^*=Nb_n*2/(Ba_n+La_n)$

Table 5-4 summarises the major geochemical features of the different groups of samples. The Northland Group 1 basalts have relatively low silica contents, low Sr and high Nd isotope ratios, relatively high $^{206}Pb/^{204}Pb$, but low $^{207}Pb/^{204}Pb$ ratios compared with the other groups of Northland rocks. The Group 3 samples and Mercury basalts have similar compositions, relatively high silica contents and high Sr and low Nd isotope ratios, low $^{206}Pb/^{204}Pb$, but relatively high $^{207}Pb/^{204}Pb$ and $^{208}Pb/^{204}Pb$. The Group 2 samples have intermediate compositions in the sense that their Sr and Nd isotope ratios similar to Group 1, but their Pb isotope ratios are more similar to the group 3 and Mercury. In addition, the Group 2 rocks have similar LIL element abundances to Group 1 but with negative Nb anomalies which are a feature of Group 3 and Mercury.

High $\Delta^{207}Pb/^{204}Pb$ and $\Delta^{208}Pb/^{204}Pb$ in Groups 2 and 3 of the Northland rocks and Mercury basalts are similar to both the basement rocks and Pacific ocean sediments. In detail, most of them plot towards the basement rock field, except for one sample which has Pb isotope ratios higher than the basement. The Pacific sediments data scatter widely and overlap those for the Groups 2 and 3 of the Northland and Mercury samples. The Group 1 Northland basalts appear different, with relatively high $^{206}Pb/^{204}Pb$, and plot near the field for the Auckland basalts.

The isotope characteristics of the three groups of the Northland and Mercury rocks are illustrated on selected isotope-isotope diagrams (Fig. 5-9). The Group 1 basalts have restricted Sr isotope ratios but variable Pb isotope ratios, therefore, they plot on a vertical array on a $\Delta^{208}Pb/^{204}Pb$ - $^{87}Sr/^{86}Sr$ diagram (Fig. 5-9a). The Group 2 basalts have low Sr isotope ratios, similar to the Group 1 basalts, but Pb isotope ratios similar to Group 3 and Mercury. Therefore, the Group 3, Mercury and Group 2 rocks plot on a near horizontal array on the $\Delta^{208}Pb/^{204}Pb$ - $^{87}Sr/^{86}Sr$ diagram with Group 2 at the end connecting to Group 1. A similar picture can be seen on a diagram of $\Delta^{208}Pb/^{204}Pb$ ~$^{143}Nd/^{144}Nd$ diagram (Fig. 5-9b). The implications of these trends is discussed in later sections.

A recent study of the geochronology on the Northland volcanic rocks shows that the K-Ar ages are between < 1 Ma to ~ 10 Ma. (Smith et al. 1993). One date of a Mercury basalt gives a K-Ar age about 6 Ma. The Northland volcanic activity was long lived and has different geochemical characteristics, but there is no relationship between ages and geochemical features. Although the available age data show that 5 of 7 samples from the Northland Group 3 have older ages (6.9 - 9.6 m.y.), the other two samples have ages of 0.3 and 0.71 Ma. (Smith et al. 1993). In addition, the Groups 1 and 2 have K-Ar ages between 0.19 to 9.7 m.y., which are similar to those from Group 3.

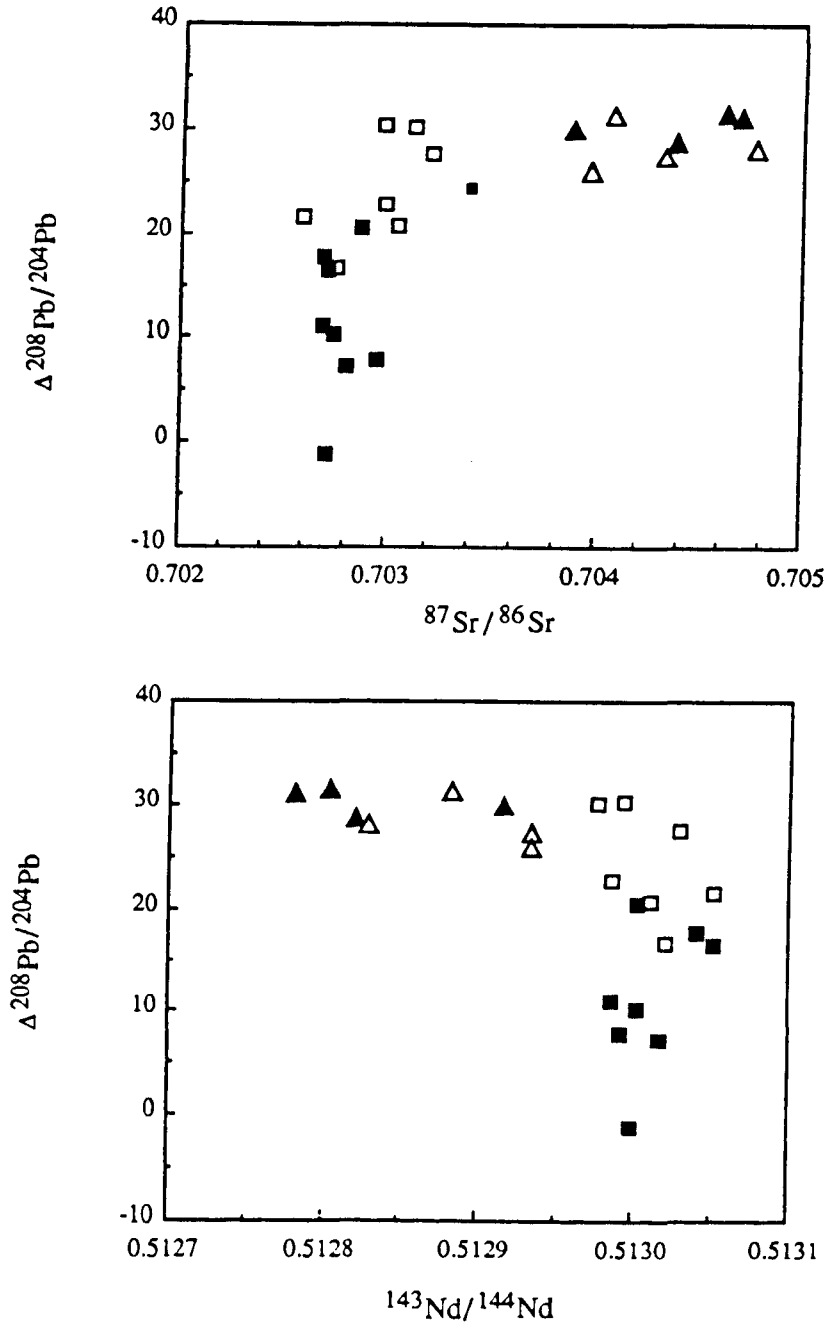

Fig. 5-9 Isotope diagrams showing the relationship between Pb, Sr and Nd isotope ratios in the Northland and Mercury samples. Group 1 has rather constant Sr and Nd but variable Pb isotope ratios, with low $^{208}Pb/^{204}Pb$ relative to $^{206}Pb/^{204}Pb$. In contrast, the Group 3 and Mercury samples have constant Pb but variable Sr and Nd isotopes and high $^{208}Pb/^{204}Pb$ relative to $^{206}Pb/^{204}Pb$ ratios. Whereas the Sr and Nd isotope ratios in Group 2 are similar to Group 1, but the Pb isotope ratios are similar to those in Group 3.

5-4. Fractional Crystallisation Processes

Major elements vary significantly within each group of samples and some trends between trace and major elements have been noted (Fig. 5-4, 5). These are likely to be due to fractional crystallisation during magma evolution.

MgO and Ni contents are sensitive to fractional crystallisation processes when olivine is one of major crystallising mineral phases. MgO contents vary widely in the Northland samples, which overlap each other in different groups, but they tend to be lower than in the Auckland basalts.

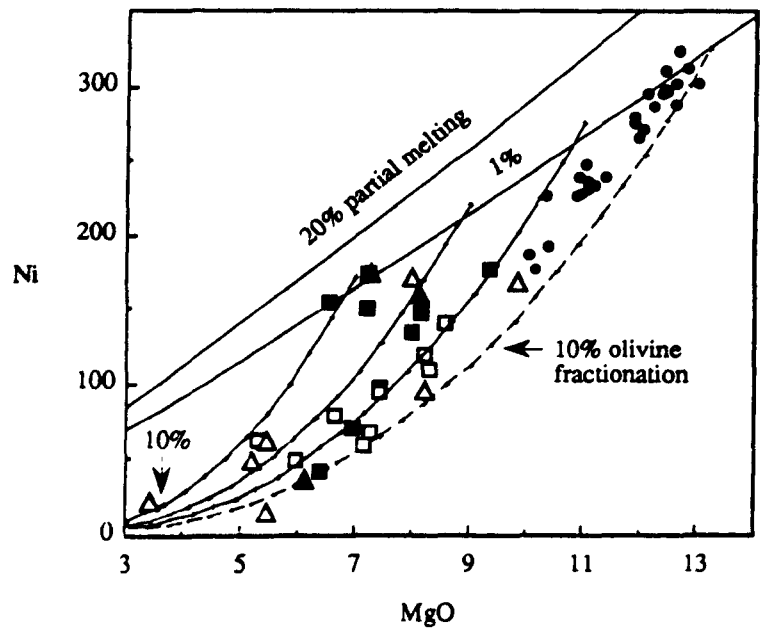

Fig. 5-10 Ni against MgO, showing the effects of olivine fractionation. Olivine fractionation lines were calculated following models of Hart and Davis (1978). The Auckland basanites are shown for comparison. Filled circles are the Auckland basalts and the rest of symbols are as the same as in Fig. 5-2.

The positive correlation between Ni and MgO may reflect olivine fractionation. However, because that Ni partition coefficient into olivine correlates negatively with the MgO content in the liquid, the positive correlation between Ni and MgO does not necessarily require that the

Northland basalts underwent more fractionation than in the Auckland basalts. On Fig. 5-10, following the Hart and Davis (1978) model, the data show that the Northland and Mercury rocks may have olivine fractionation from very little to more than 10%.

However, olivine may not be the only mineral phase to have fractionated from the magmas. On an Al_2O_3 vs. SiO_2 diagram (Fig. 5-3a), it can be seen that olivine fractionation tends to result in an increase of Al_2O_3 without increasing SiO_2 significantly, which is not consistent with some of the data arrays. This suggests that other mineral phases may also be involved in the magma evolution. Plagioclase has higher Al_2O_3 contents than the bulk rock compositions, and so fractionation of plagioclase and olivine will reduce the rate of increase of Al_2O_3 with SiO_2. Moreover, clinopyroxene is also required to account for the decrease in CaO with increasing SiO_2 shown by the data trends (Fig. 5-3c).

One way to examine fractional crystallisation is to use major element least-squares models and results are presented in the Appendix (element microprobe data for the mineral composition used in the least-square models are listed Appendix C3-3-1). Although there are wide variations within each group the results show some difference in calculated mineral assemblages between the groups. Average amounts of olivine, clinopyroxene and plagioclase removed by fractional crystallisation are 14%, 25% and 55% respectively in Group 1, and 25%, 35% and 34% in Group 2 and 29%, 29% and 39% in Group 3. These differences are expressed by different trends in major element diagrams (Fig. 5-3). Degrees of fractional crystallisation within each group vary from a few to more than 30%, and on average, 60% in Group 1, 81% in Group 2 and 68% in Group 3. Fitting residuals generally are small (most between 0.02 and 0.14) and so suggest that samples within each group may be related to one another by fractional crystallisation.

Some trace element data seem consistent with these models. Incompatible element contents should increase with fractionation i.e. La increases with SiO_2 in each group of samples, except for the Mercury rocks. Sr should be compatible on the basis of calculated cumulate assemblages if its partition coefficient for plagioclase is ~ 3, similar to recent experiment results (Blundy and Wood 1991). This is consistent with the broad negative trend between Sr and SiO_2 in the Group 3 samples (Fig. 5-5d). However, other groups scatter or show a broad positive trend in this diagram which indicates that some variations may be due to other processes, such as partial melting and contamination, or hetergeneity in the sources, which will be discussed further below.

5-5. Assimilation Processes

The fractional processes discussed above cannot be responsible for the significant variations in isotope compositions between and within some groups of samples. These may be due to different mantle source regions, however, the possible effects of crustal assimilation have to be examined first.

5-5.1 Group 1 basalts

Most of the samples in this group have low SiO_2, but high MgO contents, low $^{87}Sr/^{86}Sr$ and high $^{143}Nd/^{144}Nd$ ratios. There is no significant co-variation between $^{87}Sr/^{86}Sr$ and SiO_2 (Fig. 5-11), where the latter is considered as an indicator of fractionation. The basement rocks in New Zealand are Torlesse metamorphic rocks with high $^{87}Sr/^{86}Sr$ (on average ~0.715) and low $^{143}Nd/^{144}Nd$ (on average ~0.5122) isotope ratios. They also have high $^{207}Pb/^{204}Pb$ relative to their $^{206}Pb/^{204}Pb$ isotope ratios. These signatures are very different to those observed in most of the Group 1 basalts, and therefore, it would appear that they have not assimilated significant crustal material during fractionation.

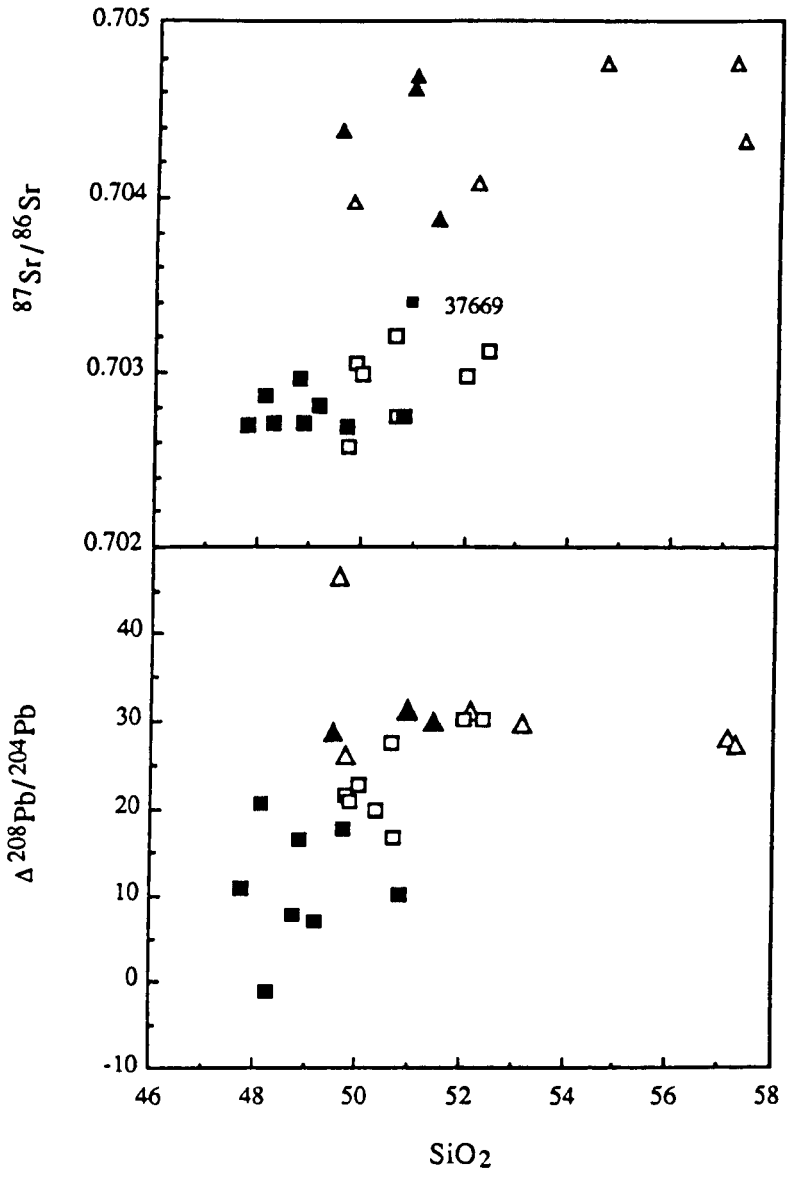

Fig. 5-11 (a) $^{87}Sr/^{86}Sr$ and (b) $\Delta^{208}Pb/^{204}Pb$ vs. SiO_2. Group 1 tends to have both low isotope ratios and SiO_2, whereas Group 3 and Mercury Island have similar SiO_2 to Group 2, but much higher $^{87}Sr/^{86}Sr$ and $\Delta^{208}Pb/^{204}Pb$. These diagrams also show that there are no significant correlations between $^{87}Sr/^{86}Sr$ and $\Delta^{208}Pb/^{204}Pb$ with SiO_2 within each group.

However, sample 37669 is an exception. It has lower Nd, but high Sr isotope ratios than the other samples in this group. Although its $^{143}Nd/^{144}Nd$ ratio is similar to the Group 3 basalts, it has lower $^{87}Sr/^{87}Sr$ relative to its Nd isotope ratios and so differs from the Group 3 basalts.

One explanation is that it was significantly contaminated. Mixing and AFC calculations indicate that the isotope composition of 37669 cannot be generated by mixing Group 3 with group 1 magma, however it might reflect contamination with the Torlesse basement. The calculation results are shown on Fig. 5-12, and they indicate that 37669 may have undergone 30~50% (r= 20%) AFC processes, depending on the choice of isotope compositions in the primary magma and Torlesse basement rocks. On the trace element ~ $^{87}Sr/^{86}Sr$ diagrams, AFC modelling is also consistent with the data (Fig. 5-13). The degrees of fractionation required by this model are also consistent with the major element least-squares model calculation.

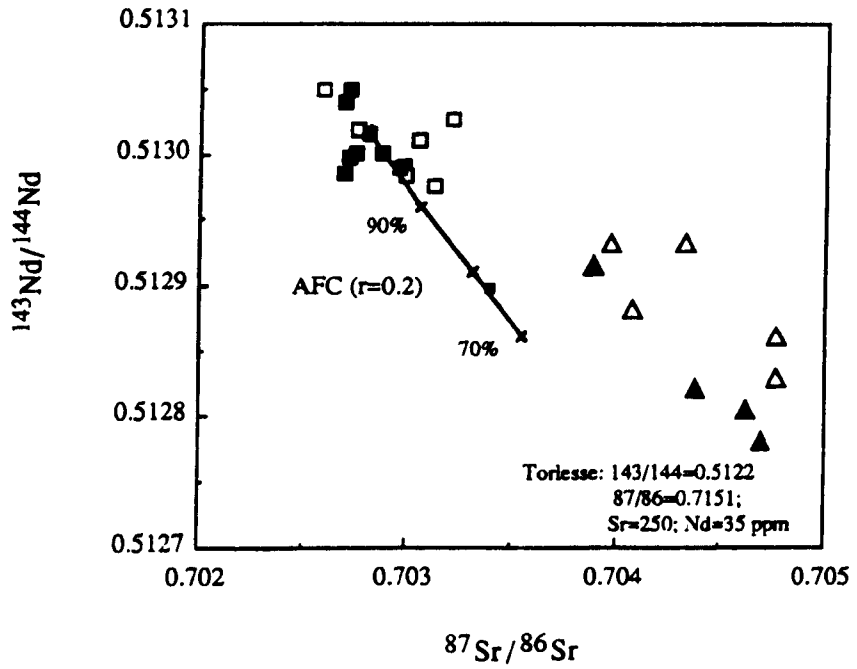

Fig. 5-12 $^{143}Nd/^{144}Nd$ vs. $^{87}Sr/^{86}Sr$ showing AFC model calculations using average compositions of the Torlesse basements (Graham et al. 1992). The results seem to indicate that sample 37669 with significant lower Nd and higher Sr isotope ratios can be generated by 20-30% of assimilation fractionation crystallisation from a parental melt with compositions similar to Group 1. However, the Group 3 and Mercury samples appear not to fit this model, and this could be due to either a component with higher $^{87}Sr/^{86}Sr$ ratio or having different parental magma compositions than Group 1.

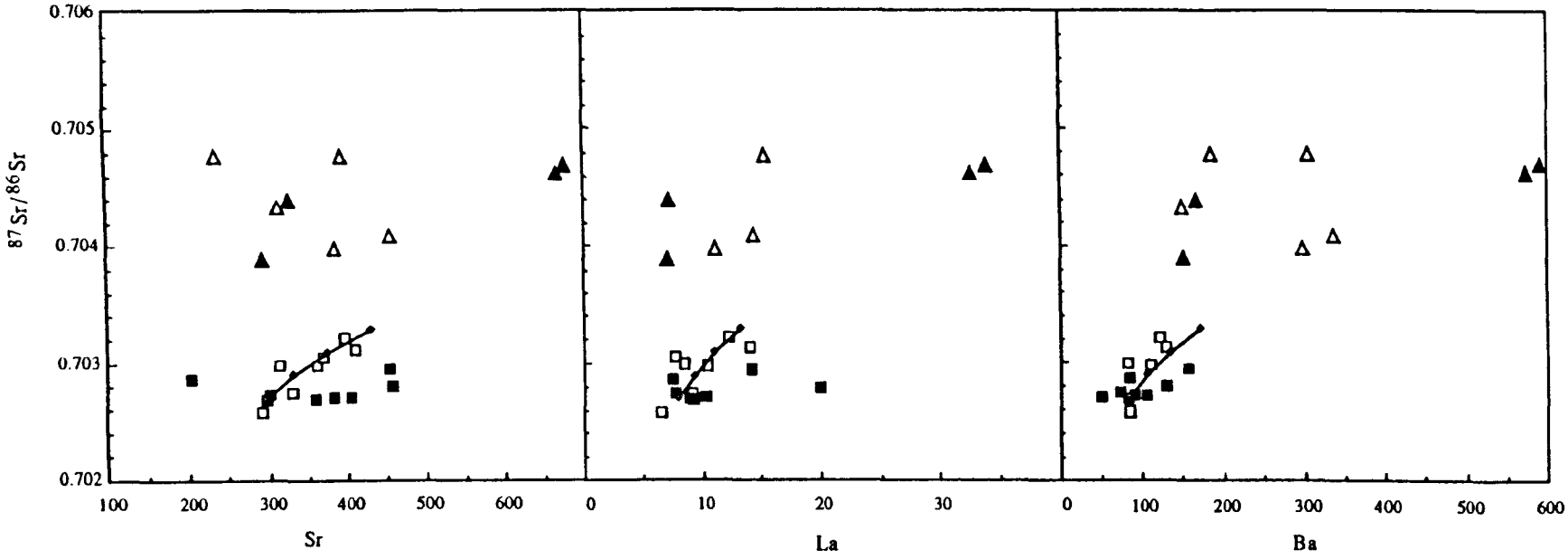

Fig. 5-13 Diagrams showing $^{87}Sr/^{86}Sr$ against selected incompatible elements. Groups 1 and 3 have very different $^{87}Sr/^{86}Sr$ ratios, and both of them show no significant correlations between $^{87}Sr/^{86}Sr$ with Sr, La and Ba. Group 2 has a positive correlation in all three diagrams. AFC model calculations using average compositions of Torlesse appear to fit the Group 2 trends.

5-5.2 Group 2 basalts

These samples have similar Nd and Sr isotope compositions to those in Group 1. However, on the Pb isotope diagrams and $\Delta^{208}Pb/^{204}Pb$ vs $^{87}Sr/^{86}Sr$ and $^{143}Nd/^{144}Nd$ diagrams (Fig. 5-8 and 9), they plot on an extension of trends formed by the data from the Group 3 basalts, with the basement rocks at the other end. Their Pb isotope ratios are similar to those from TVZ, which could have been contaminated by the basement rocks (Graham et al. 1992; Hedenquist and Gulson 1992). They have a small negative Nb anomaly, which is similar to the basement rocks. Moreover, there are positive correlations between $^{87}Sr/^{86}Sr$, SiO_2 and incompatible elements, such as Sr, Ba and La in this group of samples (Fig. 5-11 and 13). This suggests that the samples in Group 2 of the Northland basalts may have been contaminated by either Group 3 magma or basement rocks.

To investigate which is the more likely contaminant, the Group 3 basalts or the basement rocks, and how much contamination occurred, calculations have been carried out using the AFC model (DePaolo 1981). The results, shown on a $^{87}Sr/^{86}Sr$ vs Sr diagram (Fig. 5-13), appear to indicate that the Group 2 magma underwent AFC processes with less than 30% fractional crystallisation and 20% contamination by the basement rocks. Such calculations also show that Group 3 is not a suitable contaminant, since if the Group 2 samples were contaminated by Group 3 magmas, they would have had lower $^{87}Sr/^{86}Sr$ and different correlations with Sr contents (Fig. 5-13). The correlation between La and $^{87}Sr/^{86}Sr$ ratios in these samples is also consistent with the AFC model (Fig. 5-13).

A negative Nb anomaly is another feature which distinguishes this group from the Northland Group 1 basalts. However, this AFC model seems unable to generate the Nb anomaly by contamination with the basement rocks. Although the basement rocks have relatively low Nb contents (6-16 ppm) (Graham, 1985, Mortimer and Roser, 1992), because Nb

is a highly incompatible element, Nb contents in the samples should increase with increasing AFC and correlate positively with $^{87}Sr/^{86}Sr$. This is not what is observed (Fig. 5-14). In addition, although Nb/La ratios may be reduced by AFC processes, calculations indicate that Nb/La ratios should only be slightly changed with increasing of $^{87}Sr/^{86}Sr$ (Fig. 5-14).

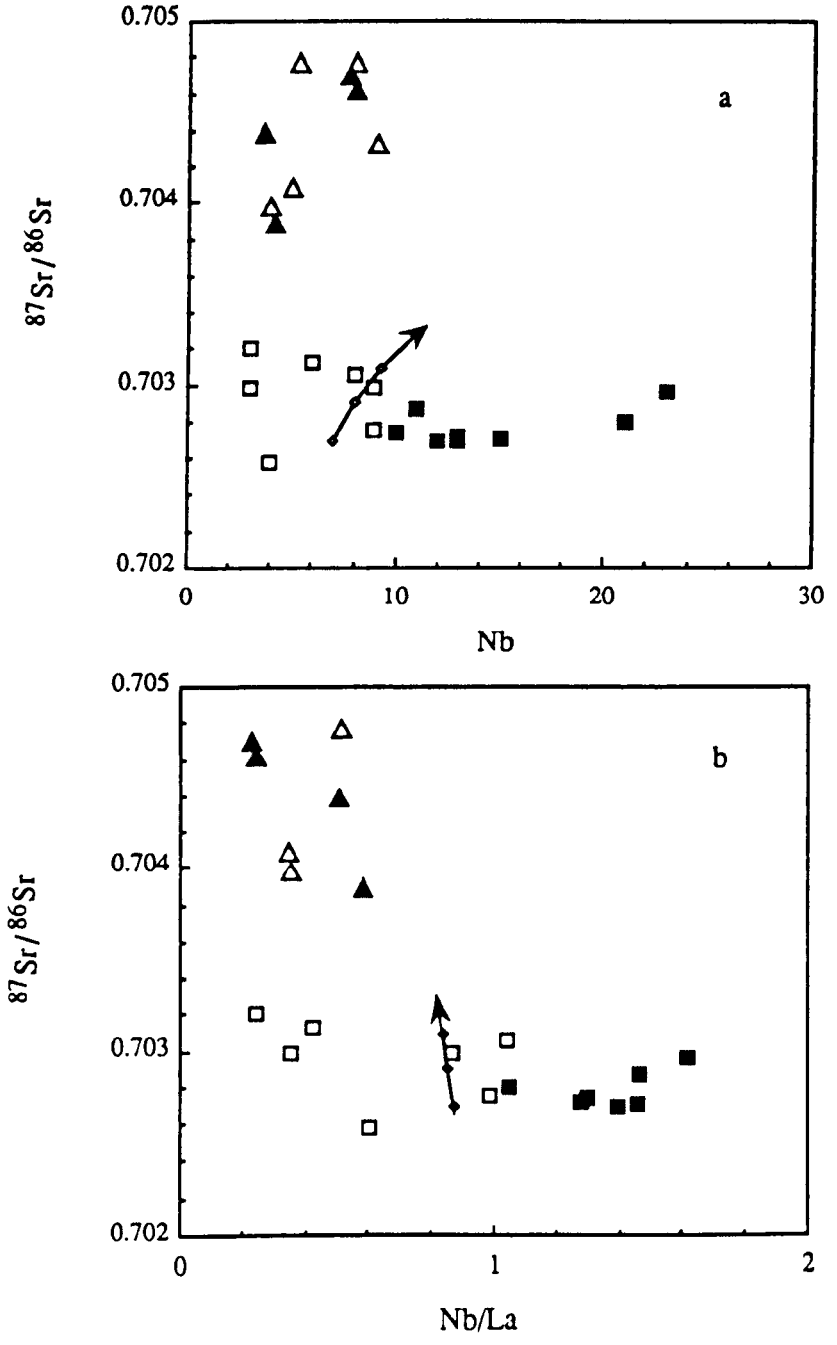

Fig. 5-14 $^{87}Sr/^{86}Sr$ against Nb and Nb/La. One major difference between Groups 1 and 2 is that Group 2 has lower Nb and Nb/La than Group 1. If the correlations between $^{87}Sr/^{86}Sr$ with Sr, La and Ba (Fig. 5-13) were due to AFC processes, the Nb content within Group 2 should increase with $^{87}Sr/^{86}Sr$, and Nb/La should hardly change. This is not what is observed.

Other explanations of the negative Nb anomaly in the Group 2 samples are that it was a feature from their mantle source regions, or a product of partial melting processes, in which case it may not have been associated with the variation of isotope compositions. Nonetheless, the Group 2 Northland basalts have relatively small Nb anomalies and lower Sr and Pb isotope ratios than the Group 3 basalts. Using the parameter, $Nb/Nb^*=Nb_n*2/(Ba_n+La_n)$, to describe the Nb anomaly relative to Ba and La, and excluding two samples for which there are no Ba data, the rest of the samples plot on broad trends of Nb/Nb^* vs $^{87}Sr/^{86}Sr$ and Nb/Nb^* vs $^{206}Pb/^{204}Pb$ (Fig. 5-15). These diagrams confirm that the samples in Groups 2 and 3 with higher $^{87}Sr/^{86}Sr$ and $^{206}Pb/^{204}Pb$ tend to have lower Nb/Nb^*, and implies a relationship between the size of the Nb anomaly and the variation in isotope ratios. Since it appears very difficult to generate the Nb anomaly by AFC processes, the observed trends of isotope compositions and trace elements may be inherited from their mantle sources. This will be discussed further below.

5-5.3 The Northland Group 3 and Mercury rocks

The Group 3 and Mercury rocks have similar isotope ratios to the basalts from the Taupo volcanic zone (TVZ), with higher $^{87}Sr/^{86}Sr$, lower $^{143}Nd/^{144}Nd$, and higher $^{207}Pb/^{204}Pb$ relative to their $^{206}Pb/^{204}Pb$ isotope ratios compared with the Group 1 basalts. On isotope - isotope diagrams, they trend away from Group 1, but towards an end-member of the Torlesse basement rocks (Fig. 5-7, 5-8). Several studies on the basalts from TVZ inferred that they have been significantly contaminated by the basement rocks (Graham et al. 1992; Hedenquist and Gulson 1992). Therefore, several questions may be asked, (i) whether the Group 3 basalts underwent AFC processes? (ii) To what extent their isotope compositions have been modified by contamination by the basement rocks, and (iii) what is the primary composition of the subduction related basalts?

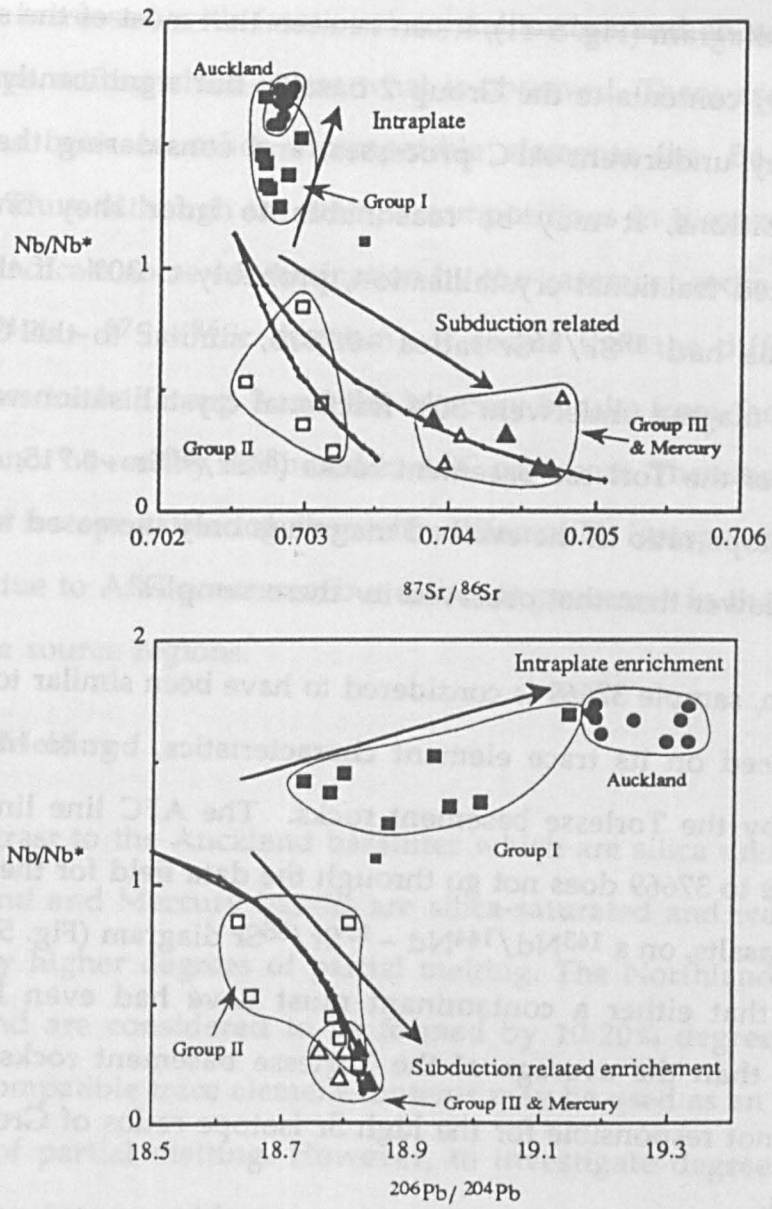

Fig. 5-15 Nb/Nb* vs. (a) $^{87}Sr/^{86}Sr$ and (b) $^{206}Pb/^{204}Pb$. Group 1 has high Nb/Nb*, restricted and low $^{87}Sr/^{86}Sr$, and variable $^{206}Pb/^{204}Pb$; therefore, they plot vertically in Fig. 5-15a and horizontally in Fig. 5-15b. The Auckland basanites are plotted for reference and they are at the high end of the Group 1 trends. Group 2 has similar $^{87}Sr/^{86}Sr$ to Group 1, but low Nb/Nb* and $^{206}Pb/^{204}Pb$. The Group 3 and Mercury samples tend to have even lower Nb/Nb*, and higher $^{87}Sr/^{86}Sr$ and $^{206}Pb/^{204}Pb$ ratios than Group 2. Thus, Nb/Nb* ratio appears to correlate negatively with $^{87}Sr/^{86}Sr$ and $^{206}Pb/^{204}Pb$ between the Groups 2 and 3 samples. Curves in the diagrams illustrate models which involve mantle source enrichment by slab derived fluids using end members in Table 5-5. See text for discussion.

The Group 3 rocks tend to have higher silica contents and Sr isotope ratios, and lower Nd isotope ratios, than Groups 1 and 2. However, on a $^{87}Sr/^{86}Sr$ ~SiO_2 diagram (Fig. 5-11), it can be seen that most of the samples have similar SiO_2 contents to the Group 2 basalts, but significantly higher $^{87}Sr/^{86}Sr$. If they underwent AFC processes, and considering they were basaltic compositions, it may be reasonable to infer they only had undergone limited fractional crystallisation, probably c. 30%. If the most parental magmas had $^{87}Sr/^{86}Sr$ ratios ~0.7028, similar to the Group 1 basalts, and the magma underwent 30% fractional crystallisation with 20% of assimilation of the Torlesse basement rocks ($^{87}Sr/^{86}Sr$ ~0.715, Graham 1985), the Sr isotope ratio in the evolved magma is only increased to 0.7031, which is much lower than that observed in these samples.

In addition, sample 37669 is considered to have been similar to the rest of Group 1 based on its trace element characteristics, but to have been contaminated by the Torlesse basement rocks. The AFC line linking the Group 1 basalts to 37669 does not go through the data field for the Group 3 and Mercury basalts, on a $^{143}Nd/^{144}Nd$ ~ $^{87}Sr/^{86}Sr$ diagram (Fig. 5-12). This may indicate that either a contaminant must have had even higher Sr isotope ratios than the average of the Torlesse basement rocks, or AFC processes are not responsible for the high Sr isotope ratios of Group 3 and Mercury rocks.

The Group 3 and Mercury samples have the most radiogenic Sr isotope ratios and lowest Nb/La ratios. The model calculations indicate that Nb/La cannot be changed so much by reasonable degrees of AFC processes. Thus, 37669 has contaminated signatures, high Sr and low Nd isotope ratios, but without significant negative Nb anomaly, consistent with a contamination model.

Another observation is that there are no significant correlations between incompatible element abundances and $^{87}Sr/^{86}Sr$ in these samples

(Group 3 and Mercury) (Fig. 5-13). If their isotope compositions had been significantly changed during AFC processes, incompatible element contents should be increased with fractional crystallisation and so would correlate with isotope ratios, which is not what is observed. There are also no clear correlations between other incompatible elements (i.e. Ba and La) and $^{87}Sr/^{86}Sr$. Thus, although the isotope compositions in these samples might appear to indicate some contamination by the basement rocks (such as on a $\Delta^{208}Pb/^{204}Pb \sim {}^{87}Sr/^{86}Sr$ diagram), it seems that the different isotope compositions in the Group 3 and the Mercury basalts from those in Groups 1 and 2 cannot be readily attributed to AFC processes. Therefore, the high Sr and low Nd isotope ratios together with different Pb isotope arrays may not be mainly due to AFC processes, but rather to processes in the evolution of their mantle source regions.

5-6. Partial Melting

In contrast to the Auckland basanites which are silica undersaturated, the Northland and Mercury basalts are silica-saturated and were probably generated by higher degrees of partial melting. The Northland basalts are tholeiitic, and are considered to be formed by 10-20% degrees of partial melting. Incompatible trace element contents may be used as an indicator of the degree of partial melting. However, to investigate degrees of partial melting using incompatible trace element contents, source compositions need to be known, and these are often not very well constrained. Thus, direct comparison of incompatible trace element contents may not reflect degrees of partial melting during their generation. For example, the Northland Group 3 and Mercury samples have higher abundances of highly incompatible element contents, such as Ba, Rb and La but not Nb, than Groups 1 and 2. This may be inherited from enriched sources, rather than result from smaller degrees of partial melting.

Thus, it is difficult to estimate an exact value of degrees of partial melting. If it is assumed that the Northland Groups 1 and 2 rocks were derived from similar source regions for the Auckland basalts, because they have broadly similar isotope ratios the Northland rocks may be generated by 10 - 15% partial melting.

The Northland group 3 and Mercury basalts (SiO_2 < 54%) have similar major element compositions to Group 2, but very different isotope compositions, and so they must be derived from different mantle sources. They may be generated by similar degrees of partial melting in which case their high LIL element contents are due to more enriched mantle sources.

Groups 1 and 2 have similar Sr and Nd isotope ratios, but different Pb isotopes, which might be due to contamination. However, another profound difference between them is the Nb anomaly, since Group 1 has a positive Nb anomaly and Group 2 has a negative one. The discussion above suggested that a negative anomaly is difficult to be generated via AFC processes. An alternative model is that such negative anomalies are generated during partial melting if there are residual Nb compatible mineral phase(s) in the source regions. Ti-phases, such as rutile, have been invoked (Ryerson and Watson 1987), because they may have high partition coefficient for Nb (McCallum and Charette 1978; Green and Pearson 1987). However, experimental studies indicate that melts in equilibrium with rutile should be saturated in Ti and this requires TiO_2 contents much higher than those observed (Green 1981; Ryerson and Watson 1987). Thus, it is concluded that the negative Nb anomalies in the Northland Groups 2, 3 and Mercury samples are a feature of their mantle source regions.

5-7. Mantle sources

The previous discussion suggested that the different isotope and trace element signatures of the different groups of Northland and Mercury rocks are difficult to attribute to assimilation or partial melting processes. For example, the Northland Group 3 and Mercury samples could not be generated from parental melts with compositions similar to Group 1 through AFC processes. Therefore, they are likely to reflect different compositional characteristics of their mantle source compositions which may be attributed to different mantle enrichment processes.

5-7.1 Intraplate enriched mantle sources

Because the Group 1 basalts have low Sr and high Nd isotope ratios, they are considered to be derived from isotopically depleted mantle source regions, broadly similar to the more enriched MORB. However, their higher incompatible trace element contents and low Sr and high Nd isotope ratios would suggest that these enrichments are relatively young.

Although their Sr and Nd isotope ratios are fairly homogeneous the Group 1 basalts have a relatively wide range of Pb isotope ratios (Fig. 5-8). In comparison with the other Northland and Mercury rocks, they have lower $^{207}Pb/^{204}Pb$ and $^{208}Pb/^{204}Pb$ relative to their $^{206}Pb/^{204}Pb$ ratios, and so lower $\Delta^{208}Pb/^{204}Pb$ and $\Delta^{207}Pb/^{204}Pb$. However, the Group 1 rocks also exhibit a negative correlation between $^{143}Nd/^{144}Nd$ vs. $^{206}Pb/^{204}Pb$ which appears to extend to the Auckland basalts (Fig. 5-16). There are two possible interpretations of this correlation. First, such variations may reflect previous melt generation and emplacement processes in the evolution of their source regions. Because U is more incompatible than Pb, and Nd is more compatible than Sm during mantle partial melting, with time, enriched mantle has lower $^{143}Nd/^{144}Nd$ and higher $^{206}Pb/^{204}Pb$ than depleted mantle source regions.

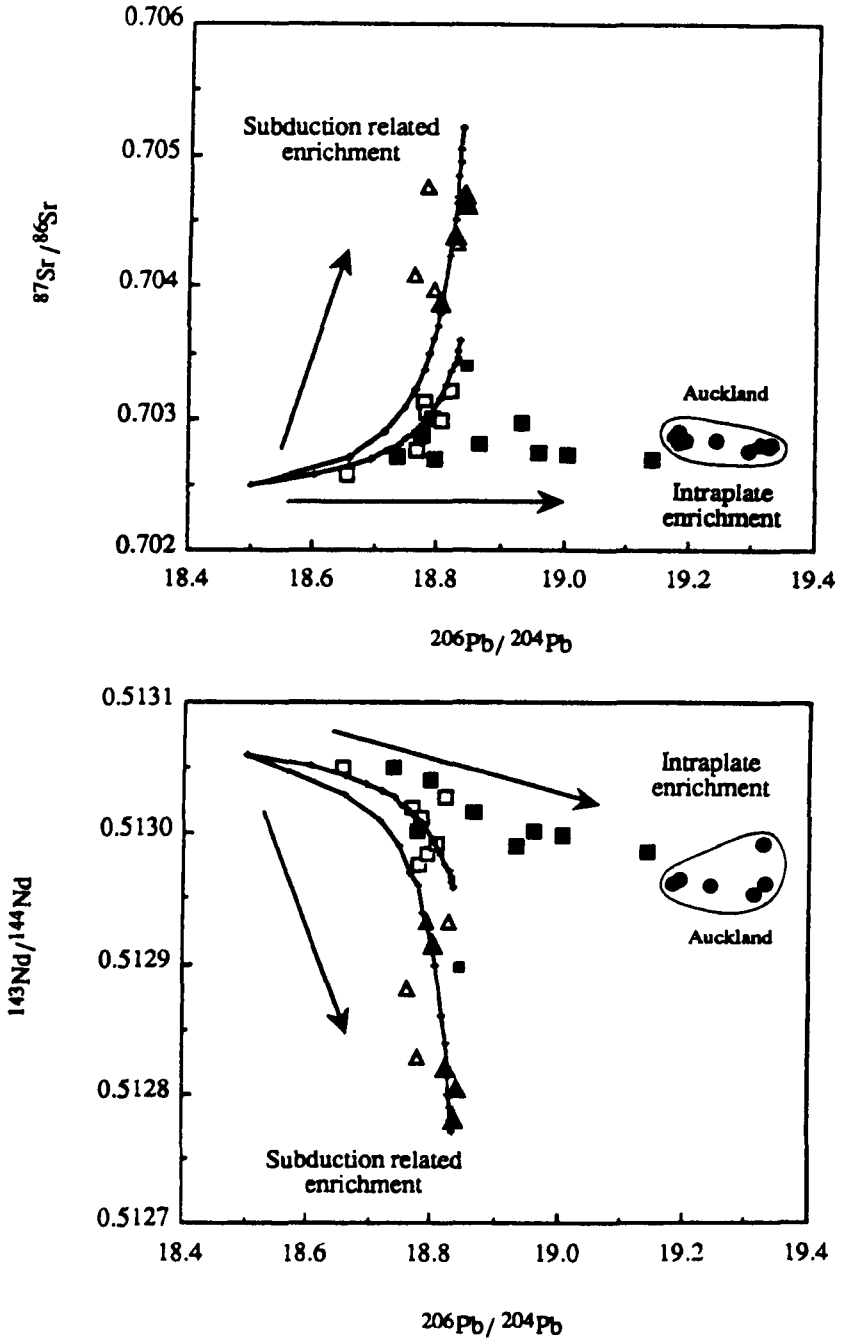

Fig. 5-16 (a) $^{87}Sr/^{86}Sr$ and (b) $^{143}Nd/^{144}Nd$ vs. $^{206}Pb/^{204}Pb$ illustrating the isotope differences between the different groups. These differences suggest that the different groups were derived from different mantle sources. Subduction related fluid enrichment models, following McCulloch and Gamble (1991), have been proposed to interpret the geochemical features in Groups 2 and 3 and Mercury samples. The end-member compositions used in the model calculations are listed in Table 5-5. The models seem to fit the Groups 2 and 3 and Mercury data arrays, but Group 1 may have been generated from mantle source regions enriched by OIB-like components. See text for discussion.

Second, the isotope variations might reflect mantle mixing associated with the introduction of an enriched component into depleted mantle. The

former could be a small degree melt from an enriched source, or it could involve a contribution from recycled oceanic crust, which has high U/Pb and so, with time, high Pb isotope ratios (see chapter IV for discussion). They have similar or slightly higher Nb/Nb* ratios, but lower Sm/Nd ratios and so lower $^{143}Nd/^{144}Nd$ ratios.

5-7.2 Subduction related mantle sources

The Group 3 and Mercury rocks are characterised by relatively high LIL and LREE abundances together with higher Sr, but lower Nd isotope ratios, and higher $\Delta^{208}Pb/^{204}Pb$ than Group 1. Although similar features have been attributed to crustal contamination in TVZ basalts (Graham et al. 1992; Hedenquist and Gulson 1992), it has been argued above that the Group 3 and the Mercury rocks cannot be generated by contamination from parental magmas similar to the Group 1 basalts, and that therefore, the Group 3 and Mercury rocks have different mantle sources. Although the reasons for Nb anomalies are still debated (e.g. Arculus and Powell 1986; Perfit and Kay 1986; Kelemen et al. 1993, Hawkesworth et al. 1993), this anomaly is well known to be associated with subduction related volcanic rocks (Pearce and Cann, 1973; Perfit et al. 1980; Pearce 1982). Thus, there are similarities between the Group 3 and Mercury samples and the TVZ basalts and magmas generated from subduction related mantle sources.

High LIL element contents, and high Sr, but low Nd isotope ratios in the samples may reflect derivation from enriched mantle sources which have been metasomatised by fluids or melts from down-going slabs. Oceanic sediments have higher Sr, low Nd, high $\Delta^{207}Pb/^{204}Pb$, $\Delta^{208}Pb/^{204}Pb$ isotope ratios (Meijer 1976; Ben Othman et al 1989; McDermott and Hawkesworth 1991). Although the processes of transferring material from the down-going slab into the mantle wedge are still a major subject of debate, a simple bulk mixing model involving a few percent of oceanic sediments appears to be able to explain the relatively high Sr, low Nd

isotope compositions of arc-related rocks (McCulloch and Perfit 1981; White and Patchett 1984). The Pb isotope compositions of the Group 3 and Mercury rocks overlap with the composition of the Pacific sediments, as do other arc basalts, such as the Sunda arc system (Ben Othman et al 1989), consistent with a small contribution from oceanic sediments (Ben Othman et al. 1989). Because the Pb isotope ratios in the southern Pacific sediments overlap with those for the Torlesse basement rocks (Fig. 5-8), it is difficult to distinguish between them. However, one sample in the group 3 with higher Pb isotope ratios than the basement rocks seems to indicate that the Pacific sediments may be more suitable as an end-member to account for the Pb isotope trends for the Group 3 and Mercury samples.

There is a consensus that oceanic sediments are recycled into the mantle during subduction based on Sr, Nd, Pb, and ^{10}Be isotope and trace element evidence (such as Plank and Langmuir 1993; Ben Othman et al. 1989; Morris et al 1990). However, there is no consensus as to how these subduction related components are transferred from slabs to the mantle wedge. One hypothesis involves derivation of subduction related magmas from the slab itself, which consists of oceanic sediments and altered basalts with high Sr, low Nd and relatively high $^{207}Pb/^{204}Pb$, and can account for the isotope signatures in island arc basalts. However, other studies (such as Kelemen et al. 1993) have concluded that melts derived from partial melting of slabs will be too rich in incompatible elements and too depleted in compatible elements.

In a mixing model, only a few percent of oceanic sediments are needed in the mantle source regions of subduction related basalts to explain their isotope characteristics. However, the key trace element features of subduction related magmas, including enrichment in LIL and LRE elements but depletion of HFSE, such as Nb, Zr and Ti, cannot be simply explained by a two component mixing model. One explanation would

attribute depletion of HFSE to partial melting processes with residual Zr-rich and Ti-phases, such as zircon and rutile in the mantle wedge. However, experimental studies (Ryerson and Watson 1987) show that melts in equilibrium with Ti-phases stable in residual mantle, would have 7-9% TiO_2. This is too high for what has been observed in subduction related basalts. Ringwood (1990) suggested that partial melting of slabs under hydrous conditions would produce TiO_2 poor melts with residual mineral assemblage containing rutile, but they would be relatively SiO_2-rich. Others (such as Kelemen et al. 1990, 1992, 1993) emphasised the importance of reactions between ascending basaltic melts and depleted peridotite in the mantle wedge, since mantle orthopyroxene, olivine and spinel have higher partition coefficients for Nb relative to K and La, and Ti and Zr relative to adjacent REE on a mantle normalised diagram (Rampone et al. 1991; McDonough et al. 1992; Kelemen et al. 1993).

An alternative hypothesis is that HFSE are relatively insoluble in hydrous fluids from dehydration of a down-going slab (Ringwood 1976; Fuji 1983). The charge/radius ratios are considered to correlate with solubility (Tatsumi et al. 1986; Weaver 1991b), and Nb is less mobile than LILE and REE during dehydration. A mantle wedge metasomatised with these fluids will therefore be enriched in LILE and REE, but not Nb and Ta. However, Randle and Odling (1992) suggested that fluids in equilibrium with hydrated partially molten peridotite do not fractionate Nb from La and K. Thus, it may require the presence of some Nb compatible accessory mineral phases in the slab during dehydration. Although there is some uncertainty, this model is investigated in the next section (5-8) in the context of the Northland subduction related basalts.

5-7.3 Group 2 Northland basalts

The compositional differences between the Groups 1 and 2 basalts have been discussed in previous sections and inferred not to be primarily

due to contamination either by basement rocks or the Group 3 basalts. Thus, the Group 3 basalts may have different mantle sources from Group 1. However, group 2 basalts have geochemical features intermediate between those of Groups 1 and 3, suggesting some relationships between their mantle sources.

Their negative Nb anomaly and Pb isotope trends are similar to the Group 3 basalts, while their Sr and Nd isotope ratios are similar to the Northland Group 1 basalts. One model is that the Group 2 basalts were derived from a depleted mantle source with a contribution from fluids or melts from previously subducted slabs. Because they have relatively lower Sr and higher Nd isotope ratios, and lower $\Delta^{208}Pb/^{204}Pb$ and $\Delta^{207}Pb/^{204}Pb$ their source regions were presumably less metasomatised by subduction related fluids or melts than those for the Group 3 and Mercury basalts.

In addition, the mantle sources of the Group 2 basalts cannot be generated by adding subduction related material to the mantle source which is similar to those for the Group 1 basalts, because they have different Pb isotope trends. If the source region for the Group 2 basalts was generated by adding subduction related material, their Pb isotope trend should plot between the Group 1 and subduction related basalts. However, the Group 2 basalts plot on a extension of the subduction related basalts on both $^{207}Pb/^{204}Pb \sim ^{206}Pb/^{204}Pb$ and $^{208}Pb/^{204}Pb \sim ^{206}Pb/^{204}Pb$ diagrams. This may imply that their mantle source regions are separated spatially.

In summary, the basaltic volcanism in Northland and Mercury may have involved three components, depleted mantle, enriched mantle which may relate to recycled subducted oceanic crust, and mantle sources enriched by subduction related fluids and/or melts. These different mantle enrichment processes reflect the complexity of the tectonic setting in Northland-Auckland, New Zealand.

5-8. A model for the mantle enrichment

The discussion above suggests that both Groups 2 and 3 of the Northland basalts were derived from mantle sources which have been metasomatised by fluids (and/or melts) from the subducted slab. McCulloch and Gamble (1991) proposed a model for subduction related magmatism, which suggests that the mantle wedge was depleted by previous episodes of melt extraction, but later replenished by some non-slab derived melts (which may be from asthenosphere) and slab derived fluids (and melts). Woodhead et al (1993) studied basalts across the island arc and arc basin. From their data they concluded that the mantle source of the island arc basalts is depleted in HSFE and transition elements relative to those from arc basin basalts. They attributed this to previous melt extraction episodes, which is consistent in general with the McCulloch and Gamble model (1991). In such models the composition of the mantle wedge reflects the proportions and compositions of the melt from the asthenosphere, and slab derived fluids. The melt from the asthenosphere is assumed to have had similar isotope ratios to MORB in this model.

The most important parameter controlling an element content in slab derived fluids is its partition coefficient. For example, Nb has a low partition coefficient between residue and silicate melts, but perhaps a high partition coefficient (compatible) between residue and hydrous fluids. However, some other incompatible elements, such as Ba and La, are thought to have low partition coefficients between fluids and silicate rocks. Thus, fluids derived from the slab by dehydration would be characterised by high LILE and LREE, and fractionation of Nb from La, Ba and K.

The depleted mantle source in this modelling was chosen to be $^{87}Sr/^{86}Sr \sim 0.7025$, slightly lower than the ratios in the Group 1 basalts. Nb/Nb^* ratio in this depleted source is just above 1, which is consistent with LIL depletion in MORB-like sources, but lower than in the Group 1

Northland basalts. Relative to Group 3 and the Mercury rocks, Group 2 samples have low $^{207}Pb/^{204}Pb$ and $^{87}Sr/^{86}Sr$, but higher Nd isotope ratios. This may indicate that the mantle sources of the Group 2 Northland basalts were less enriched by slab derived fluids than the source regions of the Group 3 and Mercury rocks, assuming that the composition of the slab derived fluids remained constant. However, the Group 2 samples have only slightly higher Nb/Nb* than the Group 3 and Mercury samples, but very different Sr and Nd isotope ratios. The calculations show that it is difficult to generate these different mantle sources by only varying the proportions of the fluid. Alternatively, their source regions may have been enriched by slab derived fluids with different compositions. However, they are spatially associated, i.e. they may occur in the same area, such as Waipu-Ti Point area, which may imply that they are likely to involve the same end member components.

A down-going slab consists of three components, i.e. fresh MORB, altered crust and oceanic sediments. Thus, the composition of slab-derived fluids is controlled by the relative contributions from each of these three components. It is considered that elements in oceanic sediments and altered crust should be easier to leach out than in the un-altered oceanic crust rocks. Therefore, fluids derived from slabs at relatively shallow depth should have a large contribution from sediments and altered crust. With progressive subduction of the slab, fluids may have a higher proportion of elements from oceanic crust. In such a model, the fluids derived from a slab in different stages are likely to have different contributions from each end-member and so different compositions.

Selected data for the model calculation are listed in Table 5-5, and the calculations have been carried out using the equations given by McCulloch and Gamble (1991). The mantle wedge was depleted by previous melt extraction and then replenished by 20% incompatible elements from

asthenosphere. During subduction processes, the mantle wedge had been affected by 1 - 4% slab-derived fluids which have variable proportions of oceanic sediments, i.e. 5% for the mantle sources of the Group 2 basalts, and 13% for the mantle sources of the Northland Group 3 and Mercury basalts. The results are shown in Fig. 5-15 and 16. Although the figures very much depend on the model, they are considered to be plausible. This model can explain both Nb anomaly and isotope features in the Groups 2 and 3 rocks.

Table 5-5
Selected parameters and end-member compositions used in mantle source enrichment models

	MORB	Altered MORB	Sediments	D (res/melt)	D (res/fluid)
Pb (ppm)	0.5	0.4	20	0.01	0.07
Sr (ppm)	90	110	350		0.1
Nd (ppm)	7.3	7.3	25		0.15
$^{206}Pb/^{204}Pb$	18.5	18.5	18.9 -19.0		
$^{87}Sr/^{86}Sr$	0.7025	0.705	0.712		
$^{143}Nd/^{144}Nd$	0.51306	0.51306	0.512		
Ba (ppm)	10	26	1000	0.01	0.08
Nb	2	2	1.25	0.01	1.2
La (ppm)	3	3	20	0.01	0.1

	Slab For the group 2 basalts	Slab 2 For the group 3 basalts
MORB	90%	77%
Altered MORB	5%	10%
sediments	5%	13%
Pb (ppm)	21	43
Sr (ppm)	1040	1260
Nd (ppm)	55	64
Ba (ppm)	750	1754
Nb (ppm)	1.6	1.6
La (ppm)	38	52
$^{87}Sr/^{86}Sr$	0.704	0.706
$^{143}Nd/^{144}Nd$	0.51291	0.5127
$^{206}Pb/^{204}Pb$	18.85	18.84

It is noticeable that the Group 1 has diverse trends on Fig. 5-8, 15 and 16. These indicate that their mantle sources were enriched by a different

component through different processes. The arrays of the Northland Group 1 basalts seem to indicate an end member component with slightly low $^{143}Nd/^{144}Nd$ ratios (Fig. 5-16), but similar $^{87}Sr/^{86}Sr$ ratios (Fig. 5-16) and higher $^{206}Pb/^{204}Pb$ ratios with slightly higher Nb/Nb* ratio relative to the depleted mantle wedge (Fig. 5-15). On these diagrams, it can be seen that the Auckland basanites plot close to this more enriched component. It can be argued that the Auckland basanites were derived from mantle sources which had been metasomatised by melts that incorporated recycled oceanic crust. Thus, a similar origin may be proposed for the Northland Group 1.

5-9. Summary

The samples from the Northland volcanic field and Mercury Island have different major, trace and isotope compositions compared with those from the Auckland Volcanic Field. They are mainly silica saturated with lower abundances of highly incompatible elements, and they therefore are likely to be generated by relatively large degrees of partial melting

In detail, the Northland samples can be divided into three groups, Groups 1, 2, 3 and the Mercury basalts which are similar to group 3. Both Groups 1 and 2 basalts have low Sr, high Nd isotope ratios, which are similar to those for MORB and some OIB, and high LIL and LRE element abundances. However, Group 1 has a positive Nb anomaly, in contrast to the negative Nb anomalies in Group 2. Group 3 of Northland, and the Mercury basalts, have much higher Sr, but lower Nd isotope ratios, and a large negative Nb anomaly, similar to those of TVZ basalts. Pb isotope ratios in Group 1 have higher $^{206}Pb/^{204}Pb$ than the rest of the Northland basalts, whereas those in Group 2 are similar to Group 3 and Mercury samples, with relatively lower $^{206}Pb/^{204}Pb$, but higher $\Delta^{207}Pb/^{204}Pb$ and $\Delta^{208}Pb/^{204}Pb$.

It has been argued that the key geochemical features in the different groups were mainly inherited from their mantle source regions and not the

result of AFC processes. Group 1 basalts have trace element patterns similar to those from Auckland, and they were probably derived from mantle source regions which contain a component of recycled oceanic crust.

However, the negative Nb anomaly in the Group 2, 3 and Mercury samples is a well known characteristic associated with subduction related magmatism. Because Group 2 has lower Sr isotope ratios and less negative Nb anomalies than Group 3 and the Mercury samples, they seem to have been derived from a mantle source region which was less metasomatised by slab-derived fluids. However, model calculations suggested that it is difficult to generate mantle source regions for Group 2 and 3 without changing the metasomatic fluid compositions. Instead, fluids derived from a slab at different stages of subduction may have different element and isotope compositions, because some components in oceanic sediments and altered ocean crust are inferred to be more readily leached out than those from unaltered oceanic crustal rocks.

On the basis of these considerations, and using the model of McCulloch and Gamble (1991), calculations show that the mantle sources for Groups 2 and 3 basalts are likely to have been enriched by fluids derived from similar slabs but at different stages. The Group 2 mantle source region has less slab-derived fluid (~5%), and that fluid contains a lower contribution from sediments and altered oceanic crust, than the Group 3 mantle, which had 13% fluid. Thus, it is inferred that the Group 2 mantle source regions may involve fluids at a latter stage of dehydration than that for the Group 3 and Mercury rocks.

Therefore, different mantle enrichment processes, intraplate and destructive margin mantle metasomatism, are responsible for different geochemical features in various Northland and Mercury basaltic rocks, which is consistent with the complexity of the tectonic settings in this area.

Chapter Six

Summary: U-Th-Pb fractionation in selected case studies

6-1. Introduction

U and Th are major heat producing elements, therefore their distribution is important to models of the Earth's interior. In addition, natural isotopes of U and Th decay to isotopes of the same element, Pb. This unique isotope system therefore provides constraints for element flux models which other isotope systems cannot provide. Previous chapters presented the results of a number of detailed geochemical and petrogenetic studies. These studies provide new insight into U-Th-Pb fractionation in igneous carbonate and silicate systems, metamorphism in the lower lower crust and melt generation in the upper mantle, and on the effects of recycled crustal material on the geochemical variations in the upper mantle. This chapter summarises the main conclusions from each study and provides brief speculation on the general U-Th-Pb fractionation in mantle and crustal processes.

6-2. Petrogenesis of carbonatites and the implications for small degrees of partial melting in the upper mantle

Carbonatites are relatively uncommon and they have very different major and trace element patterns from silicate rocks, However, their isotope ratios are often similar to OIB (Basu and Tatsumoto, 1980; Bell, et al. 1982; Nelson et al. 1988). The study in Chapter 2 confirms that the Jacupiranga carbonatites have similar isotope signatures to those in the

oceanic basalts from the Walvis Ridge and Tristan da Cunha, and in the continental flood basalts of Parana. Thus, they were derived from mantle sources with regional isotope characteristics.

In general, there are two kinds of petrogenetic models for the generation of carbonatites; (i) liquid immiscibility and (ii) very small degrees of partial melting. Experimental studies indicate that there is liquid immiscibility gap between silicate and carbonate melts (Kjarsgaad and Hamilton 1989, Baker and Wyllie 1990), and so, carbonatite melts can be generated by segregation from a carbonate-rich silicate magma, but at relatively low pressures (< 25kb). This study demonstrated that there are some differences in isotope ratios between the carbonatites and associated silicate rocks at Jacupiranga, and so they are not in geochemical equilibrium. One explanation is that the carbonatite complex formed from several batches of magmas derived by small degrees of partial melting from the heterogeneous source regions in the upper mantle.

The significance of the minor and trace element contents of carbonatite melts is that they are believed to be important agents for metasomatism and the transport of elements in the mantle. Although there are wide variations of trace element abundances in carbonatites, most of the available data show that carbonatite melts preferentially carry more U relative to Pb, and so they have high U/Pb ratios. This can be demonstrated by both measured U/Pb and Pb isotope ratios, and in Fig. 2-9 it can be seen that carbonatite melts have higher U/Pb ratios than most small degree melts of the upper mantle. Therefore, mantle metasomatism by carbonatite melts may be an important mechanism to fractionate U/Pb. Their high U/Pb, low Rb/Sr and Sm/Nd ratios will result, with time, in radiogenic Pb, and relatively un-radiogenic Sr and Nd isotope compositions. If a carbonatite metasomatised mantle source has $\mu \sim 30$, which is the average of the measured values in carbonatites, radiogenic Pb

isotope ratios similar to HIMU OIB will be developed in ~1 Ga. Although carbonatite metasomatism has been recognised in mantle xenoliths (Yaxley et al. 1991 and Rudnick et al. 1993; Hauri et al 1993), this process has not been related to HIMU OIB components. There may be several reasons for this. First, the major and trace element compositions of primary carbonatite melts in the mantle are not precisely known, and so their signatures are not yet fully recognised. Second, if carbonatites can be used as analogue of primary carbonatite melts in the mantle, their trace element patterns are very different from those considered to be associated with HIMU OIB. This may indicate that carbonatite metasomatism may not play such a significant role in generation of HIMU mantle, perhaps because carbonatite metasomatism operates mainly in the upper mantle, where heterogeneities cannot survive for long beneath the mantle lithosphere.

6-3. Southern Africa granulite xenoliths: U-Th-Pb fractionation in lower crustal processes

The lower crust has long been considered as an important reservoir with un-radiogenic Pb isotope compositions to complement the more radiogenic Pb in the upper crust and mantle (Davis 1984; Newsom et al. 1986). However, recent studies of lower crustal xenoliths have shown that some xenoliths do not have significantly unradiogenic Pb isotope ratios, and so doubts have been raised over the general unradiogenic nature of the lower crust (Rudnick and Goldstein 1990).

The granulite xenoliths studied from southern Africa have similar mafic, major element compositions, but they are divided into two suites with different generation ages. Those from northern Lesotho are inferred on both the Sm-Nd and Pb-Pb isotope systems to have been derived from the mantle in the Proterozoic. In contrast, the samples from Markt and the Britstown group are thought to have been derived from the mantle in the Archaean, on the basis of Pb isotopes in both the whole-rock and mineral-

whole rock systems, even though their Sm-Nd system has been reset by Proterozoic and later events. Both suites of the granulites are characterised by unradiogenic Pb isotope ratios, and so fractionation of U from Pb resulted in low μ in the precursors to the granulites. Major and trace element evidence indicates that igneous cumulation processes played an important role.

This study on lower crust xenoliths from southern Africa therefore provides another example of low μ in the lower crust, and demonstrates that the role of cumulation processes may be as important as granulite metamorphism in the differentiation of major and trace elements in the lower crust. There are several hypotheses about the cause of U-Pb fractionation with the major one perhaps being dehydration during granulite metamorphism, which results in the preferential depletion of LIL including U. Such processes mainly play a major role in metamorphic terrains that contain intermediate to acid rocks with OH-bearing mineral phases, such as biotite (van Calsteren et al. 1986). Crystal cumulation is probably the predominant process in the lower crust sampled as xenoliths, since most lower crust xenoliths are mafic and attributed to underplating of mantle derived magma (Rogers and Hawkesworth 1982; Rudnick 1986, Kempton et al., 1990; Loock et al. 1990). Whether this reflects a spatial relationship between them, with mafic granulite xenoliths being derived from the bottom of the lower crust and samples from metamorphic terrains from shallower levels, is not clear.

Although the lower crust has been shown to have low μ, it need not have un-radiogenic Pb isotope ratios, since that will depend on how long this low μ environment has been preserved, ie. the age of the system. This means that some material may not have been old enough to have developed un-radiogenic Pb, for example the lower crustal xenoliths from Chudleigh and McBride in north Queensland (Rudnick and Goldstein

1990). Thus, Pb isotope compositions in the lower crust are age dependent, and various model calculations suggested that the lower crust is a reservoir of relatively un-radiogenic Pb isotope composition (such as Fig. 3-10).

6-4. Studies of Volcanism in Northland-Auckland Peninsula, NZ: Effects of recycling crustal material in the upper mantle

Chapters 4 and 5 presented the results of studies on Miocene-Recent basalts from the Northland-Auckland peninsula in North Island New Zealand. These volcanic fields are > 500km away from the present subduction zone and so in an intraplate tectonic settings. The volcanic rocks range from silica-undersaturated basanites to silica-saturated tholeiites and andesites. The silica-under-saturated rocks are mainly restricted to the Auckland volcanic field, with the others largely in the Northland field.

Most of the rocks underwent some fractional crystallisation, but this is not the major processes responsible for the overall geochemical variations. Crustal contamination has, in general, not been significant in the generation of these rocks. Therefore, most of their geochemical features are due largely to either partial melting processes, or to source compositions.

Since the silica-undersaturated rocks are mainly exposed in the Auckland volcanic field, the inferred degrees of partial melting appear to increase from the Auckland to the Northland volcanic field, and this may be accompanied by changes of the depths of melting regions from south to north. Isotopically two kinds of mantle sources regions can be identified, those replenished intraplate melts and those enriched by subduction related processes.

The Auckland basalts and the Northland Group 1 tholeiites have relatively low Sr, high Nd isotope, and high Nb/Ba and Nb/Rb ratios, and so they are considered to be derived from melt enriched source regions. In

contrast, the Northland Group 2 and 3 and the Mercury tholeiites and andesites tend to have relatively high Sr, low Nd and negative Nb anomalies, and so they have some link with subduction related processes. The Pb isotope compositions are also different in the two major suites, with $\Delta^{207}Pb/^{204}Pb$ and $\Delta^{208}Pb/^{204}Pb$ ratios being higher in the magmas derived from subduction related sources than in those from the intraplate replenished source regions.

Moreover, on the basis of Sr and Nd isotope and trace element features, e.g. high Nb/Ba, Nb/Rb, and Nb/La, the intraplate source regions are inferred to have been replenished by a component containing recycled oceanic crust, which is similar to HIMU (Weaver 1986, 1991; Chauvel et al. 1992). However, since their Pb isotope ratios are much lower than HIMU OIB, such as St Helena, this component is presumed to be relatively young.

This study therefore demonstrate that subduction processes result in two different fractionation patterns for U, Th and Pb. At relatively shallow level, fluids derived from dehydration of the slabs metasomatise the mantle wedges and result in relatively low U/Pb and high $\Delta^{207}Pb/^{204}Pb$ and $\Delta^{208}Pb/^{204}Pb$ due to the introduction of continental Pb. Whereas at deep level, the mantle is modified by residual material from recycled slabs with high U/Pb, and so radiogenic Pb tends to be developed .

6-5. U-Th-Pb fractionation and exchange in different reservoirs

The individual studies outlined above provide information for U-Th-Pb fractionation in crustal and mantle processes, and so they have implications for general models of U-Th-Pb fractionation in the Earth and element fluxes between different reservoirs.

Within the continental crust, the lower crust has low U/Pb and the upper crust higher U and Pb, but with higher μ. This results in the radiogenic Pb isotope ratios which are often observed in upper crustal rocks.

There are many ways that lower crustal components can be introduced into the upper crust, such as tectonic uplift and partial melting. Tectonic movements can bring material from the lower crust up into the upper crust, and vice versa which results in granulite grade metamorphic rocks exposed at the surface.

Partial melting of the lower continental crust is believed to be the main process responsible for granite genesis, whereby lower crustal material has been transferred into the upper crust, including U, Th and Pb. There have been a number of studies on the isotope compositions of granites in Precambrian provinces (Dickin, 1981; Clayburn, 1988; Farmer, 1992), which provide evidence that low U/Pb and Rb/Sr crustal material has been involved as parts of the sources of these granites. However, evidence that granulite xenoliths are residues after partial melting is more difficult to establish, and, most granulite xenoliths have been attributed to underplating of mantle derived magmas (Rogers and Hawkesworth 1982; Rudnick 1986, Kempton et al. 1990, Loock et al. 1990; Rudnick 1992a). Rudnick (1992b) argued that most post Archaean granulite terrains are also unlikely to be the residues after granite extraction, because such residues should have positive Eu anomalies since post-Archaean granites have been documented to have negative Eu anomalies (Taylor and McLennan, 1985), and this has not been observed in the rocks from granulite terrains. Rudnick (1992b) proposed a model in which granites were generated by partial melting of evolved crustal material rather than of basaltic precursors. However, underplating of mantle derived magmas in the lower crust, such as those represented by mafic granulites xenoliths, had an important role in the generation of evolved crustal material and in providing heat for differentiation within the crust.

The upper mantle is the source of primary crustal material, and so it has been depleted in trace element and isotope features, such as low

incompatible element contents and low $^{87}Sr/^{86}Sr$, and high $^{143}Nd/^{144}Nd$ in MORB. Since U is more incompatible than Pb, μ is expected to be low. However, Pb isotope ratios vary widely in mantle derived rocks. It has been argued that the Pb isotope compositions of MORB are controlled by a kinetic mechanism (Galer and O'Nions 1988; White 1993), in which the upper mantle is enriched by a flux from the lower mantle while being simultaneously depleted by magma extraction.

There is evidence (Tatsumoto 1969; Kay et al. 1980; Tera et al. 1986; Morris et al. 1990) that crustal components have been recycled into the mantle and subsequently result in enrichment and heterogeneity in the mantle. Subduction at plate margins is presumably one of the major ways by which crustal material is introduced back into the mantle. In this study it has been demonstrated that enrichment by components related to subduction can be subdivided into shallow and deeper level processes. Shallow processes tend to introduce more LIL, such as Rb and Ba, than HFS elements (Nb, Zr and Ti) and to result in mantle with high Sr and low Nd isotope compositions, and relatively high $^{207}Pb/^{204}Pb$ and $^{208}Pb/^{204}Pb$, together with relatively low μ.

In general, MORB and OIB have significant lower $^{207}Pb/^{204}Pb$ ratios than the continental crust, although OIB may have high or low $^{206}Pb/^{204}Pb$, as in HIMU and EMI. This has been considered to relate to whether sediment has been subducted deep into mantle basalt source regions. Whether subducted slabs have reached the lower mantle continues to be debated, nonetheless, these source regions seem to be characterised by less convection and so different isotope systems can be preserved for long periods of time. For example, St Helena basalts have been modelled from mantle source regions which had high μ for ~2 Ga (Chauvel et al. 1992). EMI source regions characterised by lower $^{206}Pb/^{204}Pb$, but high $\Delta^{207}Pb/^{204}Pb$ may have been developed over similar periods of time. These

components have been sampled by plumes which transfer material from deep mantle source regions to the surface. However, they may also be transported from deeper source regions to the depleted upper mantle by agents such as carbonate and silicate melts generated by small degrees of partial melting. Such mechanisms may be more common than large plumes expressed in some oceanic islands. In addition this recycling in general may be on much shorter time scales than that required to develop HIMU and EMI end-members. The intraplate basalts in the North-Auckland Peninsula with OIB geochemical signatures may provide a good example.

Overall, the element distribution (and redistribution) and the element fluxes within the Earth is not fully understood, but this study has provided more information necessary to set up an improved model of U-Th-Pb fractionation and related geological processes operating in the Earth's interior.

Reference

Adam J., 1990. The geochemistry and experimental petrology of sodic alkaline basalts from Oatlands, Tasmania. J Petrol. 31, 1201-1223.

Adam J., T. H. Green and S. H. Sie, 1993. Proton microprobe determined partitioning of Rb, Sr, Ba, Y, Zr, Nb and Ta between experimentally produced amphiboles and silicate melts with variable F content. Chem. Geol. 109, 29-49.

Allègre C. J., B. Dupré and E. Lewin, 1986. Thorium/Uranium ratio of the Earth. Chemical Geology 56, 219-227.

Allègre C.J. and D. Rousseau,1984. The growth of the continental through geological time studies by Nd isotope analysis of shale. Earth Planet. Sci. Lett. 67, 19-34.

Amaral, G., 1978. Potassium-Argon studies on the Jacupiranga alkaline district, state of Sao Paulo, Brazil, Pro. First Int. Sym. on Carbonatites: Brasilia, departmento Nacional da Producao Mineral, 297–302.

Andersen, T. and P.N. Taylor, 1988. Pb isotope geochemistry of the Fen carbonatite complex, S.E. Norway: Age and petrogenetic implications. Geochim. Cosmochim. Acta, 52: 209–215.

Arculus R. J. and R. Powell, 1986. Source component mixing in the regions of arc magma generation. J. Geophys. Res. 91 (B6), 5913-5926.

Baker M. B. and P. J. Wyllie, 1990. Liquid immiscibility in a nephelinite-carbonatite system at 25 kbar and implication for carbonatite origin. Nature, 346, 168-170.

Ballance, P. F. and K. B. Spörli, 1979. Northland Alochthon. J. Royal Soc. of New Zealand, 9, 259-275.

Barton E.S. and A. J. Burger, 1983. Reconnaissance isotopic investigation of the marginal zone of the Proterozoic Namaqua Mobile Belt, Upington Geotraverse. Spec. Publ. Geol. Soc. S. Afr. 10, 173-192.

Basu A. R. and M. Tatsumoto, 1980. Nd-isotopes in selected mantle derived rocks and mineral and their implications for mantle evolution. Contrib. Mineral. Petrol. 75, 43-54.

Basu, A.R., P.R. Renne, D. Mertz and R. J. Poreda, 1993. Alkalic igneous complexes of the Deccan and Parana: implication for the origin of continental flood basalts (CFB). AGU Fall Meeting, EOS, 74, 43: 552.

Becccaluva, L., Barbieri, M., Born, H., Brotzu, P., Coltorti, M., Conte, A., Garbarino, C., Gomes, C.B., Macciotta, G., Morbidelli, L., Ruberti, E., Siena, F. and Traversa, G., 1992. Fractional crystallisation and liquid immiscibility processes in the alkaline-carbonatite complex of Juquia (Sao Paulo, Brazil). J Petrol., 33: 1371–1404.

Bell K., J. Blenkinsop, T. J. S. Cole and D. P. Menagh, 1982. Evidence from Sr isotopes for long-lived heterogeneities in the upper mantle. Nature 298, 251-253.

Bell, K. and J. Blenkinsop, 1987. Nd and Sr isotopic compositions of east Africa carbonatites: Implications for mantle heterogeneity. Geology, 15: 99–102.

Bell, K. and J. Blenkinsop, 1989. Neodymium and strontium isotope geochemistry of carbonatites. In: K. Bell (Editor), Carbonatite: Genesis and Evolution. Unwin Hyman, pp. 278–299.

Bell, K. and T. Peterson, 1991. Nd and Sr isotope systematics of Shombole volcano, East Africa, and the links between nephelinites, phonolites and carbonatites. Geology, 19: 582–585.

Ben Othman D., M. Polve and C. J. Allegre, 1984. Nd-Sr isotopic composition of granulites and constraints on the evolution of the lower crust. Nature 307, 510- 515.

Ben Othman D., W. M. White and J. Patchett, 1989. The geochemical of marine sediments, island arc magma genesis and crust-mantle recycling. Earth Planet. Sci. Lett. 94, 1-21.

Blundt J. D. and B. J. Wood, 1991. Crystal-chemical control on the partitioning of Sr and Ba between plagioclase feldspar, silicate melts and hydrothermal solutions. Geochim. Cosmochim. Acta 55, 193-209.

Boyd, F. R. (1989) Compositional distinction between oceanic and cratonic lithosphere. Boyd, F.R., 1989. Earth Planet. Sci. Lett., 96, 15–26.

Brey, G. and D. H. Green, 1975. The role of CO_2 in the genesis of olivine melilitite. Contrib. Mineral. Petrol., 49, 93-103.

Brey, G. and D. H. Green, 1977. Systematic study of liquidus phase relations in olivine melilitite + H_2O + CO_2 at high pressures and petrogenesis of an olivine melilitite magma. Contrib. Mineral. Petrol., 61, 141-161.

Brey, G., W.R. Brice, D.J. Ellis, D.H. Green, K. L. Harris and I.D. Ryabchikov, 1983. Pyroxene-carbonate reactions in the upper mantle. Earth Planet. Sci. Lett., 62: 63–74.

Brothers, R. N. and M. Delaloye, 1982. Obducted ophiolites of North Island, New Zealand: Origin, age emplacement and tectonic implications for Tertiary and Quaternary volcanicity. New Zealand J. Geology and Geophysics, 25, 257-274.

Brothers, R. N., 1986. Upper tertiary and Quaternary volcanism and subduction zone regression, North Island, New Zealand. J. Royal Soc. New Zealand 16, 275-298.

Bryner V., 1991. Motukorea: The evolution of an eruption centre in the Auckland Volcanic Field. M.S. thesis in University of Auckland, New Zealand.

Burton K. W., A. S. Cohen, and R. K. O'Nions, 1993. Sm, Nd, U and Pb diffusion in garnet. Terra nova 5, 382.

Campbell I. H., 1977. A study of macro-rhythmic layering and cumulate processes in the Jimberlana intrusion, Western Australia. Part 1: the upper layered series. J. Petrol. 18, 83-215.

Chaffey D. J., R. A. Cliff and B. M. Wilson, 1989. Characterization of the Ht Helena source. In Magmatism in the ocean basins (eds. A. D. Saunders and M. J. Norry), Geol. Soc. Spec. Publ. 42, 257-276.

Chase, C. G., 1981. Ocean island Pb: two stage histories and mantle evolution. Earth Planet. Sci. Lett., 52: 277–284.

Chauvel C., A. W. Hofmann and P. Vidal, 1992. HIMU-EM: The French Polynesian connection. Earth Planet. Sci. Lett. 110, 99-119.

Chow T. J., 1970. Isotopic identification of industrial pollution lead. In Second International Clean Air Congress.

Clague, D. A. and F. A. Frey, 1982. Petrology and trace element geochemistry of the Honolulu volcanics, Oahu: implications for the oceanic mantle below Hawaii. J. Petrol., 23, 447-504.

Clayburn J. A. P., 1988. The crustal evolution of Central Scotland and the nature of the lower crust: Pb, Nd and Sr isotope evidence from Caledonian granites. Earth Planet. Sci. Lett. 90, 41-51.

Clifford T. N., E. F. Stumfl, A. J. Burger, T. S. McCarthy and D.C. Rex, 1981. Mineral chemical and isotopic studies of Namaqualand granulites South Africa: a Grenville analogue. Contrib. Mineral. Petrol. 77, 225-250.

Cohen, A. S., R. K. O'Nions, and M. J. O'Hara, 1991. Chronology and mechanism of depletion in Lewisian granulites. Contrib. Mineral Petrol., 106: 142–153.

Cohen, R. S. and R.K. O'Nions, 1982. Identification of recycled continental material in the mantle from Sr, Nd and Pb isotope investigation. Earth Planet. Sci. Lett., 61, 73-84.

Cole J. W., 1986. Distribution and tectonic setting of late Cenozoic volcanism in New Zealand. In Late Cenozoic Volcanism in New Zealand (ed. I. E. Smith), the Royal Soc. of New Zealand Bull. 23, pp. 7-20.

Cornell D. H., C. J. Hawkesworth, P. W., van Calsteren and W. D. Scott, 1986. Sm-Nd study of Precambrian crustal development in the Prieska-Copperton region, Cape Province. Trans. Geol. Soc. S. Afr. 89, 17-28.

Dalton J. A. and B. J. Wood, 1993. The compositions of primary carbonate melts and their evolution through wallrock reaction in the mantle. Earth Planet. Sci. Lett., 119: 511–525.

Davies J. H. and F. von Blanckenburg, 1995. Slab breakoff: A model of lithosphere detachment and its test in the magmatism and deformation of collisional orogens. Earth Planet. Sci. Lett. 129, 85-102.

Davis G. F., 1984. Geophysical and isotope constraints on mantle convection: an interim synthsis. J. Geophys. Res. 89 (B7) 6017-6040.

Dawson J. B., 1984. Contrasting type of upper mantle metasomatism. In Kimberlite II: The Mantle and Crust - Mantle relationship (ed J. Kornprobst), Elsevier, Holland, pp. 289-294.

De Wit M. J., C. Roering, R. J. Hart, R. A. Armstrong, C. E. J. De Ronde, R. W. E. Green, M. Tredoux, E. Peberdy and R. A. Hart, 1992. Formation of an Archaean continental. Nature 357, 553-562.

DePaolo D. J., 1981. Trace element and isotopic effects of combined wallrock assimilation and fractional crystallization. Earth Planet. Sci. Lett 53, 189-202.

Dia A., C. J. Allegre and A. J. Erlank, 1990. The development of continental crust through geological time: the South Africa case. Earth Planet. Sci. Lett. 98, 74-89.

Dickin A. P., 1981. Isotope geochemistry of Tertiary igneous rocks from the Isle of Skey, NW Scotland. J. Petrol. 22, 155-189.

Dickinson, W. R. and W. S. Snyder, 1979, Geometry of subducted slabs related to San Andeas transform. J. Geology, vol. 87, 609-627.

Downes H., C. Dupuy and A. F. Leyreloup, 1990. Crustal evolution of the Hercynian belt of Western Europe: Evidence from lower-crustal granulite xenoliths (French Massif Central). Chem. Geol. 83, 209-231

Dupré B. and C. J. Allègre, 1983. Pb-Sr isotope variation in Indian Ocean basalts and mixing phenomena. Nature 303, 142-146.

Dupre B. and N. T. Arndt, 1990. Pb isotopic compositions of Archaean komatiites and sulfides. Chem. Geol. 85, 35-56.

Eggler D. H., 1987. Solubility of major and trace elements in mantle metasomatic fluids: experimental constraints. In Mantle Metasomatism (eds. M. A. Menzies and C. J. Hawkesworth), Academic Press Inc Ltd (London), pp. 21-44.

Eggler, D.H., 1989. Carbonatites, primary melts and mantle dynamics, In: Keith Bell (Editor), Carbonatite: Genesis and Evolution, Unwin Hyman, pp. 561–579.

Ellam R. M. and K. G. Cox (1989) Proterozoic lithospheric source for Karoo Magmatism: evidence from the Nuanetsi picrites. Earth Planet. Sci. Lett. 92, 207-218.

Erlank A. J., F. G. Waters, C. J. Hawkesworth, S. E. Haggerty, H. L. Asopp, R. S. Richard and M. A. Menzies, 1987. Evidence for mantle metasomatism in perdotite nodules from the kimberlite pipes, South Africa. In Mantle Metasomatism (eds. M. A. Menzies and C. J. Hawkesworth), Academic Press Inc Ltd (London), pp. 221-311.

Erlank, A.J. (Ed.), 1984. Petrogenesis of the volcanic rocks of the Karoo Province. Spec. Publ. Geol. Soc. S. Afr. 13, 394 pp/

Esperanca S. R. W. Carlson and S. B. Shirey, 1988. Lower crustal evolution under central Arizona: Sr, Nd and Pb isotopic and geochemical evidence from the mafic xenoliths of Camp Creek. Earth Planet Sci. Lett. 90, 26-40.

Falloon, T. J. and D. H. Green, 1989. The solidus of carbonated, fertile peridotite. Earth Planet. Sci. Lett., 94: 364–370.

Farmer G. L., 1992. Magmas as tracers of lower crustal composition: an isotopic approach. In The Continental Lower Crust (eds.. D. M. Fountain, R. J. Arculus, R. W. Key), Elsevier Science Publisher, pp. 363-390.

Faure G. and P. M. Hurley, 1963 The isotopic composition of strontium in oceanic and continental basalt: application to the origin of igneous rocks. J. Petrol. 4, 31-50.

Faure G.,1986. Principles of Isotope Geology. John Wiley & Sons.

Fitton J. G., D. James and W. P. Leeman, 1991. Basic magmatism associatedwith Late Cenozoic extension in the western United Sates: Compositional variations in space and time. J. Geophys. Res. 96, 13,693-13,711.

Francis D. and J Ludden, 1990. The Mantle source for olivine Nephelinite, basanite and alkiline olivine basalt at Fort Selkirk, Yukon, Canada. J. Petrol. 31, 371-400.

Fraser K. J. and C. J. Hawkesworth, 1992. The petrogenesis of group 2 ultrapotassic kimberlites from Finsch Mine, South Africa. Lithos 28, 327-345

Fraser, K. J., C. J. Hawkesworth, A. J. Erlank, R. H. Michell and B. H. Scott-Smith, 1985/1986. Sr, Nd and Pb isotope and minor element geochemistry of lamproites and kimberlites. Earth Planet. Sci. Lett. 76, 57-70.

Fuji N., 1983. Low velosity zone along the subducted slab caused by dehydration. Oji International Seminar Formation of Ocean Margins, Tokyo.

Fujimaki H., M. Tatsumoto, and K.-I. Aoki, 1984. Partition coefficients of Hf, Zr and REE between phenocrysts and groundmass. J Geophys. Res. 89, B662-B672.

Galer S. J. G. and R. K. O'Nions, 1988. Residence time of thorium, uranium and lead in the mantle with implications for mantle convection. Nature 316, 778-782.

Gallagher, K. G. and C. J. Hawkesworth, 1992. Dehydration melting and the generation of continental flood basalts. Nature, 358, 57-59.

Gaspar J. C. and P. J. Wyllie, 1983. Magnetite in the carbonatites from the Jacupiranga complex, Brazil. Am. Min., 68: 195–213.

Gast P. W., G. R. Tilton and C. Hedge, 1964, Isotopic composition of lead and strontium from Ascension and Gough Islands. Science 145, 1181-1185.

Gill J., 1981. Orogenic Andesites and Plate Tectonics.

Gittins J., 1989. The origin and evolution of carbonatite magmas. In: Keith Bell (Editor), Carbonatite: Genesis and Evolution, Unwin Hyman, pp. 580–600.

Graham I. J., B. Gulson, J. W. Hedenquist and K. Mizon, 1992. Petrogenesis of late Cenozoic volcanic volcanic rocks from the Taupo Volcanic

Zone, New Zealand, in the light of new lead isotope data. Geochim. Cosmochim. Acta, 56, 2797-2819.

Gramham I. J., 1985. Rb-Sr Geochronology and geochemistry of Torlesse metasediments from the central North Island, New Zealand. Chem. Geol. 52, 317-331.

Green D. H. and M. E. Wallace, 1988. Mantle metasomatism by ephemeral carbonatite melt. Nature 336, 459-462.

Green T. H., 1981. Experimental evidence for the role of accessory phases in magma genesis. J. Volcanol. Geotherm. Res. 10, 405-422.

Green T. H., S. H. Sie, C. G. Ryan and D. R. Cousens, 1989. Proton microprobe-determined partitioning of Nb, Ta, Zr, Sr and Y between garnet, clinopyroxene and basaltic magma at high pressure and temperature. Chem. Geol. 74, 201-216.

Green T. I. and J. J Pearson, 1987. An experimental study of Nb and Ta partitioning between Ti-rich minerals and silicate liquids at high pressure and temperature. Geochim. Cosmochim. Acta 51, 55-62.

Grey C. M. and V. M. Oversby, 1972. the behaviour of Lead isotopes during granulite facies metamorphism. Geochim. Cosmochim. Acta 36, 930-952.

Griffin W. L., D. A. Carswell, P. H. Nixson, 1979. Lower-crust granulites and eclogites from Lesotho, southern Africa, The mantle sample: Inclusions from kimberlites and other volcanics (ed. Boyd et al.). American Geophysical Union, Washington D.C., 59-86.

Haggerty S. E., 1989. Mantle metasomes and the kinship between carbonatites and kimberlites. In: Keith Bell (Editor), Carbonatite: Genesis and Evolution, Unwin Hyman, pp. 546–560.

Hamilton D. L., P. Bedson, and J. Esson, 1989. The behaviour of trace elements in the evolution of carbonatites. In: Keith Bell (Editor), Carbonatite: Genesis and Evolution, Unwin Hyman, pp. 405–427.

Harris N. B. W., C. J. Hawkesworth, P. van Calsteren and F. McDermott, 1987. Evolution of continental crust in southern Africa. Earth Planet. Sci. Lett. 83, 85-93.

Hart S. R., 1984. A large-scale isotope anomaly in the Southern Hemisphere mantle. Nature 309, 753-757.

Hart S. R., C. Brooks, T. E. Krogh, G. L. Davis and D. Nava, 1970. Ancient and modern volcanic rocks, A trace element model. Earth Planet. Sci. Lett. 10, 17-28.

Hart, S. R. and K. E. Davis, 1978. Nickel partitioning between olivine and silicate melt. Earth Planet. Sci. Lett. 40, 203-219.

Hart, S. R. and T. Dunn, 1993. Experimental cpx/melt partitioning of 24 trace elements. Contrib. Mineral. Petrol. 113, 1-8.

Hart, S. R., 1988. Heterogeneous mantle domains: signatures, genesis and mixing chronologies. Earth Planet. Sci. Lett. 90, 273-296.

Hart, S.R. and T. Dunn, 1993. Experimental cpx/melt partitioning of 24 trace elements. Contrib. Mineral. Petrol. 113: 1–8.

Harte B., 1983. Mantle peridotites and processes- the kimberlite samples. In Continental and Mantle xenoliths (eds. C. J. Hawkesworth and M. Norry), Shiva, UK, pp. 46-91.

Harte B., P. A. Winterburn and J. J. Gurney, 1987. Metasomatic and enrichment phenomena in garnet peridotite facies mantle xenoliths from the Matsoku kimberlite pipe, Lesotho. In Mantle Metasomatism (eds. M. A. Menzies and C. J. Hawkesworth), Academic Press Inc Ltd (London), pp. 125-144.

Hartnady C., P. Joubert and C. Stowe, 1985. Proterozoic crustal evolution in southwestern Africa. Episodes 5, 236-244.

Hauri E., N. Shimizu, J. J. Dieu, and S. R. Hart, 1993. Evidence for hotspot-related carbonatite metasomatism in the oceanic upper mantle. Nature 365, 221-227.

Hawkesworth C. J. and A. G. Marlow, 1983. Isotope evolution of the Damara orogenic belt. Geol. Soc.S. Afr. Spec. Publ. 11, 397-407.

Hawkesworth C. J., A. J. Erlank, J.S. Marsh, M.A. Menzies and P. van Calsteren, 1983. Evolution of the continental lithosphere: evidence from volcanics and xenoliths in South Africa. In Continental Basalts and Mantle Xenoliths (eds C.J. Hawkesworth and M.J. Norry), Shiva, UK, pp. 111-138.

Hawkesworth C. J., A. J. Erlank, P. D. Kempton, and F. G. Waters, 1990. Mantle metasomatism: Isotope and trace-element trends in xenoliths from Kimberley, South Africa. Chem. Geol. 85, 19-34.

Hawkesworth C. J., K. Gallagher, J. M Hergt and F. McDermott, 1993. trace element fractionation processes in the generation of island arc basalts. Philos. Trans. R. Soc. London A 342, 179-191.

Hawkesworth C. J., N. W. Rogers, P. W. C. van Calsteren and M. A. Menzies, 1984. Mantle enrichment processes. Nature 311, 331-335.

Hawkesworth, C. J., K. Gallagher, S. Kelley, M. Mantovani, D. W. Peate, M. Regelous, and N. W. Rogers, 1992. Parana Magmatism and the opening of the South Atlantic. In: B.C. Storey, T. Alabaster and R.J. Pankhurst (Editors), Magmatism and the causes of continental break-up. Geol. Soc. Lond. Spec. Publ. 68: 221–240.

Hawkesworth, C. J., Kempton, P. D., Rogers, N. W., Ellam, R. M. and van Calsteren, P. W., 1990. Continental mantle lithosphere and shallow level enrichment processes in the Earth's mantle. Earth Planet. Sci. Lett. 96: 256–268.

Hawkesworth, C. J., M. J. Norry, J. C. Roddick and R. Vollmer, 1979, $^{143}Nd/^{144}Nd$ and $^{87}Sr/^{86}Sr$ ratios from the Azores and their significance in LIL-element enriched mantle. Nature 280, 28-31.

Hawkesworth, C.J., M.S.M. Mantovani, P.N. Taylor, and Z. Palacz, 1986. Evidence from the Parana of south Brazil for a continental contribution to Dupal basalts. Nature, 322: 356–359.

Hedenquist, J. W. and B. L. Gulson, 1992. Intrusive and basement rock sources of lead in hydrothermal systems of the Taupo Volcanic Zone, New Zealand. Geochim. Cosmochim. Acta, 56, 2821-2829.

Heming R. F. and P. R. Barnet, 1986. The petrology and petrochemistry of the Auckland Volcanic Field. In Late Cenozoic Volcanism in New Zealand (ed. I. E. Smith), the Royal Soc. of New Zealand Bull. 23, pp. 64-75.

Herz, N., 1977. Timing of spreading in the South Atlantic: information from Brazilian alkalic rocks. Geol. Soc. America Bull. 88: 101–112.

Hirose. K. and I. Kushiro, 1993. Partial melting of dry peridotites at high pressures: Determination of compositions of melts segregated from peridotite using aggregates of diamond. Earth Planet. Sci. Lett. 114, 477-489.

Hoernle K., G. Tilton and H.-U. Schmincke, 1991. Sr-Nd-Pb isotopic evolution of Gran Canaria: evidence for shallow enriched mantle beneath the Canary Islands. Earth Planet. Sci. Lett. 106, 44-63.

Hofmann A. W. and M. D. Feigenson, 1983. Case studies on the origin of basalts: I Theory and reassessment of Grenada basalts. Contrib. Mineral. Petrol. 84, 382-389

Hofmann, A. W. and W. M. White, 1982. Mantle plumes from ancient oceanic crust. Earth Planet. Sci. Lett., 57: 421–436.

Hofmann A. W., K. P. Jochum, M. Seufert and W. M. White, 1986. Nb and Pb in oceanic basalts; new constraints on mantle evolution. Earth Planet. Sci. Lett. 79, 33-45.

Hole M. J., 1988. Post-subduction alkaline Volcanism along the Antarctic Peninsula. Geol. Soc. London J. 145, 985-988.

Hole M. J., G. Rogers, A.D. Saunders and M. Storey, 1991. Relation between alkalic volcanism and slab-window formation. Geology 19, 657-660.

Hole M. J., P. D. Kempton and I. L. Millar, 1993. Trace-element and isotopic characteristics of small-degree melts of the asthenosphere: Evidence from the alkalic basalts of the Antarctic Peninsula. Chem. Geol. 109, 51-68.

Huang, Y.-M., P. W. van Calsteren, and C. J. Hawkesworth, 1994. Implication for the evolution of the lithosphere in southern Africa from isotope systematics in granulite xenoliths. ICOG, Berkeley, California.

Hussak, E. 1892. Ueber Brazilit, ein neues Tantal (Niob) Mineral von der Eisenmine Jacupiranga. Neues Jahrb. Min. Geol. Pal., 2: 141–159.

Ireland T. R., 1992. Crustal evolution of New Zealand: Evidence from age distributions of detrital zircons in West Province paragneisses and Torlesse greywacke. Geochim. Cosmochim. Acta 56, 911-920.

Irving A., 1978 A review of experimental studies of crystal/liquid trace element partitioning. Geochim Cosmochim Acta 42, 743-770.

Ito E., W. M. White and C. Göpel, 1987. The O, Sr, Nd and Pb isotope geochemistry of MORB. Chem. Geol. 62, 157-176.

Jones, A. P., 1989. Upper–mantle enrichment by kimberlitic or carbonatitic magmatism. In: Keith Bell (Editor), Carbonatite: Genesis and Evolution, Unwin Hyman, pp. 448–463.

Kay, R. W., S.-s. Sun, and C.-H. Lee-Hu, 1978. Pb and Sr isotopes in volcanic rocks from the Aleutian islands and Pribilof islands, Alaska. Geochim. Cosmochim. Acta 42, 263-273.

Kelemen P. B. H.J.B. Dick and J. E. Quick, 1992. Formation of harzburgite by pervasive melt-rock reaction in the upper mantle. Nature 358, 635-641.

Kelemen P. B., N. Shimizu and T. Dunn, 1993. Relative depletion of niobium in some arc magmas and the continental crust: partitioning of K, Nb, La and Ce during melt/rock reaction in the upper mantle. Earth Planet. Sci.Lett. 120, 111-134.

Kelemen P. B, R. J. Kinzler, K. T. M. Johnson and A. J. Irving, 1990. High field strength element depletions in arc basalts due to mantle-magma interaction. Nature 345, 521-524.

Kempton P. D. and R. S. Harmon, 1992. Oxygen isotope evidence for large-scale hybridization of the lower crust during magmatic underplating. Geochim. Cosmochim. Acta 56, 971-986.

Kempton P. D., 1987. Mineralogic and geochemical evidence for different styles of metasomatism in spinel lherzolite xenoliths: enriched mantle source regions of basalts? In Mantle Metasomatism (eds. M. A. Menzies and C. J. Hawkesworth), Academic Press Inc Ltd (London), pp. 45-90

Kempton P. D., H. Downes and D. Ionov, 1993. Deep crustal xenoliths: evidence for extreme compositional diversity in the lower crust beneath European rifts. Terra Nova 5, 427.

Kempton P. D., R. S. Harmon, C. J. Hawkesworth and S. Moorbath, 1990. Petrology and geochemistry of lower crustal granulites from the Geronimo Volcanic Field, southeastern Arizona. Geochim. Cosmochim. Acta 54, 3401-3426.

Kinny, P. D., W. Compston, J. W. Bristow, and I. S. Williams, 1989. Archaean mantle xenocrysts in a Permian Kimberlite: Two generation of kimberlitic zircon in Jwaneng DKz, Southern Botswana. In: Kimberlites and Related Rocks (Eds. Ross, J. et al.). Geol. Soc. Aust. Spec. Publ. 14, 833–842.

Kjarsgaad B. A. and D. L. Hamilton, 1989. The genesis of carbonatites by immiscibility. In Carbonatite: Genesis and Evolution (ed K. Bell), Unwin Hyman, pp. 448-463.

Kramers J. D. and I. N. Tolstikhin, 1994. U-Th-Pb systematics, Earth accretion and crust-mantle evolution. Abstracts of the Eighth International Conference on Geochronology, Cosmochronology and Isotope Geology, US Geological Survey Circular 1170, pp. 179.

Kramers J. D., 1979. Lead, uranium, strontium potassium and rubidium in inclusion-bearing diamonds and mantle-derived xenoliths from southern Africa. Earth Planet. Sci. Lett. 42, 58-70.

Kwon, S.-T., G. R. Tilton, and M. H. Grunenfelder, 1989. Lead isotope relationships in carbonatites and alkalic complexes: An overview. In: Keith Bell (Editor), Carbonatite: Genesis and Evolution, Unwin Hyman, pp. 360–387.

Le Maitre R.W., 1989. A classification of igneous rocks and glossary of term. Blackwell Sci. Publ. London.

Le Roex A. P., R. A. Cliff and B. J. I Adair, 1990. Tristan da Cunha, South Atlantic: Geochemistry and petrogenesis of a basanite-phonolite lava series. J Petrol. 31, 779-812.

Leeman W. P., M. A. Menzies, D. J. Matty and G. F. Embree (1985) Strontium, neodymium and lead isotopic compositions of deep crustal xenoliths from the Snake River Plain: evidence for Archaean basement. Earth Planet. Sci. Lett. 75, 354-368.

Lloyd F. E., 1987. Characterization of mantle metasomatic fluids in spinel lherzolites and alkali clinopyroxenites from the West Eifel and Southwest Uganda. In Mantle Metasomatism (eds. M. A. Menzies and C. J. Hawkesworth), Academic Press Inc Ltd (London), pp. 91-124.

Loock G., H.-G. Stosch and H. A. Seck, 1990. Granulite facies lower crustal xenolith from the Eifel, West Germany: petrological and geochemical aspects. Contrib. Mineral. Petrol. 105, 25-41.

Malpas, J., K. B. Spörli, P. M. Black, I. E. M. Smith, 1992. the Northland ophiolite, New Zealand and implications for plate tectonic evolution of the S. W. Pacific. Geology, 20, 149-152.

Marsh J. S., 1989. Geochemical constraints on coupled assimilation and fractional crystallization involving upper crustal compositions and continental tholeiitic magma. Earth Planet. Sci. Lett. 92, 70-80.

McCallum I. S. and M. P. Charette, 1978. Zr and Nb partition coefficients: Implications for the genesis of Mare basalts, Kb REEP, and sea floor basalts. Geochim. Cosmochim. Acta 42, 859-869.

McCulloch M. T. and J. A. Gamble, 1991. Geochemical and geodynamical constraints on subduction zone magmatism. Earth Planet. Sci. Lett. 102, 358-374.

McCulloch M. T. and M. R. Perfit, 1981. 143Nd/144Nd, 87Sr/86Sr and trace element constraints on the petrogenesis of Aleutian island arc magmas. Earth Planet. Sci. Lett. 56, 167-179.

McDermott F. and C. Hawkesworth, 1991. Th, Pb and Sr isotope variations in young island arc volcanics and oceanic sediments. Earth Planet. Sci. Lett. 104, 1-15.

McDonough W. F., M. T. McCulloch and S. S. Sun, 1985. Isotopic and geochemical systematics in Tertiary - Recent basalts from southeastern Australia and implications for the evolution of the sub-continental lithosphere. Geochim. Cosmochim. Acta 49, 2051-2067.

McDonough, W. F., 1990. Constraints on the composition of the continental lithospheric mantle. Earth Planet. Sci. Lett., 101: 1–18.

McDonough, W. F., H. -G. and N. G. Ware, 1992. Distribution of titanium and the rare earth elements between peridotitic minerals. Contrib. Mineral. Petrol. 110, 321-328.

McGetchin T. R. and G. V. Ullrich, 1973. Xenoliths in maars and diatremes with inferences for the Moon, Mars and Venus. J. Geophys. Res. 78, 1832-1853.

McKenzie, D. and M. J. Bickle, 1988. The volume and composition of melt generated by extension of the lithosphere. J. Petrol. 29, 625-679.

McKenzie, D. and R. K. O'Nions, 1991. Partial melt distributions from Inversion of rare earth element concentrations. J. Petrol., 32: 1021–1091.

Meen, J. K., J. C. Ayers and E. J. Fregeau, 1989. A model of mantle metasomatism by carbonated alkaline melts: Trace-element and isotopic compositions of mantle source regions of carbonatite and other continent igneous rocks. In: Keith Bell (Editor), Carbonatite: Genesis and Evolution, Unwin Hyman, pp. 464–499.

Meijer A., 1976. Pb and Sr isotopic data bearing on the origin of volcanic rocks from the Mariana island-arc system. Geol. Soc. Am. Bull. 87, 1358-1369.

Melcher, G. C., 1966. The carbonatites of Jacupiranga, São Paulo, Brazil, In: O.F. Tuttle and J. Gittins (Editors), Carbonatites, Chaucer Press, pp. 169–181.

Menzies M., 1990. Effects of small volume melts. Nature 343, 312-313.

Menzies, M. A., 1983. Mantle ultramafic xenoliths in alkaline magmas: evidence for mantle heterogeneity modified by magmatic activity. In: C.J. Hawkesworth and M. Norry (Editors), Continental Basalts and Mantle Xenoliths, Shiva, UK, pp. 92–110.

Menzies, M. and V. R. Murthy, 1980. Mantle metasomatism as a precursor to the genesis of alkali magmas-isotope evidence. Am. J. Sci., 280, 622-638.

Mezger K., E. J. Essene and A. N. Halliday, 1992. Closure temperature of the Sm-Nd system in metamorphic garnets. Earth Planet. Sci. Lett. 113, 397-409.

Moorbath S., H. Welke, and N. H. Gale, 1969. The significance of Lead isotope studies in ancient high-grade metamorphic basement complexes as exemplified by the Lewisian rocks of northwest Scotland. Earth Planet. Sci. Lett. 6, 245-256.

Morris J. D., W. P. Leeman and F. Tera, 1990. The subducted component in island arc lavas: constraints from Be isotopes and B-Be systematics. Nature 344, 31-36.

Mortimer, N. and B. P. Roser, 1992. Geochemical evidence for the position of the Caples-Torlesse boundary in the Otago Schist, New Zealand. J. Geol. Soc., London 149, 967-977.

Nelson, D. R., A. R. Chivas, B. W. Chappell, and M. T. McCulloch, 1988. Geochemical and isotopic systematics in carbonatites and implications for the evolution of ocean-island sources. Geochim. Cosmochim. Acta, 52: 1–17.

New Y. Y., 1976. Electron-probe studies of earlier pyroxenes and olivines from the Skaergaard intrusion, East Greenland. Contrib. Mineral. Petrol. 55, 105-126.

Newsom H. E., W. M. White, K. P. Jochum and A. W. Hofmann, 1986. Siderophile and chalcophile element abundances in oceanic basalts, Pb isotope evolution and growth of the Earth's core. Earth Planet. Sci. Lett. 80, 299-313.

Nixon, P. H. (Ed.), 1987. Kimberlitic xenoliths and their cratonic setting in mantle xenoliths. John Wiley & Sons Ltd., 215–240.

Norry M. J., and J. G. Fitton, 1983. Compositional differences between oceanic and continental basic lavas and their significance. In Continental Basalts and Mantle Xenoliths (eds C.J. Hawkesworth and M.J. Norry), Shiva, UK, pp. 5-19.

Oxbough E. R., 1964. Petrological evidence for the presence of amphibole in the upper mantle and its petrogenetic and geophysical implications. Geol. Mg. 101, 1-19.

Paterson, L. A., 1993. Partitioning of REE between carbonatitic melts and CO_2 vapour: some unusual examples from Haast, New Zealand. EOS, Trans. Am. Geophys. Union 74, 340.

Pearce J. A. and J. R. Cann. 1973, Tectonic setting of basic volcanic rocks determined using trace element analyses. Earth Planet. Sci. Lett. 19, 290-300.

Pearce, J. A., 1982. Trace element characteristics of lavas from destructive plate boundaries. in Andesites: Orogenic Andesites and Related Rocks (ed. R.S. Thorpe), pp. 525-548.

Peate, D. S., C. J. Hawkesworth, M. Mantovani and W, Shokowsky, 1990. Mantle plume and flood-basalt stratigraphy in the Parana, South America, Geology 18, 1223-1226.

Peate, D. W., C. J. Hawkesworth, and M. S. M. Mantovani, 1992. Chemical stratigraphy of the Paraná lavas (South America): classification of magma types and their spatial distribution. Bull Volcanol., 55: 119–139.

Perfit M. R., D. A. Gust, A. E. Bence, R. J. Arculus and S. R. Talyor, 1980. Chemical characteristics of island-arc basalts: implications for mantle sources. Chem. Geol. 40, 227-256.

Perfit, M. R. and R. W. Kay, 1986. Comment on "Isotopic and incompatible element constraints on the genesis of island arc volcanics from the Cold Bay and Amak Island, Aleutians, and implications for mantle structure', by J. D. Moris and S. R. Hart. Geochim Cosmochim Acta 50, 477-481.

Placz, Z. A. and A. D. Saunders, 1986. Coupled trace element and isotope enrichment in the Cook - Austral - Samoa islands, southwest Pacific. Earth Planet, Sci. Lett. 79, 270-280.

Plank T. and C. H. Langmuir, 1993. Trace elements from sediment input to volcanic output at subduction zones. Nature 362, 379-743.

Potts P. J., O. W. Thorpe, M. C. Isaacs and D. W. Wright, 1985. High precision instrumental neutron-activation analysis of geological samples employing simultaneous counting with both planar and coaxial detectors. Chem. Geol. 48, 145-155.

Rampone E., P. Bottazzi and L. Ottolini, 1991. Complementary Ti and Zr anomalies in orthopyroxene and clinopyroxene from mantle xenoliths. Nature, 354, 518-520.

Randle H. A. and N. W. A. Odling, 1992. Experimental evidence for the role of fluids in subduction zone. EOS Trans. Am. Geophys. Union 73, 637.

Renne, P. R., M. Ernesto, I. G. Pacca, R.S. Coe, J. M. Glen, M. Prevot and M. Perrin, 1992. The age of Parana flood volcanism, Rifting of Gondwanaland, and the Jurassic-Cretaceous Boundary. Science 258, 975–979.

Richardson S. H., J. J. Gurney, A. J. Erlank and J. W. Harris, 1984. Origin of diamonds in old enriched mantle. Nature 310, 198-202.

Richardson, S. H., A. J. Erlank, A. R. Duncan, and D. L. Reid, 1982. Correlated Nd Sr and Pb isotope variation in Walvis Ridge basalts and implications for the evolution of their mantle source. Earth Planet. Sci. Lett. 59: 327–342.

Ringwood A. E., 1976. Petrogenesis in island arc systems. In Island Arcs, Deep Sea Trenches and Back-Basins, (eds. M. Talwani and W. C. Pitman), Maurice Ewing Series 1, AGU 1977, pp. 311-324.

Ringwood A. E., 1990. Slab-mantle interaction; 3 Petrogenesis of intraplate magma and structure of the upper mantle. Chem. Geol. 82, 187-207.

Robey J. van A., 1981. Kimberlites of the central Cape Province, R.S.A., Unpubl. Ph.D. thesis, Univ. Cape Town, R.S.A.

Roden M. F., F. A. Frey and D. M. Francis, 1984. An example of consequent mantle metasomatism in peridotite inclusions from Nunivak Island, Alaska. J. Petrol. 25. 546-577.

Roden, M. F., V. R. Murthy and J. C. Gaspar, 1985. Sr and Nd composition of the Jacupiranga carbonatite. J. Geol. 93: 212–220.

Rodgers, K. A., R. N. Brothers and E. J. Searle, 1975. Ultramafic nodules and their host rocks from Auckland, New Zealand. Geol. Mag. 112, 160-174.

Roedder, P. L. and R. F. Emslie, 1970. Olivine-liquid equilibrium. Contrib. Mineral. Petrol. 29, 275-289.

Rogers J. J. W. and J. A. S. Adams, 1975. Uranium, Thorium In Handbook of Geochemistry (ed K. H. Wedepohl), Verlag, Heidelberg, Chapter 90 and 92.

Rogers N. W. and C. J. Hawkesworth, 1982. Proterozoic age and cumulate origin for granulite xenoliths, Lesotho. Nature 299, 409-413.

Rogers N. W., 1977. Granulite xenoliths from Lesotho kimberlites and the lower continental crust . Nature 270, 681-684.

Rogers, N. W., C. J. Hawkesworth and Z. A. Palacz, 1992. Phlogopite in the generation of olivine-melilitites from Namaqualand, South Africa and implications for element fractionation processes in the upper mantle. Lithos, 28: 347–365.

Rout, D. J., J. Cassidy, C. A. Locke and I. E. M. Smith, 1993. Geophysical evidence fro temporal and structural relationships within the monogenetic basalt volcanoes of the Auckland volcanic field, northern New Zealand. J. Volcanol. Geother. Res. 57, 71-83.

Rudnick R. L. and S. L. Goldstein, 1990. The Pb isotopic compositions of lower crustal xenoliths and the evolution of lower crust Pb. Earth Planet. Sci. Lett. 98, 192-207.

Rudnick R. L. and T. Presper, 1990. Geochemistry of intermediate-to high-pressure granulites. In: D. Vielzeuf and Ph. Vidal (Editors), Granulites and crustal evolution , Kluwer Academic Publishers, pp. 523–550.

Rudnick R. L., 1990. Nd and Sr isotopic compositions of lower-crustal xenoliths from north Queensland, Australia: Implications for Nd model ages and crustal growth processes. Chem. Geol. 83, 195-208.

Rudnick R. L., 1992a. Xenolith - Samples of the lower continental crust, in The continental Lower Crust (eds.. D. M. Fountain, R. J. Arculus and R. W. Kay), Elsvier. pp. 269-315.

Rudnick R. L., 1992b. Restites, Eu anomalies and the lower continental crust. Geochim. Cosmochim. Acta 56, 963-970.

Rudnick R. L., W. F. McDonough and B. W. Chappell, 1993. Carbonatite metasomatism in the northern Tazanian mantle: petrographic and geochemical characteristics. Earth Planet. Sci. Lett. 114, 463-475

Rudnick R. L., W. F. McDonough, M. T. McCulloch and S. R. Taylor, 1986. Lower crustal xenoliths from Queensland, Australia: evidence for deep crustal assimilation and fractionation of continental basalts. Geochim. Cosmochim. Acta 50. 1099-1115.

Ryerson, F. J. and E. B. Watson, 1987. Rutile saturation in magmas: Implications for Ti-Nb-Ta depletion in island-arc basalts. Earth Planet. Sci. Lett., 86, 225-239.

Skinner E. M. W., K. S. Vijljoen, T. C. Clark and C. B. Smith, 1992. The petrograph, tectonic setting and emplacement ages of kimberlites in the south western border region of the Kaapvaal craton, Prieska area, South Africa. Proc. 5th Int. kimberlite Conf. I. In Kimberlites, Related Rocks and Mantle Xenoliths (ed. H.O.A. Meyer and O.H. Leonardos), CPRM Spec. Publ. 92/1, Brasilia, pp. 80-97.

Skinner, D. N. B., 1986. Neogene volcanism of the Hauraki Volcanic Region. In Late Cenozoic Volcanism in New Zealand (ed. I.E.M. Smith). The Royal Soc. New Zealand Bull., 23, 21-47.

Smith C. B. , 1983. Pb, Sr and Nd isotopic evidence for sources of southern African cretaceous kimberlites. Nature 304, 51-54.

Smith C. B., T. C. Clark, E. S. Bartonand and J. W. Bristow, 1993. Emplacement ages of kimberlite occurrences in the Prieska Province, southwest border of the Kaapvaal craton. submitted to Chem. Geol. (Isotope Geosciences section).

Smith, A. D., 1993. The continental mantle as a source for a hotspot volcanism. Terra Nova 5, 452-460.

Smith, I. E. M., T. Okkada, T. Itaya and P. M. Black, 1993. Age relationships and tectonic implications of late Cenozoic volcanism in Northland, New Zealand. New Zealand J. Geol. Geophys. 36, 385-393.

Song Y. and F. A. Frey, 1989. Geochemistry of peridotite xenolith in basalts from Hannuaba, Eastern China: Implications for subcontinental mantle heterogeneity. Geochim. Cosmochim. Acta 53, 97-113.

Spera F. J., 1987. Dynamics of translithospheric migration of metasomatic fluid and alkaline magma. In Mantle Metasomatism (eds. M. A. Menzies and C. J. Hawkesworth), Academic Press Inc Ltd (London), pp. 1-20.

Stacey, J.S. and J. D. Kramers, 1975. Approximation of terrestrial lead isotope evolution by a two - stage model. Earth Planet. Sci. Lett. 26, 207–221.

Staudigel H., K.-H. Park, M. Pringle, J. L. Rubenstone, W. H. F. Smith and A Zindler, 1991. the longevity of the South Pacific isotopic and thermal anomaly. Earth Planet. Sci. Lett. 102, 24-44.

Stern, T., E. G. C. Smith, F. J. Davey and K. J. Muirhead, 1987, Crustal and upper mantle structure of the northwestern North Island, New Zealand, from seismic refraction data. Royal Astronomical Society Geophysical J., 91, 913-936.

Stosch H.-G., G. W. Lugmair and H. A. Seck, 1986. Geochemistry of granulite facies lower crust xenoliths: implications for the geological history of the lower continental crust underneath the Eifel, West Germany. The Nature of the Lower Continental Crust (ed. Dawson et al.) Geol. Soc. Lond. 331-350.

Sun S.-s. and W. F. McDonough, 1989. chemical and isotopic systematics of oceanic basalts: implications for mantle composition and processes. In Magmatism in the Ocean Basin (eds. A.D. Saunders and M.J. Norry), Geol. Soc. Spec. Publ. No. 42, pp. 313-345.

Sweeney, R.J., D. H.Green and S.H. Sie, 1992. Trace and minor element partitioning between garnet and amphibole and carbonatitic melt. Earth Planet. Sci. Lett., 113: 1–14.

Tatsumi Y., D. L. Hamilton and R. W. Nesbitt, 1986. Chemical characteristics of fluid phase released from a subducted lithosphere and origin of arc magma: Evidence from high pressure experiments and natural rocks. J Volcanol. Geotherm. Res. 29, 293-309.

Tatsumoto M. , 1969. Lead isotopes in volcanic rocks and possible ocean-floor thrusting beneath island arcs. Earth Planet. Sci. Lett. 38, 177-210.

Taylor H. P., 1980. The effects of assimilation of country rock by magma on $^{18}O/^{16}O$ and $^{87}Sr/^{86}Sr$ systematics in igneous rocks. Earth Planet. Sci. Lett. 47, 243-254.

Taylor S. R. and S. M. Mclennan, 1985. The Continental crust: its composition and evolution. Blackwell, Oxford.

Tera F., L. Brown, J. Morris and I. S. Sacks, 1986. Sediment incorporation in island-arc magmas: Inferences from ^{10}Be. Geochim. Cosmochim. Acta 50, 535-550.

Thorkelson, D. J. and R. P. Taylor, 1989, Cordilleran slab windows. Geology 17, 833-836.

Turner, S., M. Regelous, S. Kelley, C. Hawkesworth, and M. Mantovani, 1994. Magmatism and continental break-up in the South Atlantic: high precision ^{40}Ar-^{39}Ar geochronology. Earth Planet. Sci. Lett. 121: 333–348.

Ulbrich, H.G.J. and C. B. Gomes, 1981. Alkaline rocks from continental Brazil. Earth Sci. Rev., 17: 131–154.

van Calsteren P. W., P. D. Kempton and C. J. Hawkesworth, 1988. Depletion of U in the lower crust: evidence from granulite xenoliths from southern Africa. Chem. Geol. 70, 74 (abstr.).

van Calsteren, P. W. C., N. B. W. Harris, C. J. Hawkesworth, M. A. Menzies and N. W. Rogers, 1986. Xenoliths from southern Africa: a perspective on the lower crust, The nature of the lower continental crust. Geol. Soc. Lond. Spec. Publ. 24: 351–362.

van Calsteren, P.W., Huang, Y.-M. and Hawkesworth, C.J., 1993. Pb isotope evolution in the continental lithosphere, southern Africa: a xenolith perspective. Terra Nova, 1, 5: 33.

Walker R. J., R. W. Carlson, S. B. Shirey and F. R. Boyd, 1989. Os, Sr, Nd and Pb isotope systematics of southern Africa peridotite xenoliths: Implications for the chemical evolution of subcontinental mantle. Geochim. Cosmochim. Acta 53, 1583-1595.

Wass, S., 1980. Geochemistry and origin of xenolith-bearing and related alkali basaltic rocks from the southern Highland, New South Wales, Australia. American J Sci., 280, 639-666.

Watson, E. B., D. Ben Othman, J.-M. Luck and A. W. Hofmann, 1986. Partitioning of U, Pb, Cs, Yb, Hf, Re and Os between chromian diopsidic pyroxene and haplobasaltic liquid. Chem. Geol. 62: 191–208.

Weaver B. L. and J. Tarney, 1981. Lewisian gneiss geochemistry and Archaean crust development models. Earth Planet. Sci Lett. 55, 177-180.

Weaver B. L., 1991. Trace element evidence for the origin of ocean-island basalts. Geology 19, 123-126.

Weaver B. L., D. A. Wood, J. Tarney and J. L. Joron, 1986. Role of subducted sediment in the genesis of ocean-island basalts: Geochemical evidence from South Atlantic Ocean islands. Geology 14, 275-278.

Weaver S. D. and I. E. M. Smith, 1989. New Zealand intraplate volcanism. In "In intraplate volcanism in Eastern Australia and New Zealand, (eds. R. W. Johson, J. Knutson and S. R. Taylor), pp. 157-188.

Weaver, B. L., 1991. The origin of oceanic island basalt end-member compositions: trace element and isotopic constraints. Earth Planet. Sci. Lett. 104, 381-397.

Wendlandt, R. F. and W. J. Harrison, 1979. Rare earth partitioning between immiscible carbonate and silicate liquids and CO_2 vapour: Results and implications for the formation of light rare earth-enriched rocks. Contrib. Mineral. Petrol. 69: 409–419.

Wheatley, M. R. and N. M.S. Rock, 1988. A Macintosh program to generate normalized multi-element spidergrams. Am. Mineral. 73, 919–921.

White W. M. and J. Patchett, 1984. Hf-Nd-Sr isotopes and incompatible element abundances in island arcs: implications for magma origins and crustal-mantle evolution. Earth Planet. Sci. Lett. 67, 167-185.

White W. M., 1993. $^{238}U/^{204}Pb$ in MORB and open system evolution of the depleted mantle. Earth Planet. Sci. Lett. 115, 211-226.

White, W. M. and A. W. Hofmann, 1982. Sr and Nd isotope geochemistry of oceanic basalts and mantle evolution. Nature 196, 821-825.

White, W. M., 1985. Sources of oceanic basalts radiogenic isotopic evidence. Geology 13, 115-118.

Wilson A. H. and R. W. Carlson, 1989. A Sm-Nd and Pb isotope study of Archaean greenstone belts in the southern Kaapvaal Craton, South Africa. Earth Planet. Sci. Lett. 96, 89-105.

Wilson J. R. and S. B. Larsen, 1985. Two-dimensional study of a layered intrusion-the Hyllingen Series, Norway. Geol. Mag. 122, 97-124.

Wöner, G., A. Zindler, H. Staudigel and H.-U. Schmincke, 1986. Sr, Nd and Pb isotope geochemistry of Tertiary and Quaternary alkaline volcanics from West Germany. Earth Planet. Sci. Lett. 79, 107-119.

Wood, I. A., 1991. Thermoluminescence dating gives new ages for some Auckland basalts. Geol. Soc. N. Z. Misc. Publ., 59A, 147.

Woodhead, J., S. Eggins and J. Gamble, 1993. High field strength and transition element systematics in island arc and back-arc basin basalts: evidence for multi-phase melt extraction and a depleted mantle wedge. Earth Planet. Sci. Lett., 111, 491-504.

Woodward, D. J., 1970. Interpretation of gravity and magnetic anomalies at Hokianga, Northland. New Zealand J. Geol. Geophys., 13, 364-369.

Woolley, A. R., M.W. Barr, G. C. Jones, F. Wall and C. T. Williams, 1991. Extrusive carbonatites from the Uyaynah Area United Arab Emirates. J. Petrol. 32: 1143–1167.

Yaxley G. M, A. J. Crawford, and D. H. Green, 1991. Evidence for carbonatite metasomatism in spinel peridotite xenolith from Western Victoria, Australia. Earth Planet. Sci. Lett. 107, 305-317.

Zindler A. and S. Hart, 1986. Chemical Geodynamics. Ann. Rev. Earth Planet. Sci. 14, 493-571.

Zindler A. E. Jagoutz and S. Goldstein, 1982. Nd, Sr and Pb isotopic systematics in a three-component mantle: a new perspective. Nature 298, 519-523.

Appendix

Appendix A Analytical Techniques

A1 Sample crushing and mineral separation

Fresh samples were selected to be used in this study and any weathered surface was removed before and during samples crushing. Samples with size bigger than 5 cm were split using a hydraulic slitter, then they were crushed in a hardened steel jaw crusher. A part of the crushates of granulite and carbonatite samples were taken for mineral separation and the rest was ground to < 200 mesh in an agate-lined swing mill or an agate satellite ball mill.

Some minerals in carbonatites and granulites were separated for isotope analyses. Apatite and carbonatite, (mainly calcite) were separated by hand-picking under a binocular microscrope from sieved crushates of the carbonatites. Garnet, clinopyroxene and plagioclase from granulites were separated using a Frantz electro-magnetic separator and then hand picked under a binocular microscrope. Then mineral separates were powdered by grounding with a mortar and a pestle.

A2 X-ray fluorescence (XRF) analyses

Major and some trace elements (Ba, Rb, Sr, Nb, Zr, V, Y, Zn, Cu, Cr and Ni) were measured at the Open University using an ARL 8420+ dual goniometer wavelength dispersive XRF spectrometer equipped with 3 kw Rh anode end-window Xay-ray tube and diffracting crystals AX06 (multilayer), PET (penta-erythrytol), Ge111, LiF200 and LiF220. Elemental

intensities are corrected for back ground and known peak overlap interferences. Instrumental intensity drift was corrected using a drift monitor. Calibration lines are produced from measuring of reference materials with a wide range of compositions.

A2-1 Major element analysis preparation

Sample powders were dried in a oven at 110°C for overnight. Dried powders were weighed out 0.7000±10 g with 5 times of Johnson Matthey Spectroflux 100B (lithium metaborate/tetraborate flux) into cleaned Pt-5% Au crucibles. Crucibles with well mixed powders were put in an preheated furnace at 1100°C for 15 minutes for fusion. The melts were swirled repeatly to ensure complete dissolution and homogenisation, and then poured into a heated brass mould and pressed with a plunger to form a glass disc for XRF spectrometer analysis.

Volatile contents (mainly H_2O and CO_2) cannot be analysed by this technique and they are accounted as loss on ignition (LOI). Silica crucibles were pre-ignited for 20 minutes at 1000°C. Samples were weighed out precisely between 1-2 g into the crucibles and ignited in a furnace at 1000°C for 30 minutes. LOI was worked out by the weight change of the crucibles.

Carbonatite samples were prepared as above but they were mixed with 50% silica to avoid cracking of the glass discs during cooling. Element abundances were calculated using normal silicate calibration and corrected for the dilution. SiO_2 was adjusted relative to BCS368 and BCS393 carbonatite standards.

A2-2 Trace element analysis preparation

9-10 g of a sample was weighed into a re-sealable plastic bag and mixed with 0.6-0.7 ml PVP binder (polyviny pyrollidone methy cellulose). The well mixed powder was put into a pellet mould (35 mm diameter) and

pressed at pressure of 10 tonnes per sq. inch. The pellet was dried overnight at 105 °C.

A3 Instrumental neutron activation analysis (INAA)

REE and U, Th, Sc, Ta, Hf and Co were measured by INAA at the Open University. 0.300±10 g of rock powder was weighed and sealed into a polythene capsule. Nine samples and two standards (Ailsa Craig microgranite and Whin Sill dolerite) were packed into a cylinder, together with weighed laquered iron foil between each capsule to monitor the neutron flux along the cylinder.

Samples were irradiated at the Imperial College Reactor Centre in a thermal flux of $5*10^{12}$ n cm^{-2} s^{-1} for 24-30 hours. Measurements were carried out at the Open University a week after irradiation to allow decay of short lived nuclides. The instrument was equipped with two detectors, a coaxial Ge(Li) and a low energy photon spectrometer, to count the induced radioactivity. Samples were counted twice over a period of one month, the first time for 800 sec. and six to ten hour in the second period, the latter was to improve precision on values of long lived isotope. Details of analysis procedures have been described by Potts et al. (1985).

A4 Isotope Analysis Techniques

Isotope analyses, including both isotope dilution for trace element contents (Sr, Nd, Pb, U, Th) and isotope compositions, were carried out in the radiogenic isotope laboratory at the Open University, in which clean air is supplied to maintain a positive air pressure. Subboiling Teflon distilled HF, Quartz distilled HCl and HNO_3, and water purified with Mili-Q-reverse osmosis were used for Sr and Nd analyses. Reagents were further purified by Teflon-two-bottle distillation for Th and U analyses and two times Teflon-two-bottle distilled reagents and water for Pb isotope analyses. Routine blanks for Sr, Nd and Pb were 0.5, 1, 1ng, respectively. Standard

techniques were used for Sr, Nd, Pb U and Th separation and are described briefly as bellow.

A4-1 Samples dissolution

Because a variety of samples have been studied, including carbonate and silicate rocks, metamorphic and volcanic rocks, there are slight difference in dissolution methods. Teflon oven-bombs and Savillex bombs, depending on samples, were used to dissolve samples. Teflon oven-bombs were used for granulite whole-rocks and mineral separates of garnet and clinopyroxene because garnet and some accessary mineral phases were difficult to dissolve, whereas Savillex bombs were used for young basalts, carbonate and plagioclase. Silicate rocks were dissolved in $HF+HNO_3$. Carbonate samples were dissolved initially in HCl and further in $HF+HNO_3$ for silicate residues. The sample solutions were treated with 15M HNO_3 and 6M HCl repeatedly to break formed fluorides and dissolved completely, then the samples were evaporated to dryness under evaporation hoods. Isotope dilution samples were added with proper amounts of relevant spikes mainly before digestions and then were treated the same as isotope composition samples.

A4-2 Element separation

(Rb) Sr and (Sm) Nd samples re-dissolved in 1 ml of 2.5 HCl and loaded on preconditioned ion-exchange columns of Bio-rad AG50W X8 100 mesh resin. Rb, if it is required, and Sr were collected after washing the columns in 2.5 M HCl, following the column calibration. MREE fraction were collected in 3M HNO3, and Sm and Nd separated further using reverse ion-exchange columns contained 1 g teflon powder (Voltaf 300LD Pl micro) and 100 g DEP (di(2-ethylhexy)phosphate).

Pb isotope samples were re-dissolved in 1M HBr and loaded on columns, which were made with 2ml polythene pipette tips containing 5

drops of Dowex 200-400 mesh anion exchange resin. Pb fraction was collected in 6M HCl after washing the columns with 1M HBr. Pb fraction was further purified by re-passing samples through the columns.

U and Th samples were taken up in 7M HNO3 and loaded on 4ml Dowex 200-400 mesh anion exchange columns. Th and U fractions were collected in 6M HCl and 1M HBr respectively after washing.

A4-3 Mass spectrometry

All isotope dilution for element concentrations, except Th, were measured on a Vacuum Generators Isomass 54E solid source mass spectrometer, and the other measurements were carried out on a Finnegan MAT 261. Sr and Nd samples were loaded with H_3PO_4, Pb was loaded with silica gel+H_3PO_4, and U and Th were loaded with graphite. Sr, Nd and Pb isotope ratios were measured statically. Sr isotope fractionation during run was corrected to $^{86}Sr/^{88}Sr = 0.1194$ and Nd isotope fractionation was corrected $^{146}Nd/^{144}Nd = 0.7219$. NBS 987 (Sr), J+M Nd and NBS 981(Pb) standards were routinely measured with samples to monitor mass spectrometer.

Appendix B Petrology and Mineralogy of Samples

Samples from the Jacupiranga carbonatite complex

HB001 is a pyroxenite with euhedral granular texture. The pyroxenes are high Ca diopside with Wo over 50%, indicative of crystallization in a high $CaCO_3$ environment. There are a few small flakes of micas in fractures between the pyroxenes, and these are considered to be secondary. Analyses of magnetite show high TiO_2 (10–11%) and Al_2O_3 ~3.5%. It is inferred to be cumulitic based on texture and mineral compositions.

HB004 is a brown and white banded sample with a total SiO_2 content of about 20%. The white layers are mainly composed of calcites with scattered olivine, phlogopite and magnetite. The brown layers consist of olivine, phlogopite and calcite. Olivines have been corroded by phlogopite microcrystals and calcite, suggesting that phlogopite was formed by reaction between fluids and olivine. The phlogopites have Al_2O_3 (10–7.5%) and BaO (<0.1%) and FeO (>4%).

HB005 is a carbonatite with SiO_2 <10%, consisting mainly of calcite, dolomite, apatite, phlogopite, olivine and magnetite. The carbonate minerals are predominantly calcite with a few dolomite grains (2 in 20 analyses), occurring as xenomorphic crystals. Twinning is common. The calcites contain 1–2% MgO and 0.68–0.8% SrO and 0.08–0.2% BaO, whereas the dolomites contain less SrO (0.2) and almost no BaO. Phlogopite is euhedral (>0.5 mm) and appears to be primary. It has higher Al_2O_3 (12–15%) and BaO (0.2–1.3%), and lower FeO (2–3%), and hence it is chemically different from those in HB004. Olivine has Fo 95–96, which is much higher than that in olivines (Fo 88–92) in basic and/or ultrabasic silicate rocks, but similar to olivines (Fo 96) in metamorphic limestone. Magnetite occurs scattered throughout the sample and the analyses show TiO_2 0.5–5%, and low Al_2O_3 of ~1.5%.

HB008 was split up into two parts: one (HB008–1) is similar to HB001 and the other (HB008–2) is similar to HB004.

HB009 has a dark layer sandwiched between carbonatite, and it was also split into two subsamples. HB009–1 consists of olivine, microcrystalline phlogopite and calcite, with SiO_2 = ~20%. It is similar to HB004. HB009–2 is mainly composed of calcite, with some apatite and a few sulphides.

HB010 is a carbonatite similar to HB005. The olivines have Fo 95–96, and serpentinization is seen along the fractures in the olivine crystals. Apatite is distributed heterogeneously as mineral aggregates. It appears in two distinct habits: (i) as small isolated oval grains within the carbonatitic minerals, with diameter 0.1–1 mm. These apatite crystals usually are slightly rounded and corroded. (ii) As idiomorphic prisms 1–5 mm in diameter in aggregates. Electron probe analyses indicate that the apatites are fluorapatite with 5–6% F.

HB011 is a carbonatite similar to HB010, but with fewer silicate phases (olivine and phlogopite) and magnetite.

Appendix C Modelling Calculations and Some Results

C-1 Source composition inferred from a trace element diagram

Nb/Ba and Nb/K_2O vs. Nb diagrams have been used following Hofmann and Feigenson (1983) for discussion of trace element behaviour during partial melting and source composition in Chapter IV. This section examines the calculation equations induced from simple batch partial melting model, which used to draw the several conclusions for the mantle source composition of the Auckland basalts.

During partial melting, a highly incompatible element content in a melt can be described as $C_l=C_s/(F*(1-D)+D)$ using batch melting model; where D is partition coefficient of a element and F is degree of partial melting; C_l and C_s are element abundances in melt and in the melt derived source. When considering only highly incompatible elements, D is << 1, then the equation can be simplified to

$$C_l=C_s/(F+D) \qquad (1)$$

A trace element ratio involving two incompatible elements Elements 1 and 2, such as Nb and Ba, can be written as

$$R=\frac{C_{l1}}{C_{l2}}=\frac{C_{s1}}{C_{s2}}*\frac{(F+D_2)}{(F+D_1)} \qquad (2)$$

Eq (1) can be rewritten as $F=\frac{C_{s1}}{C_{l1}}-D_1$, and substituting F in Eq. (2) and re-orgnise it,

$$R=\frac{C_{s1}}{C_{s2}}+\frac{(D_2-D_1)}{C_{s2}}*C_{l1}$$

This is a linear equation which gives relationship between a trace element ratio and abundance, for instance Nb/Ba vs. Nb. A few implications can be drawn from this equation.

First, when two trace elements have the same partition coefficients ($D_2=D_1$), the regression line will be horizontal.

Second, when Element 2 has a higher partition coefficient than Element 1 ($D_2 > D_1$), the regression line will have a positive slope; whereas $D_2 < D_1$, the regression line will have a negative slope. Therefore, this diagram can be used to compare relatively partition coefficients of two elements.

Third, because a slope involves an element abundance (slope = $(D_2-D_1)/C_{s2}$) exactly difference between partition coefficients of two elements cannot be easily worked out from a data trend without knowledge of the contents in the source.

Fourth, a element ratio in the source can be worked out using intersection of a data array (ie. when $C_{l1} = 0$, then $R = C_{s1}/C_{s2}$).

C-2 Pb isotope calculations

Pb isochron and isotope evolution model calculations have been used largely in the Chapter III, and following is the calculation equations used in this Chapter.

C-2-1 Pb - Pb isochron

Isochron calculation assumes that a suite of rocks have the same initial isotope ratios and different μ ($^{238}U/^{204}Pb$) since their generation. Thus, Pb isotopes in the rocks can be described as:

$$^{206}Pb/^{204}Pb=a_o + \mu\,(e^{(\lambda t)}-1); \qquad ^{207}Pb/^{204}Pb=b_o + \mu\,(e^{(\lambda' t)}-1)/137.88$$

where $\lambda = 1.55125*10^{-10}$ and $\lambda'=9.8485*10^{-10}$. The relationship between $^{206}Pb/^{204}Pb$ and $^{207}Pb/^{204}Pb$ in the samples can be written as:

$$^{207}Pb/^{204}Pb = a + b * {}^{206}Pb/^{204}Pb,$$

where $a = b_0 - a_0 * (e^{(\lambda' t)}-1)/(e^{(\lambda t)}-1)/137.88$, $b=(e^{(l' t)}-1)/(e^{(l t)}-1)/137.88$. Therefore, the Pb isotope ratios in this suite rocks with different μ will have linear relationship and the slope only depends on the age. If there is any independent data for the initial ratio, individual μ for each sample can be calculated from their present isotope ratios; or with knowledge of μ then the initial ratios can be calculated.

C-2-2 The Pb evolution model

Pb evolution is modelled for the southern Africa lithosphere in Chapter III, which involves one-stage and two-stage Pb evolution calculations followed Faure (1986).

One stage Pb evolution is calculated for the time integrated μ with provided initial ratio. The equations are as follows:

$$^{206}Pb/^{204}Pb=a_0 + \mu\,(e^{(\lambda t)} - 1); \qquad ^{207}Pb/^{204}Pb=b_0 + \mu\,(e^{(\lambda' t)} - 1)/137.88$$

When U/Pb is fractionated during partial melting and fractional crystallisation, a series of rocks will have different μ values and, with time, develops different Pb isotope ratios. Their $^{206}Pb/^{204}Pb$ and $^{207}Pb/^{204}Pb$ ratios plot along a line, $^{207}Pb/^{204}Pb=a + b * {}^{206}Pb/^{204}Pb$, in which slope of the line give a μ fractionation age value in the source.

The Pb evolution model used in Chapter 2 is two-stage model of Pb evolution for the southern African lithosphere mantle. Basic idea is that the southern African mantle was homogeneous before the Archaean and major fractionation of U/Pb was due to Archaean continental crust extraction from the mantle. The present compositions in the southern Africa continental mantle are represent by the mantle xenoliths from kimberlites, Group 2 kimberlites, and some flood basalts, which have partially overlapping Pb isotope compositions.

The first assumption, a homogeneous mantle before Archaean in the southern African mantle is not likely to be valid, however, there is not enough information for the compositions for the mantle before the Archaean. The data from Archaean cratons were used to calculate μ_1, using above single stage equations, and different μ_1 values (given in the chapter) may strongly indicate that the evolution of Archaean mantle was multiple stage as discussed in the chapter. Thus, the value μ_1 chosen in the calculation only can be considered an average one.

Second assumption for this two stage model is that fractionated post-Archaean mantle essentially has been as a closed system and this seems to be confirmed by many previous studies on the mantle xenoliths and mantle derived components as discussed in the Chapter.

Two stage evolution equations are given as follows:

$$^{206}Pb/^{204}Pb = a_1 + \mu_2(e^{(\lambda t_1)}-1) \qquad (1)$$

$$^{207}Pb/^{204}Pb = b_1 + \mu_2(e^{(\lambda' t_1)} - 1)/137.88 \qquad (2)$$

where $a_1 = a_0 + \mu_1(e^{(\lambda t_0)} - e^{(\lambda t_1)})$; $b_1 = b_0 + (\mu_1(e^{(\lambda' t_0)} - e^{(\lambda' t_1)})/137.88$

μ_1 is as discussed above and given from an average value from the Archaean greenstone data. The age t_1 is also given from the our xenoliths data which is close to an average age of Archaean craton generation (3.6~2.6 Ga). However, present Pb isotope ratios in different mantle regions cannot be measured directly, and so μ_2 cannot be calculated from Eqs 1 and 2. What can be used to infer mantle compositions is mantle derived rocks with different ages, such as the northern Lesotho granulite xenoliths and the mantle xenoliths from southern Africa kimberlites. The Pb isotope evolution in these rocks are:

$$^{206}Pb/^{204}Pb = a_1 + \mu_2(e^{(\lambda t_1)}-e^{(\lambda t_2)}) + \mu_2(e^{(\lambda t_2)}-1) \qquad (3)$$

$$^{207}Pb/^{204}Pb = b_1 + (\mu_2(e^{(\lambda' t_1)} - e^{(\lambda' t_2)}) + \mu_3(e^{(\lambda' t_2)} - 1))/137.88 \quad (4)$$

where t_2 is the age of the samples when they were derived from their mantle sources, for the northern Lesotho granulite samples which is ~1.2-1.4 Ga, and for the mantle xenoliths in the southern African kimberlites which is ~150 Ma. Their initial Pb isotope ratios should satisfy both a linear trend (data array): $^{207}Pb/^{204}Pb = a + b*^{206}Pb/^{204}Pb$ (Eq 5) and Eqs 3 and 4. Substituting Eqs 3 and 4 into Eq 3, μ_2 can be extracted from a rewritten equation:

$$\mu_2 = (b_1 - a - b(a_1 + \alpha_1) + \beta_1)/(\alpha_2 - \beta_2/137.88)$$

where $\alpha_1 = \mu_1(e^{(\lambda t_1)} - e^{(\lambda t_2)})$; $\beta_1 = (\mu_1(e^{(\lambda' t_1)} - e^{(\lambda' t_2)})/137.88$; $\alpha_2 = (e^{(\lambda t_1)} - 1)$ and $\beta_2 = (e^{(\lambda' t_1)} - 1)/137.88$;

The calculations suggests (shown as evolution lines in diagrams) the mantle derived rocks, the Group 2 kimberlites, mantle xenoliths and and flood basalts may be derived from different mantle regions with different μ_2, which represents U/Pb fractionation in different parts of the continental lithosphere mantle. Pb isotope compositions in these young mantle derived rocks plot on a Archaean granulite samples trend, which indicates major U/Pb fractionation in the mantle beneath southern Africa. The trend can be described as following a isochron equation:

$$^{207}Pb/^{204}Pb = a + b * ^{206}Pb/^{204}Pb,$$

where $a = b_1 - a_1 *(e^{(\lambda' t_1)} - 1)/(e^{(\lambda t_1)} - 1)/137.88$,
$b = (e^{(\lambda' t_1)} - 1)/(e^{(l\lambda t_1)} - 1)/137.88$

From the definition of a isochron equation, this indicates that they should have had the same initial Pb isotope ratios and the time (t_1) represents their generation age, ie. the U/Pb fractionation in the continental lithosphere mantle beneath southern Africa occurred during the generation of the Archaean crust.

C-3 Calculation result of major element least-square fit model

C-3-1 Calculation result of the Auckland and Northland samples

	Parental	F	Melt	ol	cpx	pla	Mt	Res
Auckland	L1	0.772	B5	0.29	0.34	0.31	0.05	0.02
	L8	0.98	L4	0.27	0.18	0.55	0.00	0.03
	L6	0.631	B1	0.29	0.29	0.36	0.05	0.04
	L6	0.95	L10	0.47	0.16	0.38	0.00	0.03
	L6	0.896	L11	0.21	0.41	0.33	0.05	0.00
	L6	0.961	L7	0.50	0.22	0.28	0.00	0.01
	L8	0.667	B7	0.31	0.28	0.36	0.05	0.02
	L8	0.792	L11	0.38	0.31	0.26	0.05	0.05
	L8	0.635	B3	0.16	0.38	0.39	0.08	0.01
	L8	0.92	L3	0.43	0.24	0.27	0.05	0.05
	L8	0.903	L5	0.29	0.35	0.27	0.09	0.01
	L8	0.815	SCB13	0.35	0.32	0.30	0.03	0.03
	L8	0.572	44071	0.23	0.42	0.27	0.09	0.92
	L8	0.515	44079	0.24	0.42	0.26	0.09	1.04
Group 1	44055	0.396	37669	0.13	0.27	0.55	0.05	0.07
	44055	0.627	44036	0.14	0.28	0.52	0.06	0.05
	44055	0.738	44040	0.05	0.23	0.63	0.09	0.02
	44055	0.558	44042	0.12	0.31	0.54	0.03	0.05
	44055	0.533	44048	0.13	0.29	0.52	0.07	0.08
	44055	0.585	44050	0.18	0.22	0.55	0.05	0.14
	44055	0.757	44052	0.22	0.15	0.55	0.08	0.12
Group 2	37653	0.864	37682	0.22	0.35	0.37	0.07	0.07
	37653	0.932	37697	0.64	0.31	0.00	0.05	0.26
	37653	0.912	37702	0.00	0.71	0.25	0.05	0.06
	37653	0.765	44018	0.22	0.31	0.39	0.08	0.02
	37653	0.818	44020	0.27	0.13	0.58	0.02	0.57
	37653	0.589	44027	0.20	0.29	0.46	0.05	0.02
Group 3	42547	0.591	42556	0.29	0.27	0.38	0.07	0.11
	42547	0.911	42563	0.50	0.17	0.33	0.00	0.08
	42550	0.677	42565	0.26	0.25	0.46	0.03	0.08
	42550	0.572	44022	0.14	0.50	0.31	0.04	0.18
	42550	0.515	44034	0.23	0.31	0.42	0.05	0.12
	42550	0.517	44043	0.23	0.31	0.42	0.05	0.12
	44410	0.95	44411	0.41	0.20	0.39	0.00	0.02

C-3-2 Major element compositions of phenocrysts used in the calculation

	SiO_2	TiO_2	Al_2O_3	Fe_2O_3	FeO	MgO	CaO	Na_2O	K_2O
Olivine	39.71	0	0.04	2.55	12.76	44.38	0.34	0.37	0
Pyroxene	45.12	3.11	7.68	0.07	7.05	12.15	22.75	0.93	0
Feldspar	52.92	0.34	29.17			0.03	12.5	3.95	0.38

Appendix D Published abstracts

Appendix D-1

EUG Conference VII, April, 1993, Terra nova 5, 437

Isotope variation in Jacupiranga carbonatite complex, Brazil: Evidence for a multiple small degree melting origin

Y. -M. Huang, P. W. van Calsteren and C. J. Hawkesworth

Department of Earth Sciences, Open University, Milton Keynes, UK

The 130 Ma old Jacupiranga carbonatite complex, consists of pyroxenite, peridotite, ijolites, fenites, nepheline syenites and carbonatite, intruded into the late Precambrian folded mica schists and syntectonic granodiorite belt of east Brazil. $^{87}Sr/^{86}Sr$ ratios range from 0.7047 to 0.7056, $^{143}Nd/^{144}Nd$ ratios are 0.51251 to 0.51264 and $^{206}Pb/^{204}Pb$ ratios range between 17.0~18.2. Most of them have high Th/U ratios and $^{208}Pb/^{204}Pb$ ratios (37.9~40.2) relative to $^{206}Pb/^{204}Pb$, and with time integrated Th/U>4. Initial Sr and Pb isotope ratios indicate systematic differences between pyroxenite and carbonatite and they are negatively correlated. Thus the pyroxenites have higher $^{206}Pb/^{204}Pb$ ratios (17.65~17.60) and lower $^{87}Sr/^{86}Sr$ ratios (0.7047) than the carbonatites (17.45~17.0, 0.7049~0.7054 respectively).

The negative Pb-Sr isotope correlation between carbonatite and pyroxenite precludes the possibility of binary mixing because Sr /Pb ratios are dramatically different in carbonatites and pyroxenites. Moreover the constant Nd isotope compositions with variable Sr isotope ratios are inconsistent with AFC involving a crustal component. In addition, the relationship between Sr content and Sr isotope ratios further precludes a mixing or AFC model. Therefore, the isotopic compositions are considered to be primary features inherited from the mantle sources associated with incipient magmatism of the Tristan de Cunha hotspot and the opening of the south Atlantic Ocean. This relationship between carbonatite and associated silicate rock does not directly support a liquid immiscibility model, but favours a multiple small degree partial melting event to count for the variable isotopic compositions.

Appendix D-2

Eighth International Conference on Geochemical, Cosmochronology and Isotope Geology, June, 1994, Abstracts of ICOG-8 (US Geological Survey Circular 1107), pp. 145

Implication for the evolution of the lithosphere in southern Africa from isotope systematics in granulite xenoliths

Huang, Y-M., van Calsteren, P. and Hawkesworth, C. J.
Department of Earth Sciences, Open University, Milton Keynes MK7 6AA, U.K.

The nature and evolution of the lower crust around the margins of Archaean cratons is not well constrained. New data are presented on granulite facies xenoliths from kimberlite pipes in N. Lesotho and the Markt area, Namaqualand, southern Africa, close to the margins of the Kaapvaal Craton. Granulites from both areas have similar major element compositions with SiO_2 between 46-51%. Sr and Nd isotope ratios are 0.70479-0.70723 and 0.51251-0.51149 respectively in the Markt granulite xenoliths, which have, on average, higher Sr and lower Nd isotope ratios than those in the N. Lesotho granulites[1]. Whole rock Sm-Nd isotope data from the Markt granulites scatter on an errochron, corresponding to 1.18±0.2 Ga, within error of the age of 1.24±0.17 Ga for the N. Lesotho granulites. Selected mineral (cpx, gt, plag)-whole rock isochrons from Markt yield ages of 851±56 and 604±36 Ma, and one from Lesotho gives an age of 595±10 Ma.

Measured $^{206}Pb/^{204}Pb$ ratios from the N. Lesotho granulites range from 16.25 to 17.58, and $^{207}Pb/^{204}Pb$ from 15.19 to 15.58. All but two of the granulites from N. Lesotho fall on an array which yields an age of 1.49±0.36 Ga. This age is indistinguishable within error from their Sm-Nd whole rock age. In contrast, the Markt granulites have $^{206}Pb/^{204}Pb$ ratios in the range 15.17 to 17.67, with relative low $^{207}Pb/^{204}Pb$ ratios between 14.87 to 15.10. These data fall on a trend corresponding an age of 3.19±0.04 Ga, which is much older than either the Pb-Pb age for the N. Lesotho samples and their own Sm-Nd age. Mineral-whole rock Pb-Pb isochrons from two Markt granulites with low whole rock Pb isotope ratios give ages of 2.93±0.07 and 2.91±0.08 Ga, respectively.

Thus, both Sm-Nd and Pb-Pb whole rock ages indicate that the N. Lesotho granulite xenoliths were mostly derived from a Proterozoic lower

crust. However, taken at face value, Pb isotope data for the granulite xenoliths from Markt indicate Archaean ages. Correlations between major and trace element data indicate that the granulite xenoliths from Markt are genetically related and preclude simple mixing models for the Pb-Pb trend. Contamination from kimberlites is also unlikely because there is no correlation between Pb contents and isotope compositions. There are two explanations for the Pb and Nd isotope systems, one is that the Pb-Pb trend from the Markt granulites was been inherited from an Archaean lithospheric mantle source and the Sm-Nd whole rock age represents the time of the lower crust generation. Alternatively, ages of 2.9 Ga yielded by the mineral-whole rock isochrons from two U-depleted samples represent early metamorphic ages, and the Markt granulites are inferred to have been derived from the mantle in the Archaean, probably at 3.2 Ga as indicated by the whole rock Pb-Pb age. In this explanation, the Nd whole rock age may reflect re-equilibration in an Archaean lower crust during the generation of Proterozoic crust, which in turn implies that Sm and Nd have higher diffusion rates than U and Pb, consistent with the conclusions of recent geochronological studies[2,3].

1 Rogers and Hawkesworth, 1982, Nature 299, pp. 409-413.
2 Burton et al., 1993, Terra Nova 5, pp. 382.
3 Mezger et al., 1992, Earth Planet. Sci. Lett. 113, pp. 397-409.

Appendix D-3

Goldschmidt Conference, Aug. , 1994, Mineralogical Magazine 58A 432-433

OIB-like magmatism in Auckland, New Zealand

Y.-M. Huang, P. van Calsteren and C. Hawkesworth
the Open University, Milton Keynes, MK7 6AA, UK;

P. Black and I. Smith
the University of Auckland, New Zealand

Introduction

Continental volcanic rocks with isotope and trace element compositions similar to oceanic island basalts (OIB) are often attributed to deep seated mantle plumes. Radiogenic isotope ratios in oceanic basalts are widely modelled in terms of contributions from different mantle components, similarly perceived to reside at depth in the upper mantle. It is therefore of interest to investigate the isotope and trace element characteristics of continental intraplate basalts generated in response to regional plate interactions, since by implication they are derived from relative shallow levels in the sub-continental mantle. This study reports major, trace element and radiogenic isotope data on 100,000 year old to historic volcanic rocks from the Auckland volcanic field in the Northland-Auckland peninsula, New Zealand. The volcanic field is situated c. 500 km west of the active Taupo Volcanic Zone, and magmatism may be a response to the development of a slab window after cessation of subduction under the Northland-Auckland peninsula.

Geochemical Results

The Auckland rocks analysed are silica undersaturated basanites and alkali basalts (SiO_2 40-46%) with high MgO (10-12.5%). The basanites have lower SiO_2, Al_2O_3 and higher CaO than the alkali basalts. Although the basanites have the higher incompatible element contents , both groups exhibit similar smooth patterns on mantle normalised diagrams. Such patterns tend to peak at Nb and Ta, and so the rocks are characterised by high Nb/Ba, Nb/Rb and Nb/La ratios. They are therefore more similar to HIMU OIB (Table 1) than any of the other proposed mantle components (Weaver 1991)

$^{87}Sr/^{86}Sr$ and $^{143}Nd/^{144}Nd$ ratios are in range 0.70275 - 0.70294 and 0.51294 - 0.51299, respectively. Thus, their source regions were depleted

relative to the bulk earth, but less than MORB source, and consequently they plot between MORB and HIMU on a Nd-Sr diagram. Most Pb isotope ratios measured also exhibit a limited range, with $^{206}Pb/^{204}Pb$ = 19.18 to 19.33, although three samples have significantly lower Pb isotope ratios and higher Pb contents. The majority of samples therefore have Pb isotope ratios similar to the more radiogenic Pb ratios observed in MORB, but they are significantly less radiogenic than HIMU OIB. Basanites and alkali basalts have very similar radiogenic isotope ratios.

Discussion

The samples analysed here have high MgO contents with high compatible element contents (e.g. Ni = 177-323 ppm). Using the Hart and Davis model (1978), calculations indicate that the more evolved samples have only undergone 5-7% olivine fractionation. Thus, they are considered as primary or near primary compositions. Similar isotope and highly incompatible trace element ratios, but variable major and incompatible trace element abundances, indicate that they may be related to each other by different degrees of partial melting of similar mantle sources.

The observed incompatible element features in the Auckland rocks, i.e. that Nb and Ta are relatively more enriched than LILE and LREE, are also a feature of HIMU OIB (Table 1, Weaver 1991). It has been argued that the HIMU component has been derived from subducted oceanic crust from which LIL and LRE elements have been preferentially removed by dehydration. It has been inferred from the radiogenic Pb isotope characteristics of OIB, that HIMU has high U/Pb and that this is the results of Pb loss into fluids from dehydration of slab or oceanic sediments (Weaver 1991; Chauvel et al. 1992). The incompatible trace element characteristics in the Auckland basalts (Table 1 and Fig. 1), together with their Sr and Nd isotope compositions are similar to HIMU basalts, however, the Pb isotope ratios are much lower than those from HIMU OIB. This could be because either they had lower U/Pb ratios in their mantle source and/or insufficient time has passed since high U/Pb ratios developed. The precise U/Pb ratios in the mantle sources are difficult to assess. However, relatively low Nb/U ratios (35) in the Auckland basalts indicates that U is relatively enriched.

The undersaturated silicate contents (SiO_2 40-44%) in the basanites suggest they were generated by relatively small degrees of partial melting of the mantle. Undersaturated silicate melts with K_2O/Na_2O <1 can be generated from a carbonate-enriched mantle sources, such as melilitites. Another possible mantle source is amphibole-bearing lherzolites. The glasses in amphibole lherzolite xenoliths tend to have lower silica and

higher alkali contents than glasses from anhydrous lherzolites (Francis and Ludden 1990), and a recent experimental study indicated that primary basanites can be generated from amphibole-bearing garnet lherzolite source (Adam 1990). Thus, the Auckland basalts may have been derived from metasomatised mantle at relatively shallow depths.

Oceanic intraplate volcanism has usually been attributed to mantle plumes. However, the geological setting of the Auckland volcanism is more easily explained in terms of a slab window model. (e.g. Hole et al. 1991). There is evidence that the Pacific oceanic crust was subducted beneath the Northland - Auckland peninsula and subduction related volcanic rocks (Miocene) are found in the nearby Coromandel peninsula. However, subduction in the Northland - Auckland peninsula has stopped and, at present, subduction related volcanism is expressed by the Taupo volcanic zone. The Auckland post-subduction basalts have a similar tectonic setting and geochemical features to the Antarctic peninsula basalts (Hole et al. 1993), consistent with a similar mantle source with HIMU-like signatures at relatively shallow levels in the southern hemisphere.

Reference

1 Adam, J. (1990) Journal of Petrology, 31, 1201-1223.

2 Chauvel, C., Hofmann, A. and Vidal, P. (1992) Earth Planet. Sci. Lett., 110, 99-119.

3 Francis, D. and Ludden, J. (1990) Journal of Petrology, 31, 371-400.

4 Hole, M., Rogers, G., Saunders, A. and Storey, M. (1991) Geology, 19, 657-660.

5 Hole, M., Kempton, P. and Millar, I. (1993) Chemical Geology, 109, 51-68.

6 Weaver, B., Wood, D., Tarney, J. and Joron, J.-L. (1987) Alkaline igneous rocks: Geological Society of London Special Publication (eds. Fitton and Upton), 30, 253-267.

7 Weaver, B. (1991) Earth Planet. Sci. Lett., 104, 381-397.

Fig. 1 Ba/Nb, La/Nb and Ba/La ratios vary systematically between the OIB end members (Weaver 1991 and Weaver et al. 1987). This diagram shows that these incompatible trace element ratios in the Auckland basalts are similar to the HIMU OIB.